Structural and Fluid System Evolution in the Otavi Mountainland (Namibia) and its Significance for the Genesis of Sulphide and Nonsulphide Mineralisation

Inaugural - Dissertation

zur Erlangung der Doktorwürde
der
Naturwissenschaftlich-Mathematischen
Gesamtfakultät
der
Ruprecht-Karls-Universität
Heidelberg

vorgelegt von
Diplom-Geologe

Carsten Laukamp

Heidelberg 2006

Structural and Fluid System Evolution in the Otavi Mountainland (Namibia) and its Significance for the Genesis of Sulphide and Nonsulphide Mineralisation

Inaugural - Dissertation

zur Erlangung der Doktorwürde
der
Naturwissenschaftlich-Mathematischen Gesamtfakultät
der
Ruprecht-Karls-Universität
Heidelberg

vorgelegt von
Diplom-Geologe Carsten Laukamp
aus Großauheim, Hessen
Tag der mündlichen Prüfung: 16.01.2007

Gutachter: Prof. Dr. Thilo Bechstädt
Geologisch-Paläontologisches Institut
Ruprecht-Karls-Universität Heidelberg
Im Neuenheimer Feld 234
D-69120 Heidelberg
Deutschland

Prof. Dr. Hartwig E. Frimmel
Institut für Mineralogie und Kristallstrukturlehre
Julius-Maximilians-Universität Würzburg
Am Hubland
D-97074 Würzburg
Deutschland

okuhakula omamanya

"curing the stones"
Bushmen mining ceremony

Before smelting could begin there had to be a ceremony known as *okuhakula omamanya*, literally "curing the stones." Once the master smelter had lighted the furnace with a glowing piece of charcoal brought from the village hearth, he faced the east and, with arms raised, offered a prayer to the spirits which climaxed with an invocation to the stones themselves:

I pray, I pray, I pray!
All ye spirits from the other door [from the other side],
May the grudging one stay away!
May the generous one come!
The stone [the ore] runs like the tortoise. [Smelting is slow work.]
Run fast, like a girl going for water!
May the stone bring us luck [permit us to acquire] a slave, an ox, a goat, beads, bracelets and anklets.
May the quantity of iron be like a mountain of [edible] caterpillars,
A cloud of locusts!
A big, big head [block of iron]!
Much molten iron!

(Estermann, 1976)

Zusammenfassung

Das Otavi Bergland (Namibia) liegt im nördlichsten Teil des nördlichen Vorland Falten- und Überschiebungsgürtels des Pan-Afrikanischen Damara Orogens. Neoproterozoische Plattformkarbonate (Otavi Gruppe) lagern dem Paläoproterozoischen Grundgebirge des „Grootfontein Inlier“ und siliziklastischen Sedimenten des Kryogeniums (Nosib Gruppe) auf. Die damarische Otavi Gruppe führt verschiedene Typen von sulfidischen und sulfidfreien Buntmetall-Lagerstätten. Ziel der vorliegenden Studie war es, die geodynamische Entwicklung des Otavi Berglandes und die daran gekoppelten hydrothermalen Systeme zu beschreiben sowie ein Modell zur Bildung der Lagerstätten zu erstellen. Ein weiterer Schwerpunkt lag in der Betrachtung möglicher Liefergesteine der Buntmetalle. Die Geländearbeit im Otavi Bergland und strukturgeologische, petrographische und geochemische Studien an Proben der Lagerstätten und der Paleo- und Neoproterozoischen Gesteinseinheiten wurden mit Ergebnissen weiterer Mitarbeiter, bestehend aus Analysen stabiler und radiogener Isotope, kombiniert.

Das Paläoproterozoische Grundgebirge des „Grootfontein Inlier“ gliedert sich in den „Grootfontein Metamorphic Complex“ und den „Grootfontein Mafic Body“. Haupt- und Spurenelement-Zusammensetzungen des Paläoproterozoischen Grundgebirges weisen auf eine Intrusion dioritischer bis granitischer Schmelzen in einem konvergenten plattentektonischen Regime hin. Eine Korrelation mit anderen Grundgebirgsanteilen des südlichen Sao Francisco-Kongo Kratons und spät-Eburnische Rb-Sr Alter (1816 ± 26 Ma) von Hellglimmern aus Pegmatiten-Intrusionen deuten auf eine Bildung des „Grootfontein Metamorphic Complex“ während der Eburnischen Orogenese hin. Geochemische Analysen an Gabbros des „Grootfontein Mafic Body“ zeigen jedoch eine deutlich abweichende Zusammensetzung, die für eine Intrusion in einem kontinentalen Regime spricht. Unterschiedliche Magmenquellen oder eine teilweise Kontamination durch ältere Grundgebirgskörper könnten dabei eine wichtige Rolle gespielt haben.

Während des Zerfalls Rodinias im Neoproterozoikum bildete sich ein Horst- und Graben-System im Paläoproterozoischen Grundgebirge aus, das durch siliziklastische Sedimente der Nabis Formation verfüllt wurde. Die Horst- und Grabenbildung wurde von der Intrusion tholeiitischer Vulkanite der Askevold Formation begleitet, deren Vorkommen bereits aus dem südlichen Otavi Bergland bekannt waren und in dieser Studie auch im zentralen Otavi Bergland nachgewiesen wurden. Nabis und Askevold Formation sind Teil der damarischen Nosib Gruppe, die während der Pan-Afrikanischen Orogenese grünschieferfaziell überprägt wurde (M1). In der Askevold Formation enthaltene Magnetite bildeten sich nach den vulkanogenen Massivsulfid-Lagerstätten (VMS) der Nosib Gruppe. Pb-Pb Datierungen an Magnetiten der Askevold Formation ergeben ein Alter von 587 ± 12 Ma und zeigen eine Bildung der VMS-Vererzungen im Kryogenium an. Die Hauptphase der Pan-Afrikanischen Orogenese erfolgte nach der Ediakarischen Bildung der Magnetite. Hieraus ergibt sich das Höchstalter dieser Orogenese im Otavi Bergland.

Anhand strukturgeologischer und petrographischer Analysen konnte eine dreiphasige Überprägung der Damara Supergruppe und von Anteilen des sie unterlagernden Grundgebirges durch die Pan-Afrikanische Orogenese festgestellt werden: Vermutlich verursachten Kollisionsprozesse im westlich gelegenen Kaoko Gebirgsgürtel die Ost-West gerichtete Verkürzung während des frühen Ediakariums (D1). Die darauf folgende Hauptphase der Pan-Afrikanischen Orogenese (D2) entstand durch die Konvergenz und schließlich Kollision der Sao Francisco-Congo und Kalahari Kratone im späten Ediakarium bis frühen Kambrium und verursacht eine Nord-Süd gerichtete Einengung. Dextrale Seitenverschiebungen und Abschiebungen waren das Ergebnis der späten Pan-Afrikanischen Anhebung der nördlichen Platform (D3) während der späten Kollision zwischen Sao

Francisco-Congo und Kalahari Kraton. Die während des Kryogeniums angelegten Grabenbrüche wurden während der gesamten Pan-Afrikanischen Orogenese und während späterer plattentektonischer Prozesse, vermutlich auch der Öffnung des Südatlantiks in der Kreide, reaktiviert.

Zusammenfassend ergibt sich folgendes Modell für eine Entwicklung der Buntmetall-Lagerstätten im Otavi Bergland: Die Zirkulation mineralgesättigter Lösungen aus tieferen Beckenbereichen und die Mobilisierung bestimmter Buntmetalle durch die Pan-Afrikanische Regionalmetamorphose wurde durch einzelne Phasen der Pan-Afrikanischen Orogenese im Damara Gebirgsgürtel gesteuert. Sie führten zur Bildung von sulfidischen und sulfidfreien Buntmetallvorkommen in den Karbonaten der Otavi Gruppe. Syntektonische Granitintrusionen im zentralen Damara Gebirgsgürtel kontrollierten vermutlich die Zirkulation hydrothermaler Wässer. Als Liefergesteine der Buntmetalle können außer dem „Grootfontein Mafic Body“ auch intermediäre bis mafische Gesteine des „Grootfontein Metamorphic Complex“ gedient haben. Geochemische Analysen an siliziklastischen und vulkanischen Gesteinen der Nosib Gruppe sowie an Sulfiderzvorkommen in der Otavi Gruppe unterstützen die Annahme, dass die Askevold Formation und die daran gebundenen VMS-Vererzungen eine weitere Quelle für Buntmetall-Vererzungen im Otavi Bergland waren.

Zn-Pb Sulphide des Berg Aukas-Typs wurden während D1 in sedimentären und tektonischen Brekzien abgelagert. Zirkulierende hydrothermale Wässer erzeugten eine weitere Brekziierung, die zu einer weiteren Konzentration der Zn-Pb Sulphide führte. Vermutlich wurden die Berg Aukas-Typ Lagerstätten während D2 hydrothermal alteriert und dienten damit als Vorläufer späterer Buntmetall-Vererzungen. Syn-D2 wurden auch die Cu-As-reichen Sulfosalze und Pb-Cu-Zn Sulphide des Tsumeb-Typs in Karströhren und Störungsbrekzien, die an Schnittbereichen verschiedener Störungssysteme entstanden, abgelagert. Während D3 wurden die primären Sulfid-Vererzungen des Tsumeb- und vermutlich auch des Berg Aukas-Typs wiederholt remobilisert. Dies führte zu einer Verdrängung der primären Erzkörper und/oder einer Ausfällung in weitere D2-Strukturen (z.B. Kombat Mine). Erste Rb-Sr Datierungen an Zinksilikaten (Willemit), die vornehmlich Zn-Sulfide des Berg Aukas-Typs ersetzten, ergaben Alter von 562 bis 436 Ma und weisen damit auf eine gleichzeitige Bildung mit den Tsumeb-Typ Lagerstätten und deren Remobilisaten hin. Dies wird durch die Ausfällung der Zinksilikate in Pan-Afrikanischen Störungszonen bestätigt. Die Ausfällung von Pb-Zn-Cu Vanadaten fand im späten Oligozän bis Pleistozän statt ((U-Th)/He an Descloizit) in post-damarischen Karstfüllungen, Brekzien und Nord bis Nordost streichenden Störungen statt. Die Eigenschaften der Fluideinschlüsse und O- und C-Isotopensignaturen von Karbonatzementen, die an die Vanadate gebunden sind, sprechen für eine tief greifende Zirkulation mäßig erhitzter meteorischer Wässer in einem kontinentalen Klima. Laut den Untersuchungen der Pb-Isotopen und der Haupt und Spurenelemente, spiegelt die Zusammensetzung der Vanadate die Zusammensetzung der primären sulfidischen Buntmetall-Lagerstätten aus ihrer näheren Umgebung wieder.

Summary

The Otavi Mountainland (OML) in Namibia is located in the northernmost part of the northern foreland fold and thrust belt of the Pan-African Damara Orogen. Neoproterozoic platform carbonates (Otavi Group) rest unconformably on the Paleoproterozoic basement of the Grootfontein Inlier and Cryogenian rift sediments (Nosib Group). The Damaran Otavi Group is host for various types of sulphide and nonsulphide mineralisation. The aim of this study was to establish a model of the structural and fluid system evolution of the OML, in order to constrain the sources of the ore forming fluids and to understand the timing and the formation of several types of base metal ore deposits in this target area. Field work and structural analysis, petrographic and geochemical studies of samples from mining sites and the Paleoproterozoic and Neoproterozoic successions were accompanied by analysis of stable and radiogenic isotopes by co-workers.

The Paleoproterozoic basement comprises the Grootfontein Metamorphic Complex and the Grootfontein Mafic Body. The obtained major and trace element compositions of the Grootfontein Metamorphic Complex suggest a magmatic evolution from dioritic towards granitic compositions in a convergent tectonic setting. A correlation with other basement units of the southern margin of the Sao Francisco-Congo Craton and a late-Eburnean Rb-Sr age of micas from pegmatitic intrusions in the Grootfontein Metamorphic Complex (1.816 ± 26 Ma) indicate a formation of the Paleoproterozoic basement that was related to the Eburnean orogeny. The acquired distinctly different chemical compositions of gabbros of the Grootfontein Mafic Body suggest an emplacement in a continental regime and could be related to distinct magma sources or to contamination from older basement rocks. Beside the Grootfontein Mafic Body, intermediate to mafic rocks of the Grootfontein Metamorphic Complex could have been source rocks for base metal mineralisation in the OML.

Due to the Neoproterozoic break-up of Rodinia, a horst-graben-system evolved in the Paleoproterozoic basement, which was filled by siliciclastic rocks (Nabis Formation). Related rift volcanics of the Askevold Formation, which were already known from the southern OML, have been now observed in the central OML as well. Geochemical studies on these rift volcanics yield a tholeiitic composition. Both the Nosib and the Askevold formations are part of the Damaran Nosib Group, which was deformed during the Pan-African orogeny under greenschist facies conditions (M1). A Pb-Pb age of 587 ± 12 Ma was obtained for pre Pan-African magnetites from the Askevold Formation, whose segregations postdate VMS-type ores, contained in the Nosib Group. This age points to a Cryogenian deposition of the VMS-type ores and results in a maximum age of the Pan-African orogeny in the OML. Comparative geochemical studies on siliciclastic and volcanic rocks from the Nosib Group as well as on sulphide ores hosted by the Otavi Group indicate the Askevold Formation and related VMS-type deposits as favourable sources for base metals deposited in the OML.

Structural and petrographic analyses suggest a three-staged Pan-African overprint in the OML: 1. Early Ediacaran E-W shortening (D1) that was presumably caused by collisional processes in the Kaoko Belt. 2. The main deformational event and the related N-S shortening in late Ediacaran to early Cambrian times (D2), which were due to convergence and finally collision of the Sao Francisco-Congo and Kalahari Cratons. 3. Dextral strike slip and extensional normal faulting (D3), which were triggered by the late Pan-African uplift of the Northern Platform during the waning stages of the convergence between the Sao Francisco-Congo and Kalahari Cratons. The Cryogenian rift-related normal faults were reactivated throughout the Pan-African orogeny and later deformational events, presumably such as the opening of the southern Atlantic in Cretaceous times.

The formation of sulphide and nonsulphide mineralisation, hosted by platform carbonates of the Damaran Otavi Group, resulted from circulation of basinal and/or metamorphic brines and

were correlated with the successive deformational events of the Pan-African orogeny. During D1, Zn-Pb sulphides of the Berg Aukas-type were deposited in sedimentary and tectonic breccias. Percolating hydrothermal fluids caused further brecciation, leading to further refining of the Zn-Pb sulphide ores. Paragenetic and geochemical studies suggest that Berg Aukas-type deposits could have been subject to hydrothermal remobilisation during D2 and therefore acted as precursor for later phases of base metal mineralisation. In a second stage (syn-D2), hydrothermal fluids were triggered by the regional metamorphism (M1) and by the emplacement of syntectonic granites in the central Damara Belt. Cu-As-rich sulphosalts and Pb-Cu-Zn sulphides of the Tsumeb-type were emplaced in karst pipes and fault breccias, which developed at cross junctions of different tectonic trends. During D3, repeated remobilisation of primary Tsumeb-type and eventually also Berg Aukas-type deposits resulted in direct replacement of the primary ores and/or further distribution of sulphide ore into D2-structures (e.g. Kombat). Synchronous to and possibly also after the formation of Tsumeb-type deposits and their subsequent remobilisation, Zn-silicate ore (willemite) locally replaced primary Zn sulphides of the Berg Aukas-type, as indicated by preliminary Rb-Sr ages in the range from 562 to 436 Ma and by their localisation in Pan-African shear zones. As suggested by (U-Th)/He ages on the Zn-Pb vanadate descloizite ranging from Late Oligocene to Pleistocene, the precipitation of the vanadates commenced significantly after the Pan-African orogeny. Fluid inclusions characteristics and O and C isotope signatures of carbonate cements, related to the formation of the vanadates, indicate that a circulation of slightly heated meteoric fluids took place during a phase of deep continental weathering in the late Kenozoic. This circulation fostered the formation of supergene Pb-Zn-Cu vanadates in post-Damaran karst fillings, solution collapse and tectonic breccias and North- to NE-striking faults. According to our Pb-isotope and major and trace element studies, the chemical composition of the vanadate ores reflects the original composition of the primary sulphide deposits in the same area.

Part 1: General introduction and main results

This thesis is based on a project about the structural and fluid system evolution of the Otavi Mountainland (OML) in northern Namibia. The thesis comprises a general introduction including the main results (Part 1) and five chapters (Part 2 - 6), corresponding to several independent studies which were previously published or submitted to peer reviewed journals:

- Part 2:
  Title: Geodynamic evolution of the Otavi Mountainland (Namibia): Implications for Pan-African Damara orogeny and metallogeny
  Authors: Carsten Laukamp, Thilo Bechstädt, Maria Boni
  Status: Submitted to Journal of African Earth Sciences

- Part 3:
  Title: Geochemistry and geochronology of Paleoproterozoic basement rocks of the Grootfontein Inlier (Namibia)
  Authors: Carsten Laukamp, Jens Schneider, Maria Boni, Thilo Bechstädt
  Status: Submitted to Precambrian Research

- Part 4:
  Title: Geology, geochemistry and metallogenetic significance of Cryogenian rift volcanics in the Otavi Mountainland (Namibia)
  Authors: Carsten Laukamp, Jens Schneider, Maria Boni, Thilo Bechstädt
  Status: Submitted to South African Journal of Geology

- Part 5:
  Title: Willemite (Zn_2SiO_4) as a possible Rb-Sr geochronometer for dating nonsulphide Zn-Pb mineralisation: examples from the Otavi Mountainland (Namibia)
  Authors: Jens Schneider, Maria Boni, Carsten Laukamp, Thilo Bechstädt, Volker Petzel
  Status: Accepted by Ore Geology Reviews

- Part 6:
  Title: Vanadate ores in the Otavi Mountainland (Namibia): geological setting, mineralogy, geochemistry, formation timing and relation with the "African Erosion Cycle"
  Authors: Maria Boni, Rosario Terracciano, Noreen Evans, Carsten Laukamp, Jens Schneider, Thilo Bechstädt
  Status: Submitted to Economic Geology

According to the published or submitted studies, each part consists of an abstract, introduction, results, discussion, conclusions and acknowledgements.

1.1 Objectives

The aim of this project was to develop a genetic model for the mineralisation of sulphide and nonsulphide ores, hosted by the sediments of the Damara Supergroup in northern Namibia. As most of the base metal deposits in the OML show a clear structural control (Innes and Chaplin, 1986; Lombaard et al., 1986) and because of the lack of reliable ages of base metal mineralisation as well as of the country rocks (e.g., Haack, 1993; Frimmel et al., 2004), an attempt was made to re-evaluate the deposit types and to assign the observed mineralisation phases to distinct deformational stages belonging to the geodynamic evolution of the OML. Therefore a detailed structural study of certain key areas in the OML was undertaken with the aim of obtaining a sound geodynamic model (Part 2). The main focus was put on the Pan-African (Damaran) orogeny, because this event was suggested as the driving force for the hydrothermal activity in the OML (Hughes, 1979; Pirajno and Joubert, 1993; Frimmel et al., 1996a). However, particular care was also taken in determining the geological and morphoclimatic characteristics, which are at the base of the Gondwanan (willemites) and post-Gondwanan (vanadates) nonsulphide deposits in the same area. Cement stratigraphic and petrographic studies enabled a comparison of tectonic related cements with the hydrothermal gangue of the base metal ores in the OML. In order to identify the possible sources of the metals, present in sulphide and nonsulphide ores in the OML, geochemical and isotopic analyses were undertaken not only on metallic ore samples, but also on possible source rocks such as the Paleoproterozoic basement and the early Damaran Nosib Group as well as on sulphide and nonsulphide samples (Part 3, 4).

The structural, cement stratigraphic and geochemical studies were then complimented with preliminary age datings of nonsulphide mineralisation (Part 5, 6).

1.2 Introduction

The Otavi Mountainland (OML) is located in northern Namibia and consists of a Paleoproterozoic basement, which is overlain by the sedimentary successions of the Neoproterozoic Damara Supergroup. The Proterozoic strata are intruded by presumably Karoo-aged dykes and partly covered by clastic sediments of the Cambrian to Jurassic Karoo Supergroup, the Cretaceous Etendeka Group and the Cenozoic Kalahari Sequence.

The platform carbonates of the Damara Supergroup are hosts for polymetallic sulphide and nonsulphide deposits, amongst which are world famous deposits such as the Tsumeb and Berg Aukas mines. Mining of the base metal deposits was presumably started by the Bergdama tribe, which introduced copper smelting into Namibia (Cairncross, 1997). At the end of the 19th century the Otavi Mountainland was occupied by Europeans. The first mining concession was granted to the South West Africa Company (SWACO) in 1890 (Misiewicz, 1988). Since then mining of base metal deposits in the OML was conducted by several companies. The first comprehensive overview on the geology of the OML was presented by Schneiderhöhn (1929). Further important works on the regional geology of the OML were produced by Söhnge (1957), Hedberg (1979) and Miller (1997). Recent studies concerning the ore deposits of the OML were published by Lombaard et al. (1986), Innes and Chaplin (1986), Deane (1995), Frimmel et al. (1996a), Chetty and Frimmel (2000), Melcher (2003) and Melcher et al. (2003, 2006).

1.3 Geological Setting

1.3.1 The Damara Orogen and the Damara Belt

The Otavi Mountainland is part of the NE-trending Damara Belt in northern and central Namibia. The Damara Belt (Fig. 1.1) is the intracontinental branch of the Damara Orogen and was generated during the Pan-African collision of the Sao Francisco-Congo and Kalahari Cratons (Fig. 1.2). Three major zones, divided by NE-trending lineaments, can be

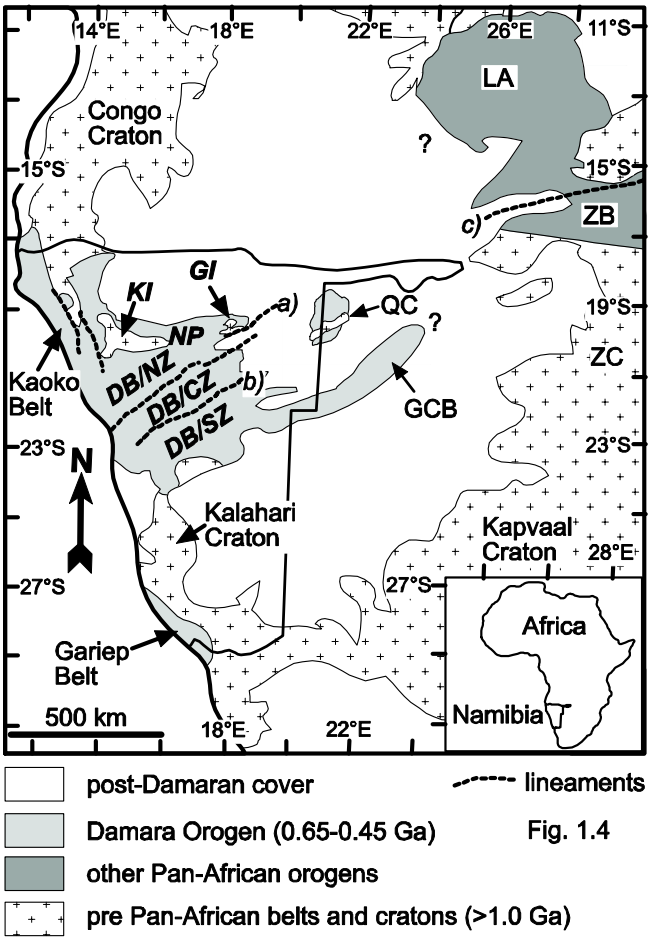

Fig. 1.1: Proterozoic mobile belts and cratons of South western Africa with selected lineaments and metamorphic zones of the Damara Belt; Lineaments: a) - Grootfontein lineament, b) - Okahandija Lineament; c) - Mwembeshi shear zone; DB – Damara Belt, CZ – Central Zone, NZ – Northern Zone, SZ – Southern Zone, GCB – Ghanzi-Chobe Belt, GI – Grootfontein Inlier, KI - Kamanjab Inlier, LA – Lufilian Arc, QC – Quangwadum Complex, ZB – Zambezi Belt, ZC - Zimbabwe Craton (Map modified after GSN, 1999; Rainaud et al., 2005; Singletary et al., 2003).

distinguished according to their stratigraphic, tectonic and metamorphic characteristics in the Damara Belt: the Northern, the Central and the Southern Zone (Miller, 1983a) (Fig. 1.1). The OML is located at the transition of the Northern Zone to the Northern Platform (NP, Fig. 1.1), which consists of Cryogenian and Ediacaran platform carbonates. In order to avoid confusion about depositional and tectonic processes in this thesis, the term "Pan-African orogeny" is used instead of "Damaran orogeny" in the presented thesis, whereas the term "Damaran" is restricted to the deposition of the Damara Supergroup and their subunits. Exceptions are made for specific terms of the nomenclature for southern Africa, such as "Damara

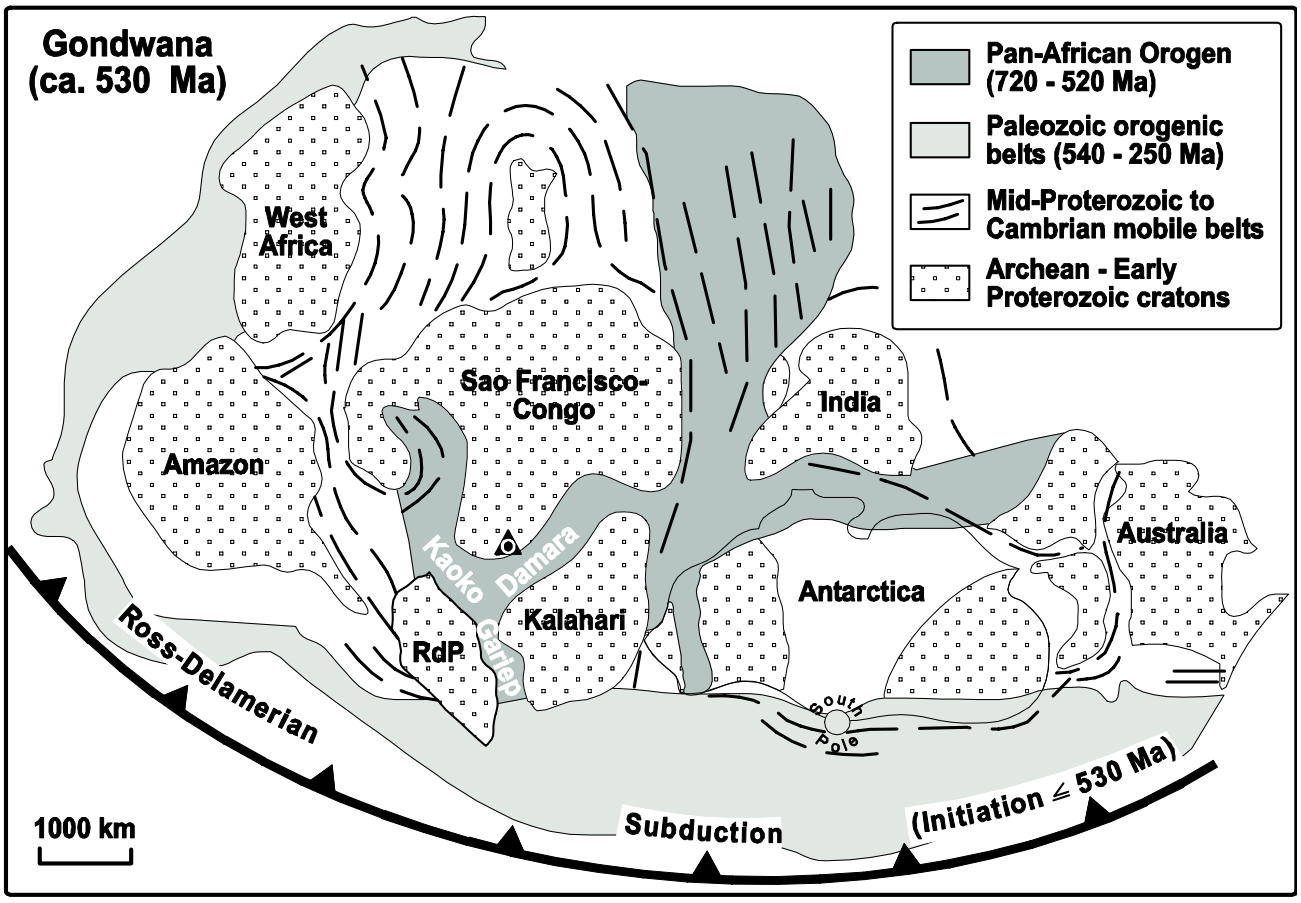

Fig. 1.2: Map of the Gondwana supercontinent at the end of Neoproterozoic and beginning of Cambrian time (modified from Foster and Gray, 2000; Grey et al., 2006), showing the extent of the Pan-African orogeny and the continental margin Ross-Delamerian orogeny (modified from Meert, 2003; Grey et al., 2006). White letters represent the belts of the Damara Orogen. The triangle at the southern margin of the Sao Francisco-Congo craton indicates the position of the Otavi Mountainland.

Orogen" as the collective term to describe the Damara, Kaoko and Gariep Belts and "Damara Belt" defining the intracontinental branch of the Damara Orogen.

The tectonic evolution of the north-eastern Damara Orogen can be divided in four major stages: 1) Formation and generation of the Paleoproterozoic basement during the Eburnean orogeny (Tegtmeyer and Kröner, 1985), 2) pre Pan-African rifting, 3) Pan-African orogeny with the formation of the Damara Belt and 4) post Pan-African uplift and extension. The tectonic evolution of the Paleoproterozoic basement (Grootfontein Inlier) is summarised in Part 3 (Fig. 1.3). The second tectonic event was caused by Cryogenian rifting, which was due to the break-up of Rodinia and the related opening of an inland branch of the Adamastor Ocean (Hartnady et al., 1985; Frimmel et al., 1996). The Pan-African orogeny caused three deformational events in the OML (Fig. 1.3): D1 with early Ediacaran E-W shortening, D2 with late Ediacaran to early Cambrian N-S shortening and D3 with an early Paleozoic uplift (Part 2). D1 could have been due to the accretion of a Coastal Terrane to the Kaoko Belt in the west, immediately before the suturing of the Rio de la Plata and Sao Francisco-Congo Cratons (Goscombe et al., 2005; Part 2).

1.3.2 Geology of the Otavi Mountainland

The main deformational event of the Pan-African orogeny in the OML (D2) was related to the convergence and collision of the Kalahari and Sao Francisco-Congo Cratons. The late Pan-African uplift of the Northern Platform (D3), which led to a fragmentation of the OML by extensional normal faults, was due to the waning stages of the convergence between the Kalahari and Sao Francisco-Congo Cratons (Grey et al., 2006). D3 passed over into the post Pan-African uplift and extension, characterised by normal faulting and reactivation of NE-trending structures (Söhnge, 1957).

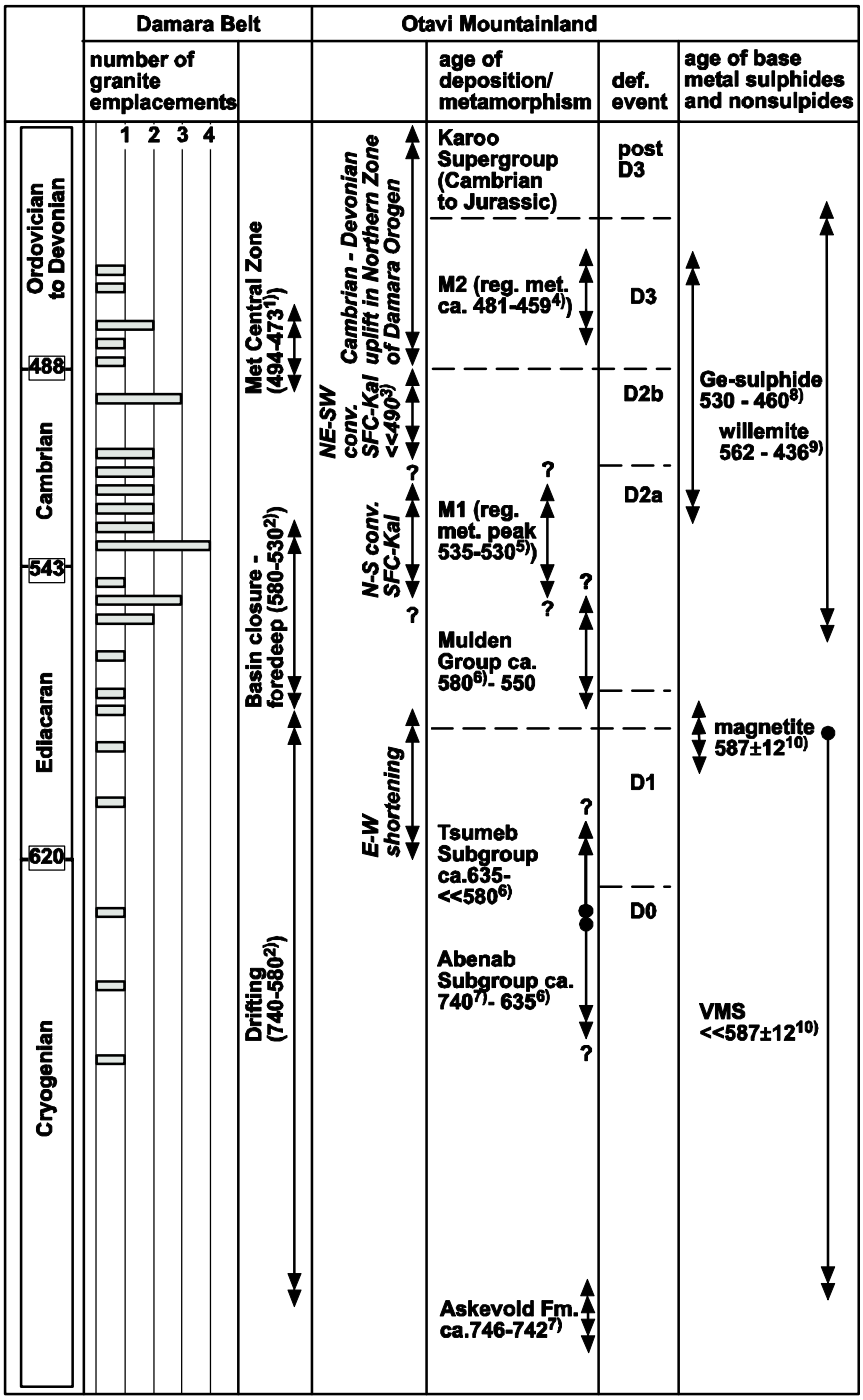

Fig. 1.3: Structural evolution of the OML modified after Part 2 (mean ages in Ma). Kal – Kalahari Craton, SFC – Sao Francisco-Congo Craton. Lines with double arrows give a maximum timing if not extended by a question mark. Black points at the end of a line represent a dated age. Histogram of emplacement ages (Rb-Sr whole rock, U-Pb zircon) of syntectonic granites according to Haack et al. (1988), Miller (1983a) and references therein, Passchier et al. (in press), Seth et al. (2002).
[1)]Goscombe et al. (2005); [2)]Frimmel (2004); [3)]Singletary et al. (2003); [4)]Haack et al. (1980), Haack (1983); [5)]Clauer and Kröner (1979), Goscombe et al. (2004); [6)]Hoffmann et al. (2004); [7)]Burger and Coertze (1973), Hoffman et al. (1996); [8)]Melcher et al. (2006); [9)]Schneider et al. (in press); [10)]Laukamp et al. (Part 3).

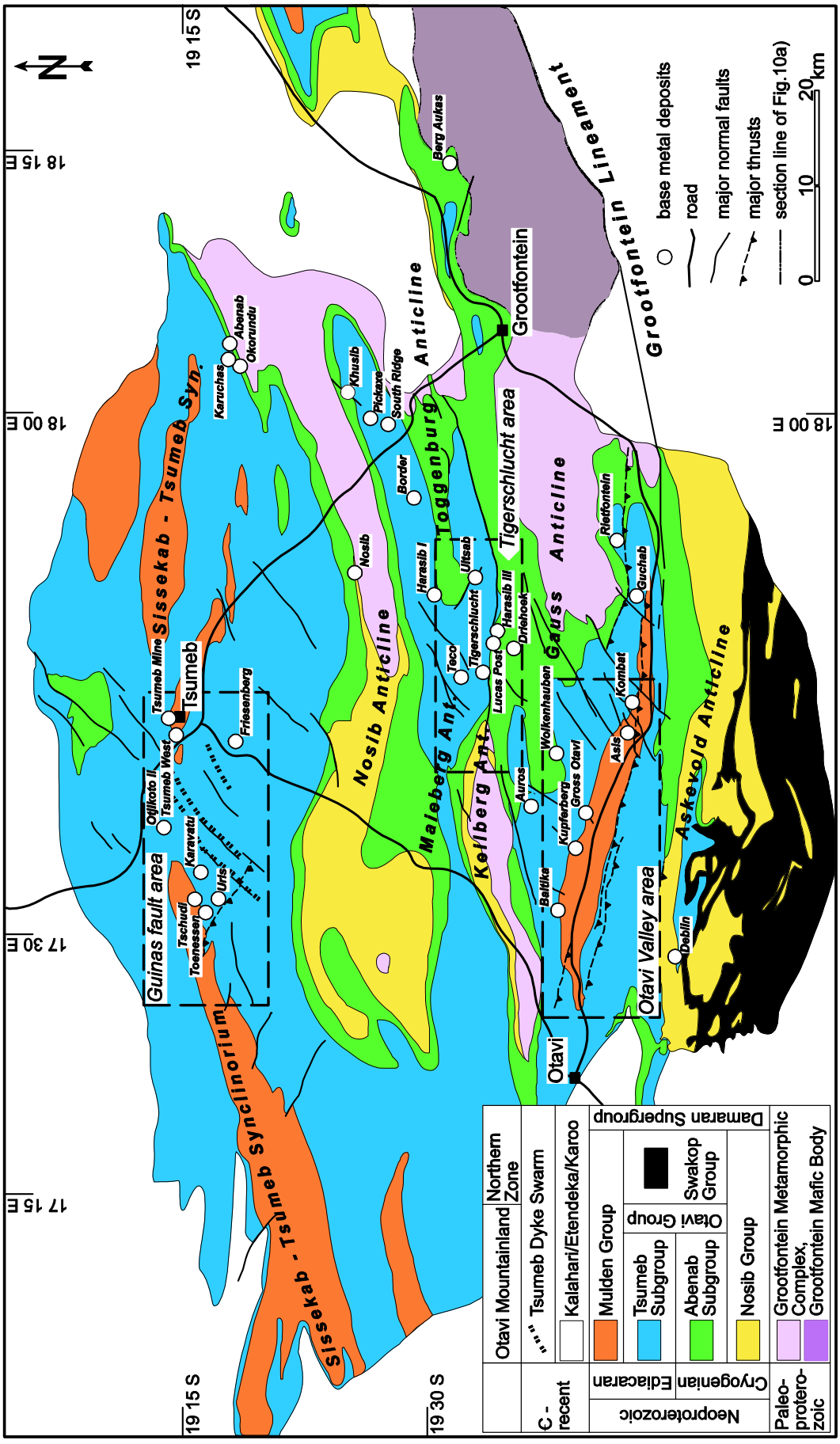

Fig. 1.4: Geological map of the Otavi Mountainland with key areas and localities of discussed sulphide and nonsulphide occurrences.

D2 was accompanied by a greenschist facies metamorphism (M1, Fig. 1.3) of the Otavi and Mulden Groups with peak conditions of around 530 - 535 Ma (Clauer and Kröner, 1979; Goscombe et al., 2004). The metapelites from the eastern Northern Zone, 50 km SW of Otavi (Fig. 1.4) were overprinted by amphibolite facies metamorphism during D2 (estimated peak cinsitions: 635°C at 8.7 kbar; Goscombe et al., 2004). This supported the southward increasing grade of syn-D2 metamorphism towards the hinterland of the Otavi Mountain fold and thrust belt (Coward, 1981). Clauer and Kröner (1979) described a second, low-grade metamorphic event (M2, Table 2) around 455 Ma (K-Ar, 250 - 300°C at 2 kbar) in the Mulden Group from the Etosha Pan northwest of Tsumeb, whereas Haack (1983) published K-Ar cooling ages of ca. 300°C at around 481 ± 25 Ma. Similar ages of this metamorphic event, ranging from 469 ± 12 to 445 ± 11, were determined by Ahrendt et al. (1983, K-Ar, fine mineral fractions < 2μm) on phyllites of the Kombat Fm close to the Kombat Mine (Fig. 1.4).

During the Pan-African orogeny, massive granite intrusions emplaced in the Northern, Central and Southern Zone of the Damara Belt (Miller, 1983a). Granite emplacement culminated during the late Ediacaran and early Cambrian (syn-D2a) and from late Cambrian to middle Ordovician (late D2b to syn-D3) (Fig. 1.3).

The Otavi Mountainland (OML) consists of three major rock units: 1) Igneous and metamorphic rocks of the Paleoproterozoic basement, 2) sedimentary successions of the Neoproterozoic Damara Supergroup and 3) Meso- to Cenozoic sediments and igneous dykes.

1.3.3 Paleoproterozoic basement

The presumably Paleoproterozoic basement of the OML, also called the Grootfontein Inlier, is part of the southern Congo Craton (Rainaud et al, 2005) and can be subdivided in the Grootfontein Metamorphic Complex (GMC) and the Grootfontein Mafic Body (GMB) (Geological Survey of Namibia, 1999). The GMC consists mainly of alkaline/calc-alkaline granites and granodiorites (Clifford et al., 1969), whereas the GMB is made of anorthosites, gabbros, micaceous biotite gneisses, granites and amphibolites (Martin, 1965; Söhnge, 1964; Günzel, pers. comm., 2005). The age of the Grootfontein Inlier is only poorly constrained by a Pb-Pb whole rock age of 1.946 +299/-333 Ma for gabbros of the GMB (Armstrong, 1988).

1.3.4 Damara Supergroup

The Neoproterozoic successions of the OML are part of the Damara Supergroup (Fig 1.4, Fig. 1.5). Up to 4500m thick platform carbonates of the Otavi Group rest unconformably on the Paleoproterozoic basement of the Grootfontein Inlier (GI, Fig. 1.1) and Cryogenian rift sediments of the Nosib Group. The Otavi Group is overlain by the molasse-like Mulden Group.

The Nosib Group consists mainly of siliciclastics of the Nabis Fm with intercalated metavolcanics of the Askevold Fm (Fig. 1.5). Comparable volcanic successions of the Naauwpoort Fm (Fig. 1.6) in central Namibia give a depositional age of 780-740 Ma for the Nosib Group (Burger and Coertze, 1973; Hoffmann et al., 1996). The Chuos Fm (also called Varianto Fm) consists of diamictites, pyroclastics and ironstones, which interfinger with the Nabis Fm in the central OML (own observations) and is therefore seen as part of the Nosib Group. In the southern OML the genetic relationship is veiled by the Pan-African orogeny (Part 3). The Nosib Group was deposited in a pre-Pan-African, NE trending horst-graben-system that developed due to the Cryogenian break-up of Rodinia (Hartnady et al., 1985; Frimmel et al., 1996b).

The Otavi Group is divided by the diamictites of the Ghaub Fm, aged at about 635 Ma (Hoffmann et al., 2004) into a lower Abenab Subgroup and an upper Tsumeb Subgroup (Fig. 1.5). The Abenab Subgroup comprises from bottom to top the Berg Aukas, Gauss and Auros Fms. Cap carbonates of the Berg Aukas Fm unconformably overly the diamictites of the Chuos Fm (Hoffmann et al., 2004). Massive and bedded dolomites of the Gauss Fm correspond to shallow water carbonates, which were deposited at the margin of the Otavi carbonate platform (Frimmel et al., 1996a). The Auros Fm consists of stromatolites and oolites, alternating with bedded limestones and shales. The Tsumeb Subgroup is subdivided in the Ghaub, Maieberg, Elandshoek and Hüttenberg Fms, which can be further subdivided in 8 lithozones (Fig. 1.5). A second cap carbonate sequence in the OML, represented by limestones and dolomites of the lower Maieberg Fm (T2), overlies the Ghaub diamictites (T1). In the central OML, the dolomites of the upper Maieberg Fm (T3) and the lower Elandshoek Fm (T4)

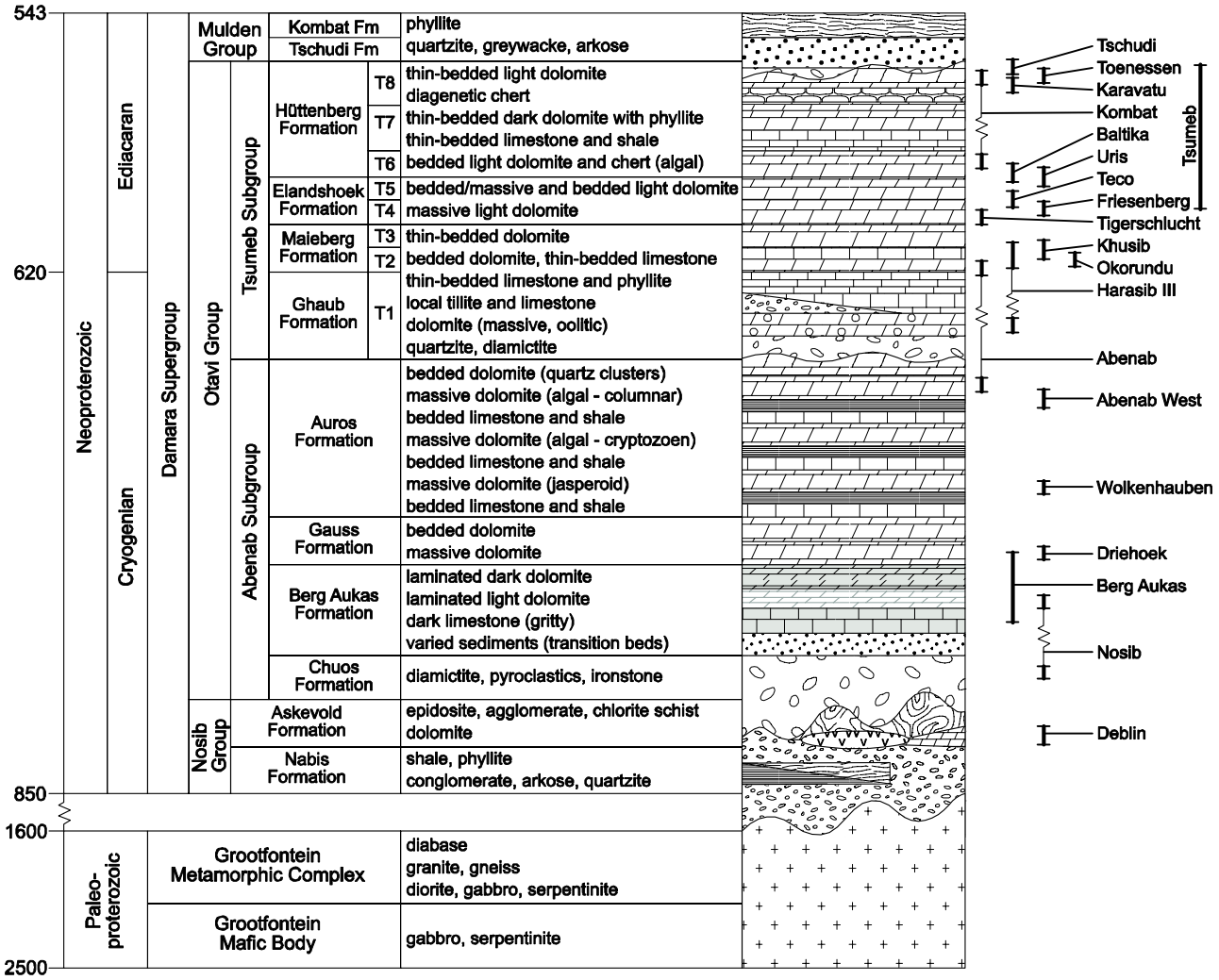

Fig. 1.5: Stratigraphy of the Otavi Mountainland (ages of eras and periods in Ma) and stratigraphic location of selected ore deposits (stratigraphic hiatus at deposit site marked by zigzag line between locations).

are characterised by synsedimentary brecciation (Günzel, pers. comm. 2004). Bedded dolomites of the upper Elandshoek and lower Hüttenberg Fms are followed by lagoonal deposits of the middle Hüttenberg Fm (T7) (Söhnge, 1957). Stromatolitic and oolitic dolomites with intercalated cherts occur in the upper Hüttenberg Fm (T8). The Otavi Group was deposited as a carbonate platform on the southern margin of the stable crust of the Congo Craton (Prave, 1996). However, large-scale growth faults and synsedimentary breccias in the Tsumeb Subgroup indicate reactivation of pre-Damaran basement structures and the evolution of small-scale basins in the area of the Grootfontein basement high (Dürr and Dingeldey, 1997; Part 2, 3).

The Mulden Group is subdivided in the Tschudi and Kombat Fms (Fig. 1.5). The Tschudi Fm occurs predominantly in NE- to E-trending synclines in the Northern OML, such as the Tschudi syncline (Fig. 1.4), and consists of conglomerates, sandstones, quartzites and arkoses. The angular unconformity between the Otavi Group and the Tschudi Fm is represented by the filling of karst depressions by the Tschudi conglomerates (Misiewicz, 1988) and Pan-African thrusting of the carbonates over the siliciclastic rocks (Laukamp et al., 2006). Also the sedimentary infill of karst pipes in the OML (e.g. Tsumeb pipe, Kombat Mine) is correlated to the Mulden Group (Lombaard et al., 1986). The Kombat Fm is confined to the Otavi Valley and comprises shales and phyllites, which were characterised as low grade metamorphic equivalents of the Tschudi Fm (Söhnge, 1957). In contrast to this, Deane (1995) suggested an onlap of the Kombat shales over the carbonates of the Tsumeb Subgroup, related to a drowning of parts of an Otavi Valley subbasin during

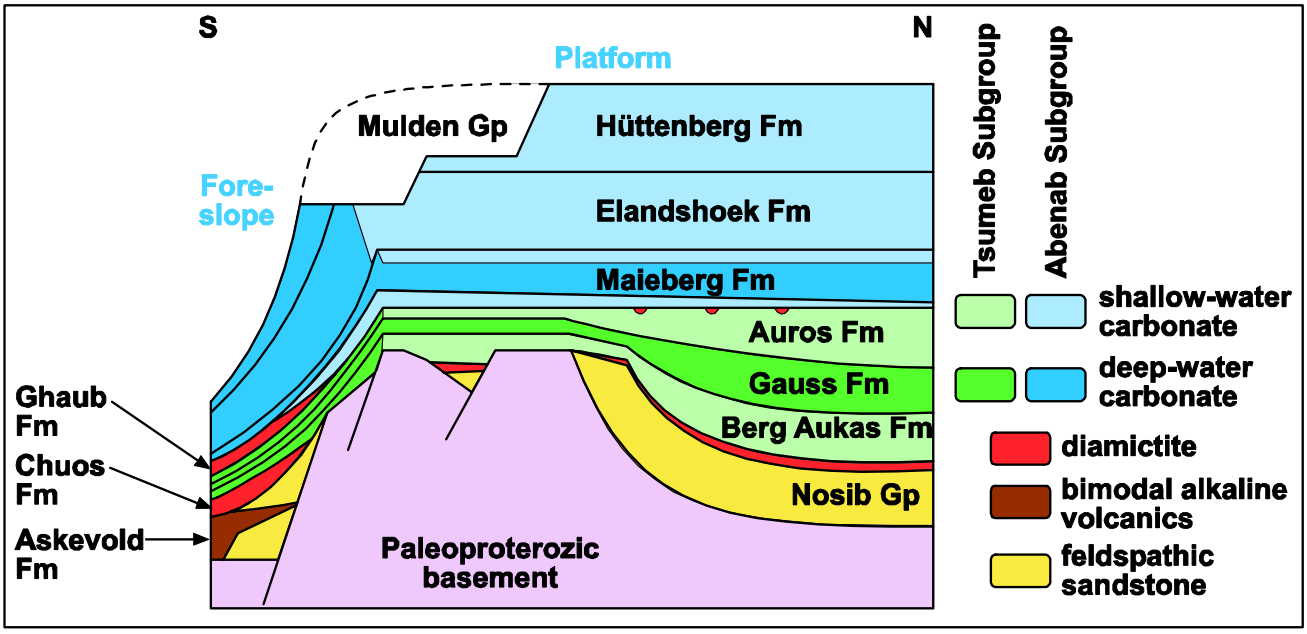

Fig. 1.6: Stratigraphic architecture and generalised sedimentary facies projected onto a north-south cross section of the Northern Platform and its southern foreslope (modified from Hoffman, 2004) (section not to scale).

the final stage of deposition of the Otavi Group. The presented thesis considers the Kombat Fm as part of the Mulden Group, as suggested by the preliminary geological map of the Geological Survey of Namibia (1999).

1.3.5 Post-Damaran successions

To the north, east and south the OML is covered by sediments of Paleozoic to Mesozoic, Tertiary and Quaternary age, belonging to the Karoo and Kalahari Sequences (Fig. 6.3). Additionally, the mainly siliciclastic successions of the Kalahari Sequence occur in deeply eroded, E-trending Pan-African Anticlines (King, 1951; DWA, 2002). In the northern OML, single calcalkaline lamprophyres (e.g. kersantites at the Tsumeb Pipe) as well as other kinds of dyke swarms occur, both types being presumably of Cretaceous age (Söhnge, 1957). Basalts of the Etendeka Group, related to the break-up of Gondwana and the formation of the South Atlantic Ocean in the Early Cretaceous, could have extended to the southern OML (Marsh et al., 2003). Tertiary and Quaternary deposits were accumulated in post-Damaran karst structures (Pickford, 1993, 2000) and as eolian sands (Kalahari sands) and calcrete cover.

1.4 Methods

The results of this study are based on the work carried out during three field seasons (2003 to 2005) in the Otavi Mountainland. The work was mostly concentrated on three "key areas", namely the Guinas Fault area in the north-western, the Tigerschlucht area in the central and the Otavi Valley area in the southern OML. Additional field studies were carried out around selected ore deposits/occurrences. The mentioned areas, other selected outcrops of the Paleoproterozoic basement and the Nosib Group, as well as drill cores from Abenab, the Guinas Fault area, Khusib Springs, Kombat and Tsumeb, provided by Ongopolo Mining and Processing Limited (OMPL), were sampled for further analytical studies. In the following chapters a short overview on the used methods is listed. Detailed descriptions about the methods are given in the respective parts.

1.4.1 Sedimentology, petrography and cement stratigraphy

Samples from the Paleoproterozoic basement, the Damara Supergroup and contained sulphide and nonsulphide occurrences were analysed for their sedimentological, petrographic and cement stratigraphic characteristics, using optical microscopy techniques.

1.4.2 Structural Geology

A detailed structural study of the key areas, selected outcrops and mining sites was conducted during the field seasons from 2003 to 2005. Results of these studies are presented in geological maps of the key areas and stereographic projections in Part 2. Orientated samples were taken for microstructural analysis on thin sections (e.g. determination of deformation phases and metamorphic events; sense of displacement; strain analysis). - Part 2 - 6.

1.4.3 Cathodoluminescence

Polished thin sections of country rocks, ores and gangue mineralisation were examined by conventional and cold cathodoluminescence (CL) petrography utilising a CITL 8200 Mk3 Cold Cathodoluminescence instrument at the Geological-Palaeontological Institute, University of Heidelberg, operating at 23-25 kV voltage and 500-550 µA beam current. Based on variations of elemental species in the crystal lattice and the related varying luminescent characteristics of the distinct materials, different generations of carbonate cements and zonings of cements are visible with the cathodoluminescence technique. - Part 5 and 6.

1.4.4 SEM/EDS

Scanning electron microscope (SEM) observations and semi-quantitative major element analyses were undertaken on polished and carbon coated thin sections of country rocks, ores and gangue mineralisation using a LEO 440 with a Link ISIS EDS at the Mineralogical Institute, University of Heidelberg. In the SEM technique an electron beam is emitted to interact with the surface of a sample, leading to the subsequent emission of secondary electrons. The backscattered electrons are used for the visualisation of the chemical composition. Brighter areas in the backscatter image represent a higher average atomic number. In the EDS technique, the energy spectrum of the emitted characteristic X-ray radiation is determined by a semiconductor detector. The quantitative chemical composition of the analysed material can be estimated by comparison of intensities of characteristic X-rays from standards with intensities from the sample material. - Part 3, 4 and 6.

1.4.5 Fluid inclusion analysis

Microthermometric analytical measurements on fluid inclusions of carbonate and silicate cements were carried out in cooperation with other authors at the Geological-Palaeontological Institute, University of Heidelberg, using a Linkam MDS 600 heating/freezing stage and at the Dipartimento di Scienze della Terra, Università di Napoli, Italy, using a Linkam THMSG 600 heating/freezing stage. Salinities of fluid inclusions can be calculated from the final ice melting temperature (Bodnar, 1993). The formation temperature can be determined from liquid/vapour ratio, homogenisation temperature and hydrostatic pressure (Bakker, 2003). - Part 6.

1.4.6 Major and trace element geochemistry

Sample preparation of whole rocks and ore minerals was carried out at the Geological-Palaeontological Institute, University of Heidelberg, using a jaw crusher and a tungsten-carbid sieve mill (Scheibenschwingmühle). Major and trace elements were measured by ACME laboratories in Vancouver, Canada. From each pulverised sample, 2 g were digested with Aqua Regia (HCl - HNO3) at 95°C. The measurements were performed on a Perkin Elmer Elan 6000 ICP-MS in the 4A+B Group (24 elements), 1T-MS Group (16 elements) and 1-DX Group (36 elements). For interpretation, the obtained data were compared by factor analyses. Variation diagrams were constructed for comparison with published experimentally determined rock compositions of known formation. - Part 3, 4 and 6.

1.4.7 Stable and radiogenic isotopes

In cooperation with other authors of the respective papers, the following radiogenic isotope systems were used to constrain ages of mineral samples:

- Pb-Pb of magnetite - Part 4
- Rb-Sr of mica and willemite - Part 3, 5
- (U/Th)-He of Pb-Zn-Cu vanadates - Part 6

The following stable and radiogenic isotope ratios were measured for comparative analyses in cooperation with other authors of Part 6:

- $^{18}O/^{16}O$ and $^{13}C/^{12}C$ of carbonate powders
- $^{87}Sr/^{86}Sr$ of gangue carbonate minerals
- $^{206}Pb/^{204}Pb$, $^{207}Pb/^{204}Pb$, $^{208}Pb/^{204}Pb$ of descloizite, galena and dolomite

	Berg Aukas-type	Tsumeb-type
Host-rock	Abenab Subgroup and lower Tsumeb Subgroup	Elandshoek and Hüttenberg Formations (dolomites), T4 through T8 zones
Shape of orebody	Stratiform lenses, discordant breccias	Discordant pipe, filled with breccia and sandstone; structural control
Ore mineralogy	Sphalerite, galena (pyrite, chalcopyrite, tennantite)	Tennantite, galena, sphalerite, pyrite, bornite, chalcopyrite, germanite
Ore geochemistry	Zn>Pb; low Cu, Ag, As, Ge, Ga, Cd	Pb>Cu=Zn, Considerable As, Ag, Cd, Ge, Ga, W
Fluid inclusions	ca. 23 wt.% NaCl eq., 137 to 255°C	22.3 wt.% NaCl eq., >212°C (dolomite III)
Fluid source	Basinal brines	Orogenic fluids
Age	635 to 750 Ma ?	460 to 530 Ma?

Tab. 1.1: Major types of base metal mineralisation in the OML.

1.5 Base metal mineralisation in the Otavi Mountainland

Over 600 occurrences of base metal mineralisation are known from the 10.000 km² large OML (Cairncross, 1997). The two economically most important types comprise the Tsumeb- and the Berg Aukas-type mineralisation. Both are hosted by carbonates of the Otavi Group, with the Tsumeb-type occurring in the upper Tsumeb Subgroup and the Berg Aukas-type predominantly in the upper Abenab and lower Tsumeb Subgroup. A recent summary of the two main types is given in Table 1 (Melcher et al., 2006).

The absolute age of primary base metal sulphides in the OML is not well constrained. Based on preliminary Re-Os analyses of Ge-rich sulphide ores, Melcher et al. (2003) reported an age of 530 Ma for the main ore phase of the Tsumeb Pipe deposit. A minimum age for Berg Aukas-type mineralisation could be deduced by the dating of nonsulphide minerals which replace sphalerite, from the Berg Aukas and Abenab mines. Schneider et al. (in press) obtained Rb-Sr ages of ca. 493 to 560 Ma from willemites replacing primary sulphides (Part 5). Model ages of ore samples from the Tsumeb Pipe and the Kombat Mine range from 600 to 530 Ma (Allsopp et al., 1981; Hughes et al., 1984; Kamona et al., 1999), but recent studies question the reliability of these dates (e.g., Haack, 1993; Frimmel et al., 2004).

Types of sulphide mineralisation from the OML are described in the subsequent chapters 1.5.1 to 1.5.6. Nonsulphide mineralisation from the OML is described in Part 5 for the Zn-silicates and in Part 6 for the Vanadates.

1.5.1 VMS-type

VMS-type ores occur in the southernmost OML, which is part of the Northern Zone of the Damara Belt. The low grade Cu-Ag-Au mineralisation is associated with metavolcanics and chlorite schists of the Askevold Fm, intercalated in clastic rocks of the Nabis Fm and dolomitic marbles, which could be related to the lower Abenab Subgroup (Söhnge, 1957). Main primary sulphides comprise chalcopyrite, chalcocite and bornite, whereas supergene sulphides are represented by chalcocite and neodigenite (Emslie, 1981). The metavolcanics and chlorite schists contain layers of magnetites and pyrites (Part 4).

1.5.2 Berg Aukas-type

The type locality of Berg Aukas is located in large scale folded dolomites of the Abenab Subgroup east of Grootfontein (Fig. 1.4), resting on the basement high of the Grootfontein Inlier. Hypogene Zn-Pb dominated sulphides were enriched along a bedding parallel fault breccia (Northern Ore Horizon, Fig. 6.5) and in collapse breccias (Central Ore Body) (Verwoerd, 1957). Misiewicz (1988) described saline brines (ca.

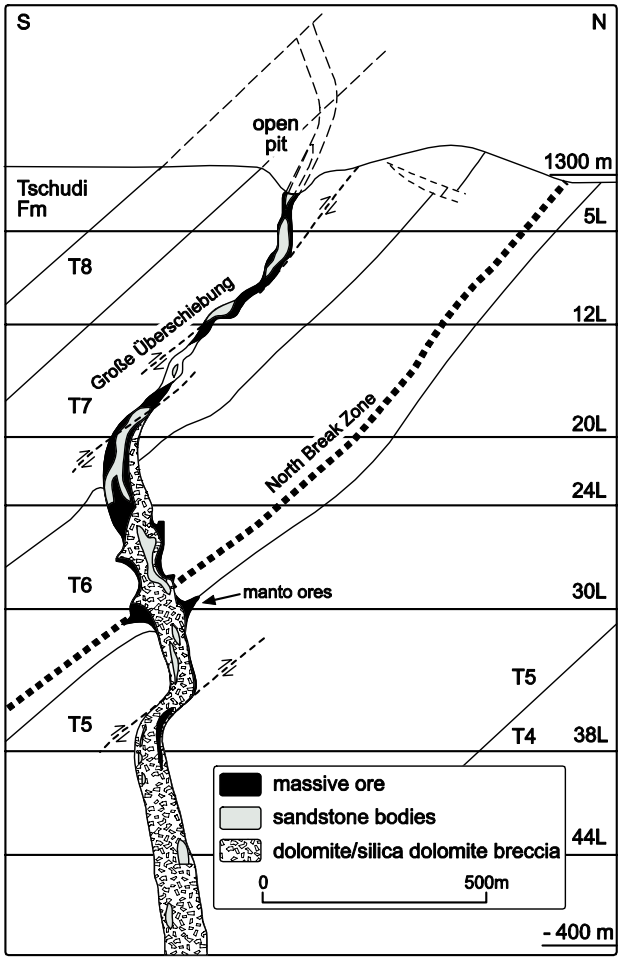

Fig. 1.7: The Tsumeb Pipe orebody (modified from Lombaard et al., 1986; Hughes, 1987).

23 wt.% NaCl equivalent) and homogenisation temperatures ranging from 92°C to 210°C from sphalerite and related carbonate gangue. Further Berg Aukas-type deposits and similar occurrences are located in the central to eastern OML (e.g. Abenab Pipe, Harasib, Border, Pickaxe, South Ridge, Fig. 1.4). Carbonate cements accompanying the primary sulphides are characterised by a high salinity and formation temperatures ranging from 137°C to 255°C assuming a hydrostatic pressure of 0.5 kbar (Misiewicz, 1988). Compared to the host rocks, the carbonate cements indicate no significant enrichment in trace elements and REE, suggesting together with the fluid characteristics a fluid-rock interaction largely within the depositional basin of the Otavi Group (Chetty and Frimmel, 2000). Two models are suggested for the formation of Berg Aukas-type deposits: 1) MVT-style mineralisation prior to the Pan-African orogeny due to basin dewatering processes (Pirajno and Joubert, 1993; Chetty and Frimmel, 2000) and 2) syn Pan-African emplacement (Hughes, 1979).

1.5.3 Tsumeb-type

The Tsumeb Pipe deposit (Fig. 1.7), represented in the type locality of Tsumeb, is extensively described in Lombaard et al. (1986). The reported summary of this complex deposit is mainly in accord with the latter paper, if not mentioned otherwise. The ore bodies are located in a discordant breccia pipe, which is originated by the dissolution of the carbonate host rocks by meteoric water prior to syn-D2 folding and shearing and hydrothermal alteration syn- and post-D2. Upward progression of the collapse brecciation through the whole overlying succession of the Tsumeb Subgroup finally allowed siliciclastic material of the Tschudi Fm to influx into the cavernous conduit down to level 36 (T5). Deposition of the feldspathic sandstone, which is correlated to the Mulden Group, occurred prior to D2, as indicated by syn-D2 deformed sandstone bodies. Base metal mineralisation occurs in four different types, divided according to the degree of metal concentration, structural position and state of oxidation: A) Massive Peripheral Ores replace the feldspathic sandstone and extent laterally into a dolomite breccia. B) Manto Ores comprise massive sulphides, extending from the margin of the breccia pipe into the country rocks. They are confined to the lower T6 and controlled by structures, which developed prior to the formation of the karst pipe (Hughes, 1979), C) Disseminated and Stringer Ores comprise a variety of sulphide mineralisation. Amongst these are disseminated replacements of feldspar and Cu-rich veins in the feldspathic sandstone and irregular blebs to discontinuous veins associated with altered breccia bodies and steep fractures. Further on Hughes (1979) described massive sulphides as vug-filling, which is predominantly preserved in the silicificated lower levels of the breccia pipe. D) Secondary Ores, derived by supergene alteration of the primary sulphides, are enriched in two oxidation zones.

The emplacement of base metal mineralisation is related to the ascent of metal-bearing hydrothermal fluids prior to the waning stages of the deformation and a significant enhancement of permeability could be due to the main deformational event (Ypma, 1978). However, Hughes (1987) and Maiden and Hughes (2000) discuss a pre-D2 mineralising event for Tsumeb. Up to its closure in 1996 the Tsumeb Mine produced about 30 Mt of ore grading 10% Pb, 4,3% Cu and 3,5% Zn. Apart from the high concentration of As,

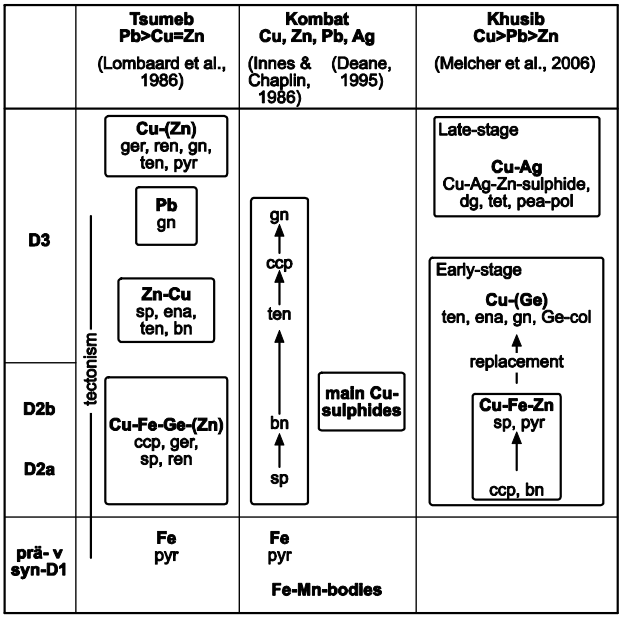

Fig. 1.8: Paragenetic sequence of major Tsumeb-type deposits in the OML. Deformational stages according to Part 2. For abbreviations see Appendix.

Melcher et al. (2006) emphasise the high amount of Cu-thiogermanate minerals like germanite and renierite. The paragenetic sequence of the hypogene mineralisation determined by Lombaard et al. (1986) started with early pyrite, followed by the main mineralisation with Cu-Fe-Ge(-Zn) sulphosalts and sulphides (Fig. 1.8). Commencing sulphide mineralisation was dominated by Zn-Cu sulphides, which was finally displaced by galena. The metal to sulphur-ratio increases with the deposition of this sequence.

Homogenisation temperatures of fluid inclusions in quartz gangue of the main mineralisation vary between 170°C and 245°C, accompanied by an increasing CO_2 amount to the higher temperatures and decreasing depth (Ypma, 1978). Carbonate cements accompanying the main mineralising and subsequent sulphide remobilisation exhibit formation temperatures of about 275°C (Chetty and Frimmel, 2000). Quartz-gangue, related to Pan-African recrystallisation of the sulphides, contains 3-phased fluid inclusions ($H_2O \pm CO_2$ + vapour) with homogenisation temperatures of 100 to 185°C (Ypma, 1978). Salinities of gangue minerals associated with Tsumeb-type ore in the OML range from 17 to 23 wt% NaCl (Chetty and Frimmel, 2000). Significant elevation of Chondrite normalised REE patterns of carbonate cements (Cc II) related to remobilised sulphide ore point to extensive interaction of the mineralising fluids with non-carbonate rocks of the Damara Supergroup or the basement in the OML (Chetty and Frimmel, 2000). In the Tsumeb and Kombat deposits most fluid inclusions have been destroyed by deformation of the host mineral. Preservation was enabled by protection due to an environment of more ductile material (e.g. Cu-sulphides, Ypma, 1978).

Amongst further Tsumeb-type deposits in the OML are Kombat (Innes and Chaplin, 1986; Deane, 1993), Khusib Springs (Melcher et al., 2006) and several occurrences in the north-western OML like Tsumeb West and Uris (Fig. 1.4). At the Kombat and Tsumeb West deposits, Pb- and Cu-sulphides were remobilised into D2b structures (Innes and Chaplin, 1986; Deane, 1993; Part 2). Recent studies on Tsumeb-type deposits suggest that hydrothermal fluids were generated during prograde metamorphism of the Pan-African orogeny and migrated along Pan-African faults (Pirajno and Joubert, 1993). Based on fluid inclusion studies on massive sulphides (Ypma, 1978), Chetty and Frimmel (2000) calculated a formation temperature of ca. 405°C for Tsumeb-type mineralisation in the Kombat Mine. Sediments and mafic rocks of the Damara Supergroup and contained VMS-type deposits (Part 4) that were leached by the northward migrating fluids.

1.5.4 Nosib-type

The Nosib-type comprises disseminated Cu-Pb(-Zn) mineralisation in arkoses, conglomerates and diamictites of the Nosib Group, close to the tectonic contact with overlying laminated dolomites of the Abenab Subgroup. Pyrite, chalcocite, galena, sphalerite and bornite represent the main sulphides. Secondary mineralisation is made of Cu carbonates, Pb oxides and Pb-Cu vanadates.

1.5.5 Tschudi-type

The stratiform Tschudi-type is confined to the Sissekab-Tsumeb-synclinorium in the north-western OML (Fig. 1.4). At the Tschudi Mine, low-grade Cu mineralisation impregnates sandstones and conglomerates at the base of the Mulden Group. The ore body shows a slight zoning with chalcocite as the main sulphide at the bottom to a combination of bornite, chalcopyrite and pyrite at the top. Misiewicz (1988) suggested metal precipitation by replacement of diagenetic pyrite.

1.5.6 Other mineralised areas

Several different types of mineralisation occur in the north-western OML (Fig. 1.4). Almost all deposits and major occurrences are located in the area west of Tsumeb and northeast of the Guinas Fault (Fig. 1.4) and are characterised by a significant amount of Cu-sulphides. Tsumeb West and Uris are Tsumeb-type deposits, related to structurally controlled karst pipes. Further occurrences of Cu sulphides are bound to sedimentary breccias (e.g. Karavatu) and/or located beneath silicified horizons (Venter, 1977), which can be represented by large chert nodules or due to syn-deformational silicification, such as along the Guinas Fault (De Bever, 1997). The Otjikoto 2-prospect comprises mainly bornite and chalcocite enriched along a bedding parallel fault in the T7 lithounit, which developed during D2. Low-grade Cu deposits are located in sandstones and conglomerates in karst depressions at the base of the Mulden Group (e.g. Tschudi; Misiewicz, 1988). Southwest of the Guinas Fault, primary sulphides are enriched in breccias in the Hüttenberg Fm (e.g. Lucky Friday, Blackjack; Fig. 1.4; Osterman, 1990) or represented only by small specks of galena, which are distributed over the area without any stratigraphic or tectonic control. Local supergene Zn-enrichments related to mass flow breccias in the T7 lithounit, could have larger Zn-Pb-mineralised root zones in lower stratigraphic levels (Osterman, 1990). The grade of Zn is fairly high for this region (22.8% Zn), but the occurrences are very small.

Several base metal sulphide prospects of the Berg Aukas-type occur in the central OML, namely in the area of the eastern Maieberg Anticline, the eastern Keilberg Anticline, the western Gauss Anticline and in the northern limb of the Toggenburg Anticline (Fig. 1.4). Galena, sphalerite, chalcocite and pyrite are hosted by sedimentary, tectonic and solution collapse breccias in the Maieberg and Elandshoek Fms (e.g. Border, Harasib 1) (Misiewicz, 1988). The mineralised breccias are situated in the hanging wall of shear zones in the lower Tsumeb Subgroup (e.g. Teco) or tectonised contact of the Tsumeb Subgroup to shales of the Auros Fm. These shales show a strong impregnation by Fe-hydroxides (e.g. Harasib 3, Lucas Prospect). In the hanging wall of some of these deposits, Zn-Cu-Pb vanadate ores are emplaced in karst breccias (e.g. Harasib 3) (Van der Westhuizen, 1984). The Khusib Springs deposit in the eastern central OML is a high-grade, bedding parallel Cu-Zn-Pb deposit, replacing limestones of the lower Tsumeb Subgroup (Melcher et al., 2006).

Base metal sulphide deposits in the northern limb of the Otavi Valley syncline in the southern OML (Fig. 1.4) are closely related to tectonic structures, such as NE- and E-striking normal faults (Innes and Chaplin, 1986). In the Kombat Mine, galena, chalcopyrite and bornite as main primary sulphides are hosted by sedimentary and tectonic breccias and are closely related to sandstone bodies, which are very similar to the Damaran karst infill of the Tsumeb Pipe. The genetic relationship to the Tsumeb-type deposits is supported by high amount of Cu sulphosalts (e.g. tennantite) and a similar paragenetic sequence of base metal sulphide ores and carbonate generations (Frimmel et al., 1996a) (Fig. 1.8). Deane (1995) emphasised the role of the unconformable contact to the hanging wall phyllites and shales of the Kombat Fm as a seal for ascending metalliferous fluids. Based on fluid inclusion studies on massive sulphides (Ypma, 1978), Chetty and Frimmel (2000) calculated a formation temperature of ca. 405°C for Tsumeb-type mineralisation in the Kombat Mine. Smaller pendants to the Kombat Mine can be found in the eastern (e.g. Guchab) and western Otavi Valley syncline (Baltika - Kupferberg area, Fig. 1.4), but most of theses are lacking of the Damaran karst infill. Layered Fe-Mn-bodies are confined to the Kombat Mine and predate the sulphide formation (Innes and Chaplin, 1986). In single deposits in the Otavi Valley, sphalerite was replaced by willemite (e.g. Baltika, Part 5). Unlike other areas in the OML, Zn-Cu-Pb vanadate ores are not only emplaced in karst structures in the hanging wall of the primary sulphide ore bodies, but also associated with N-trending joints (Van der Westhuizen, 1984).

A detailed description of the Berg Aukas and Abenab deposits in the east and northeast of the OML is given in Part 5 and 6.

1.6 Main results

Research undertaken for this thesis produced a number of significant insights into various aspects of the geology and metallogeny of the OML including:

- The formation and consolidation of the Paleoproterozoic basement and its metallogenetic significance
- Cryogenian rifting and formation of VMS-type deposits
- Pan-African geodynamic evolution of north-eastern Namibia and formation of sulphide and nonsulphide deposits in the OML
- The formation of post-Damaran nonsulphide deposits

1.6.1 The Paleoproterozoic basement of the OML

The Paleoproterozoic basement of the OML comprises the Grootfontein Metamorphic Complex (GMC) and the Grootfontein Mafic Body (GMB). Geochemical studies suggest a magmatic evolution from dioritic towards granitic compositions in a convergent tectonic setting. These events could have been related to the Eburnean orogeny as is indicated by late-Eburnean Rb-Sr ages of micas from pegmatitic intrusions in the granodiorites (1.816 ± 26 Ma) (Part 3). A rather imprecise, but nevertheless similar age of 1.946 +299/-333 Ma obtained for gabbros of the GMB (Pb-Pb whole rock, Armstrong, 1988) provides additional support for this hypothesis. The major and trace element composition of gabbros of the GMB indicate emplacement in a continental regime and differ distinctly from the granites and diorites of the GMC, suggesting a regional shift in the geochemical characteristics of the magmas. The variable geochemical patterns of the GMB could be the result of distinct magma sources, or differential contamination from older basement rocks. Negative Sr anomalies could have been caused by pre-Damaran weathering and erosion processes, as suggested for the case of the Franzfontein Granites (Clifford et al., 1969). Petrographic studies of the granitic, dioritic and gabbroic rocks indicate at least two metamorphic overprints of the Paleoproterozoic basement of the OML. Presumably the two events consisted of a retrograde metamorphism prior to the Pan-African orogeny and a greenschist to amphibolite facies metamorphism during the Pan-African orogeny.

A petrographic and geochemical comparison of granites and diorites of the GMC with other pre-Damaran basement rocks in Northern Namibia highlights similarities with the Franzfontein granites in the Kamanjab Inlier further to the west (Clifford et al., 1969), as well as to the Archean Huab Massif (Seth et al., 1998). Geochemical studies of the GMB reveal similarities to other anorthositic bodies in the south-western part of the Sao-Francisco Congo Craton, such as the Kunene Complex described by Silva (1990) and Mayer et al. (2004).

No important mineral occurrences have been identified in the pre-Damaran basement of the OML. However, Littmann et al. (1997) described Cu-Ni-(PGE) sulphide mineralisations, (Fe-Ti-V) oxide occurrences and high REE contents from the Kunene Anorthosite Complex. The Geological Survey of Namibia (www.mme.gov.na/gsn/download.html, Oct. 2006) has also summarised the occurrences of several prospects for base and precious metal ores in other parts of the pre-Damaran plutonic basement of northern Namibia. In the Huab Massif (Fig. 3.1) and Abbabis Complex, hydrothermal gold-bearing quartz veins are associated with base metals. Additionally, Cu-Au mineralisation in the Abbabis Complex occurs at the contact of the igneous basement and quartzites of the Nosib Group as well as in brecciated aplites.

As outlined in previous sections, the basement of the OML was overprinted by greenschist facies metamorphism, presumably during the Pan-African orogeny. Although the main deformation was accommodated by distinct Damaran sedimentary lithologies (Maclaren, 1991), an intense compositional change of basement rocks in the Grootfontein Inlier and a release of economically important elements could have been protracted during the Pan-African orogeny. The presented geochemical data highlight a considerable enrichment in Y, precious metals (e.g. Au) and transition elements such as V, Ni, Cu and Zn in GMB rocks (Fig. 4.2). The diorite sample from the Toggenburg Anticline (CL53) is also enriched in Cu, Ni, V and Zn, implying a close relationship with the GMB. Base metal ore deposits in the northern OML are known for their wide and peculiar assemblages of arsenic sulphides and sulphur-salts, of both hypogene and supergene origin (tennantite, enargite, renierite; acc. to Lombaard et al., 1986). High As contents were also detected in diorites and granites of the GMC and the Keilberg mica schist (Fig. 3.7).

1.6.2 Cryogenian rifting and VMS-type deposits

Siliciclastic rocks of the Nosib Group were deposited in NE-trending grabens that formed during the Cryogenian break-up of Rodinia and the related opening of the Adamastor Ocean (Unrug, 1997) with the Khomas Trough as its intracontinental branch (Kukla and Stanistreet, 1991). Geochemical studies on the metavolcanic rocks support the classification of the Askevold Fm as intracontinental rift volcanics (Part 4). Intercalated metavolcanics of the Askevold Fm are comparable to the Naauwpoort Fm in the Northern Zone of the Damara Belt for which ages of ca. 742 ± 25 Ma (Burger and Coertze, 1973) and 746 ± 2 Ma (Hoffmann et al., 1996) have been determined. These volcaniclastic rocks were described only from the southern OML adjacent to the Northern Zone margin (Söhnge, 1957). This thesis provides data on comparable tholeiitic volcaniclastic rocks in the central OML. Conversely, Pan-African shear zones, represented by the Keilberg quartzitic micaschist (Part 2, 3), could also point to large scale displacement between the Paleoproterozoic basement and the early Damaran volcaniclastic rocks in the central OML. Magnetite-rich layers occur in the schistose Askevold Fm in both central and southern OML. Pb-Pb age determinations for the magnetite yield ca. 587 ± 12 Ma. The magnetites occur predominantly as euhedral grains, but also feature in healed fractures in deformed VMS-type sulphides. This estimate therefore provides an important constraint (the first published) on the minimum age for VMS-type deposits in the Nosib Group. Additionally, the magnetites show quartz and phyllosilicate strain shadows that could have only developed during the Pan-African orogeny. Therefore the maximum age of the Pan-African orogeny in the OML is about middle Ediacaran, just prior to D2 deformation and the subsequent deposition of the late Ediacaran Mulden Group.

1.6.3 Pan-African geodynamic evolution and base metal deposits of the Otavi carbonate platform

The Pan-African orogeny was the driving force for hydrothermal activity, fostering the formation of base metal sulphide and nonsulphide deposits in the OML. In southern Africa the Pan-African orogeny was related to the assembly of western Gondwana, commencing in the middle to late Neoproterozoic (Porada, 1989; Unrug, 1996; Trompette, 1997; Condie, 2002). The amalgamation of the Sao Francisco-Congo, Kalahari and Rio de la Plata Cratons resulted in the formation of the Damara Orogen, comprising the Damara, Kaoko and Gariep Belts (660-500 Ma, Goscombe et al., 2003). The Damara Belt is likely to extend further to the east into other Pan-African belts, forming the Damara-Lufilian-Zambezi Orogen (DLZ). The collision of the Rio de la Plata Craton with the Kalahari and Sao Francisco-Congo Cratons respectively preceded the suturing along the DLZ.

The Pan-African overprint of the OML happened in three stages: D1 was represented by late Cryogenian to middle Ediacaran E-W shortening, presumably triggered by the accretion of a coastal terrane in the Kaoko region (Goscombe et al., 2005). D2 comprised late Ediacaran to early Cambrian N-S shortening, caused by the collision of the Sao Francisco-Congo and Kalahari Cratons and was accompanied by greenschist facies metamorphism (M1; Clauer and Kröner, 1979; Goscombe et al., 2004). D3 was related to early Paleozoic uplift, which was accompanied by zeolite to prehnite-pumpellyite facies metamorphism (M2) around 481-459 Ma (Haack et al., 1980; Haack, 1983). Post-Pan-African reactivation of large scale normal faults is envisaged by parallel aligned dyke swarms of presumably Karoo-age (Söhnge, 1957).

The distinct stages of base metal mineralisation were correlated with deformational stages of the Pan-African orogeny in this study (Fig. 1.9). In order to understand the sequence of the single stages, the major types of mineralisation in the OML (Berg Aukas- and Tsumeb-type) are critically reviewed in this thesis.

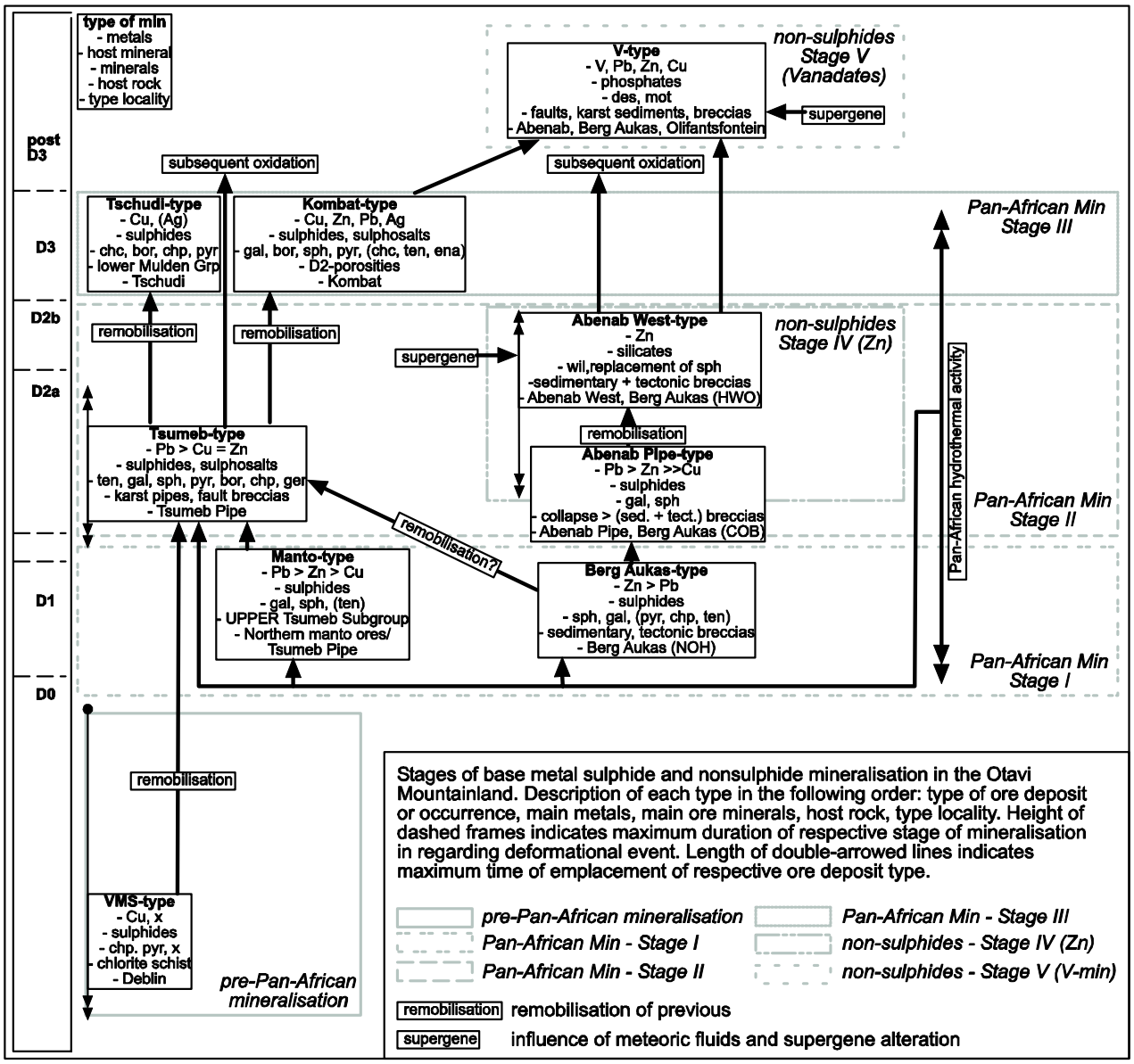

Fig. 1.9: Flow chart of development of sulphide and nonsulphide mineralisation in the OML.NOH- Northern Ore Horizon, COB - Central Ore Body, HWO - Hanging Wall Orebody. For abbreviations of minerals see Appendix.

1.6.3.1 Characteristics of Berg Aukas- and Tsumeb-type

Previous researchers classified Berg Aukas-type deposits in the OML as MVTs that formed due to basin dewatering processes either prior to the Pan-African orogeny (Pirajno and Joubert, 1993; Chetty and Frimmel, 2000) or during (Hughes, 1979). The discrimination of Berg Aukas-types from Tsumeb-types was primarily based on: different deposition environments; fluid salinity; depositional temperature of sulphide and gangue mineralisation; distinctly different paragenesis of the ore assemblage; and different lead-isotope trends (Melcher et al., 2006).

Berg Aukas-type deposits are located mainly in the Abenab Subgroup and lower Tsumeb Subgroup in the central and eastern OML, resting directly on top of the Paleoproterozoic basement highs or separated only by thin successions of the Nosib Group (Fig. 1.3; Hedberg, 1979, Fig. 26). Additionally, Berg Aukas-type deposits occur in less deformed areas than Tsumeb-type deposits (Part 2, Fig. 2.13). Nevertheless, in some Berg Aukas-type localities primary sulphides are hosted by bedding parallel tectonic breccia horizons (e.g. Berg Aukas, Northern Ore Horizon, Part

6, Fig. 6.5). Therefore the depositional sites of both deposit types allow us to constrain the relative timing with respect to the deformational phases of the Pan-African orogeny. Berg Aukas-type deposits could have evolved during or after the first stage of the Pan-African orogeny (D1), which still would allow suitable conditions for low temperature fluids to be responsible for formation of the deposit (Chetty and Frimmel, 2000). The Tsumeb-type deposits are mainly located along or close to major Pan-African fault systems (Part 2) and evolved over several stages throughout the Pan-African orogeny as is implied by remobilised massive sulphides (Hughes, 1979; Innes and Chaplin, 1986; Deane, 1993; authors observations, 2004/2005) and the fluid characteristics (Ypma, 1978; Chetty and Frimmel, 2000). The depositional site may point also to the distinctly varying paragenesis of both deposit types. For example, the lithological type and thickness of the underlying strata could have provided different metals, and the architecture of the fluid pathways could have controlled the degree of fluid rock interaction. Hughes (1987) discriminated different Pb isotope trends for Berg Aukas-, Khusib- and Tsumeb-type ore. However, preliminary Pb isotope studies on sulphide and nonsulphide ores in the OML indicate a dependency of Pb isotope ratios of the various deposits to their location and the underlying strata, regardless of the type of deposit. (Part 6; Schneider, pers. comm., 2005).

1.6.3.2 Stage I: Pan-African mineralisation - Berg Aukas-type

The first stage of major deposition of base metal sulphides in the OML occurred during D1 (Fig. 1.9) and comprises Berg Aukas-type mineralisation as well as the northern Manto-Ores of the Tsumeb Pipe, described by Hughes (1979). Precipitation of the Zn-Pb dominated sulphide ore took place in sedimentary and tectonic breccias (e.g. Berg Aukas, Northern Ore Horizon). A further refining of these ores developed due to collapse brecciation at the depositional sites (e.g. Berg Aukas, Central Ore Body), which was caused by solution processes due to the circulation of hydrothermal fluids (Misiewicz, 1988). A tectonic component of this brecciation is evident from the Abenab Pipe deposit in the north-eastern OML (Part 6). The Manto-Ores of the northern part of the Tsumeb Pipe show compositions similar to the Berg Aukas-type and were emplaced prior to the syn-Damaran karstification (Hughes, 1979). Further indications for Stage I ores in Tsumeb-type deposits were obliterated by the following stages of Pan-African mineralisation.

1.6.3.3 Stage II: Pan-African mineralisation - Tsumeb-type

The second stage comprises the main sulphide mineralisation of the Tsumeb-type and evolved during D2. Hydrothermal fluids were triggered by the regional metamorphism (M1), which reached upper greenschist facies in the Nosib Group and lower greenschist facies in large areas of the Otavi platform carbonates (Part 2, Fig. 2.13). Furthermore, emplacement of syntectonic granites in the central Damara Belt could have fostered the hydrothermal activity (Miller, 1983a; Fig. 1.2). Adequate fluid pathways for mineralising fluids could have been Pan-African thrusts and reactivated E-W striking lineaments (Deane, 1995; Part 2, Table 2.4).

Cu-As rich sulphur-salts and Pb-Cu-Zn sulphides were emplaced in karst pipes and fault breccias (e.g. Tsumeb Pipe), which developed at cross junctions of different tectonic trends (Part 2). The main Cu-sulphide deposition at the Khusib, Kombat and Tsumeb Mines were related to Stage 2 (Fig. 1.6; Part 1, Fig. 1.5). The Berg Aukas-type deposits could have been partly remobilised during Stage 2. Melcher et al. (2006) suggested an upgrading of Zn-rich deposits, such as Berg Aukas-type deposits in the central and eastern OML by hydrothermal fluids to form Tsumeb-type ore bodies as at Khusib.

1.6.3.4 Stage III: Pan-African mineralisation - remobilisation of primary sulphides

The third stage of Pan-African mineralisation in the OML involved repeated remobilisation of the primary Tsumeb-type and eventually also Berg Aukas-type deposits to form complex ore bodies such as the Tsumeb Pipe. This process led to a direct replacement of the primary ores and/or to further distribution of sulphide ore into D2-structures. The remobilised material could have been transported by hydrothermal fluids along sedimentary (e.g. T8 chert layers at Karavatu) and tectonic structures (e.g. mineralised shear zones at the Tsumeb Mine or Otjikoto 2). Remobilised ore bodies were reported from several localities in the OML (e.g. Tsumeb Pipe, Hughes,

1979; Tsumeb West, authors observations), but extensively described from the Kombat Mine (Innes and Chaplin, 1986; Deane, 1995) and are therefore summarised as the "Kombat-type" in Fig. 1.6. The repeated remobilisation of primary ores could have involved the addition of further elements which were transported by new fluid pulses that originated in the central regions of the Damara Belt, causing the complex polymetallic deposits at Tsumeb, Kombat and Khusib (Fig. 1.5).

The driving force for the hydrothermal fluids could has been the second regional metamorphism in the OML, which accompanied D3 and reached at least zeolite to prehnite-pumpellyite facies in the Kombat phyllites close to the Kombat Mine and in siliciclastic rocks of the Mulden Group in the Etosha Pan northwest of Tsumeb during Ordovician times (Clauer and Kröner, 1979; Ahrendt et al., 1983) (Fig. 1.2). Synchronous regional metamorphism in the Central Zone included migmatisation and granite emplacement (Goscombe et al., 2005), pointing to further regional triggers of hydrothermal activity in the Damara Belt. The related uplift of the Northern Platform caused extensional faulting along pre-D3 structures and a conjugate set of NE and NW-striking faults opening new fluid pathways.

1.6.3.5 Stage IV: nonsulphides - Zn silicates

In the OML, the Zn-silicate willemite occurs as fine-grained to granular masses in tectonic breccias (e.g. Abenab West) and replaces sphalerite, developing a boxwork structure (e.g. Berg Aukas, Hanging Wall Horizon), and the host carbonates. Later generations of willemite form radiating prismatic needles. Willemite has been evaluated as a potential Rb-Sr geochronometer and was used to directly date nonsulphide Zn-mineralisation in the OML (Part 5). The most reliable age data were obtained from coarse-grained, well-crystallised willemite samples from Berg Aukas, which yield Rb-Sr ages of 499 ± 63 Ma (MSWD = 2.6) and 493 ± 2 Ma (MSWD = 1.2). These, along with less reliable ages ranging from 560 to 500 Ma, reveal an overall syn-D2 timing for Stage IV mineralization (Fig. 1.6) synchronous with the formation of Tsumeb-type deposits and their subsequent remobilisation. A syn- to post-D2 age of early willemite is supported by the emplacement of massive willemite along a syn-D2 shear zone at Abenab West (Part 5), which is also chosen as the type locality for this ore stage. This supports the Pan-African alteration of Berg Aukas-type deposits by percolating hypogene-hydrothermal fluids (as suggested previously by Melcher et al., 2006), rather than supergene weathering of the associated primary sulphide ores. Accordant to Stage II, the trigger for the circulation of fluids leading to the hydrothermal alteration of the primary sulphides could be the regional metmamorphsim (M1) and/or granite emplacement in the central zone of the Damara Belt.

1.6.3.6 Stage V: nonsulphides - vanadates

Stage V comprises supergene Pb-Zn-Cu vanadates that occur in post-Damaran karst fillings, solution collapse and tectonic breccias, and along faults at various localities of the OML (Part 6). North- to NE-trending faults were reactivated during post-Damaran deformational phases such as the opening of the southern Atlantic in Cretaceous times (Raab et al., 2002) (Part 2), and served as hosts for supergene V-Pb-Zn-Cu occurrences. The vanadates follow the formation of all base metal sulphides and the early willemites in the OML, but their relative timing with respect to supergene Zn- and Pb-carbonates remains unclear. Varying Cu (mottramite) and Zn (descloizite) contents reflect the original composition of the primary sulphide deposits in the same area (Van der Westhuizen et al., 1984, 1988). Studies of fluid inclusions and O and C isotope signatures of carbonate cements, related to the formation of the vanadates, suggest that slightly heated meteoric fluids circulated during a phase of deep continental weathering, resulting in the precipitation of vanadates. Pb-isotopic compositions of the vanadates are identical to their precursor sulphides, excluding the input of Pb from external sources. The clearly distinct Pb isotope signatures of the primary sulphides as well as of the related vanadates could indicate different ages of the respective deposits or variable sedimentary successions of the underlying strata. Senut et al. (1992) and Pickford (1993, 2000) used fossil remnants in the karst fillings in order to date the vanadate ores and obtained ages ranging from Middle to Upper Miocene and Pleistocene respectively. The presented (U-Th)/He analyses on descloizites from various localities in the OML suggest ages ranging from Late Oligocene to Pleistocene for the vanadate ores, pointing to their formation during the "African Erosion Cycle".

1.6.3.6 Metal sources

Deposition of sulphide ores in the Otavi carbonate platform resulted from circulation of basinal or metamorphic brines, which leached the Paleoproterozoic basement or siliciclastic and volcaniclastic rocks of the Nosib Group (Pirajno and Joubert, 1993; Chetty and Frimmel, 2000). Furthermore, distinct horizons within the Otavi Group could have been leached during ore forming processes (Chetty and Frimmel, 2000; Melcher et al., 2006). Zn-silicates originated from alteration of Berg Aukas-type sulphides by hypogene-hydrothermal fluids (Part 5). Sulphide ores and Zn-silicates were altered from the end of the Mesozoic throughout the Tertiary, resulting in the formation of Pb-Cu-Zn vanadates (Part 6). The driving processes for the circulation of ore-forming fluids were the deformational events during the Pan-African orogeny and emplacement of syntectonic granites in the Damara Belt (Part 2, Part 1). These events produced several stages of sulphide and even nonsulphide deposition in the Otavi Group (Fig. 1.6, Part 1). Pan-African lineaments, reverse faults and large thrusts located in the Damara Belt, could have been the conduits of such ore-forming fluids (Part 2, Part 3). Petrographic, major and trace element as well as radiogenic isotope studies on samples of the Paleoproterozoic basement and metavolcanic and clastic rocks of the Nosib Group provide information about the source rocks for the base metals in sulphide and nonsulphide deposits in the Otavi carbonate platform. The Paleoproterozoic basement and the Askevold Fm, containing VMS-type deposits, were subject to at least greenschist facies metamorphism during the Pan-African orogeny (Part 2), leading to an intense compositional change of these sequences (Part 3, 4).

On the basis of Sr-isotope studies, Chetty and Frimmel (2000) excluded magmatic sources (Innes and Chaplin, 1986) for the sulphide ore forming fluids and favour circulation of basinal or metamorphic brines. A mixture of basement-derived Pb and more radiogenic Pb, which was added through syn-orogenic brines, was suggested by Frimmel et al. (2004). Geochemical studies of galena from various localities in the OML and samples from the Askevold Fm show similar distribution patterns of trace elements (Part 4), but differ from trace element patterns of the GMC (Part 3). Therefore, adequate source rocks of base metal sulphides in the Otavi Group could have been the Askevold Fm and VMS-type deposits contained within it. Metavolcanics in the central OML could be hosts for further VMS-type deposits, representing a further source for base metal sulphide deposits in the northern OML, such as the Tsumeb Pipe.

Sr-studies on willemite mineralisation and adjacent cements suggest small scale fluid systems during the deposition of the Zn-silicates as is shown by contrasting initial 87Sr/86Sr ratios of the Rb-Sr isochrons obtained for single samples of the same deposit (Berg Aukas, Part 5). Some of the circulating ore-forming fluids could have been contaminated by carbonate host rocks of the ore deposits, whereas others reflect a more intense interaction with gangue of the primary sulphides.

Pb isotope signatures of Pb-Zn-Cu vanadates are in agreement with adjacent sulphide ores, defining these as the direct precursors for the vanadate ores. Sr isotope signatures of the carbonate gangue of Pb-Zn-Cu vanadate ores suggest contamination of supergene fluids by carbonate cements of the host rocks, but also a local contribution of radiogenic Sr from hydrothermal dolomites associated with primary sulphides, shales of the Otavi Group, or Paleoproterozoic basement rocks. Mafic minerals (biotite, hornblende) from the basement or the newly formed clays in the shales originating from weathered basement could have been a vanadium source. Geochemical studies show that gabbroic rocks of the GMB, but also diorites from Berg Aukas and the Toggenburg Anticline have a significantly higher V-content than granites and granodiorites of the GMC. This characterises not only the GMB as possible source rock for V-mineralisation in the OML (Verwoerd, 1957), but also other intermediate to mafic rocks of the Paleoproterozoic basement. The deep circulation of meteoric fluids during the Cenozoic could have enabled the leaching of V-rich metavolcanics of the Askevold Fm and deposition of vanadate ores. But the largest portion of the V is contained in magnetites, which are not very susceptible to weathering.

Part 2: Geodynamic evolution of the Otavi Mountainland (Namibia): Implications for Pan-African Damara orogeny and metallogeny

Abstract

The Otavi Mountainland (OML) is part of the foreland fold and thrust belt of the inland branch of the Pan-African Damara Orogen. It is located at the southern margin of the Sao Francisco-Congo Craton at the transition of the Northern Zone of the Damara Belt to the Northern Platform. Damaran lithologies in the OML unconformably overlie a Paleoproterozoic basement, the Grootfontein Inlier, and consist of clastic rift sediments (Nosib Group), platform carbonates of the Otavi Group and the molasse-like Mulden Group.

Pre Pan-African deformation of the Damara Supergroup is syndepositional and comprises slumping, brecciation and growth faulting. Three major Pan-African (Damaran) phases of deformation can be identified: a late Cryogenian to middle Ediacaran E-W shortening (D1), a late Ediacaran to early Cambrian N-S shortening (D2) and an early Paleozoic uplift (D3). A post Pan-African reactivation of NE-striking structures is shown by parallel aligned kersantite and gabbroic dykes of presumably Karoo-age. Based on the comparison of the tectonic evolution of the Northern Platform, the Northern Zone of the Damara Belt and other Pan-African belts in southern central Africa, either almost simultaneous suturing or a westward propagating collision of the Kalahari and Sao Francisco-Congo Cratons are possible, leading to the Damara-Lufilian-Zambezi Orogen (DLZ). The collision of the Rio de la Plata Craton with the Kalahari and Sao Francisco-Congo Cratons respectively precedes the suturing along the DLZ.

Many base metal ore deposits, both primary and secondary, are known in the OML and the majority appears to be structurally controlled. The hypogene Berg Aukas-type mineralisation consists of stratabound Zn-Pb sulphides. Tsumeb-type mineralisation comprises hypogene Pb-Cu-Zn ores and is largely hosted by breccia pipes. The breccia pipes developed at cross junctions of different tectonic trends generated during D2 and extended during D3. While the Tsumeb-type may contain remobilised material from Berg Aukas-type mineralisation, alteration of both types produced secondary ores. It is possible that throughout the Pan-African orogeny shear zones may have acted as pathway and seal for ascending metal-bearing fluids (e.g. Guinas Thrust, Teco Thrust). Structural analysis of the OML and the linking to different stages of mineralisation support a pre-D2 age for Berg Aukas-type and a syn-D2 age for Tsumeb-type ores in accord with the model of Pirajno and Joubert (1993).

2.1 Introduction

The Damara Belt can be subdivided in three major zones: the Northern, the Central and the Southern Zone (Miller, 1983a; Gray et al., 2006) (Fig. 2.1). The Otavi Mountainland (OML) is located in the northern part of the Damara Belt in Namibia, at the transition of the Northern Zone to the Northern Platform, which rests on the southern margin of the Sao Francisco-Congo Craton. The aim of this study is to unravel the geodynamic evolution of the OML, in order to gain a better understanding of the Neoproterozoic and early Cambrian evolution of the Northern Platform (also called Otavi Carbonate Platform) as well as of the genesis of the base metal mineralisation on the northern tip of the foreland fold and thrust belt of the northern Damara Orogen. An attempt is made to correlate the regional structures with other provinces of the Damara-Lufilian-Zambezi Orogen (Johnson et al., 2005 amongst others), in order to unravel the Pan-African assemblage of West-Gondwana.

This study presents results from three key areas and further key outcrops in the ca. 430 km² OML. The selection of these areas and outcrops was made on the basis of existing maps of the OML (GSN, 1999; Hedberg, 1979; Maclaren, 1991; Miller, 1983a; Van der Merwe Smit, 1959; Werner, 2005), aerial photographs and unpublished reports provided by Ongopolo Mining and Processing Limited (OMPL) and the Geological Survey of Namibia. These key areas were chosen to fulfil the following requirements: 1) distinct cross cutting relationships of the different stages of deformation and 2) visible relationships between tectonic structures and base metal

mineralisation. Field work included regional and outcrop mapping, field and underground sampling, followed by petrographic and structural analyses of about 150 thin sections.

In spite of the numerous often structurally controlled mineral deposits occurring in the OML, there is no detailed structural analysis published about this area. Former published work (Hedberg, 1979; Hughes, 1979; Miller, 1980; Coward, 1981; Miller, 1983; Deane, 1995; Melcher, 2003; Goscombe et al., 2004; Melcher et al., 2006), PhD and MSc theses (Deane, 1993; King, 1990; Van der Merwe Smith, 1959; Veldsman, 1977) and unpublished company reports (Botha, 1958; Gadd-Claxton, 1972; Venter, 1977; Osterman, 1990; Maclaren, 1991; Petzel, 1993) deal only marginally with this topic or with only local structural settings within the OML. Radiometric age data of the tectonic evolution of the Northern Platform are lacking and a well-constrained age for the orogeny of the Otavi foreland remains to be established (Prave, 1996). The OML provides an ideal area to investigate the evolution of the outermost part of a fold and thrust belt, without a major obliteration by subsequent deformational events. Its position at the far north-eastern end of the Damara Belt provides crucial information about the eastward continuation of the intracontinental branch of the Pan-African Damara Orogen.

2.2 Geological Setting of the OML and the Damara Belt

2.2.1 Pan-African tectonic belts in south-western Africa

The Damara Belt is the intracontinental branch of the Damara Orogen, which also comprises the Kaoko Belt in north-western and the Gariep Belt in south-western Namibia. The Damara Orogen evolved during the late Neoproterozoic to early Paleozoic Pan-African event (660-500 Ma, Goscombe et al., 2003), due to the assembly of West-Gondwana (Porada, 1989; Unrug, 1996; Trompette, 1997; Condie, 2002). The Sao Francisco-Congo and Kalahari Cratons and the Rio de la Plata Craton situated in Africa and South America respectively were involved in this process. The continuity between the Damara Belt and the Lufilian Arc and the Zambezi Belt of central Africa (Fig. 2.1) is indicated by prominent linear magnetic anomalies across NW-Botswana (Pretorius, 1984; Hartnady et al., 1985) and a similar tectonostratigraphic evolution of these Neoproterozoic suture zones (summarised in Johnson et al., 2005). The Okahandja Lineament in the Central Zone of the Damara Orogen (CZ in Fig. 2.1) possibly continues into the Mwembeshi Shear Zone in Zambia, representing a major ENE-trending transcontinental shear zone from south-western to central Africa (Unrug, 1983). This author suggested that the Damara Belt could be divided from the Lufilian Arc by a sinistral strike slip zone, which could be orientated perpendicular to the general north-eastern strike of the Damara Belt. Conversely, recent studies discuss a westward continuation of the Lufilian Arc into the West Congo Belt (Porada and Berhorst, 2000), leaving the eastward continuation of the Damara Belt open.

2.2.2 Tectonic evolution of the Northern Platform

The oldest relics of crustal forming processes in the OML date back to the Eburnean (ca. 2 Ga; Part 3). The Grootfontein Inlier forms the pre-Damaran basement of the OML and is part of an Eburnean Orogen at the southern margin of the Congo Craton (Thomas et al., 1993, Fig. 3). Time constraints on the Neoproterozoic tectonic evolution of central and northern Namibia are not very clear. A comparison of OML related models is given in Table 1. The following outline of the tectonic evolution of the OML is taken mainly from Laukamp et al. (2006). The orogenic cycle starts with a rifting stage, which results from the break-up of Rodinia, and is accompanied by deposition of the Nosib Group. The mafic volcanic rocks intercalated in the siliciclastic Nosib Group, could be correlated with similar volcanic rocks belonging to the Naauwpoort Formation in central Namibia, which were dated at 780-740 Ma (Burger and Coertze, 1973; Hoffman et al., 1996). The rifting was due to the opening of the Adamastor Ocean (Hartnady et al., 1985; Frimmel et al., 1996b) in the area of the coastal Damaran belts and propagated from there into the continent (Porada, 1985). This rifting led to a NE-SW orientated horst-

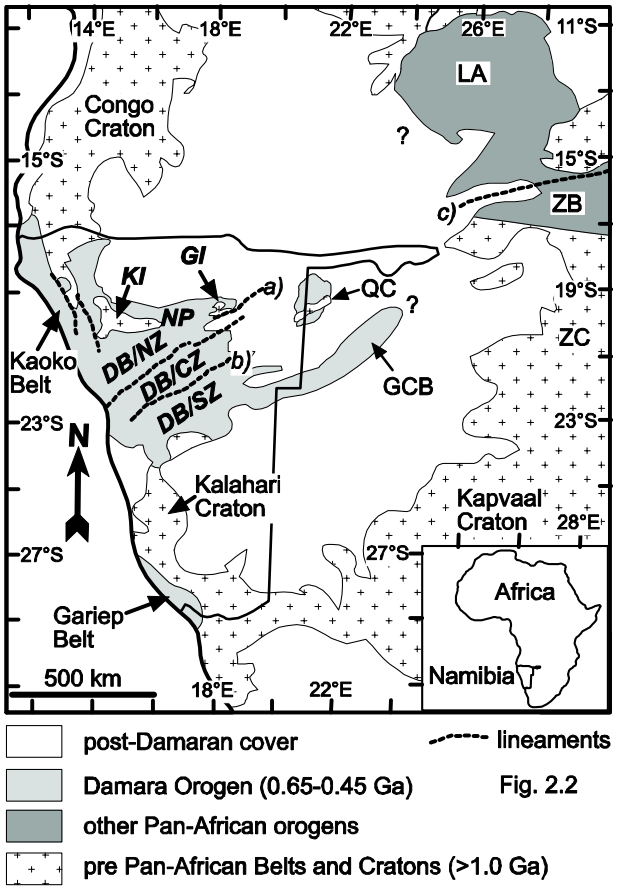

Fig. 2.1: Proterozoic mobile belts and Cratons of South-western Africa with selected lineaments and metamorphic zones of the Damara Belt; Lineaments: a) - Grootfontein Lineament, b) - Okahandija Lineament; c) - Mwembeshi Shear Zone; DB – Damara Belt, CZ – Central Zone, NZ – Northern Zone, SZ – Southern Zone, GCB – Ghanzi-Chobe Belt, GI – Grootfontein Inlier, KI - Kamanjab Inlier, LA – Lufilian Arc, QC – Quangwadum Complex, ZB – Zambezi Belt, ZC - Zimbabwe Craton (Map modified after GSN, 1999; Rainaud et al., 2005; Singletary et al., 2003)

graben-system, resulting in oceanic subbasins (Porada, 1985) or in a narrow northeast-extending oceanic branch of the Adamastor Ocean (Khomas Trough according to Kukla and Stanistreet, 1991). The development of the horst-graben-system was accompanied by sinistral strike slip movements along NE-trending lineaments (Miller, 1983; Daly, 1986), which divide the tectonometamorphic zones of the Damara Belt (Northern, Central and Southern Zone). The strike slip could have been due to a faster relative movement of the Kalahari Craton compared to the Sao Francisco-Congo Craton (Porada, 1989). One of these lineaments likely extends to the Mwembeshi Shear Zone, which separates the Pan-African Lufilian Arc from the Zambezi Belt (Porada, 1989). Movement directions along the Mwembeshi Shear Zone and their significance for the Pan-African tectonic evolution of Western Gondwana are controversial in the literature (Coward and Daly, 1984; Daly, 1986; Hartnady et al., 1985; Kukla and Stanistreet, 1991; Porada and Berhorst, 2000) but are assumed to be sinistral strike slip in recent literature (Johnson et al., 2005 amongst others). The transpressional orogeny of the Sao Francisco-Congo and Rio de la Plata Cratons in the west (Goscombe et al., 2005) forming the coastal Damaran belts preceded the collision of the Sao Francisco-Congo and Kalahari Cratons (Prave, 1996). In contrast to this, Dürr and Dingeldey (1996, 1997) deny the existence of an orogenic event in the Kaoko Belt prior to the Sao Francisco-Congo-Kalahari suturing. They relate the existence of sinistral movements along the Okahandja Lineament and dextral movements in the Gariep and Kaoko Belts to extrusion of the Sao Francisco-Congo Craton, induced by the existence of an indenter-like Kalahari Craton during the Pan-African collision between W- and E-Gondwana.

Continental convergence began in the Kaoko region successively proceeding to the east (Kasch, 1983; Goscombe et al., 2005). The first deformation of the Pan-African orogeny in the Northern Platform (D1a) is due to the ocean closure in the Kaoko region (K1 according to Coward, 1983; D1 according to Porada, 1989; Frimmel et al., 1996b; Miller, 1983), which occurred in the middle Ediacaran (before 600 Ma according to Alkmim et al., 2001; before ca. 580 Ma according to Goscombe et al., 2005), and caused N-S-trending, E-facing folds in the Kaoko Belt. A SSE-NNW shortening (D1b) (D1 according to Maclaren, 1991; K2 according to Coward, 1983; D2 according to Miller, 1983) replaced the E-W-compression, leading to northward thrusting in the Kamanjab Inlier (Fig. 2.1). D1 and D2 in the Kaoko region generated folding and bedding parallel deformation in the OML (Coward, 1981). The evolution of the Northern Platform (Miller, 1983; Porada, 1985) started in a transitional phase from the pre-Damaran extensional regime to the Damaran continental convergence between the Sao Francisco-Congo and Kalahari Cratons. Deposition of the middle part of the Otavi Group occurred around an age of 635 ± 1.2 Ma (U-Pb zircon age of the Ghaub Fm: Hoffmann et al., 2004). The platform was subject to local synsedimentary deformation (Deane, 1995; Laukamp et al., 2006; Maclaren, 1991). Miller (1983) reported thrusting of

Miller (1983) Northern (NZ) & northern Central Zone (CZ), Damara Belt	Frimmel (2004) Damara Belt tectonic setting	Maclaren (1991) with ages of sed. after Innes & Chaplin (1986) OML (prov. correlation)	Laukamp et al. (2006) OML tectonic setting	age of deposition/ metamorphism	def. event	tectonic structures/ karstification	Deane (1995) Kombat area, southern OML def. event	structures	Innes & Chaplin (1986) Kombat area, southern OML Kombat Fm.	dolomites
						karstification II	Post Karoo	N-S faults		
		D5 (fracturing, N trend, ass. with Waterberg Fault)	Late Cretaceous reactivation of Pan-African Lineaments		post D3	strike slip?	Karoo	Kombat West Fault		
D3 (480-460) Further uplift in CZ (495-460)		D4b (faulting, fracturing) D4a (cross folding, NE trend, formation of domes and basins)	Late or post-Damaran uplift in Northern Zone of Damara Orogen	M2 (reg. Met. ca. 481-459[3])	D3	normal faults (NW-SE, N-S, NE-SW) dextral strike slip (E-W), tension gashes			NE-trending strike slip faults	
Isostatic rebound in CZ (540-495)	Basin closure - foredeep (M3) 580-530	D3c (fold rupturing, NE trend) D3b (main folding, ENE trend) D3a (shearing with steep dip, NE-ENE strike) Mulden Grp. (570-550)	Collision of Kalahari and Congo Plate	M1 (reg. Met. peak 535[2])	D2b brittle	thrusting (> N - NE) F3 (E-W-axis) dextral strike slip (E-W)	D3 D2b	S3, F3 S2c, L2d, OVR, monoclinal F, ENE shearing	S3 (fracture cleavage) axial planar to chevron folds (F3) and kink bands	F3 (monoclinal folds) ass. with crenulation lineation and NE-trending S3 (fracture cleavage)
					D2a ductile	F3 (E-W-axis) (isoclinal) crenulation cleavage, S2, thrusting, slices	D2a	S2a+S2b, F2, L2a+L2b+L2c, E-W shears	Mulden Group F2 (north-verging recumbent folds) S2 (crenulation cleavage)	F2 (disharmonic folds) S2
Post-tectonic intrusion of Salem-type granites (590-570)		Emergence of Tsumeb Subgrp. (karst.) D2 (thrusting)		Mulden Group 580?- 540		karstification I				
D2 in NZ and collision in Kaoko Belt (600) D1 (~650-630)	Drifting (M2) 740-580	D1 (syn-sedimentary faults) Otavi Group (830-760)	Continental convergence in Kaoko region		D1	S1 // S0 (flexural gliding)) F2 (NW-SE-axis) F1 (NNE-SSW-axis)	D1	S1, F1, thrusts	F1 (isoclinal), S1 (axial plane cleavage)	F1 (disharmonic folds)
deposition of Otavi Group 730-~650		Northern Platform		Otavi Group 740?- 580?	D0b	slumping, growth faults				
End of rifting stage: 840-730	Rifting (M1) 770-740	Rifting Nosib Grp. (ca.1000 - 840)	Rifting stage	Nosib Group 780-740[1]	D0a	basement faulting (horst-graben)		normal faults		

Table 2.1: Structural evolution of the OML (modified after cited references); ages in Ma (1) Burger and Coertze, 1973; Hoffman et al., 1996; 2) Goscombe et al., 2004; 3) Haack et al., 1980; Haack, 1983); D: deformation, F: folding, L: lineation, M: metamorphism, OVR: Otavi Valley Rupture, S: schistosity.

the Swakop Group over the Otavi Group SE of Otavi (Fig. 2.2). The proceeding closure of the Khomas sea with subduction of the Kalahari under the Sao Francisco-Congo Craton (Miller, 1983; Kukla and Stanistreet, 1991) led to uplift and karstification of the Otavi Group (Miller, 1983). At least one phase of folding of the Otavi Group took place prior to the deposition of the molasse-like Mulden sediments on the boundary between the late Ediacaran and Early Cambrian (Deane, 1995; Hoffmann et al., 2004), followed by karstification of parts of the carbonate succession (Frimmel et al., 1996b).

The collision of the Kalahari and Sao Francisco-Congo Cratons caused the main deformational event in the OML (D2) (K3 according to Coward, 1983; D3 according to Porada, 1989; D2 and D3 according to Maclaren, 1991; D2 according to Frimmel et al., 1996b; D1 and D2 according to Deane, 1995) accompanied by up to greenschist metamorphic conditions in the southernmost OML (Innes and Chaplin, 1986; Frimmel et al., 1996b) and very low-grade metamorphism in the Mulden Fm of the Ovambo Basin north of the OML (Clauer and Kröner, 1979) with a peak metamorphism around 535-530 Ma (Goscombe et al., 2004). Goscombe et al. (2004) described metapelites, overprinted by amphibolite facies metamorphism (estimated peak-T: 635°C at 8.7 kbar), from the eastern Northern Zone, 50 km SW of Otavi, supporting the southward increasing grade of metamorphism towards the Central Zone of the Damara Belt (Coward, 1981). According to Coward (1981) granite intrusion and high temperature metamorphism in the northern and central section of the Damara Belt controlled the style and deformation intensity of the D1 and D2 structures. The dominating structures caused by D2 are the E-trending large-scale folds (Weber et al., 1983), which are open to tight and upright to northward vergent in the southern OML (Coward, 1981) (Fig. 2.3). Coward (1981) justified the onset of these structures as syn-D1, based on a first cleavage (S1) in the OML, which is comparable to the S1 in the Kaoko Belt that had higher deformation syn-D1. Further prominent features are thrusting to the north (Coward, 1981) and strike slip movements along Damaran lineaments (Coward, 1983). Deane (1995) described a variable intensity of the D2 in the southern OML and postulates thrusting of Otavi Group units with a relatively higher temperature onto the Mulden Group. West of the OML Coward (1981) described westward verging recumbent folds with a well

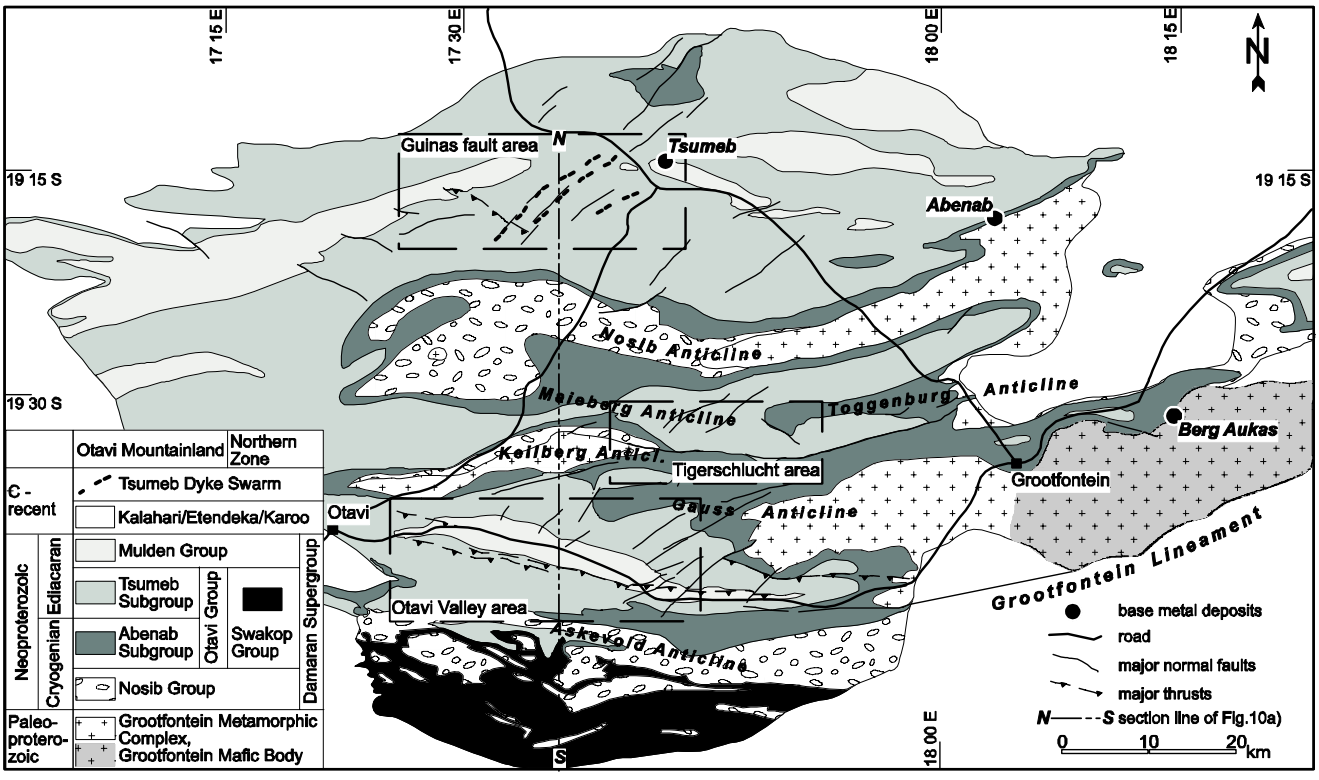

Fig. 2.2: Regional Geology of the OML compiled after Geological Survey of Namibia (GSN, 1999) and own mapping; dashed frames represent key areas for this study.

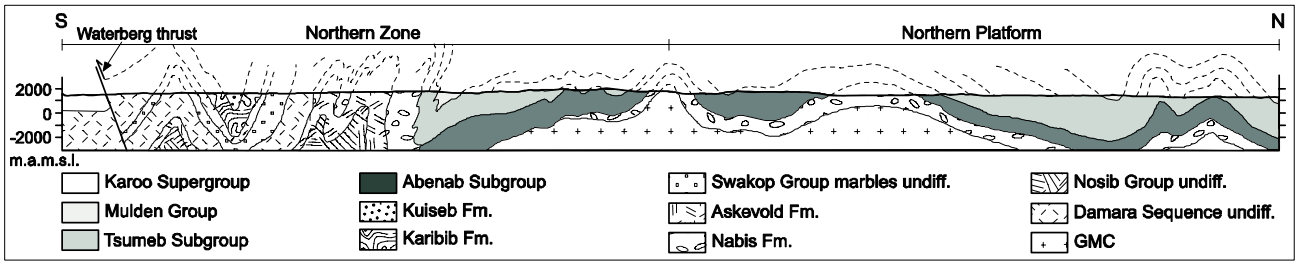

Fig. 2.3: Structural section across the Northern Platform, OML area (redrawn after Miller, 1983).

developed cleavage and ENE-trending mineral lineation. Fault inversion and thrusting of the upper Tsumeb Subgroup (Table 2.1) over the Mulden Group in the northern OML confines the thrusting event probably to the Early Cambrian (Laukamp et al., 2006). In the Kamanjab Inlier (Fig. 2.1) a higher grade Swakop Group was thrusted northwards onto lower grade Mulden schists (Coward, 1981).

During the Cambrian and Ordovician the Northern Zone of the Damara Orogen underwent a further uplift indicated by K-Ar cooling ages of ca. 300°C at ca. 481 ± 25 Ma (Haack, 1983). Dominating structures of this D3 event (D3 according to Miller, 1983 and Deane, 1995; D4 according to Maclaren, 1991) were NE-SW-striking normal faults, which were part of an extensional fault system (Laukamp et al., 2006). Frimmel et al. (1996a) described NE-trending cross warps (interference folds), but no penetrative cleavage. Deane (1995) reported NW-trending open to upright warps and estimates the age of D3 as late Ordovician. Related to these processes was the last regional metamorphic event in the Northern Platform, which is of middle Ordovician age and is recorded in the Mulden phyllites NW of the OML (Haack et al., 1980; Haack, 1980) and phyllites and schists of the Mulden Group in the Kombat area (K-Ar, fine mineral fractions < 2µm, Ahrendt, 1983). Unrug (1983) postulated a transformation of the compressional regime to a predominantly strike-slip translation in the waning stages of the Pan-African orogeny, expressed by the ENE-trending lineaments in the Damara Belt.

Coarse clastic sediments, deposited within NE-striking half-graben structures in the Northern Zone, support an Early Mesozoic tectonic reactivation of the regional lineaments in the Damara Belt (Raab et al., 2002). The post-Damaran reactivation of these structural trends is demonstrated by NE-trending dyke swarms in the Northern OML, which are presumably of a late to post-Karoo age (Söhnge, 1957).

2.2.3 Influence of the basement on the structural evolution of the OML

The Grootfontein Inlier forms the pre-Damaran basement of the OML and is part of an Eburnean Orogen at the southern margin of the Sao Francisco-Congo Craton (Thomas et al., 1993, Fig. 3; Part 3). Söhnge (1972) suggested that the basement highs (e.g. Grootfontein Inlier) exerted a strong influence on the depositional environment and tectonic structures. The influence on the tectonics is implied by more intense folding of the Damaran sediments in the Northern Zone of the Damara Orogen, just south of the Grootfontein lineament, compared to the gentle folding on the Northern Platform. The Grootfontein Lineament marks the southern scarp of the Paleoproterozoic basement high, separating the Otavi Carbonate Platform in the North from the Damara Basin in the South (Maclaren, 1991). A pre-Damaran metamorphism in parts of the Grootfontein Inlier and a medium grade Pan-African overprint are evident, but there is no direct age-dating available for deformation and metamorphism. Thrusting of the Grootfontein Metamorphic Complex onto overlying, folded, weakly metamorphosed Damaran carbonates was reported from the highly tectonised zone of the Tsumkwe Complex in the eastern prolongation of the Grootfontein Inlier at the border of Namibia and Botswana (www.mountburgess.com, Jan. 2006). Singletary et al. (2003) proposed a $^{40}Ar/^{39}Ar$ age of 533 ± 2.3 Ma for the metamorphically induced resetting of igneous muscovite in the presumably Paleoproterozoic Quangwadum Complex in north-western Botswana, lying in the north-eastern strike of the Grootfontein Inlier. The overprint was referred to north-vergent thrusting (Singletary et al., 2003).

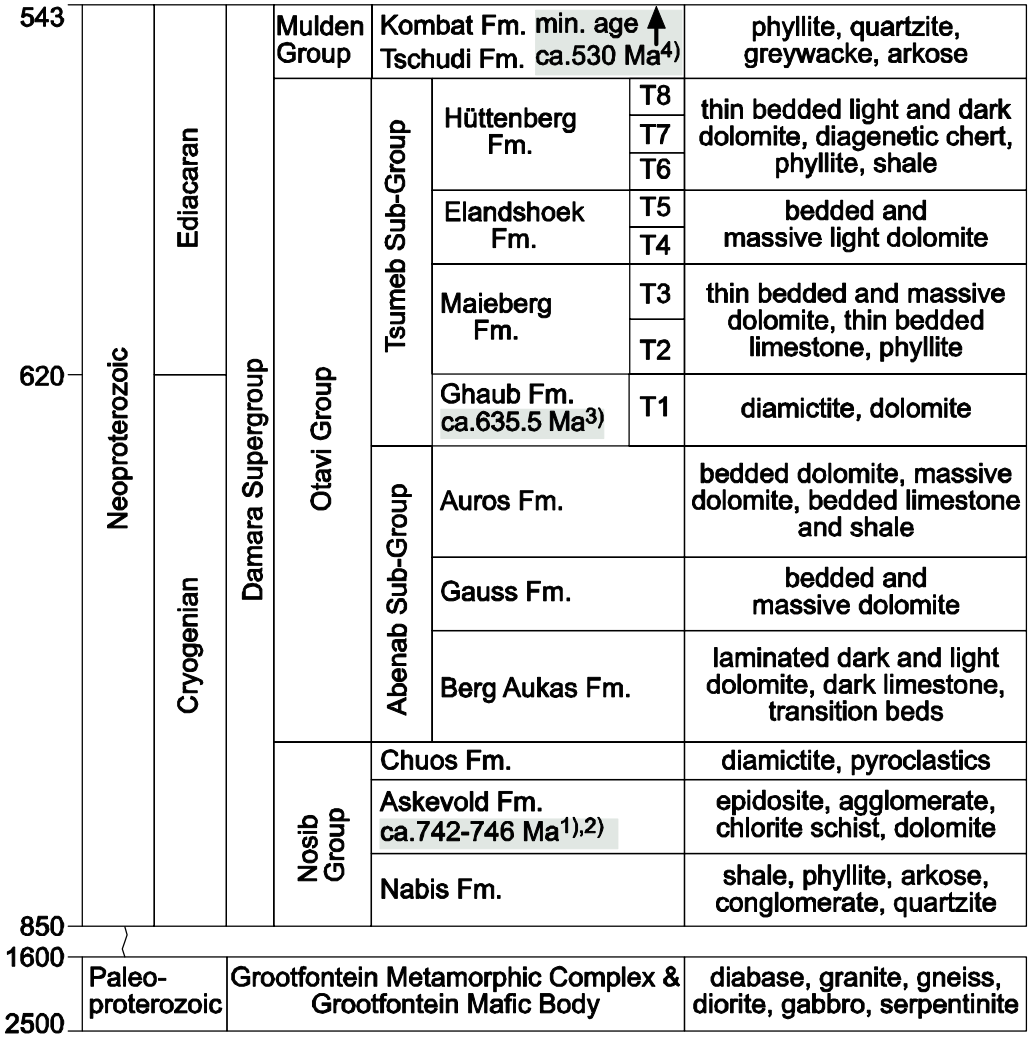

Table 2.2: Stratigraphy of the OML modified after Geological Survey of Namibia (GSN, 1999) with ages of distinct strata. [1)]Burger and Coertze, [2)]Hoffman et al., 1996, [3)]Hoffmann et al., 2004, [4)]Melcher et al., 2003.

2.2.4 Stratigraphy and deformation of the OML - the Damara Supergroup

The Damara Supergroup in the OML consists of conglomeratic siliciclastic sediments, with intercalated mafic volcanics at the base (Nosib Group), overlain by platform carbonates (Otavi Group) and by the molasse-like Mulden Group at the top (Hedberg, 1979) (Table 2.2). Sediments of the Nosib Group were accumulated in EW-striking grabens in the southern, central and eastern OML (Fig. 2.2). Occurrences of metavolcanics (Askevold Fm) and diamictites (Chuos Fm) are known from the southern OML (Söhnge, 1957) and in the Nosib Anticline (Söhnge, 1957) and can be accompanied by ironstones and dolostones. The Askevold Fm corresponds to the Naauwpoort Fm in the Northern Zone of the Damara Orogen (U-Pb zircon ages: 742 ± 25 Ma, Burger and Coertze, 1973; 746 ± 2 Ma, Hoffman et al., 1996), which indicates an early Cryogenian emplacement age for the metavolcanics in the OML. Söhnge (1957) and Van der Merwe Smith (1959) discussed a primary intrusive or sheared contact between the Askevold Fm and the siliciclastics. The contact to the surrounding lithologies is commonly masked by folding and thrusting (Brandt, 1955; Schoch, 1958), due to the Pan-African orogeny. Sandstones and shales of the Nabis Fm and diamictites of the Chuos Fm were locally deformed by intense shearing (Söhnge, 1957; Coward, 1983). Northward overturned folding was reported from the southern

limb of the Nosib Anticline (Söhnge, 1957).

The Otavi Group comprises dolostones, intercalated with limestones and shales. The lower Abenab Subgroup is separated from the upper Tsumeb Subgroup of the Otavi Group by diamictites of the Ghaub Fm (Table 2.2). The Formations of the Tsumeb Subgroup are subdivided in 8 lithozones (T1 – T8) (Söhnge, 1957 amongst others). The Nosib Group and the basal parts of the Abenab Subgroup partially exhibit an onlap onto a basement high (Söhnge, 1957; Hedberg, 1979). Ash layers interbedded in the Ghaub Fm in central Namibia reveal an age of 635 ± 1.2 Ma (U-Pb zircon, Hoffmann et al., 2004) and limit the time of deposition of the Abenab Subgroup to the Cryogenian. Thrusting occurred preferentially in shale horizons of the Auros Fm of the upper Abenab Subgroup (Table 2.2) and Hüttenberg Fm of the upper Tsumeb Subgroup (Söhnge, 1957; Verwoerd, 1957: Abenab area; Osterman, 1990: Guinas Fault area). This resulted in "tectonic squeezing" into under- and overlying dolomites (Söhnge, 1957). Besides dolostones and limestones, the Tsumeb Subgroup is characterised by synsedimentary breccias in the Maieberg and Elandshoek Fms. and cherts and shales in the Hüttenberg Fm (Söhnge, 1957). Growth faulting in the lithozones of the upper Tsumeb Subgroup (King, 1990; Petzel, 1993; Laukamp et al., 2006) indicates synsedimentary deformation in several areas.

The lower Mulden Group (Tschudi Fm) consists of quartzites, greywackes and arkoses. Basal parts of the Tschudi Fm are deposited in karst pipes and these sandstone bodies were sometimes deformed into large boudins (e.g. Tsumeb West according to Söhnge, 1972; Tsumeb Pipe, Kombat). Phyllites of the Kombat Fm, only evident in the southern OML (Otavi Valley), are assigned to the Mulden Group as well. Piercement structures of the phyllites in the Otavi Valley indicate a pre- to syn-Pan-African deposition (Deane, 1995). The Mulden Group overlies the Otavi Group unconformably (Söhnge, 1957) and deposition presumably started during (Maclaren, 1991) or after (Innes and Chaplin, 1986) the syn-D2 main folding event. Sheared contacts were reported from the north-western OML (Tsumeb mine and North Bobos prospect: Söhnge, 1957; Tschudi mine: Hiveluah, pers.comm. 2004).

The Damara Supergroup shows a general E-W-strike of the large scale folding (Söhnge, 1957; Fig. 9 in Hedberg, 1979), intersected by older (Weber and Ahrendt, 1983) or younger N-S-striking cross folding (Frets, 1969; Guj, 1970; Miller, 1980). According to Söhnge (1972) the prominent E-W- and NE-SW-striking tectonic structures trace the pre-Pan-African tectonic framework of the basement. Thrusting was reported mainly from the southern OML (van der Merwe Smith, 1959; Deane, 1995), but is also evident up to the northern OML, e.g. in the Tsumeb Pipe (Lombaard et al., 1986) and in the Guinas Fault area (Laukamp et al., 2006). Most thrusts and a penetrative cleavage are bedding parallel or cut the strata at an acute angle, where dragfolds are disrupted (Söhnge, 1957; 1972). A penetrative cleavage is dominant in limestones, calcified dolomites, calcitic and graphitic matrix of breccias, and feldspar-rich quartzites of the karst pipes (Hughes, 1979). According to Hedberg (1979) the flexural slip was concentrated in the Berg Aukas, Auros and Maieberg Fms., which contain larger amounts of limestone and shale in comparison to other formations of the Otavi Group. Silicified oolitic horizons of the upper Otavi Group in the central and north-western OML were tectonically deformed with a maximum principal stretch ratio of 2 (Laukamp et al., 2004). Söhnge (1972) and Innes and Chaplin (1986) reported tectonically induced repetition of the Damara Supergroup. Dragfolding, which was described from the Nosib and the Otavi Group, is more common in thin-bedded and less competent formations (Söhnge, 1957) and was interpreted in the southern OML to be a component of a left-lateral displacement, causing a mylonitisation of the phyllites of the Kombat Fm (Deane, 1995).

2.2.5 Key areas

2.2.5.1 Guinas Fault

The Guinas Fault is positioned in the north-western OML, approximately 22 km south-westwards of the Tsumeb Mine (Fig. 2.2). Outcropping strata comprise the lithounits T4 to T8 (Elandshoek and Hüttenberg Fms., Tsumeb Subgroup; Table 2.2) and the basal successions of the Mulden Group. Synsedimentary deformation was reported from T6 up to T8 (Veldsman, 1977; Petzel, 1993). The Neoproterozoic carbonate platform was affected by at least two phases of karsting. Dominating structural patterns are E-W-striking large-scale folds with amplitudes up to 7 km, which are in the north-western part due to NNW-SSE contraction (Veldsman, 1977) and the NW-striking

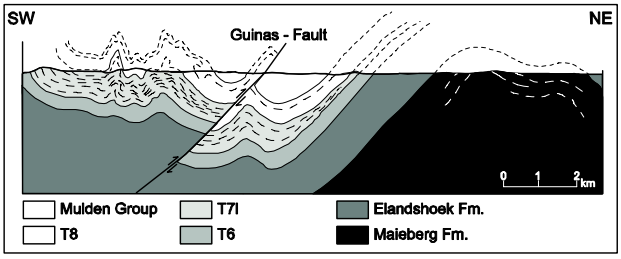

Fig. 2.4: Cross section through the Guinas Fault area (redrawn after Veldsman, 1977).

Guinas Fault (Fig. 2.5). Parallel aligned thrusts occur NE of the Guinas Fault, whereas the south is pervaded by penetrative foliation (Veldsman, 1977, Fig. 2.4). E of Karavatu (Fig. 2.5) the Heidelberg Lineament (Söhnge, 1976) comprises an about 3.5 km wide shear zone that strikes NE-SW (Veldsman, 1977). Mean values of the structural data of Veldsman (1977) are given in Fig. 2.12. Characteristic of this area are deep penetrating karst pipes, which attain at the Tsumeb pipe a depth of at least 1400 m (Lombaard et al., 1986). The karst pipes were largely filled by siliciclastics of the Mulden Group and are a typical host to base metal mineralisation. Söhnge (1957) reported NE-striking kersantite and tholeiitic dykes (e.g. Tsumeb Dyke Swarm, Fig. 2.2) of presumably Karoo-age, which could indicate a post-Damaran reactivation of NE-trending structures. Jointing occurs in E-, NW- and NE-striking directions (Botha, 1958).

2.2.5.2 Tigerschlucht

The Tigerschlucht area is located in the central OML (Fig. 2.2). The dominating structure is an E-W-striking regional fault ("Uitsab Fault", Maclaren, 1991), which juxtaposes the Gauss and Auros Formations of the upper Abenab Subgroup in the South against the T3 to T5 lithozones (Maieberg and Elandshoek Formations) of the Tsumeb Subgroup in the north. Maclaren (1991) proposed a downthrow of about 1500m to the north and a prolongation of this north-dipping structure into the northern Keilberg anticline. Like in the northern OML, the E-W-striking large scale folding is a prominent feature. Small-scale deposits of a Berg Aukas-type mineralisation (Pirajno and Joubert, 1993) are scattered mainly in the Tsumeb Subgroup in the northern part of the Tigerschlucht area, but are known also locally in the southwards sited Driehoek prospects (Misiewicz, 1988).

2.2.5.3 Otavi Valley

The third key area comprises the Otavi Valley in the southern OML (Fig. 2.2). With the exception of the T7 lithounit, the whole succession of the Tsumeb Subgroup is exposed on the flanks of the Otavi Valley. The central part is overlain by the Kombat Phyllites, which are unique to this location and are presumably related to the Mulden Group (Söhnge, 1957). A northward overturned fold that is presumably ruptured along a WNW-ESE-striking structure at deeper levels of the Otavi Valley (Otavi Valley Rupture according to Maclaren, 1991 and Deane, 1993) influences the carbonate successions and the phyllites. Tectonic repetition induced by northward thrusting is evident from the southern fold hinge (Innes and Chaplin, 1986), whereas gentle open folds occur at the northern limb (Söhnge, 1957). Deane (1995) reported from the Kombat workings monoclinal folds due to the Pan-African orogeny, which host base metal deposits in the fold hinge. These features are displaced by a NE-striking fault system (Innes and Chaplin, 1986). South of the Otavi Valley in the Askevold anticline (Fig. 2.2) Maclaren (1991) reported crenulation cleavage parallel to the axial plane of north-vergent folding. The Otavi Valley marks a transition in metamorphic grade from an anchizonal to lower greenschist facies influenced carbonate platform in the North to upper greenschist facies south of the Otavi Mountains and finally to medium grade metamorphic conditions in the northernmost Northern Zone of the Damara Belt (Goscombe et al., 2004). According to Deane (1995) the Otavi Valley originated from one of the subbasins, which pervade the Grootfontein Inlier in an approximately E-W-direction. The deformational history of the Otavi Valley was summarised in Deane (1995) and compared with our results in Table 2.1. Misiewicz (1988) assumed the Grootfontein Lineament (Fig. 2.2) as the southern scarp of the basement high of the Grootfontein Inlier that could extend into the Otavi Valley.

2.2.6 Base metal mineralisation

The OML comprises a variety of base metal deposits and occurrences in Neoproterozoic carbonates, which are structurally controlled. An overview on the two main types of primary base metal mineralisation, the Berg Aukas- and the Tsumeb-type, is given in Frimmel et al. (1996a), Melcher et al.

	Berg Aukas-type	Tsumeb-type
Host-rock	Abenab Subgroup and lower Tsumeb Subgroup	Elandshoek and Hüttenberg Formations (dolomites), T4 through T8 zones
Shape of orebody	Stratiform lenses, discordant breccias	Discordant pipe, filled with breccia and sandstone; structural control
Ore mineralogy	Sphalerite, galena (pyrite, chalcopyrite, tennantite)	Tennantite, galena, sphalerite, pyrite, bornite, chalcopyrite, germanite
Ore geochemistry	Zn>Pb; low Cu, Ag, As, Ge, Ga, Cd	Pb>Cu=Zn, Considerable As, Ag, Cd, Ge, Ga, W
Fluid inclusions	ca. 23 wt.% NaCl eq., 137 to 255°C	22.3 wt.% NaCl eq., >212°C (dolomite III)
Fluid source	Basinal brines	Orogenic fluids
Age	635 to 750 Ma ?	460 to 530 Ma?

Table 2.3: Major types of base metal sulphide deposits in the OML (modified after Melcher et al., 2006 and references therein).

(2006) and Pirajno and Joubert (1993) and summarised in Table 2.3. The stratabound Berg Aukas-type mineralisation comprises hypogene Zn-Pb dominated sulphides. Pb-, Cu- and Zn-sulphides are the major constituents of the Tsumeb-type mineralisation, which is hosted by discordant breccia pipes. The published ages of the ore deposits in the OML, mostly based on galena Pb-Pb model ages (a method now considered geochronologically not reliable), vary from middle to late Ediacaran (e.g. Haack, 1993; Frimmel et al., 2004). Melcher et al. (2006) estimate a middle to late Cryogenian age for Berg Aukas-type mineralisation and Cambrian to Ordovician age for Tsumeb-type mineralisation (Table 2.3). A preliminary study based on Re-Os isotopic dating of the Ge-rich sulphide ore from the Tsumeb Pipe (Melcher et al., 2003), assigns to this mineralisation type a model age of about 530 Ma (Re-Os, Melcher et al., 2003). No absolute dating exists for the Berg Aukas-type ores. However, a recent study carried out on the Zn-silicate willemite derived from Berg Aukas-type sulphides, resulted in Rb-Sr ages ranging from 562 to 436 Ma for these secondary minerals (Part 5). The obvious consequence of these data is the older age of the primary sulphides. Two major models for the timing of the Berg Aukas-type base metal mineralisation are discussed in the literature, which can be summarised as follows: emplacement 1) prior to (Pirajno and Joubert, 1993) or 2) during the Pan-African orogeny (Hughes, 1979).

Considering the driving factors for the circulation of base metal bearing hydrothermal fluids for both mineralisation types, the first modern theory is due to Miller (1983b). In his model, hydrothermal fluids for both mineralisation types were generated during the prograde metamorphism of the Pan-African orogeny. The fluids could have then moved along thrust zones toward the low-T northern and southern marginal zones of the Damara Belt. This model is very similar to Oliver's (1986) model of tectonically induced expulsion of fluids from orogenic belts. Pirajno and Joubert (1993) support a basin-dewatering model only for the Berg Aukas-type mineralisation, whereas they consider the later emplaced Tsumeb-type mineralisation as caused by Cu-bearing fluids generated in a further evolved metamorphic stage. During the Tsumeb-type ore stage there is evidence for some remobilisation of the Berg Aukas-type mineralisation.

2.3 Results

2.3.1 Guinas Fault

The Guinas Fault area is affected by large scale folding with a highly variable fold axis striking around E-W (Fig. 2.5, 2.6a, 2.6b). Two dominant structures in this area are the NW-striking Guinas Fault in the west and the NE-striking Heidelberg Lineament (Söhnge, 1976). The Guinas Fault divides two structural

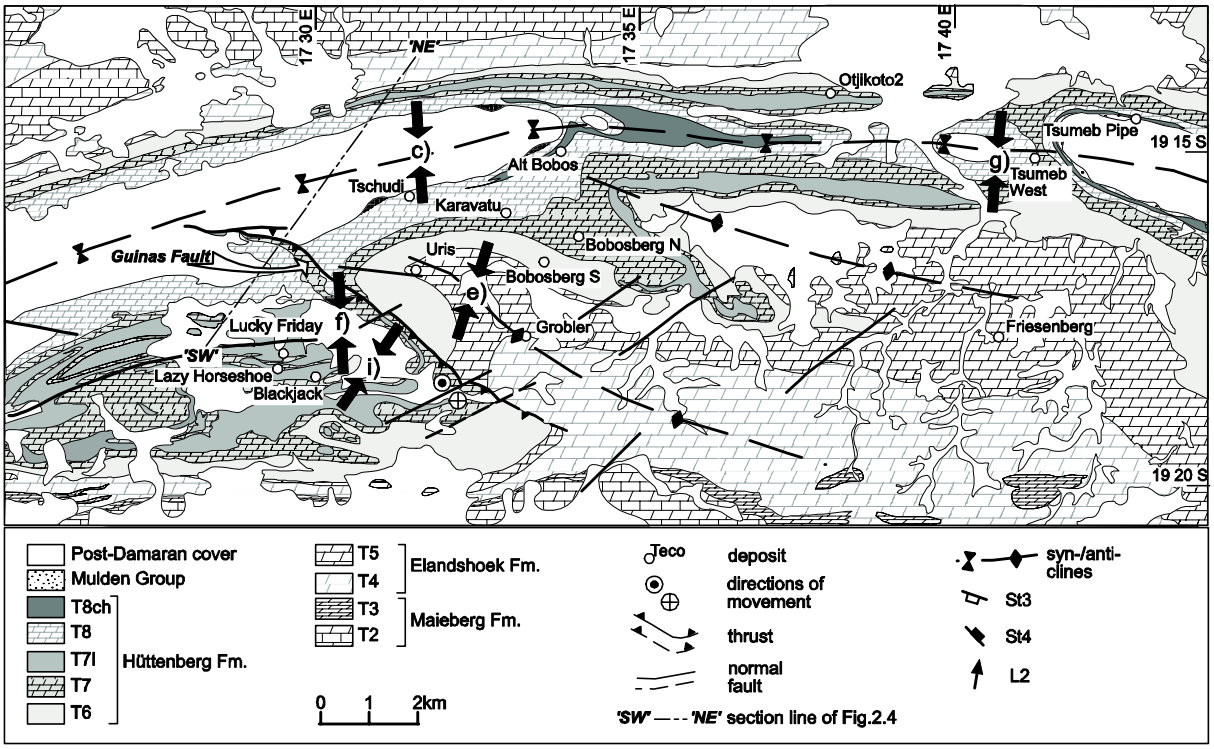

Fig. 2.5: Regional geology of the Guinas Fault area; black arrows show the main shortening direction during D2. Letters refer to Fig. 2.6.

domains. In thin bedded limestones of the T7 lithozone south of the Guinas Fault, a bedding parallel S1 and embedded chert layers are isoclinally folded around a NW-SE-axis and pervaded by a crenulation cleavage S2 (Fig. 2.10a). In dolomites of the T7 a penetrative S2 cuts a bedding parallel S1 with an angle of 25 - 30°. S2 (Fig. 2.6d) is folded around an approximately E-W- to NW-SE-axis. During the development of the isoclinal folding and S2 (D2) the shortening direction is orientated N-S to NE-SW. This is indicated by the orientation of some of the clasts in the mass flow bodies of the T7 lithounit and by small-scale thrusting and nappe stacking in the limestones (Fig. 2.10a). Thrusting south of and along the Guinas Fault cuts the former structures and slickenside lineation indicates a NNE-trending shortening direction (Fig. 2.6i). The Guinas Fault itself comprises a highly silicified oolitic dolomite terminated by a discrete floor thrust. The oolitic dolomites indicate a N-S orientated shortening direction of D2 (Fig. 2.6f). The intensive silicification obliterated the sedimentary pattern and occurred during or after this deformation (Fig. 2.10b).

In contrast to this, north of the Guinas Fault the lithologies contain almost no limestone and a crenulation cleavage is only evident in thin bedded dolomites of the T7 lithozone. The NNE-trending shortening direction is estimated from lineation (L2) preserved on S2 (Fig. 2.6e). The siliciclastics of the Mulden Group contain only one generation of cleavage, which is folded around ENE-WSW and exhibits roughly N-S-striking lineation (Fig. 2.6c). Further to the east in the vicinity of Tsumeb the platform carbonates are intensively tectonised. A penetrative cleavage and thrusts change their orientation at a small-scale (Fig. 2.6h, g), but nevertheless a folding ranging ± 20° around E-W can be observed. S2 is cut by thrusts, which show a lineation striking around N-S (Fig. 2.6g). Parallel to the Heidelberg Lineament, NE-striking normal faults and joints pervade the Guinas Fault area (Fig. 2.6j, k, o). Other major normal fault systems strike especially in the Tsumeb area NW-SE to NNW-SSE (Fig. 2.6l) and in the whole Guinas Fault area to a lesser extent N (Fig. 2.6m). Quartz veining is aligned parallel to the major fault systems (Fig. 2.6m, o) and contains NW- to NE-trending slickenside lineation (Fig. 2.6n).

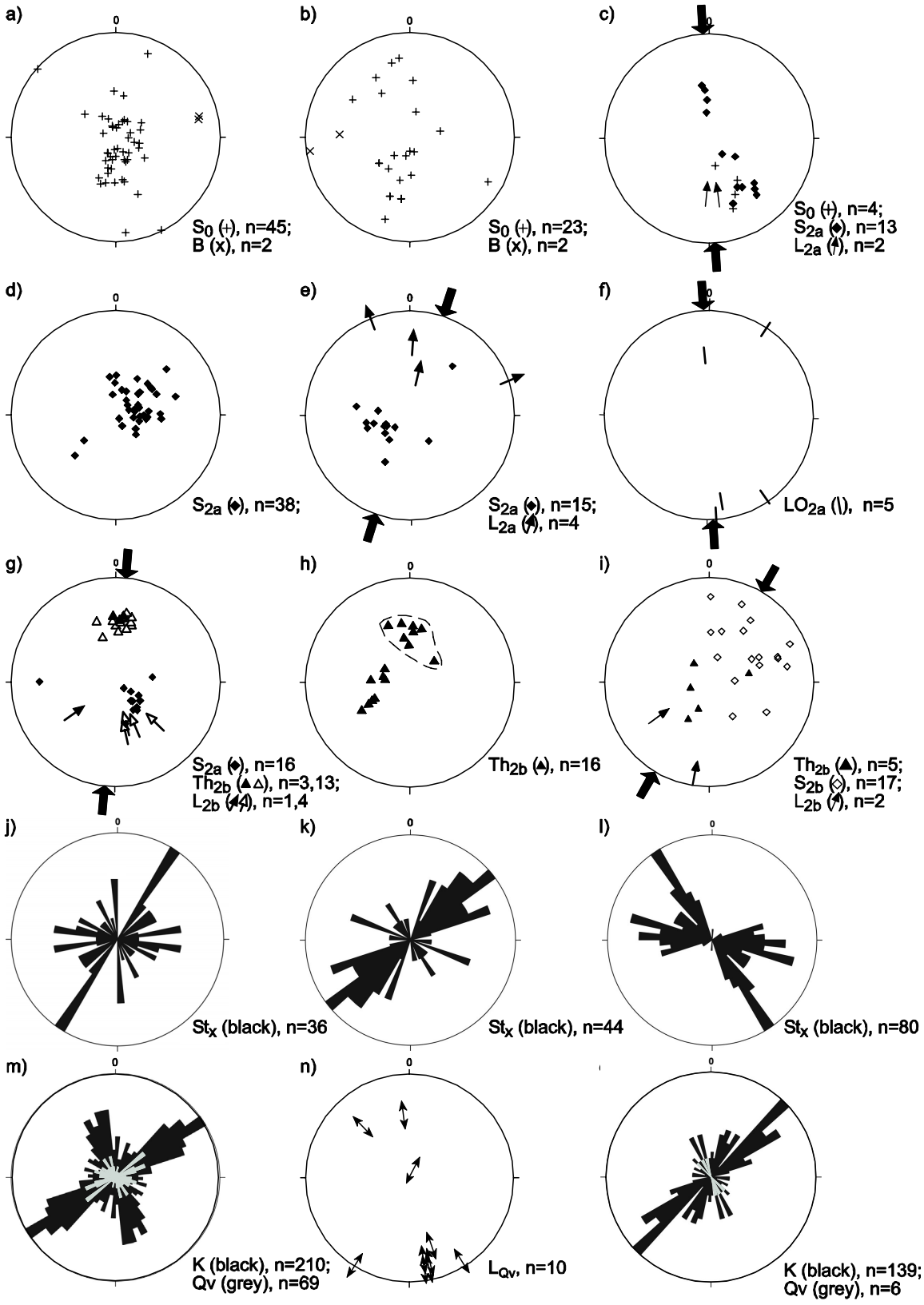

Fig. 2.6: Structural data of the Guinas Fault area: stereonets (a-i, n): equal area projection, lower hemisphere; rose diagrams (j-m, o): strike direction. Abbreviations: B = fold axis (a, b), K = jointing (m, o), Th = thrust plane, Ln = lineation, LO = long axis of elongated ooids (f), Qv = quartz filled joints (m, o), Sn = cleavage, S0 = bedding (a-c), St = normal fault (j-l). Areas: a, e: structural data north of the Guinas Fault; b, g, l, o: structural data of the Tsumeb area, solid symbols in g are measurements from this paper, white filled symbols are from Hughes (1987, Tsumeb Pipe, 35L); c: cleavage and lineation in Mulden Group; d, i, j: structural data south of the Guinas Fault; f: trend of elongated ooids of the Guinas Thrust horizon; h: D2b thrusting at Friesenberg (dashed circle) and Tsumeb West; m: normal faults, joints and quartz veining Guinas Fault area; n: lineation on quartz filling surfaces in the Guinas Fault area. Arrows give the estimated shortening direction.

2.3.2 Tigerschlucht

Large scale roughly E-W-trending folds with amplitudes about 7 to 9 km affect the whole Damaran stratigraphy in the Tigerschlucht area (Fig. 2.7, 2.8d, 2.8e) and are cut by normal faults. Asymmetric, slightly northvergent parasitic folds of decametre scale are found on the large scale folds (Fig. 2.10c).

Affected by the large scale folding is a NW-SE to E-W-striking foliation (Fig. 2.8a, b). This cleavage (S_2) is generated mostly parallel to the bedding and occurs predominantly in shales and limestones of the Auros Formation. S_2 is cut by normal faults (e.g. east of Harasib, Fig. 2.7). Lineations on the foliated surfaces are orientated randomly (Fig. 2.8a, b), but an average orientation of the shortening direction strikes N-S. In oolites of the Auros Formation (T1) in the western part of the Tigerschlucht area, the deformation is concentrated in calcified horizons, resulting in a mylonitisation (Fig. 2.10d). Intensively sheared horizons alternate with almost undeformed ones. Strain analysis of the deformed ooids in the mylonites reveals a N-S elongated, oblate strain ellipsoid (Fig. 2.8a). The close to tight folding around a NW-SE axis is overprinted by the mylonitic foliation. Thin sections confirm the macro scale view of an extreme heterogeneously deformed Auros Formation. Dolomitic and silicified oolites alternate with calcified layers, characterised by an almost complete obliteration of the ooids. The obliteration is mainly caused by grain boundary migration that results in an oblique deformation pattern (Fig. 2.10e) or regionally penetrative foliation. Twin lamellae in the calcite crystals are bent or have an irregular shape. Single sparitic dolomite crystals and recrystallised quartz aggregates, which represent former fillings of the ooids and brecciated dolomitic intraclasts have non fibrous strain shadows. Calcite veins, followed by quartz veining, are cut by the foliation. Stylolites can divide the strongly deformed from the undeformed oolitic layers (Fig. 2.10d, e). Close to the mylonites, the micas in the diamictite unit (T1) are aligned parallel to the bedding and record a syndeformational growth. In the more competent dolomites of the Elandshoek Formation, the cleavage is concentrated in thrusts (Fig. 2.10f). The orientations of the small-scale thrusts in the Tigerschlucht area are shown in Fig. 2.8c. Slickenlines on mica-rich thrust surfaces indicate a northward movement of the hanging wall (e.g. Teco Thrust). This is confirmed by Riedel shear structures (Fig. 2.8c).

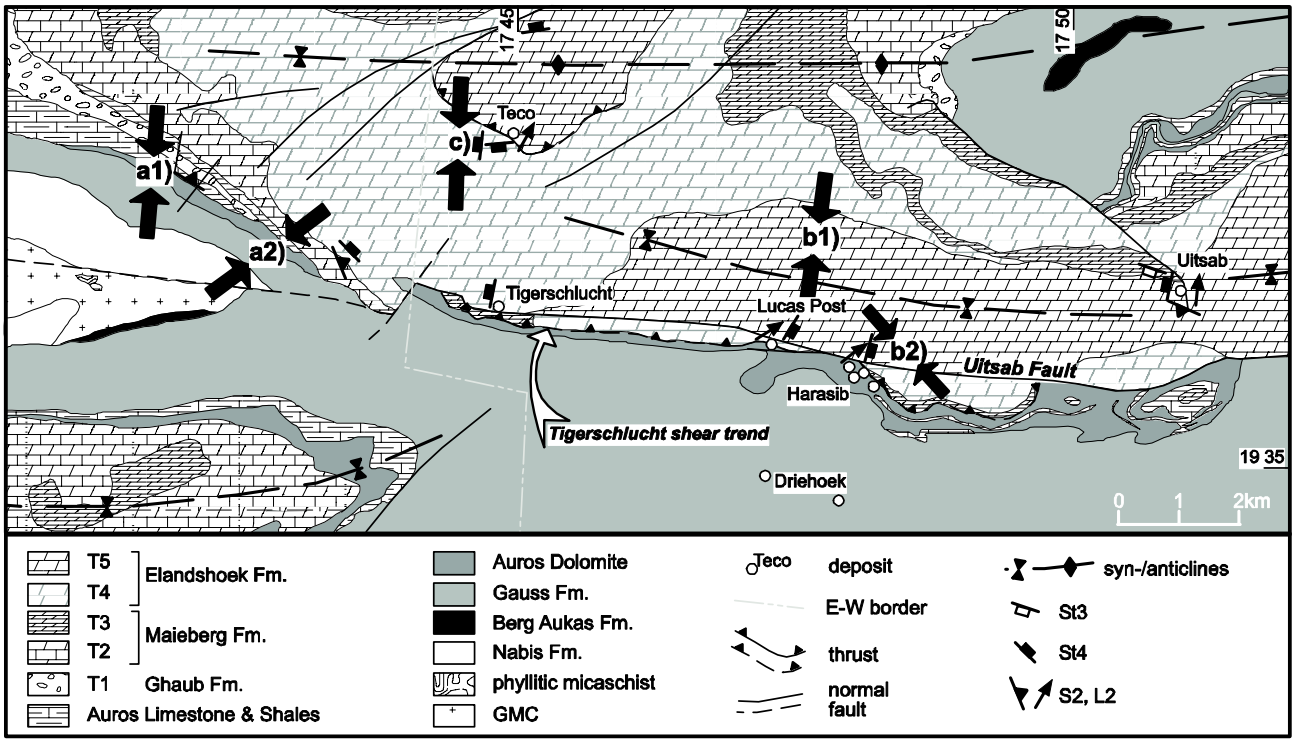

Fig. 2.7: Regional geology of the Tigerschlucht area; Geological map after GSN 1999, Werner (2005) and own regional structural mapping. Black arrows show main shortening direction during D2. Letters refer to Fig. 2.8. Post-Damaran cover sediments not shown.

Growth of quartz and mica accompanied the thrusting and sphalerite occurs along some of the surfaces (Fig. 2.8c: Min).

A detailed geological map of the Tigerschlucht area (Fig. 2.7) shows the E-W- to ESE-WNW-striking Tigerschlucht shear trend as another prominent structural feature in this part of the OML. The E-W-striking Uitsab Fault (Maclaren, 1991) is part of this regional shear trend (Fig. 2.7). The Tigerschlucht shear trend consists of subvertical to northward inclined faults, which regionally branch out like at the Lucas Post deposit. In the eastern part of the map the Tigerschlucht shear trend juxtaposes the Elandshoek Formation in the North against the upper parts of the Abenab Subgroup and the T2 to T4 lithounits. Riedel shear structures show a N- to NNW-downthrow. The Tigerschlucht shear trend can be traced to the Tsumeb-Grootfontein road in the East (GSN, 1999). West of the Tigerschlucht deposit the Tigerschlucht shear trend is displaced to the south and may continue to the West, opposing the Nabis Formation in the North against the basement in the south. Quartz veins that can reach more than 2 m in thickness are aligned parallel to the Tigerschlucht shear trend (Fig. 2.8 f, g, h, i). Striae on fault surfaces in these quartz veins are orientated NNE-SSW.

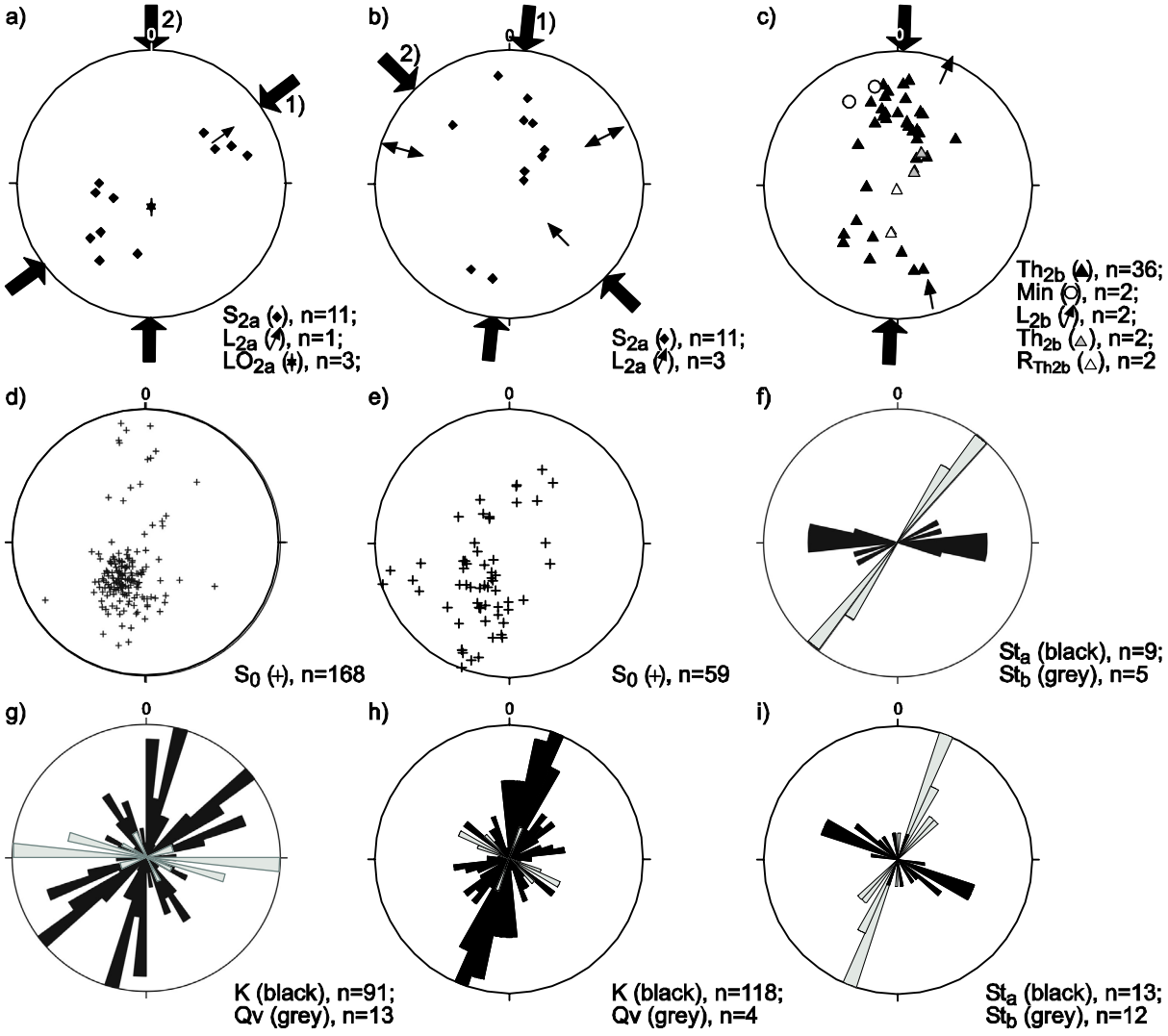

Fig. 2.8: Structural data of the Tigerschlucht area: stereonets (a - e): equal area projection, lower hemisphere; rose diagrams (f - i): strike direction. Abbreviations: Ln = lineation, LO = orientation of strain ellipsoid deduced by strain analysis of deformed oolites, K = jointing, Min = mineralised cleavage, Qv = quartz filled joints, R = Riedel shears, Sn = cleavage, S0 = bedding, St = normal fault, Th = thrust plane. Areas: a, d, f, g: structural data in the western part of the Tigerschlucht area; b, e, h, i: structural data in the eastern part of the Tigerschlucht area; c: thrusting and mineralised cleavage in Tigerschlucht area. Arrows give the estimated shortening direction.

Secondary normal faults (Stb) trend NNE to NW (Fig. 2.8f, i) and cut the first order normal faults (Sta, e.g. Tigerschlucht shear trend). The length of the larger secondary normal faults reaches about hundred metres or more, but shows mostly only very little displacement. The majority of joints are aligned parallel to the secondary normal faults (Fig. 2.8g, h).

2.3.3 Otavi-Valley

A transect through the Otavi Valley clarifies the distinctly different structural domains in respect to the Pan-African tectonic evolution (Fig. 2.9, Fig. 2.11). On the northern side bedding and synsedimentary breccias are preserved in the massive, partly oolitic dolomites of the Elandshoek and Hüttenberg formations. The dolomites show several stages of dolomitisation, dedolomitisation and silicification. Early deformation patterns of the Tsumeb Subgroup are restricted to local open rounded to subangular m-scale folds (e.g. Baltika) and to the gentle large scale folding that affects the whole northern flank of the Otavi Valley. Rare outcrops of the Kombat Formation show crenulation cleavage and contain clasts, which are orientated parallel to the main cleavage (S_2). N- to NNE-striking normal faults pervade the northern limb of the Otavi Valley and cut the penetrative cleavage of the Kombat Fm. A dextral separation along these faults is evident from the outcrop and the map scale (Fig. 2.9, Fig. 2.9g, h).

The Otavi hills on the southern flank of the Otavi Valley consist of horizontal to steep to the south or vertically inclined successions of the Maieberg, Elandshoek and Kombat Formations (Fig. 2.9d). Isoclinal folding around an ESE-trending axis and tectonic thinning can be detected at the map scale (Fig. 2.9) as well at the outcrop scale. Slices of oolitic dolomites (Maieberg Fm) are imbricated in phyllites of the Kombat Formation (Fig. 2.10g). A first cleavage (S1) in the phyllites is to some extent cut and crenulated by a second cleavage (S2) (Fig. 2.9a, Fig. 2.10h) or isoclinal folded, accompanied by a SC-fabric. Pre-S_2 quartz-veins is elongated and boudinaged. Calcite veining occurs parallel to the crenulation cleavage and bedding. South of Karlsruhe (Fig. 2.9) dolomites of the T5 lithozone are disrupted by thrusts, which contain mylonitised internal sediments. Dolomite clasts are surrounded by dolomite rich internal sediments, and are orientated roughly along a NS-axis. Macroscopically and microscopically these very fine-grained dolomitic sediments can be related to the earliest karst fillings of the OML, which are assigned to the Mulden Group (Söhnge, 1972). Isoclinal folding and imbrication of competent into incompetent layers is also seen in the Askevold Range south of the Otavi Valley (e.g. Hohentwiel). Marbles show boudinage whereas most of the strain is consumed by metavolcanics of the Askevold Fm.

Drag folds and thrusting were reported from the workings of the Kombat and Asis mines (Deane, 1995), which are situated at the centre of the Otavi Valley. The Kombat phyllites are isoclinally folded and thrusted over T8-dolomites. Stringers of sandstone are imbricated in the dolomites (Innes and Chaplin, 1986). Bedding (S0) and the penetrative foliation (S2) are folded around a NW-SE axis south of the Otavi Valley (Fig. 2.9a, d) and around a westward inclined axis in the northern limb of the Otavi Valley (Fig. 2.9e). A reliable estimation of the shortening direction during the evolution of the penetrative cleavage is only available from the north-eastern part of the Otavi Valley area (Fig. 2.9: Wolkenhauben) and is based on a distinct lineation orientated around N-S (Fig. 2.9c). Shales of the Auros Fm are tectonically thinned out parallel to the main foliation. D_2 structures are cut by N- to NNE- and ENE-striking normal faults (D_{3a}; Fig. 2.9g) like the Kombat Fault, which cut the primary sulphide ore bodies in the Kombat mining area (Innes and Chaplin, 1986). Dextral strike slip is apparent from the geological map (Fig. 2.9) and, accompanied by silicification, reported from the Kombat Mine (Deane, 1989). The Otavi Valley Rupture pervades the north-western closure of the Otavi Valley (Otavi Pforte, Fig. 2.9). Some of the N- to NNE-striking faults contain post-Karoo karst fillings (e.g. Baltika, Fig. 2.9). The main direction of jointing is parallel to the major normal faults (Fig. 2.9g, i)

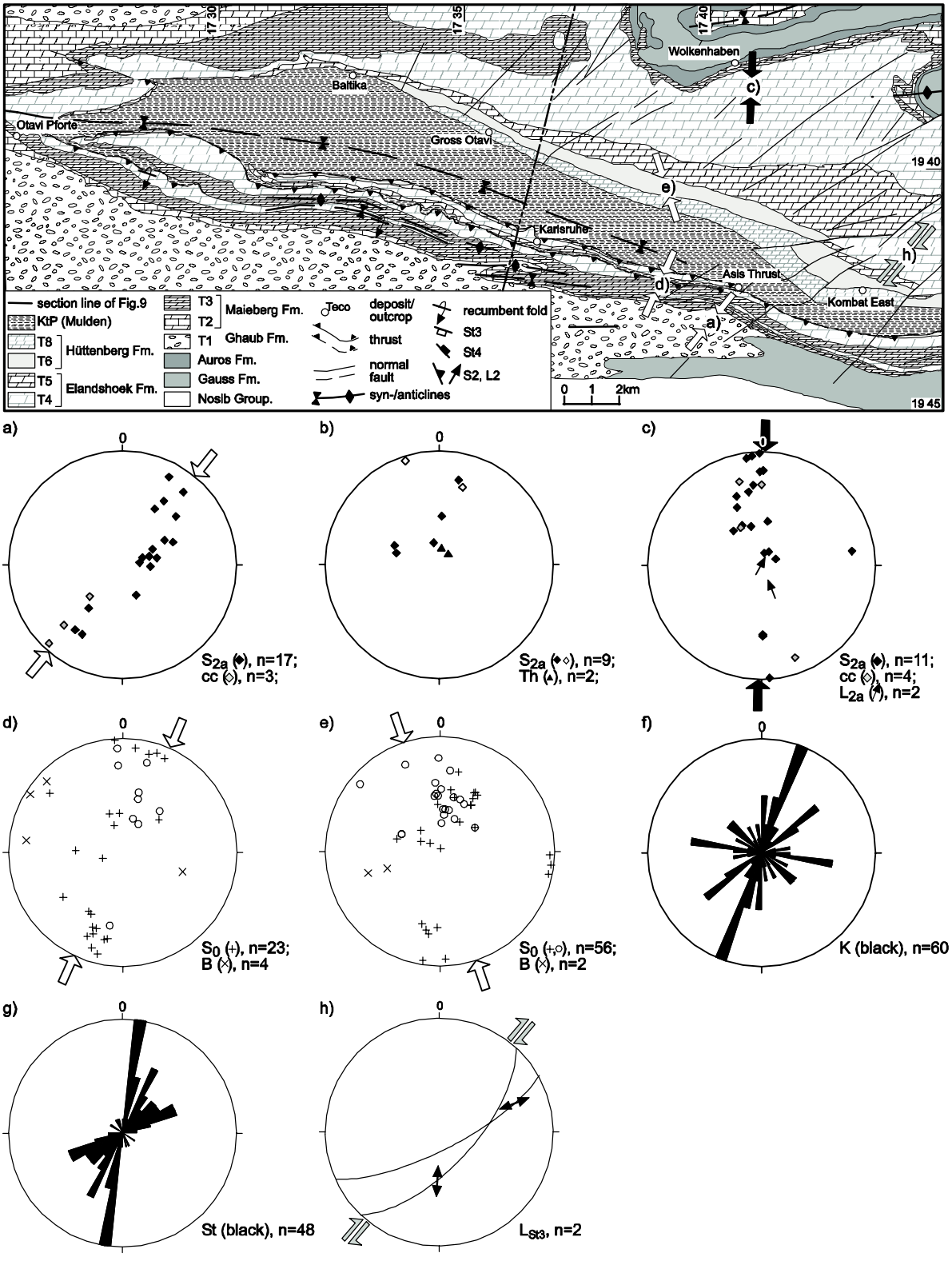

Fig. 2.9: Regional Geology and structural data of the Otavi Valley area: stereonets (a - e, h): equal area projection, lower hemisphere; rose diagrams (f, g): strike direction. Abbreviations: B = fold axis, cc = crenulation cleavage, fee = en echelon structure, K = jointing, Ln = lineation, Qv = quartz filled joints, Sn = cleavage (open diamonds from Petzel, 1992), S0 = bedding (open circles from Petzel, 1992), St = normal fault, Th = thrust plane. Areas: sets a and d: structural data from the southern limb of the Otavi Valley, sets b and e: structural data from the northern limb of the Otavi Valley, c: cleavage and lineation in Wolkenhauben area, f: joints in the Otavi Valley area, g: normal faults in the Otavi Valley area, h: slickenside lineation along dextral faults at Kombat East. Post-Damaran cover sediments are not shown. Arrows give the estimated shortening direction.

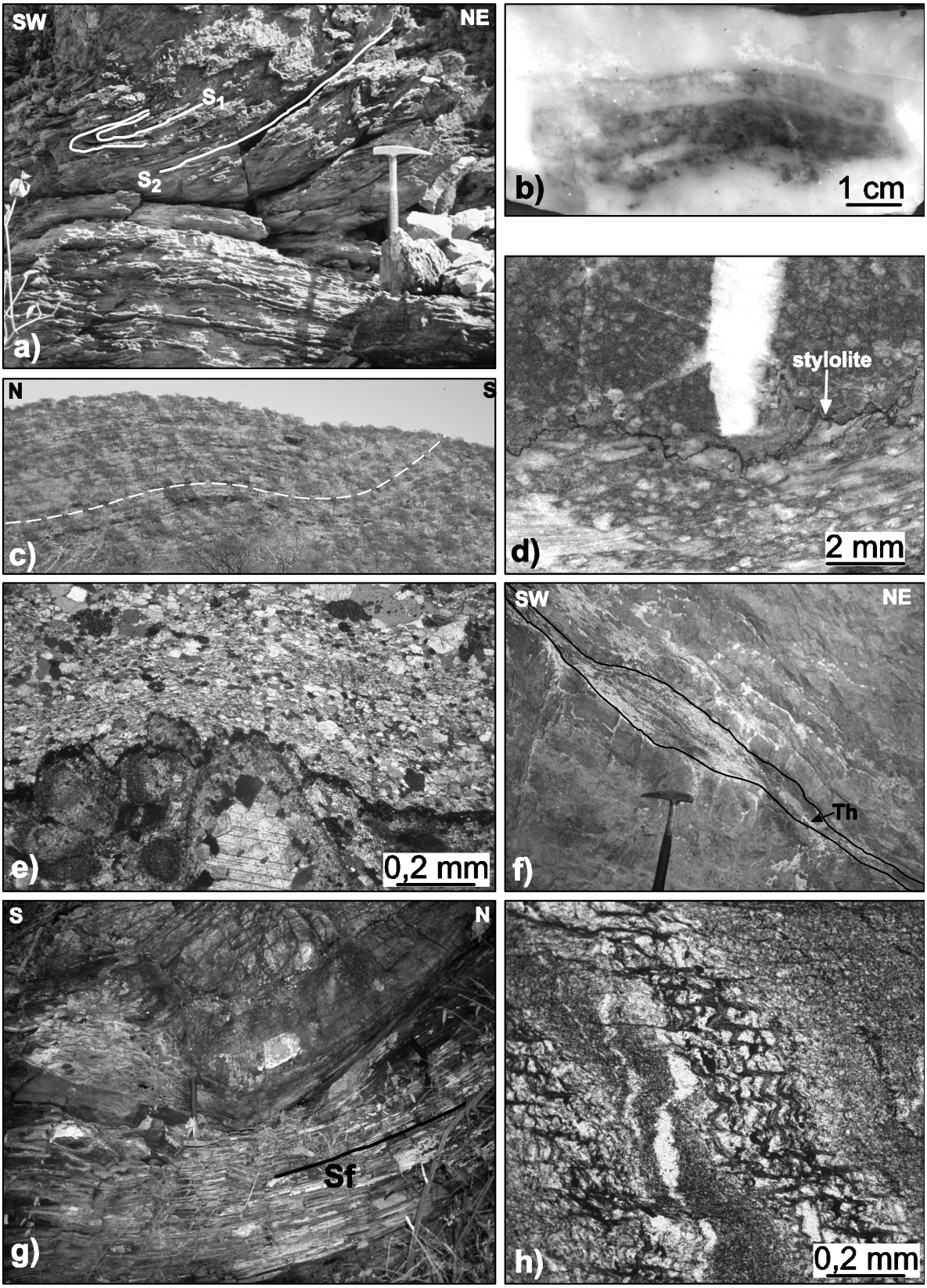

Fig. 2.10: Guinas Fault area: a) crenulated S1 and small-scale thrusting, north of Guinas Fault, b) clast of bedded oolitic dolomite in a silicified thrust horizon, Guinas Fault; Tigerschlucht area: c) large scale folding, north of Teco mineral occurrence, d) stylolite dividing the undeformed oolite in the upper part of the picture from the mylonitised oolite in the lower part, western Tigerschlucht area, scan of hand specimen, e) thin section corresponding to d), oblique foliation in lower part, parallel nicols, f) thrust horizon, Th = thrust surface, Teco mineral occurrence; Otavi Valley area: g) bedding parallel foliation (Sf) in phyllites of the Kombat Formation and imbricated slice of dolomite (T8), Asis thrust, h) crenulation cleavage (cc), thin section, Asis thrust, parallel nicols, a), f), g): hammer for scale.

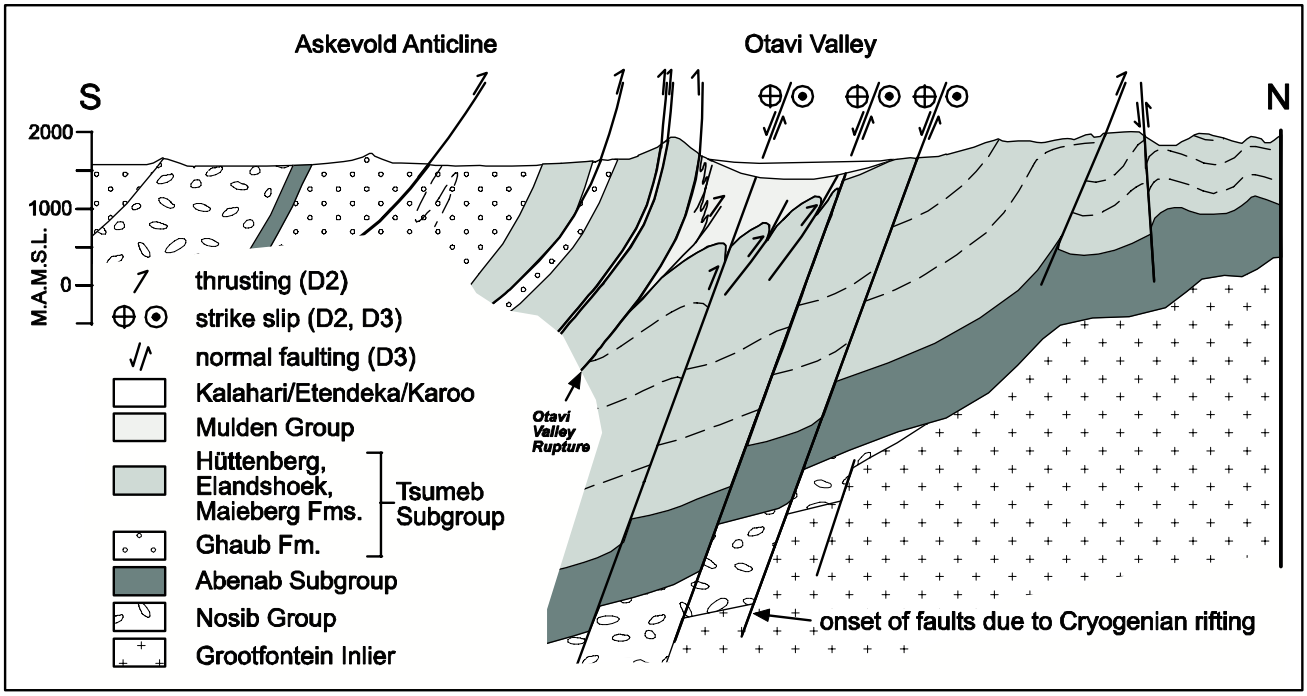

Fig. 2.11: Schematic section through the Otavi Valley (section line see Fig. 2.9).

2.3.4 Basement and quartzitic micaschists

The Paleoproterozoic basement of the OML was deformed during the Eburnean and/or Kibaran orogeny, accompanied by low to medium grade metamorphism (Thomas et al., 1993). Apart from small-scale shear zones and jointing, occurring in some of the diorites and granites, there is no indication of a later tectonic overprint in the examined basement sites. Only the basement in the eastern Tigerschlucht area (Fig. 2.9, Keilberg Farm) consists of foliated gneiss and quartzitic micaschist with a greenschist facies overprint. C-type shear bands pervade the quartzitic micaschist and extraformational hornblende-rich clasts exhibit biotite strain shadows. The precursors of the quartzitic micaschists are siliciclastic rocks, suggested by remnants of allothigene quartz clasts. The quartzitic micaschist occurs together with phyllitic micaschists, both with an approximate south-eastward dipping foliation. The phyllitic micaschists are positioned in the hanging wall of the basement and are not comparable to any other lithologies of the Damaran Supergroup in the OML. Nevertheless, these units could have served as a major detachment zone between the basement and the overlying Damara Supergroup. A similar relationship of the basement and overlying Katangan metasediments is reported from the Lufilian Arc (De Swardt and Drysdall, 1964; Unrug, 1983).

2.4 Discussion and conclusions

2.4.1 Synsedimentary deformation

The depositional environment of the Otavi Group can be summarised as a Neoproterozoic carbonate platform that developed on an unstable pre-Damaran basement high on the southern margin of the Sao Francisco-Congo Craton. Pre- and early-Damaran rift tectonics continued not only during the deposition of the Nosib Group but also thereafter and led to a distinct relief with highly variable depositional environments. Reefs composed of stromatolites and microbial mats rest on basement highs, which were characterised by a high relief. To the west and south the platform gradually deepened and was characterised by small-scaled basins, which approximately follow the E-trending Cryogenian rift structures.

Synsedimentary deformation is evident in various locations of the OML throughout the Tsumeb Subgroup. Debris-flow, talus and storm breccias are known from the Maieberg and the Elandshoek Fms. (Deane, 1993; Söhnge, 1957) and mass flow breccias were reported from the Auros Fm and the diamictites of the Ghaub Fm (Werner, 2005) as well as from the

Hüttenberg Fm (Laukamp et al., 2006). Werner (2005) assumed earthquakes as trigger for the development of mass flows in the Ghaub Fm. Slumping structures and decimetre-scale normal faulting are preserved in the Hüttenberg (Petzel, 1993) and Elandshoek Formations. Growth faulting in the Guinas Fault area is suggested by distinct thickness variations of the same lithozones south and north of the Guinas Fault and mass flow bodies south of the Guinas Fault, which contain clasts of carbonate sediments from the north-eastern area (Laukamp et al., 2006). Deformations during deposition of the Mulden Group were induced by the main phase of the Pan-African orogeny (D2) and are discussed in the respective section.

Most authors considered the southern margin of the Sao Francisco-Congo Craton as a passive plate margin during the deposition of the Damara Supergroup (Miller, 1983a; Prave, 1996). Prave (1997) stated that synsedimentary deformation during the deposition of the Otavi Group on the Northern Platform, such as metre- to decametre-scale extensional faulting, would be no evidence for synsedimentary tectonics caused by early-Damaran rifting (Dürr and Dingeldey, 1997). However, growth faulting in the north-western OML could have been related to gravity or tectonic driven extensional faulting at the western slope of the Otavi Carbonate Platform margin.

2.4.2 D1

The first deformation of the Otavi Platform carbonates, induced by the Pan-African Damaran orogeny, comprised folding around NNE-SSW (F1) and NW-SE (F2). A bedding parallel first cleavage (S1) is evident from the Hüttenberg Fm of the Guinas Fault area. As the penetrative cleavage in the Mulden Group is aligned parallel to the S2 of the underlying T8 lithozone, it is related to D2, the main deformational event of the Pan-African orogeny in the OML. This is contrary to the interpretation of Veldsman (1977), who suggested a post-Mulden age of the D1, with the main shortening direction orientated roughly N-S. There are no indications for pre-D2 deformations in the Mulden Group and a post-D1 deposition of the Mulden Group is also suggested by the unconformable contact to the underlying Otavi Group (Söhnge, 1957). Deane (1995) estimated the timeframe of the D1 at about 650 Ma. As the whole Otavi Group was affected by D1 and recent age data report a younger depositional age for the Ghaub Fm (635 ± 1.2 Ma, Hoffmann et al., 2004), we assume a late to post-Cryogenian age for D1. The deduced timeframe of ca. 635 – 580 Ma matches with the accretion of a Coastal Terrane to the Kaoko Belt, which happened immediately before the collision of the Sao Francisco-Congo Craton with the Rio de la Plata Craton (Goscombe et al., 2005).

2.4.3 D2a/D2b

The impact of deformation in the Damara Supergroup caused by D2 is concentrated in less competent rocks like limestones, shales and strongly altered lithologies (e.g. calcified dolomites) as suggested by earlier studies (Hughes, 1979; Coward, 1983; Petzel, 1993). Good examples are given by the Auros and the Kombat Formations. Due to the bedding parallel deformation the shales of the Auros Fm, which are intercalated in massive dolomites, thin out parallel to S2. Oolitic dolomites of the Auros Fm were partly silicified prior to D2 and calcification occurred prior to or during D2, enabling a mylonitisation of the calcified horizons. The phyllites of the Kombat Fm exhibit isoclinal folding and “piercement structures” in the T8 dolomites (Deane, 1995). In the OML thrusting mainly took place along these formations (Fig. 2.10a, g, h). Also between the more rigid layers a competence contrast caused a different behaviour. Veldsman (1977) for example reported boudins of chert layers embedded in foliated dolomites from the north-eastern Guinas Fault area.

The truncation of D1-structures by D2 is best shown in the incompetent layers. The crenulation cleavage transecting an older foliation is also evident in the Kombat Phyllites. If the older foliation, which is parallel aligned to the bedding in the phyllites, is related to D1, the Kombat Phyllites would be older than the Tschudi Formation and in this case they might not be part of the Mulden Group. On the other hand the earlier foliation could be related also to D2 and may be an expression of the more intense deformation in the southern OML, which caused foliation, folding and crenulation in a progressive process during the main phase of the Damara orogeny. The Otavi Valley does not necessarily originate from an eroded subsidiary intracontinental rift basin of the northern rift as suggested by Deane (1995), but could have formed by isoclinal and recumbent folding at the southern margin of the Northern Platform and subsequent erosion.

Distinct variations in style and intensity of deformation are evident from the investigated areas (Fig. 2.13a). South of the Guinas Fault, isoclinal folding, small-scale nappe stacking and thrusting are evident, whereas north of the Guinas Fault only non-penetrative cleavage can be observed. Maclaren (1991) interpreted parts of the T2 lithounit of the Maieberg Fm as a decollement-surface and the Guinas Thrust as a tectonic ramp or step fault, leading to an ascent of the decollement to higher stratigraphic levels of the Tsumeb Subgroup. Botha (1958) and Gadd-Claxton (1972) suggested a widespread silicification of the Guinas Fault area during northward or eastward thrusting along the Guinas Fault. As the upper Tsumeb Subgroup was thrusted over the Mulden Group in this area, this deformation is of post-Neoproterozoic age. Our observations reveal a change in the style of deformation and locally its direction throughout the D2. Elongated oolites of the Guinas Fault thrust horizon (Fig. 2.10b) show a N-trending shortening direction and were silicified during or after this deformation (Fig. 2.6). The shortening direction related to the sole thrust at the bottom of the Guinas Thrust horizon, which cuts the former structures, strikes NE-SW (Fig. 2.6, Fig. 2.12a). The change in the style of deformation in the oolites could have been caused by the cooling of the tectonic environment during D2. In the Tigerschlucht area the shortening direction during D2a and D2b strikes N-S, which is estimated from the lineation indicating a northward movement (Fig. 2.12a) and confirmed by the orientation of elongated oolites in the Auros Fm and northward thrusting (Fig. 2.8a, b). The role of roughly E-W orientated lineations (Fig. 2.8h) might be due to a significant strike slip component during deformation processes along the Tigerschlucht shear trend during D2b. The estimation of the shortening direction in the Otavi Valley by lineations on S2-surfaces is difficult, because of the scarcity of distinct lineations, but orientated clasts in the Kombat Fm and a north vergent crenulation cleavage support a northward directed movement during D2 (Fig. 2.10g, h, 2.12a). The EW-striking lineation in the southern limb of the Otavi Valley and the Askevold Anticline (Maclaren, 1991) is interpreted as an intersection lineation of S2 and S0/1.

The gradual cooling of the Northern Platform during D2 is shown by the change of the style of deformation. During D2a isoclinal folding of S0 and S1 was accompanied by the development of an axial plane cleavage, which changed during D2b into

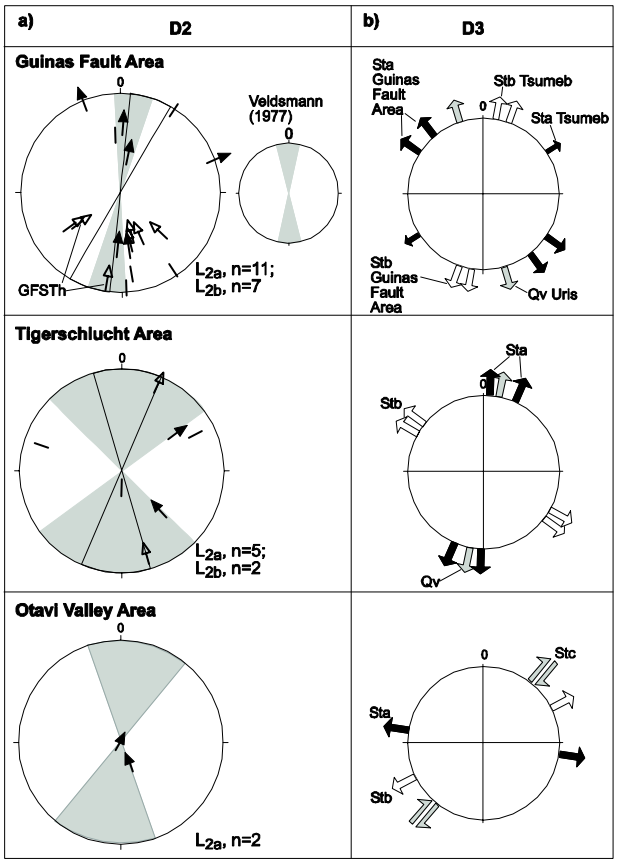

Fig. 2.12: Kinematics of the key areas during D2 and D3

a) Average orientation of the main shortening direction in the key areas during D2a (grey segments) and D2b (black framed segments), estimated from lineations (L2n), orientation of elongated components and fold axes. Arrows give lineations with known movement direction of the hanging wall (filled: D2a, open: D2b). Lines give strike of movement. GFSTh: Guinas Fault sole thrust.

b) Summary of syn-D3 extensional directions (Qv: quartz veins in grey, Sta: first order normal faults in black, Stb: second order normal faults in white, Stc: strike slip).

thrusting also along incompetent lithologies (e.g. Guinas Fault, Otavi Valley Rupture). At the southern limb of the Otavi Hills thrusting of T5 dolomites along internal sediments gives a maximum age of the thrusting syn-D2b. The internal sediments can be interpreted as karst fillings, which accumulated at the beginning of the deposition of the Mulden Group (Table 2.1, 2) in the already folded (D1) platform. This is also confirmed by various reports of thrusts transposing the karst fillings in the Tsumeb Pipe (Lombaard et al., 1986). Stringers of sandstones in the Kombat workings belong to the Mulden Group as well (Innes and Chaplin, 1986). These sandstone bodies are

elongated along S2 and late Pan-African normal faults. Their appearance as lenses orientated along the main foliation can be interpreted as a result of boudinage of karst fillings during D2. In the Tsumeb Pipe Hughes (1987) estimated the amount of displacement along bedding parallel thrusts of up to 250 m ("Große Überschiebung").

The change in the orientation of the shortening direction from D2a (N-S to NNE-SSW) to D2b (NE-SW), which is evident from the Guinas Fault area (Fig. 2.6d, i, f, e, g, 9), could have been due to different rheological characteristics of the opposed lithologies during the northward movement of the hanging wall or a regional change of the stress field during D2 caused by a transpressional orogeny in a later phase. Further indications of a transpressional orogeny were given by Coward (1983), who described westward verging recumbent folds with a well developed cleavage and ENE-trending mineral lineation west of the OML. E-striking strike slip movements in the Otavi Valley and some slickenside lineations in the Tigerschlucht area were overprinted by D3 and provide no clear indications of movement directions syn-D2.

In general, the grade of metamorphism during D2 decreased from lower greenschist facies conditions in the Otavi Valley (Innes and Chaplin, 1986) in the South to the North. In contrast to this model, higher greenschist facies conditions are evident from chlorite

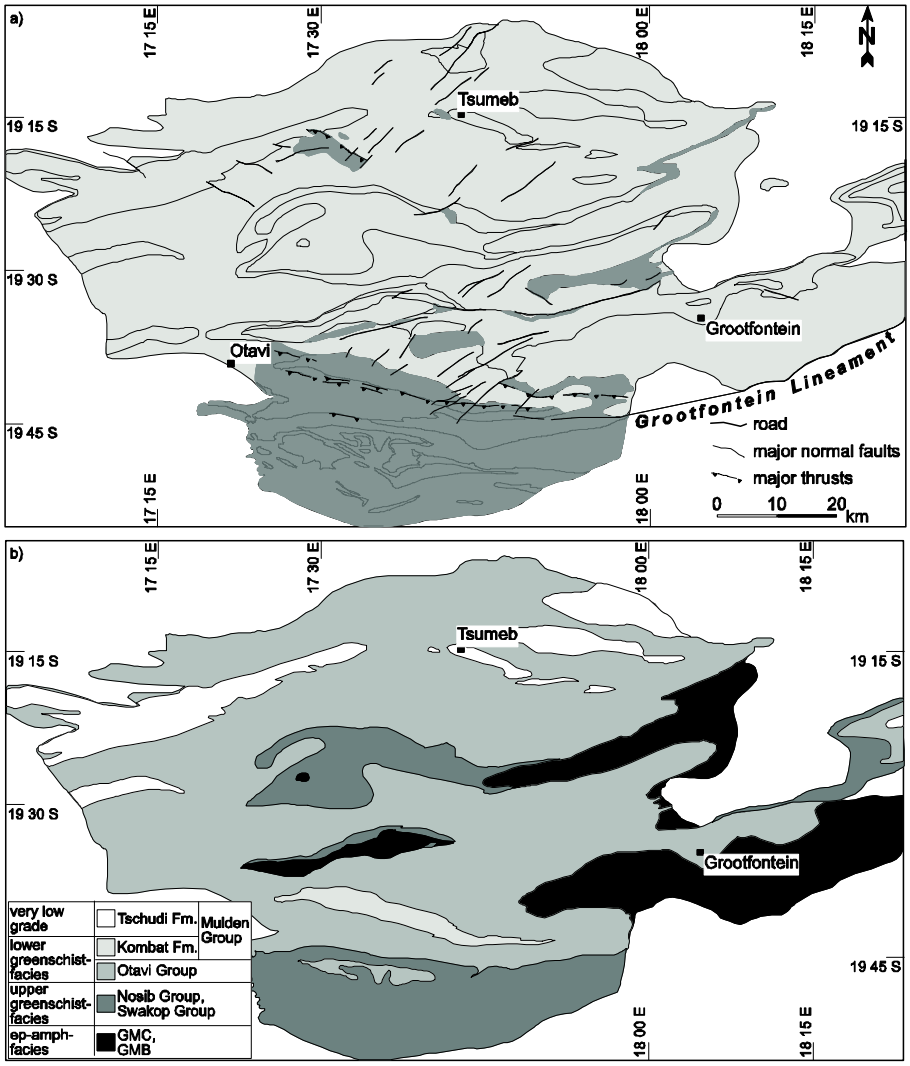

Fig. 2.13: a) Structural domains of the OML related to D2a; light grey: minor influence of deformation confined to non-penetrative cleavage; dark grey: major influence of deformation expressed by isoclinal folding, penetrative cleavage, common elongation of breccia clasts and ooids, mylonitisation, thrusting, small scale nappe stacking, common calcification of dolomites; for lithological boundaries see Fig. 2.2; b) Tectonometamorphic zones of the OML with maximum metamorphic overprint accompanying D2; GMC: Grootfontein Metamorphic Complex, GMB: Grootfontein Mafic Body.

and biotite in the Askevold Fm of the central OML (Fig. 2.13b). There is no age dating available for this metamorphism in the OML, but the peak metamorphism of the Pan-African orogeny around 535-530 Ma (Clauer and Kröner, 1979; Goscombe et al., 2004) is inferred to the D2a in the OML. A muscovite cooling age of 490 ± 2.3 Ma, which is interpreted as cooling of kyanite-grade rocks of Damaran siliciclastics of the Tsodo Hills Group (north-western Botswana) below 350-400 °C (Singletary et al., 2003) could represent a minimum age of D2b. Biotite strain shadows in the Askevold Fm of the southern OML indicate a syn-D2 age, as this would have been the only orogenic phase, which could have caused such metamorphic conditions in the Cryogenian strata. Therefore the decrease of metamorphism might only be apparent due to the dominance of dolomites in the central and northern OML, which are in general bad indicators for low grade metamorphic conditions. In addition, a deeper tectonostratigraphic level is probably outcropping in the southern OML. Nevertheless, the mineral assemblage of the Kombat Fm and the conversion of authigenic pyrite to pyrrhotite confirm greenschist facies conditions in the Otavi Valley (Innes and Chaplin, 1986). Deane (1995) suggested a syn-D2 formation of the Kombat ore bodies at temperatures around 350 – 480°C. A further increase of the metamorphic grade during D2 from the Otavi Valley to the south is envisaged in the amphibolite facies conditions reported by Goscombe et al. (2004) in the eastern part of the Northern Zone of the Damara Orogen. Pure brittle deformation of pyrite in the Askevold Fm from the Askevold Range in the southern OML indicates pT-conditions lower than 400°C and 3 kbar (Atkinson, 1975), spanning the Bt-zone in the Nosib Group from the north-eastern Northern Zone to the central OML (Fig. 2.13b). In order to classify the metamorphic zones of the Northern Zone and the Northern Platform the authors suggest a separation of the variably overprinted Damara Supergroup in distinct tectonostratigraphic levels (Fig. 2.13).

2.4.4 D3 and post-Damaran deformations

The late- (D3) and post-Damaran structures were caused by a change from a syn-Damaran compressional system to an extensional system. This change was due to uplift and denudation of the Northern Platform (Gadd-Claxton, 1972). The D3 was accompanied by zeolite to prehnite-pumpellyite facies metamorphism, which is recorded in the Mulden Group sediments in the Etosha Basin NW of the OML. This metamorphism has been dated around 481-459 Ma (Haack et al., 1980; Haack, 1983).

The major trend of syn-D3 normal faults in the OML strikes NE-SW (Table 2.1, Fig. 2.12b). In the Guinas Fault area this fault system is parallel to the Heidelberg Lineament (Söhnge, 1976). In the Otavi Valley area dextral strike slip movements are evident along the NE-SW-striking (e.g. Kombat Fault) (Fig. 2.12b), but also along E-W-striking normal faults. These faults are subsidiary structures of the Grootfontein Lineament, which juxtaposes the Northern Platform with the Northern Zone in the South (Maclaren, 1991). Unrug (1983) amongst others reported a sinistral movement along major transcurrent shear zones of southern central Africa, like the Mwembeshi Shear Zone or the Okahandija Lineament, whereas a dextral movement along these major sutures was proposed by Dürr and Dingeldey (1996) and Kukla and Stanistreet (1991). Dextral movements along NE- and E-striking strike slip faults could therefore be related to these larger lineaments, active during D2b and D3. Hanson et al. (1993) suggested a late Ediacaran-age of the Mwembeshi Shear Zone, shown by rhyolites emplaced in the dislocation zone (551±19 Ma). The onset of E-W-striking strike slip movements in the Otavi Valley occurred during D2b, shown by thrusts, which transpose these structures in the Kombat Workings. The location of major E- to ESE-striking structures along the margin of the Grootfontein Inlier, like the Tigerschlucht shear trend or the Otavi Valley Rupture, indicates a late to post-Pan-African fragmentation of the basement, presumably along pre-Pan-African rift structures. The impact of this deformation on the basement is supported by the large scale northward downthrow along the Uitsab Fault (Maclaren, 1991), located at the northern margin of the southernmost basement high of the OML (Fig. 2.2, Fig. 2.7). Here is also visible the extremely varying dip slip component of these strike slip faults. A post-Damaran early Mesozoic reactivation of the lineaments dividing the Southern, Central and Northern Zones of the Damara Orogen was reported by Raab et al. (2002). Reactivations of the NE-SW-striking structures are shown by parallel aligned kersantite and mafic dykes of presumably Karoo-age (Söhnge, 1957).

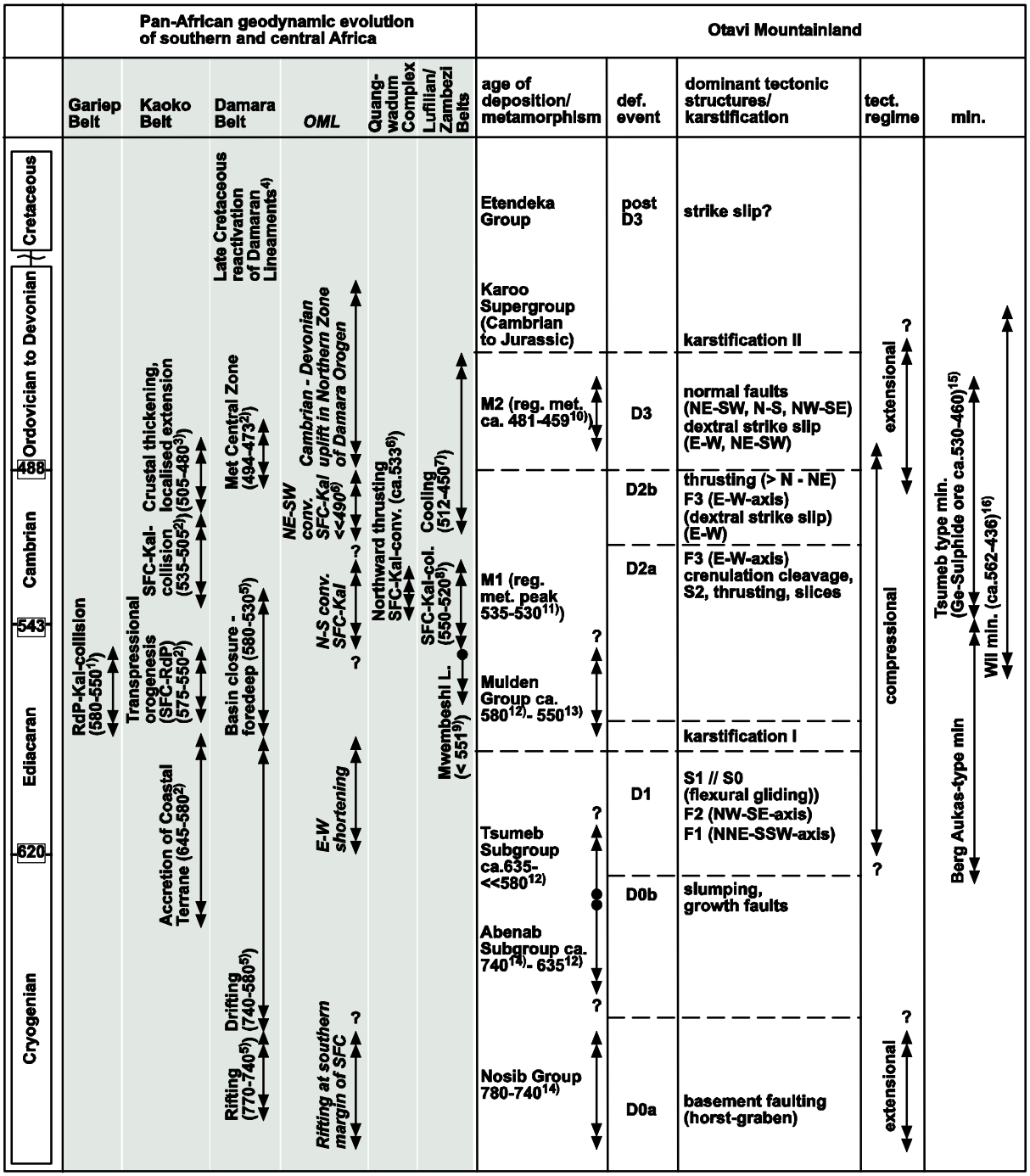

1) Frimmel & Fölling (2004)
2) Goscombe et al. (2005)
3) Gray et al. (2006)
4) Raab et al. (2002)
5) Frimmel (2004)
6) Singletary et al. (2003)
7) Porada & Berhorst (2000)
8) Johnson et al. (2005)
8) Hanson et al. (1993)
9) Haack et al., 1980; Haack, 1983
10) Clauer & Kröner, 1979; Goscombe et al. (2004)
11) Hoffmann et al. (2004)
12) this paper
13) Burger & Coertze (1973), Hoffman et al. (1996)
14) Melcher et al. (2006)
15) Schneider et al. (in press)

Table 2.4: Revised structural evolution of the OML and comparison to the Pan-African geodynamic evolution of southern and central Africa (ages in Ma). Kal – Kalahari Craton, RdP – Rio de la Plata Craton, SFC – Sao Francisco-Congo Craton. Lines with double arrows give a maximum timing if not extended by a question mark. Black points at the end of a line represent a distinct age.

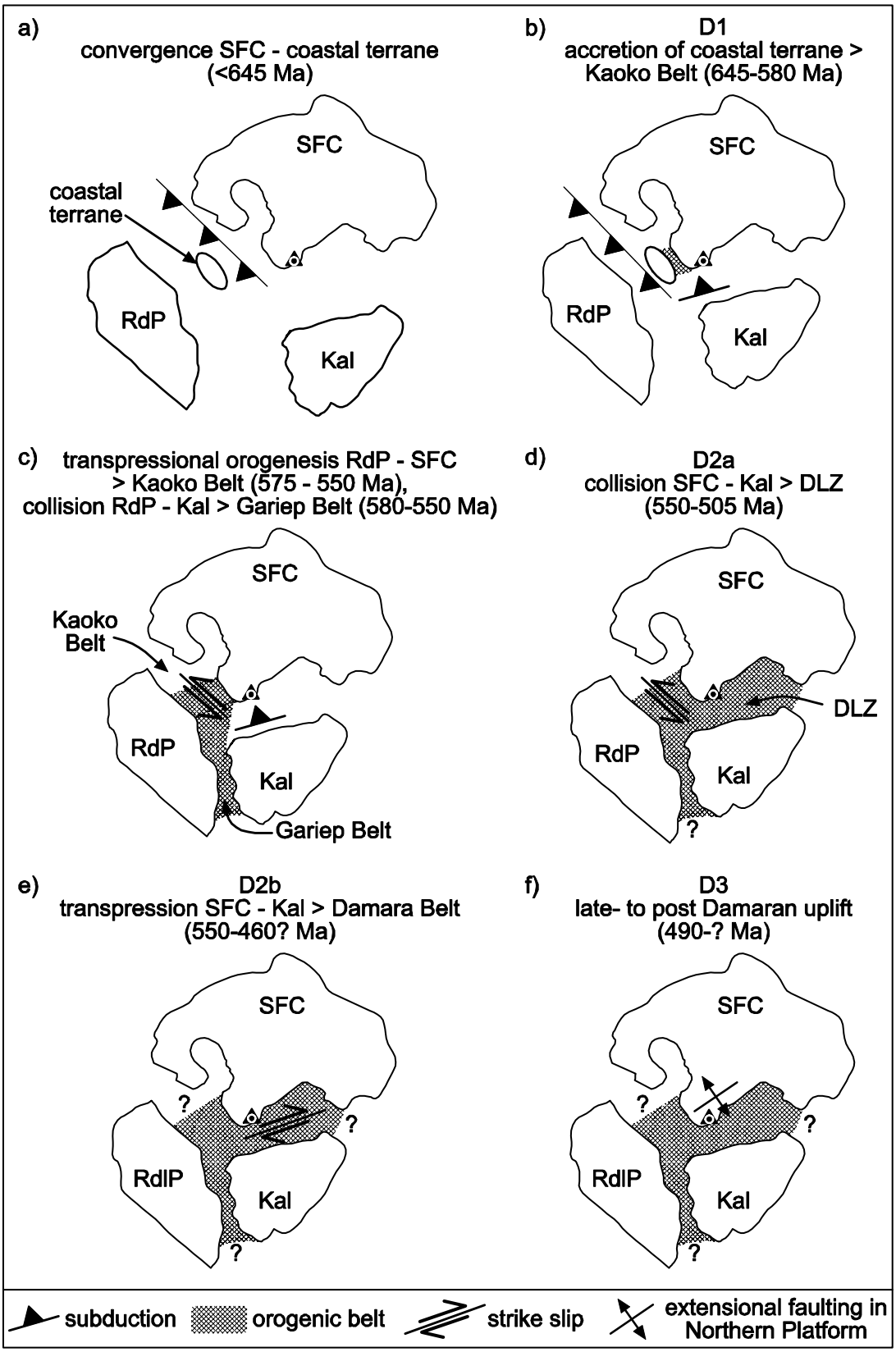

Fig. 2.14: Schematic model of plate tectonic evolution of the Sao Francisco-Congo, Kalahari and Rio de la Plata-Cratons during the Pan-African orogeny forming the Damara Orogen (references for tectonic events see Table 4; cratons after Goscombe et al. (2004) and Meert and Torsvik (2003)). Triangle marks location of the OML. Not to scale. DLZ – Damara-Lufilian-Zambezi Belt, Kal – Kalahari53raton, RdP – Rio de la Plata Craton, SFC - Sao Francisco-Congo Craton, Damaran Orogenic Belts in grey.

The orientation of further fault systems varies between the different key areas (Fig. 2.12). NW- to WNW-striking faults occur in the Guinas Fault and Tigerschlucht area. This fault system could be conjugated to the NE striking faults, but at least in the Tigerschlucht area the secondary normal faults cut the first order faults and are therefore of an later age. N-S-striking normal faulting is evident in the Otavi Valley and to a minor extent in the Guinas Fault and Tsumeb area. In the Otavi Valley the N-S-striking faulting passes into NNE- and NE-striking faults to the east, thus implying a cogenetic relationship with the latter normal faults. In contrast to this, Deane (1995) proposed a post-Karoo age of the N-S-striking faults. A reactivation of this fault direction is implied by post-Karoo karst fillings along these faults.

Widespread quartz-veining is observed in the Tigerschlucht and the Guinas-Fault area. The quartz veins in the Tigerschlucht area are parallel to the Tigerschlucht shear trend and striations on fault surfaces in the quartz veins coincide with the N-S-striking movement along the Tigerschlucht shear trend. The quartz-veining is therefore presumably related to the late or post-Damaran D3.

2.4.5 Structural domains of the OML

The presented key areas and additional localities show the characteristic partition of the OML in structural domains (Fig. 2.13a) that were already mentioned by Schwellnus (1946). The formation of these structural domains is dependent on 1) stratigraphy, 2) synsedimentary tectonics, 3) existence and spatial extent of the pre-Damaran basement, 4) pre-Damaran basement structures and graben fillings, 5) karstification and 6) distance from the Northern Zone.

1) The major influence of the stratigraphy is due to the competence contrast of the different lithologies (Hughes, 1979). Maclaren (1991) classified the sedimentary successions of the Otavi and Mulden Groups according to their competence. Dolomitic boundstones and grainstones show brittle deformation and a tendency to brecciation and thrusting. Mudstones interlayers (e.g. Auros shales) and the Kombat Phyllites accommodate the majority of strain and are isoclinally folded at the contact to the dolomites. The rheology of the lithologies appears to be a controlling factor on the distribution of deformation. The accommodation especially of syn-D2a induced strain by incompetent layers could also explain the small amount of deformation in the pre-Damaran basement with respect to the sedimentary cover, as suggested by Unrug (1983) for the Lufilian Arc. A protection of the Northern Platform by its underlying rigid and stabilised basement (Tankard et al., 1982) is only valid regarding the penetrative cleavage that is widely distributed in the Northern Zone, whereas it is confined in the OML to the more deformed structural domains.

2) Synsedimentary tectonics provide structures for the onset of further deformation. Growth faults in the middle to upper Tsumeb Subgroup, like the Guinas Fault, were inverted during the compressional phase of the Pan-African orogeny and could have been used as thrust horizons syn-D2. Additionally growth faulting causes different sedimentary environments to become closely associated, leading to the deposition and lithification of sediments with different rheological behaviour.

3) The influence of the Grootfontein Inlier on the depositional environment and tectonic structures in the OML was outlined by Söhnge (1972). The importance of the roughly ENE-trending basement high on the northward progression of the D2 should be emphasised. Basement highs may have served as ramps enabling or fostering the concentration of thrust tectonics in distinct areas like the Tigerschlucht area (e.g. Teco thrust) or the Otavi Valley area (Otavi Valley Rupture) and the decoupling of tectonic structures in the basement and the Neoproterozoic strata (sensu Butler, 1989). In fact the position of the Otavi Valley at the southern scarp of the Grootfontein Inlier might be due to the Pan-African orogeny. As shown in Fig. 2.11, the Otavi Valley is positioned at the transition of the Grootfontein Inlier and its cover units in the North to the schistose and isoclinally folded Neoproterozoic successions in the south. The basement high and the competent platform carbonates hampered the northward moving of the Damaran foreland basin units, leading to the large scale isoclinal folding and narrow sequence of thrusts at the southern limb of the Otavi Valley (Fig. 2.8).

4) Similar to the synsedimentary faults in the Otavi Groups, the pre-Damaran basement structures were reactivated and inverted. Inverted growth faults, normal faulting due to Neoproterozoic rift-processes and basement highs fostered the staircase geometry of thrusting as suggested by Coward and Daly (1984) for

the Northern Platform. In the OML a reactivation of the rift structures is exemplified by the Tigerschlucht shear trend and oblique slip faults in the Otavi Valley (see chapter 4.4).

5) Karstification of the Northern Platform preceding and accompanying the deposition of the Mulden Group was concentrated in distinct horizons of the platform carbonates like the upper Tsumeb Subgroup and caused further shear strength weakening in these lithologies. Solution collapse breccias and faulting along these karst structures are the result of this process, as exemplified by the Tsumeb Pipe.

6) Last but not least the distance of the Northern Platform from the Central Zone of the Damara Orogen plays a role in the partitioning of the OML into structural domains. During D2 the northward progression of the deformational front interacts with the already deformed platform carbonates and the adjacent lithologies. The impact of the D2 also relies on the angle of the shortening direction to pre- or early syn-D2 structures (Fig. 2.13, 2.14). Southward dipping to horizontal S1 or bedding parallel breccias could have been reactivated. This results in more intensive narrowing of the E-W-striking anticlines than of the synclines (Gadd-Claxton, 1972). Maclaren (1991) amongst others described a decrease of syn-D2 deformation from south to north. However, figure 2.13a shows, that the deformation pattern, which is due to D2a, is much more heterogeneous.

2.4.6 Pan-African belts in south-western Africa

There are 3 major phases of deformation in the OML, which can be related to the Pan-African tectonic assembly of Western Gondwana. These can be summarised as D1 (E-W shortening phase), D2 (N-S shortening phase) and D3 (uplift): the mentioned phases, together with age and location of Pan-African rifting, are presented in Table 2.4. The suturing of the Rio de la Plata Craton with the Kalahari and Sao Francisco Cratons respectively preceded the collision of the latter two cratons (Table 2.4, Fig. 2.14; Maloof, 2000). The collision of the Kalahari and Sao Francisco Cratons and the formation of the Damara-Lufilian-Zambezi Orogen (DLZ) occurred either simultaneously along the whole DLZ or started in the east commencing to the west. A diachronous deformation due to N-directed subduction of the Khomas sea and the related asymmetric ocean closure by about 540 - 520 Ma was suggested by Gray et al. (2006).

The late to post-Cryogenian D1 comprised NNE- and NW-trending folds, accompanied by flexural gliding and terminated before the deposition of the Mulden Group. This first compressional phase in the Otavi Group could be related to the accretion of a Coastal Terrane to the Kaoko region in the west, immediately before the suturing of the Rio de la Plata and Sao Francisco-Congo Cratons (645-580 Ma, Goscombe et al., 2005).

D2 represents the main deformational event in the OML and should be divided into two subphases, due to the apparent cooling of the Damaran successions and a presumable change of the shortening direction from N-S (D2a) to NE-SW (D2b) during the collision between the Sao Francisco-Congo and Kalahari Cratons. D2a was accompanied by the peak metamorphism of the Damaran orogeny in the eastern Northern Zone (535-530 Ma according to Clauer and Kröner, 1979; Goscombe et al., 2004), evidenced by syn-deformational grown phyllosilicates in S2 shear bands and early thrusts. This fits roughly with the high-angle, NNE-SSW directed convergence of the Kalahari and Sao Francisco-Congo Cratons in the western inland branch of the Damara Orogen at 535-505 Ma, as suggested by many authors (Coward, 1981, 1983; Goscombe et al., 2005; Miller, 1983a). North-vergent thrusting in the presumably Paleoproterozoic Quangwadum Complex in north-western Botswana occurred around 533 ± 2.3 Ma (Singletary et al., 2003) and coincides with the N-S contraction at the northern margin of the Damara Belt during D2a. There is evidence for a progressive change of the shortening direction during D2, leading to NE-SW contraction syn-D2b. An oblique NE-SW-striking convergence, related to the Mwembeshi Shear Zone (MSZ), is reported from the Lufilian and Zambezi Belt by Johnson et al. (2005), who emphasised the sinistral displacement along this lineament. The main collision between the Kalahari and Sao Francisco-Congo Cratons in this area took place from 550-520 Ma (Johnson et al., 2005). A lower age of ca. 551 Ma is assigned to the Mwembeshi Shear Zone by Hanson et al. (1993). Therefore the Pan-African continental collision at the eastern end of a Damara-Lufilian-Zambezi Orogen (DLZ) would have preceded the NE-SW directed collision in the west. This contradicts the eastward suture progradation proposed by Kasch (1983). The indication of sinistral movement along the

Mwembeshi Shear Zone was discussed by Porada and Berhorst (2000), pointing out the changes from sinistral to dextral movement between different segments (Johns et al., 1989). Dürr and Dingeldey (1996) related sinistral movements along the Pan-African lineaments to an early phase of the convergence between the Kalahari and Sao Francisco-Congo Cratons that was replaced by dextral movements in a later stage. Dextral movements in the OML are distinctly younger (Table 2.4) than the sinistral ones along the Mwembeshi Shear Zone (Johnson et al., 2005) and are related to the main and late stages of the Pan-African orogeny. Reasons for the different shortening directions along the DLZ during the main phase of the Pan-African orogeny, could be a response to the non-linear shape of the southern margin of the Sao Francisco-Congo Craton or generated by a later subdivision and offset of the DLZ by a perpendicular lineament (Unrug, 1983). Singletary et al. (2003) described N- to NW-trending structures north of the Quangwadum Complex (Fig. 2.1), which are due to Pan-African deformation at a promontory at the southern margin of the Sao Francisco-Congo Craton. This suggests that the Quangwadum Complex acted as a small indenter located at the southern margin of the Sao Francisco-Congo Craton (Key and Ayres, 2000) during its Pan-African amalgamation with the Kalahari Craton. A greenschist facies metamorphism during the main phase of the Pan-African orogeny is reported from several areas of the DLZ. Besides the two early Cambrian ages from the eastern Northern Zone (Goscombe et al., 2004) and the Quangwadum Complex (Singletary et al., 2003), similar ages spanning from 550-520 Ma were described from the Lufilian and Zambezi Belts (Johnson et al., 2005).

The late Pan-African uplift (D3) caused predominantly NE- and minor NW-striking normal faults but also the reactivation of NE- and E-striking dextral strike slip faults. The accompanying zeolite to prehnite-pumpellyite facies metamorphism occurred around 481-459 Ma (Haack et al., 1980; Haack, 1983). A similar timeframe of a metamorphic period at 494-473 Ma in the Central Zone of the Damara Belt has been assigned to the NNE-SSW directed shortening between the Sao Francisco-Congo and Kalahari Cratons by Goscombe et al. (2005). This phase was characterised by high-T metamorphism, which also included migmatisation and granite emplacement. This implies that the uplift in the Northern Platform was still due to continental convergence, which led to a fragmentation of the OML by extensional faulting along pre-D3 structures and a conjugated set of NE and NW-trends.

2.4.7 Remarks on base metal mineralisation in the OML

Tectonic structures provide indications for the timing of base metal mineralisation in the OML. An argument for a pre-D2 base metal mineralisation is represented by the occurrence of disseminated specks of Zn-, Pb- and Cu-sulphides in the massive dolomites of the Elandshoek Fm, which show no structural control (Veldsman, 1977). On the other hand, the multiple calcitisation and silicification phases, which frequently do not reveal a structural control either, suggest a fair permeability of the Neoproterozoic lithotypes during the Pan-African orogeny, which could have also favoured the diffusion of metal bearing fluids precipitating the sulphide specks. An example of this enhanced porosity and permeability is the concentration of base metals in mass flow breccias (Petzel, 1993). Another argument for a pre-D2 Berg Aukas-type mineralisation stage, are the frequently quoted occurrences of presumably syn-D2 deformed base metal sulphides in several localities of the OML (e.g. Kombat: Innes and Chaplin, 1986; Deane, 1995). Hughes (1979) described from the Tsumeb Pipe folding, deformation- and healing-structures and sulphide veins, which are cut by a penetrative cleavage. In some shear zones from the same pipe, galena shows orientated slickensides, whereas the remaining sulphide ores exhibit no deformation or recrystallisation (Söhnge, 1972). Additional remobilisation of former base metal sulphide bodies into D2-structures is evident from Kombat (Innes and Chaplin, 1986; Deane, 1991), Tsumeb (Hughes, 1979) and Tsumeb West. Small-scale breccia pipes, truncated by D2-thrusts, containing Zn- and minor Cu, Mn, Fe and Cd-mineralisation, were reported from the north-western OML by Petzel (1993) and De Bever (1997). Söhnge (1972) postulated the generation of the breccia pipes by dragfolding in the keel of the Tsumeb syncline, which occurred eventually even before the lithification of the dolomites. Because dragfolding is due to D2, this can, however, not be the case.

Contrary to the mainly stratabound setting of the

Berg Aukas-type ores, the breccia pipes, which are the host for the Tsumeb-type mineralisation (Table 2.3), developed at the cross junctions of different tectonic trends, like hinge zones of syn-D2 folds (F3) with D2b thrusts or late Pan-African normal faults (D3). The Tsumeb Pipe for example (Fig. 2.5) is located at the crosscutting of steep inclining, northward thrusting (Fig. 2.6g) and syn-D3 normal faulting (Fig. 2.6l). This apparent relationship is difficult to understand, because of the pre-D2b age of the Mulden Group, which occurs as karst infill. An explanation could be a pre- or early D2 onset of the karsting and filling of the karst by Mulden siliciclastics, followed by a further extension of the karst system in the OML by migrating fluids and syn-D2 and syn-D3 deformation of the weakened karst zone. Syn-D2 truncated sandstone bodies in the karst pipes and the observed multi stage brecciation of the karst infill also support this assumption. In the Kombat Mine in the Otavi Valley (Fig. 2.9, map) the primary base metal sulphide deposits are cut by post-D2 structures, like at the Kombat West Fault (Galloway, 1988). The distinct northeast-trend of the ore-bodies in the central Otavi Valley is therefore caused by the truncation of the ore bodies by post-D2 structures and does not indicate a primary emplacement along these faults. Nevertheless, later base metal mineralisation, for example supergene Cu-sulphides and -carbonates (Innes and Chaplin, 1986), was distributed along these transpressional to normal faults.

Mineralised shear zones are described from various localities in the OML (e.g. Tsumeb Pipe, according to Söhnge, 1957) and give further indications on the timing of mineralisation in the OML. Deane (1995) reported mineralisation that is associated with subvertical axial planar cleavage. Laukamp et al. (2006) emphasised the possible role of shear zones as seals for ascending metal-bearing fluids. The silicified Guinas Thrust horizon for example, may have triggered the distribution of post D2a Cu-mineralisation in the Guinas Fault area. Besides the Guinas Thrust, further shear zones and intense deformed lithologies may have acted as seals for mineralised fluids. In the northern Tigerschlucht area Pb-Zn-mineralised dolomites of the Elandshoek Fm occur beneath the Teco Thrust (Fig. 2.7), but sphalerite occurs along thrust surfaces as well (Fig. 2.8c). Along the mylonitised limestones and shales of the Auros Fm south of the Uitsab Fault, several Pb-Zn-occurrences are located (Fig. 2.7). The “Zinc-Reef” of Abenab West, containing high grade Zn-silicates possibly replacing primary sulphides, is positioned in a bedding parallel shear horizon at the contact between bedded limestone and dolostone of the Auros Fm (Verwoerd, 1957) and post-dates D2 (Part 5). The same could be said for the secondary malachite and chalcocite, originated from weathering of Cu-sulphides and described by Veldsman (1977) in several shear zones from the north-western OML.

The observed relationships between base metal mineralisation and tectonic structures in the OML allow a discrimination of the driving factors for the circulation of base metal bearing hydrothermal fluids for both the Berg Aukas- and the Tsumeb-type mineralisation. As there are clear indications for a pre-D2 age of at least parts of the primary base metal mineralisation, a basin-dewatering model as suggested by Pirajno and Joubert (1993) is favoured for the Berg Aukas-type mineralisation. Cu-bearing fluids, presumably generated during the Pan-African orogeny, led to the later emplacement of Tsumeb-type mineralisation. On their northward migration the fluids could have leached Damaran sediments and mafic rocks (Frimmel et al., 1996a) or the volcanogenic massive sulphide (VMS-type) deposits occurring in the southern OML. Remobilisation of former base metal occurrences is shown in various localities of the OML (e.g. Kombat Mine). The indicated late to post-Damaran fragmentation of the basement could give further implications on the Pan-African fluid flow. If the basement relief was less pronounced during the Pan-African orogeny, the distribution of the widely disseminated base metal mineralisation in the OML would have been eased.

2.5 Conclusions

The Pan-African Damaran orogeny caused three major deformational events in the OML in northern Namibia. A first deformation (D1), which took place in the late Cryogenian to middle Ediacaran, resulted in E-W shortening of the Otavi Group. The accretion of a coastal terrane in the Kaoko region could have been the trigger of D1. This was followed by the collision of the Rio de la Plata Craton with the Sao Francisco-Congo and Kalahari Cratons, forming the Kaoko Belt and the Gariep Belt respectively. The main deformational event in the OML, represented by D2, was caused by the late Ediacaran to early Cambrian N-S shortening, which was due to the collision of the Sao Francisco-Congo and Kalahari Cratons. The collision

happened either simultaneously throughout the DLZ or started in the Lufilian and Zambezi Belts and propagated to the west. The shortening direction could have changed to NE-SW in a late phase of D2, leading to transpression along the DLZ. During the early Paleozoic the transpressional system passed into an extensional system, caused by the late Pan-African uplift (D3). The onset of major structures in the OML, like NE-SW- and E-W-striking normal faults and strike slip faults, could be related to the pre-Pan-African rifting at the southern margin of the Sao Francisco-Congo Craton. These structures were reused throughout the Paleozoic.

The tectonic evolution of the OML led to a heterogeneous deformation pattern and distinct tectonometamorphic domains. The development of these domains was dependent on 1) stratigraphy, 2) synsedimentary tectonics, 3) nature and extension of the pre-Damaran basement, 4) pre-Pan-African basement structures and graben fillings, 5) karstification, 6) distance from the Northern Zone.

The linkage between primary base metal mineralisation and tectonic structures supports a pre-D2 age for Berg Aukas-type and a syn-D2 age for Tsumeb-type mineralisation. The stratabound Berg Aukas-type mineralisation formed by basinal brines derived from compaction and dewatering of the Otavi platform carbonates. The collision of the Sao Francisco-Congo and Kalahari Cratons led to a northward migration of metamorphic fluids that was controlled by pre- to syn-D2 structures and leached the Damaran sediments and/or VMS-type deposits in the southern OML. These Cu-rich fluids were the source of the Tsumeb-type mineralisation, which was preferentially deposited in structural and karst controlled breccia pipes in the Elandshoek and Hüttenberg Formations. The Tsumeb-type mineralisation may contain remobilised material from the older Berg Aukas-type deposits as well.

Acknowledgements

We thank Arno Günzel, Hafeni Hiveluah and Tinus Prinsloo (Ongopolo Mining and Processing Limited, Tsumeb) as well as Volker Petzel (Namibia Geological Survey) for the introduction into the field and the mines. We acknowledge the logistic support by Volker Petzel and Hartwig Frimmel (University of Würzburg). Frank Melcher (BGR) and Georg Werner (University of Heidelberg) kindly provided unpublished material. Discussions with Thomas Angerer and Jens Grimmer (University of Heidelberg) are also acknowledged. We are indebted to Deutsche Forschungsgemeinschaft (DFG) for financing this study in the framework of the Graduiertenkolleg 273 on Rock-water Interaction at Heidelberg University. Further financial support was provided by the DAAD-financed Internationales Promotionsprogramm (IPP) at the Faculty of Chemistry and Geosciences, Heidelberg University.

Part 3: Geology of Paleoproterozoic basement rocks in the Grootfontein Inlier (Namibia)

Abstract

The Proterozoic basement of northern Namibia consists of several magmatic and metamorphic inliers situated along the southern margin of the Congo Craton. In the Otavi Mountainland (OML), NE Namibia, Paleoproterozoic basement rocks are represented by the Grootfontein Inlier, which has been subdivided into the Grootfontein Metamorphic Complex (GMC) and the Grootfontein Mafic Body (GMB). Field observations, petrographical, geochemical, and geochronological data were used to put constraints on the geotectonic evolution of these units.

Main and trace element data of gabbroic rocks from the GMB indicate their emplacement in a continental regime, whereas rocks from the GMC reflect a magmatic evolution from dioritic towards granitic compositions in a convergent tectonic setting, with a waning stage producing pegmatitic intrusions. Rb-Sr dating of white mica reveals a late Eburnean age of 1.816 ± 26 Ma for this final pegmatitic stage, indicating that the basement of the OML forms part of the southern Congo Craton

which was affected by major crust-forming events and underwent consolidation during the Eburnean orogeny. This is supported by the geochemical similarity of the Grootfontein Inlier with other pre-Damaran basement complexes farther west.

3.1 Introduction

Proterozoic basement units in northern Namibia belong to the southern part of the Congo Craton and crop out in several inliers along the Kaoko Belt in the W and the northern margin of the Damara Belt (Fig. 3.1). These are, from NW to E, (i) the Kunene Complex and Epupa Inlier, (ii) the Kamanjab Inlier, (iii) the Grootfontein Inlier and (iv) the Tsumkwe-Tarikora-Massif, which is located at the border to Botswana. Other important Proterozoic basement units, such as the Abbabis Complex, are preserved in the northern, central and southern zones of the Damara Belt.

While the Paleoproterozoic units in NW Namibia have been extensively studied and are relatively well understood (e.g., Seth et al., 1998), little is known about the nature and geochronological evolution of the Grootfontein Inlier in NE Namibia. The Grootfontein Inlier consists of the Grootfontein Metamorphic Complex (GMC), which is dominated by alkaline/calc-alkaline granites and granodiorites (Clifford et al., 1969), and the Grootfontein Mafic Body (GMB), which comprises anorthosites, amphibolites, gneisses and granites (Martin, 1965; Söhnge, 1964; Günzel, pers. comm., 2004). This paper aims to characterise the Paleoproterozoic metamorphic basement in NE Namibia by means of its field occurrence and main and trace element geochemistry. Furthermore, a Rb-Sr age on pegmatite-related white mica from the GMC is presented that allows us to better constrain the geochronological evolution of the Paleoproterozoic basement in northern Namibia.

3.2 Geology

3.2.1 Pre-Damaran basement units in northern Namibia

The geochronological evolution of the Proterozoic basement is well-documented only for the Kaoko Belt in NW Namibia (Fig. 3.1). A comprehensive overview that integrates available literature data and new U-Pb zircon ages has been given by Seth et al. (1998) and reflects five phases of major crust-forming events (Table 3.1): 1) protolith emplacement ages of granitoid gneisses between 2.645 and 2.585 Ma, which were related to an Archean terrain (Seth et al., 1998), 2) intrusion of granitoid rocks in the Epupa Inlier and the Huab Massif during the Eburnean orogeny at ca. 2.000 Ma (Seth et al., 1998), 3) gneiss formation in the Epupa Inlier and the Huab Massif (Tegtmeyer and Kröner, 1985) and intrusion of the Franzfontein granitic suite (Fig. 3.1) (Burger et al., 1976) between 1.880 and 1.680 Ma, 4) tectonism in the Franzfontein granitic suite around 1.580 Ma (Burger et al., 1976), 5) syn-Kibaran intrusion of the anorthositic Kunene Complex (KC) between ca. 1.280 and 1.470 Ma and related pegmatitic dykes (1.260 ± 90 Ma; age data of

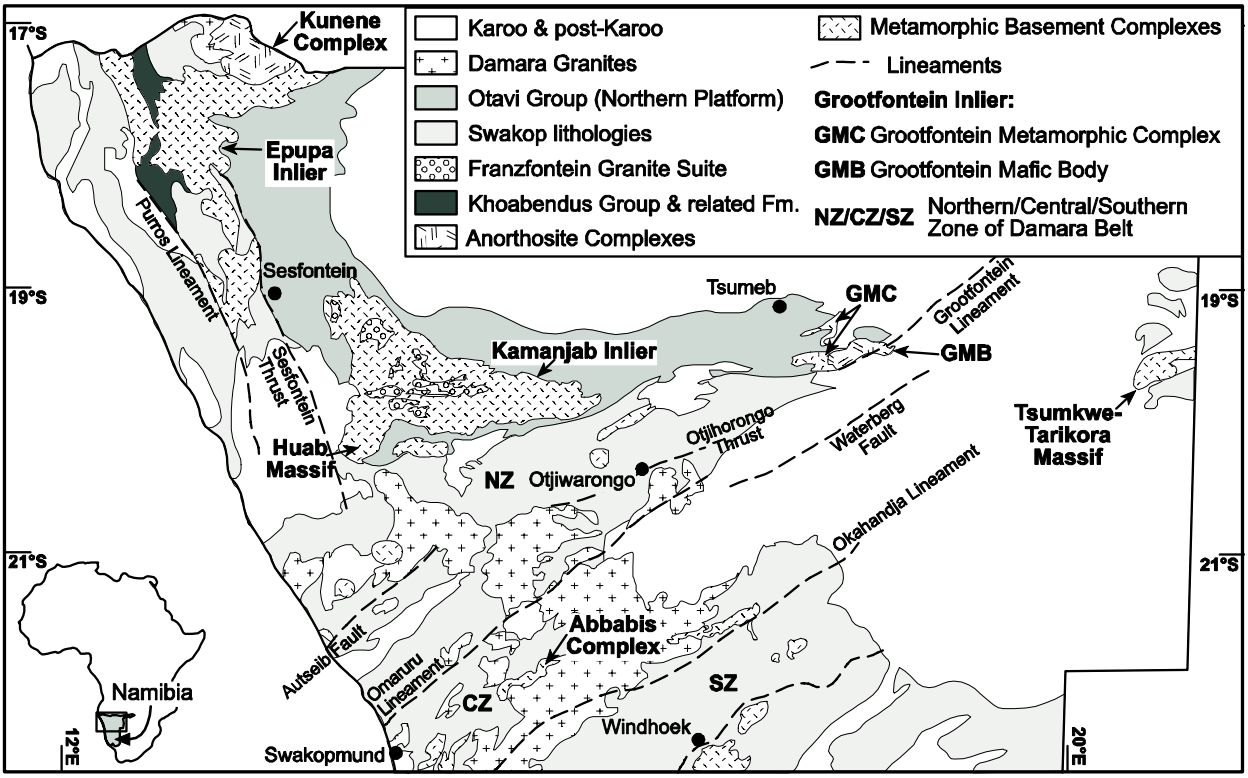

Fig. 3.1: Basement inliers at the southern boundary of the Congo Craton.

the KC with authors summarised in Mayer et al., 2004).

Jacob et al. (1978) proposed a continuous basement extension from the Huab Anticline to the Central Zone of the Damara Belt, with ages from 1.700 - 2.000 Ma. Weathering and erosion in the basement is marked by discordant whole-rock ages (Rb-Sr) of the Franzfontein Granite around 1.100 - 1.300 Ma (Burger et al., 1976; Clifford et al., 1969). Based on An/(Ab+Or+Qz) ratios, a pre-Damaran weathering episode has been postulated for the basement rocks, which are now close to or in direct contact with the overlying Neoproterozoic Otavi Group (Clifford et al., 1969). A Rb-Sr age of 560 ± 30 Ma for biotite from the Franzfontein granitic suite may reflect later a tectonothermal event related to the Pan-African orogeny (Clifford et al., 1962). Similar ages for a Pan-African overprint of the basement rocks were found by other authors (Jacob et al., 1978; Seth et al., 1998).

The basement in central and north-eastern Namibia is cut by NNE-SSW to E-W striking lineaments, which are part of a Neoproterozoic horst and graben system (Raab et al., 2002). These are, from S to N, the Okahandja Lineament, the Omaruru Lineament - Waterberg Fault System, and the Autseib Fault - Otjihorongo Thrust System, which possibly extends north-eastwards into the Grootfontein Lineament in the Otavi Mountainland (Fig. 3.1).

3.2.2 The pre-Damaran basement in the OML

In the Otavi Mountainland (NE Namibia), the pre-Damaran basement is represented by the Grootfontein Inlier, which extends from Otavi in the West to the Grootfontein Lineament in the SE, and to Abenab in the N (Fig. 3.1, 3.2). The Grootfontein Inlier has been subdivided into the Grootfontein Metamorphic Complex (GMC) and the Grootfontein Mafic Body (GMB) (GSN, 1999). The GMC emerges in several EW-striking anticlines: the Gauss Anticline in the SE, the Keilberg and Toggenburg Anticlines in the central OML, and the Nosib Anticline in the NE. However, outcrops are scarce due to widespread, post-Damaran sedimentary cover sequences. The GMC displays a diversified assemblage of plutonic rocks (Fig. 3.3), dominated by various, intensely deformed coarse-crystalline alkaline/calc-alkaline granites and granodiorites (Clifford et al., 1969). Own field observations revealed that the granodiorites of the northern Nosib Anticline contain large feldspar phenocrysts of up to 4 cm in length. Aplite dykes, less than 20 cm thick, intersect the otherwise homogenous

area	type of rock	age (Ma)	author	cycle/ orogeny
Franzfontein granites	Weathering and erosion of the Franzfontein Granitic Suite	1100 - 1300^	Clifford et al. (1969)	
Kunene Anorthosite Complex	Pegmatite dykes in the KC	1260 ± 90*	Simpson and Otto (1960)	Kibaran
Kunene Anorthosite Complex	Mangerite vein cogenetic with KC	1371 ± 2.5*	Mayer et al. (2004)	
Franzfontein granites	Tectonism of granites	1580 ± 20 (1662 ± 30* acc. to Seth et al!.)	Burger et al. (1976)	
Khoabendus Fm.	metavolcanics	1765 - 1860*	Burger and Coertze (1973)	
Epupa Inlier	augengneiss of granitic derivation	1795 + 33/-29*	Tegtmeyer and Kröner (1985)	
Franzfontein granites	Intrusion	1800 ± 80 (1838 ± 30* acc. to Seth et al.)	Burger et al. (1976)	
Huab Massif	Orthogneiss, granitic gneiss	1811 + 39/-35, 1749 + 78/-70*	Tegtmeyer and Kröner (1985)	
GMC	pegmatite dykes in the GMC	1816 ± 26 #	this study	Eburnean
GMB		1946 + 299/-333°	Armstrong (1988)	
Epupa Inlier	sheared monzogranite, possibly Epupa Inlier	1960,9 ± 0,6*, 1977,5 ± 0,6*	Seth et al. (1998)	
Epupa Inlier	granite	1985 - 1960*	Seth et al. (1998)	
Epupa Inlier	Khoabendus Fm. (rhyolite)	1987 ± 4*	Seth et al. (1998)	
W of Kamanjab	syenite	ca. 2124*	Tegtmeyer and Kröner (1985)	
Epupa Inlier ("Archean terrain")	granitoid gneiss protolith emplacement	2645 - 2585*	Seth et al. (1998)	

Tab. 3.1: Stratigraphy and geochronological evolution of the Proterozoic basement at the northern margin of the Damara belt (compiled from Hedberg, 1979; Simpson and Otto, 1960; Burger and Coertze, 1973; Burger et al., 1976; Tegtmeyer and Kröner, 1985; Armstrong, 1988; Seth et al., 1998; Mayer et al., 2004; and this study). *U-Pb and Pb-Pb zircon ages, ° Pb-Pb whole rock age, ^Rb-Sr whole rock age, # Rb-Sr mica age.

bodies. In the Toggenburg Anticline in the E, fine-crystalline, mafic igneous bodies display non-oriented jointing and quartz veining. Pegmatitic dykes containing up to 1cm large muscovite crystals intersect coarse-crystalline granites, which intruded dioritic rocks. In the Keilberg Anticline, basement rocks occur both in situ (GSN, 1999) and as fragments (granites, gneisses, schists) within diamictites of the overlying Neoproterozoic Ghaub Formation (Werner, 2005). According to Misiewicz (1988) gneissic two-mica granites occur in the Gauss Anticline. Muscovite, biotite and hornblende are the main components and epidote and calcite are alteration products. Söhnge (1957) described grey porphyritic granites comprising phenocrysts of microperthite, epidotised plagioclase, quartz and subordinate microcline. Accessories are dark green biotite, apatite, magnetite and zircon. Hornblende-rich diorites intermixed with heterogeneous granite-gneiss were reported from beneath the Nosib copper mine, which is located in the central Nosib Anticline. Broad areas of the GMC are overprinted by retrograde metamorphism, leading to chloritisation and saussuritisation (Günzel, pers. comm., 2005). Misiewicz (1988) observed hydrothermal alteration features in the Grootfontein Inlier, indicated by sericitisation of GMC granites and propylitisation of GMB gabbros.

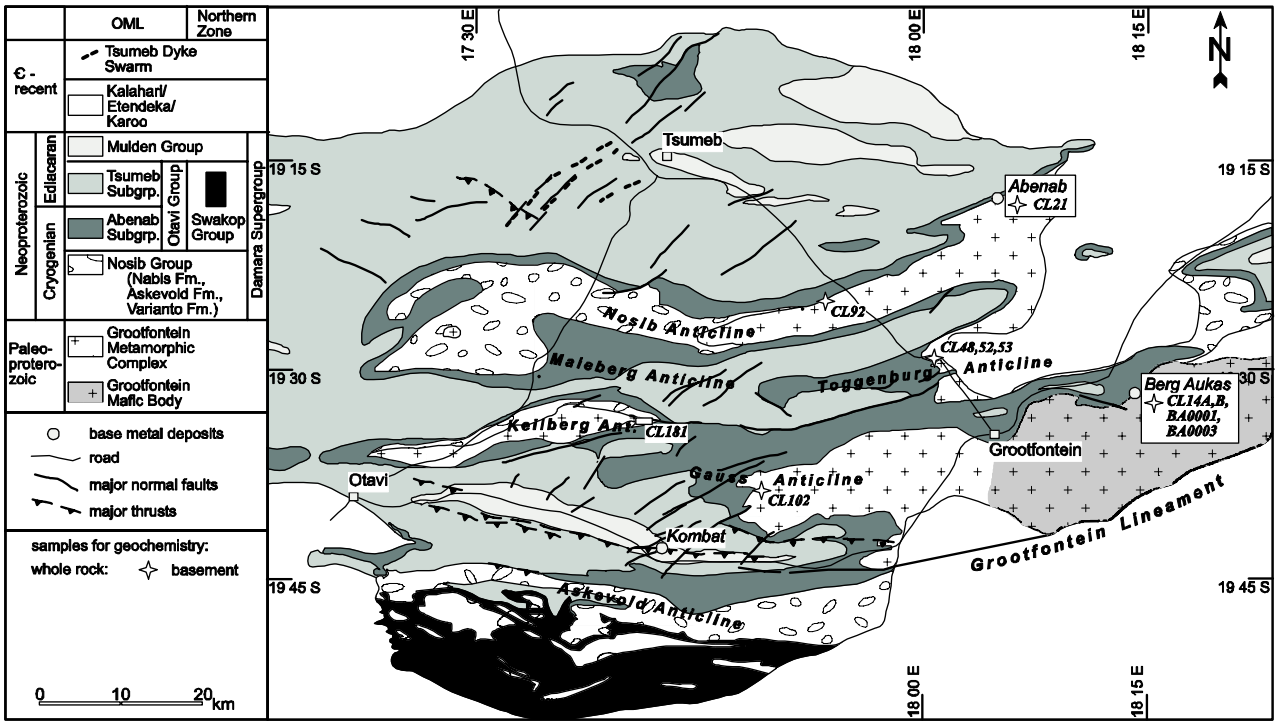

Fig. 3.2: Geological Map of the OML showing major structural elements and sample locations.

The GMB is located SE of Grootfontein (Fig. 3.2) and dominated by different generations of anorthosite (Günzel, pers. comm., 2004). Outcrops of the GMB were not encountered in the field, so that its existence relies upon drill core sampling by various mining companies and aeromagnetic surveying (GSN, 1999). Drilling sludges revealed also the presence of micaceous biotite gneisses, granites and amphibolites in the Grootfontein area (Martin, 1965; Söhnge, 1964).

Different opinions exist about the time relationships between the GMC and the GMB. Söhnge (1957) proposed an intrusion of the granitic rocks into metamorphosed mafic formations. Conversely, Misiewicz (1988) suggested an intrusive relationship of the mafics into the GMC, based on the observation of pink gneissic blocks within the basic rocks of the GMB. Hedberg (1979) linked the Grootfontein granites to the 1700-1900 Ma old Franzfontein granites (Fig. 3.1), whereas Martin (1965) and Söhnge (1964) related the Grootfontein Inlier to the Abbabis Formation in the Abbabis Complex (Fig. 3.1). Tankard et al. (1982) assigned the basement of the OML to the Huab-Grootfontein Metamorphic Suite. Rainaud et al. (2005) suggested that the Grootfontein Inlier could be part of the Kamanjab-Bangweulu arc, forming a Paleoproterozoic magmatic arc terrane, which extended from northern Namibia to northern Zambia and the Democratic Republic of Congo. The Kamanjab-Bangweulu arc was accreted to the southern margin of the Congo Craton during the Kibaran orogeny (ca. 1.400-1.000 Ma). The age of the Grootfontein Inlier is poorly constrained. Armstrong (1988) reported an imprecise Pb-Pb whole rock age of 1.946 +299/-333 Ma for gabbros occurring in the area SE of Grootfontein.

3.2.3 Neoproterozoic Damara Supergroup

The Paleoproterozoic basement of the OML is overlain by sedimentary successions of the Damara Supergroup, comprising the Nosib, Otavi and Mulden Groups. The Neoproterozoic break-up of Rodinia caused the opening of the Adamastor ocean at the western margin of the Sao Francisco-Congo Craton (Unrug, 1997). The Cryogenian development of an eastward aligned intracontinental branch of the Adamastor ocean, resulted in opening of the Khomas Trough and subsidiary basins ("Khomas Sea", Kukla and Stanistreet, 1991). This process caused an ENE-trending horst graben system in the Grootfontein Inlier (Söhnge, 1957), which was filled by sedimentary and volcanic successions of the Nosib Group. The accumulated siliciclastic rocks of the Nosib Group

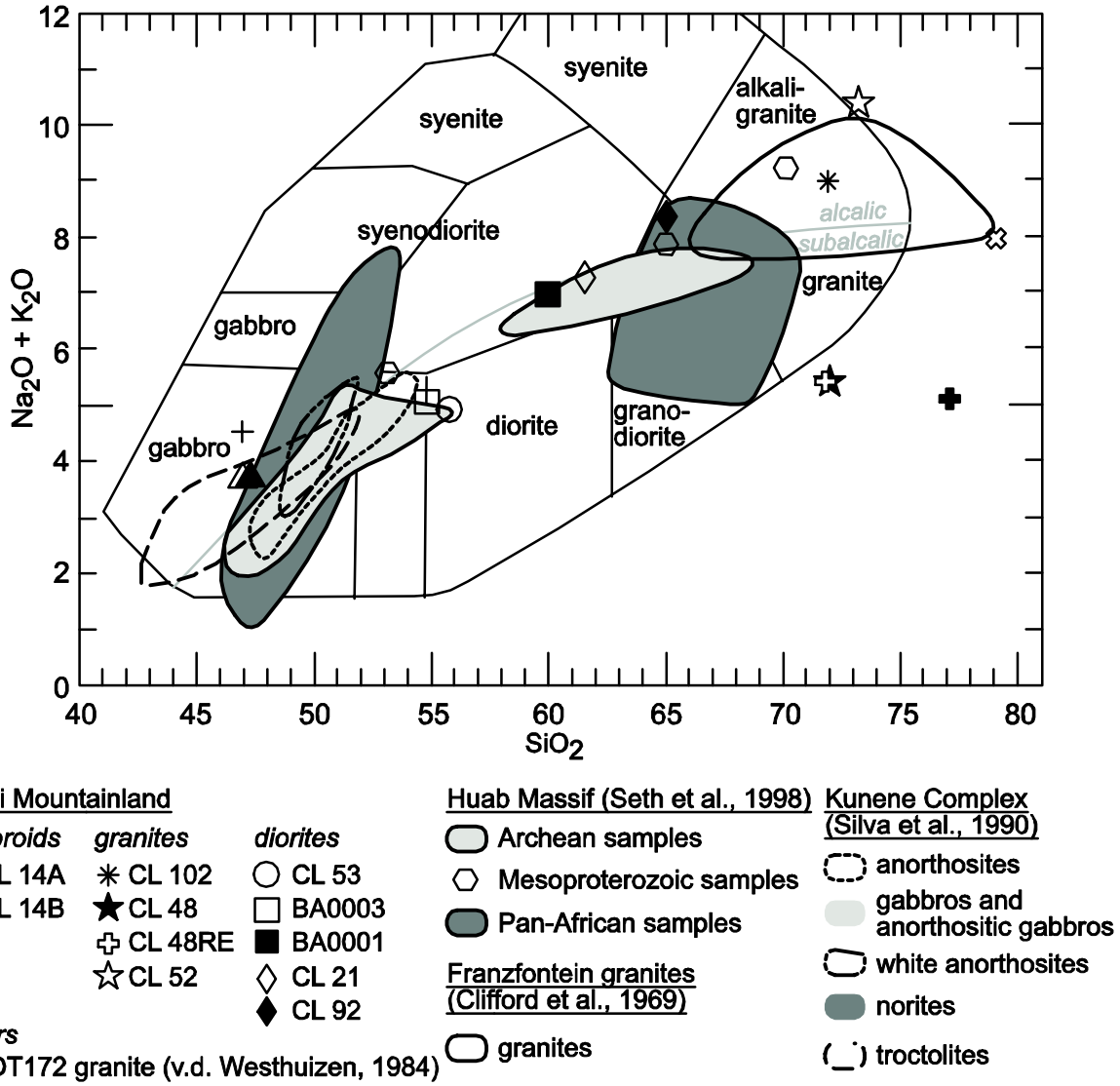

Fig. 3.3: Diagram of total alkali-silica (Cox et al., 1979; modified for plutonic rocks after Wilson, 1989) of samples from the Grootfontein Inlier and basement rocks of the southern Congo Craton and Central Damara Belt.

(Nabis Fm) reflect the composition of the subjacent basement (Hedberg, 1979) and interfinger with diamictites, pyroclastics and ironstones from the Chuos Fm (old terminology: Varianto Fm). The Grootfontein Lineament (Fig. 3.2) is a major fault at the southern scarp of the Paleoproterozoic basement that divides the Northern Platform from the Northern Zone (Miller, 1983a) (Fig. 3.1) and resulted from the Cryogenian rift processes. The rift processes were accompanied by mafic volcanism, whose relicts are represented by the Askevold Fm. The volcanic rocks of the Askevold Fm (Söhnge, 1957) can be correlated with the Naauwpoort Formation in the Northern Zone, which revealed U-Pb zircon ages of 742 ± 25 Ma (Burger and Coertze, 1973) and 746 ± 2 Ma (Hoffmann et al., 1996). In the late Neoproterozoic a carbonate platform developed on top of the Grootfontein Inlier and the siliciclastic graben fillings of the Nosib Group, represented by mainly carbonates of the Otavi Group. The Otavi Group is subdivided by diamictites of the Ghaub Fm into the basal Abenab Subgroup and the Tsumeb Subgroup on top (Hoffmann et al., 2004). During the Pan-African orogeny and related collision of the Sao Francisco-Congo and Kalahari Cratons, the Damaran successions were folded and thrusted northwards, resulting in thinning and tectonically induced repetition of the Damara Supergroup (Söhnge, 1972; Innes and Chaplin, 1986). In the greenschist-facies Northern Zone, south of the Grootfontein Lineament, the original contact from the

Nosib Group to the underlying basement was overprinted by the Pan-African orogeny. Sheared contacts of the Nosib Group with the Paleoproterozoic basement and the Abenab Subgroup were reported by Schoch (1958) and Brandt (1955).

3.3 Sampling and analytical methods

A total of 10 samples of Paleoproterozoic basement rocks were taken in the OML for petrography and geochemical analysis during field seasons from 2004 to 2005. Sample types and locations are given in Table 3.2. With exception of samples CL14 and CL21, which were collected from drill core dumps at Berg Aukas and Abenab (Fig. 3.2), respectively, the samples were taken from field outcrops. All samples were studied in thin section (Fig. 3.2 for location).

Whole rock powders were prepared using a jaw crusher and a tungsten-carbide mill at the University of Heidelberg. Analysis of the main and trace elements was performed by ACME Analytical Laboratories Ltd. (Canada). For whole rock analysis, 2.5 g of sample pulp was treated with $LiBO_2$ fusion and subsequent digestion using dilute HNO_3. Major oxides and minor elements were measured by ICP-ES and trace elements measured by ICP-MS. Sample CL14A was remeasured by ACME Analytical Laboratories Ltd. and labelled as CL14B.

White mica for Rb-Sr dating was extracted from a sample of pegmatitic dyke taken from the Farkfontein Farm northwest of Grootfontein (CL52, Fig. 3.2). The mica sample was leached in hot 1 N HCl for 15 min. and repeatedly rinsed with DDW. The dry sample was weighed and completely dissolved in a Teflon screw-top vial at 120°C. After evaporation to dryness, the residue was redissolved in 6 N HCl. One sample aliquot was spiked with a mixed ^{87}Rb-^{84}Sr tracer for Rb and Sr concentration analyses by isotope dilution, whereas an unspiked aliquot was used for determination of the $^{87}Sr/^{86}Sr$ ratio. Both aliquots were dried again and rewetted with 3 N HNO_3. Rb and Sr were separated with 3 N HNO_3 using EICHROM Sr resin on 50 µl Teflon columns following the methods of Horwitz et al. (1991a; 1991b). The first 600 µl of HNO_3 wash of the spiked aliquot were collected and used for measurement of Rb. Sr was stripped from the columns with 1 ml of H_2O. For mass spectrometry, Sr was loaded with $TaCl_5$-HF-H_3PO_4 solution (Birck, 1986) onto W single filaments. Rb was loaded with DDW onto the evaporation ribbon of a Ta double-filament assemblage. All isotopic measurements were performed at ETH Zurich (Switzerland) on a FINNIGAN MAT 262 solid-source mass spectrometer running in static multicollection mode. Sr isotopic ratios were normalised to $^{88}Sr/^{86}Sr = 0.1194$. Repeated static measurements of the NBS 987 standard over the duration of this study yielded an average $^{87}Sr/^{86}Sr$ ratio of 0.71024 ± 4 (2σ mean, n = 6). Errors and error correlations were calculated after Ludwig (1980). Individual uncertainties (2σ) are given for Rb-Sr elemental concentrations and isotope ratios (Table 3.3). Total procedure blanks amounted to 30 pg Sr and were found to be negligible. Rb-Sr ages were calculated after Ludwig (2001) using the ISOPLOT/Ex version 2.49 program, errors on the ages are quoted at the 2σ level.

3.4 Results

3.4.1 Field relationships and petrography

The Grootfontein Inlier crops out in EW-striking anticlines, which are the Gauss Anticline in the southeast (Fig. 3.2), the Keilberg and the Toggenburg Anticline in the central OML and the Nosib Anticline in the northeast. Good outcrops of the Grootfontein Inlier were found on the Polmannskloof Farm (sample CL102) and the Farkfontein Farm (samples CL48, 52, 53). Coarse crystalline granites and granodiorites (sample CL102, Gauss Anticline, Fig. 3.2) are the dominating basement rocks of the Grootfontein Inlier. Granodiorites of the northern Nosib Anticline contain large feldspar-phenocrysts with a long axis of up to 4 cm (sample CL92, Fig. 3.2, Table 3.2). Aplite dykes, less than 20cm thick, intersect the otherwise homogenous bodies. In the Toggenburg Anticline (Farm Farkfontein), fine crystalline, mafic igneous bodies (sample CL53, Fig. 3.2, Table 3.2) display non-oriented jointing and quartz veining. Coarse crystalline (grain size about 0.5 mm) granites (sample CL48, Fig. 3.2, Table 3.2) are intruded by even coarser pegmatitic dykes (sample CL52). The latter include "veins" displaying greenish chloritisation and up to 1 cm large muscovite crystals. Outcrops of the GMB have not been encountered in the field, so that its existence relies still upon drill core sampling by various mining companies and the GSN (Geological Survey of Namibia) as well as aeromagnetic surveying carried

out by the GSN and the BGR (Bundesanstalt für Geowissenschaften und Rohstoffe, Germany).

At outcrop and in hand specimens, all basement samples do not show any deformational overprint but jointing. In thin section, a foliation of the diorites is suggested by epidote and actinolite floating around large plagioclase (Fig. 3.4a). The mineral assemblage of granites and diorites of the GMC reflects distinct alteration patterns. Granites are characterised by myrmekitisation of K-feldspar. This alteration is due to the breakdown of hornblende (hastingsite), which results in silification and calcitisation of feldspars (Fig. 3.4b). The primary composition of the diorites consisted of plagioclase (ca. 50 vol. %), amphiboles (hastingsite and grammatite) and quartz. Saussuritisation of the feldspars resulted in the formation of calcite, chlorite, quartz and epidote, sometimes merged in complex aggregates. Either the same minerals, but larger in size, or only epidote and quartz can replace amphibole. The zoned epidotes are overgrown by feldspar. Other samples predominantly show a breakdown of hornblende, leading to the growth of calcite, actinolite, quartz and epidote (Fig. 3.4c). Small-scale shear zones are composed mainly of epidote, chlorite and opaque phases. Pegmatite sample CL52 from the Toggenburg Anticline contains serictised orthoclase, which exhibits distinct perthitic segregation. Quartz shows undulation and grain boundary migration. Muscovite is bent and characterised by a high content of opaque phases that are aligned along the slip planes.

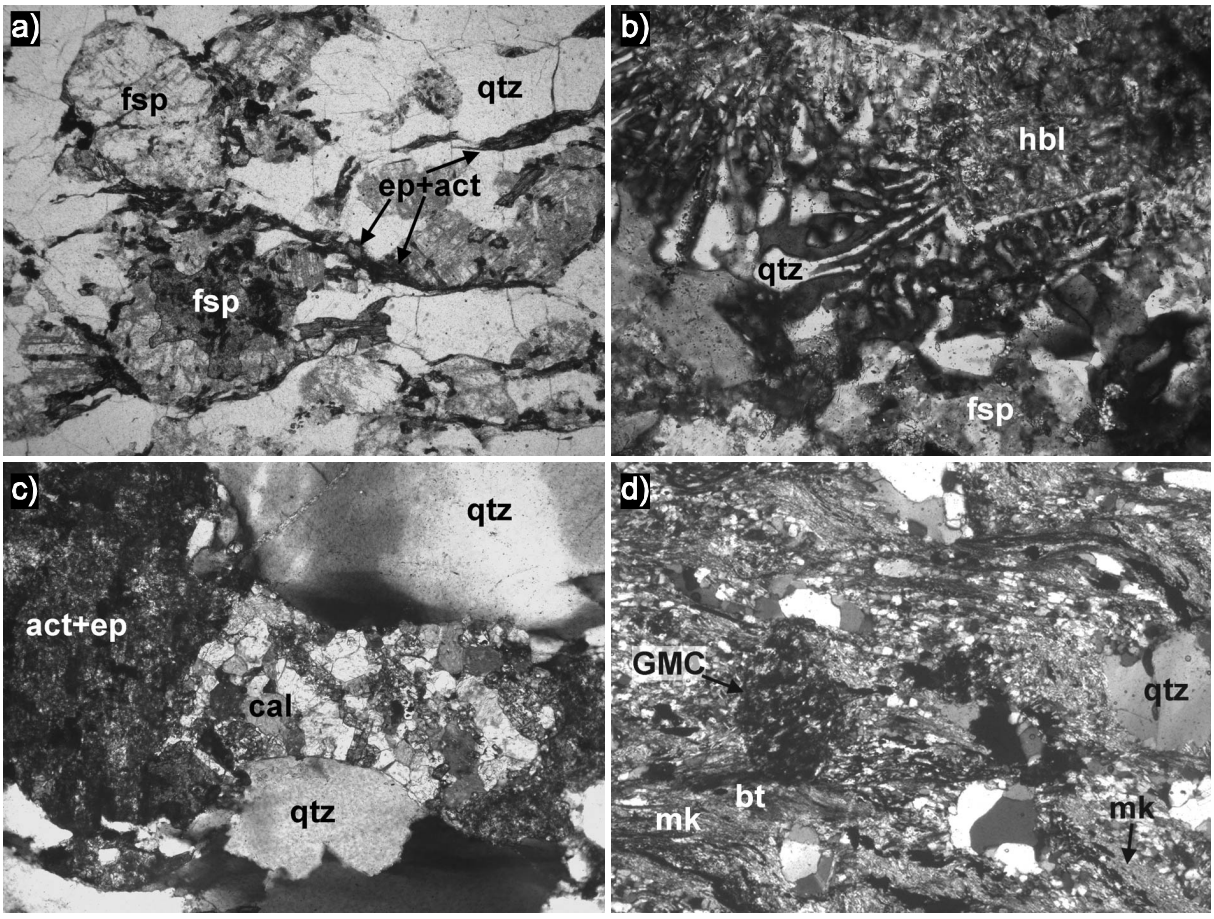

Fig. 3.4: Hand specimens and thin sections of sampled basement rocks: a) epidote-actinolite-foliation; thin section, parallel nicols, lower side: 4mm (CL53), b) breakdown of hastingsite and myrmekitisation of K-feldspar; thin section, crossed nicols, lower side: 0,5mm (CL48), c) calcite, epidote, actinolite and quartz growth due to breakdown of hastingsite; thin section, crossed nicols, lower side: 1,4mm (CL53), d) SC-pattern in quartzitic micaschist, lower side: 2,5mm (CL181). GMC: clast from Grootfontein Metamorphic Complex, act: actinolite; bt: biotite, cal: calcite, ep: epidote, fsp: feldspar, hbl: hornblende, mk: muscovite, qtz: quartz.

Locality	Abenab	Hurisib	Polmannskl.	Farkfontein	Farkfontein	Farkfontein
Sample	CL 21	CL92	CL102	CL48	RE CL48	CL52
Rock type	Syenodiorite	Granodiorite	Alkali Granite	Granite	Granite	Pegmatite
SiO2	61.50	64.98	71.89	71.93	71.76	73.14
Al2O3	16.20	16.57	15.13	15.42	15.17	14.74
Fe2O3	4.61	3.36	1.06	2.17	2.27	0.30
MgO	2.68	1.56	0.37	0.82	0.99	0.11
CaO	3.10	2.51	0.89	2.59	2.53	0.66
Na2O	2.86	4.08	3.75	3.65	3.59	3.17
K2O	4.43	4.32	5.25	1.80	1.84	7.23
TiO2	0.62	0.43	0.11	0.26	0.25	0.02
P2O5	0.24	0.18	0.21	0.04	0.04	0.08
Cr2O3	0.004	0.002	0.001	0.001	0.001	0.001
LOI	4.00	1.50	1.20	1.20	1.30	0.40
TOT/C	0.62	0.02	0.06	0.08	0.08	0.11
TOT/S	0.01	0.01	0.01	0.04	0.04	0.01
Total	99.65	99.54	99.89	99.90	99.76	99.86
A.S.I.	1.56	1.52	1.53	1.92	1.91	1.33
Ba	1215.00	1994.40	1025.70	672.10	673.00	438.70
Sc	12.00	4.00	7.00	3.00	3.00	3.00
Mo	0.30	0.30	0.40	0.20	0.30	0.30
Cu	5.40	44.90	12.10	7.30	7.00	1.50
Pb	4.10	15.90	6.90	2.50	2.60	5.50
Zn	53.00	38.00	14.00	12.00	11.00	3.00
As	0.60	< 0.5	< 0.5	0.70	0.70	< 0.5
Sb	< 0.1	< 0.1	0.20	0.10	0.10	< 0.1
Ag	< 0.1	< 0.1	< 0.1	< 0.1	< 0.1	< 0.1
Au	3.00	2.40	1.50	< 0.5	2.00	0.50
V	89.00	55.00	5.00	25.00	25.00	<5
Rb	168.20	139.90	159.00	81.60	84.50	272.80
Sr	555.30	653.70	139.50	403.30	403.50	75.00
U	1.80	0.60	1.10	0.30	0.30	0.60
Th	14.30	8.20	6.80	<1	<1	1.90
Y	15.80	9.40	18.50	4.10	4.10	8.70
Zr	130.50	196.80	39.10	129.10	133.70	13.70
Nb	10.10	6.30	8.70	1.40	1.10	8.10
Cs	11.50	5.00	1.80	2.70	3.20	7.60
Ga	19.80	18.20	12.00	12.10	12.60	13.00
Rb/Sr	0.30	0.21	1.14	0.20	0.21	3.64
La	24.30	41.40	21.20	2.80	2.70	3.30
Ce	49.20	77.10	39.80	4.50	4.60	6.30
Pr	5.47	7.97	4.91	0.74	0.67	0.82
Nd	22.80	26.50	18.70	2.70	3.00	3.40
Sm	4.40	3.80	3.70	0.70	0.70	1.00
Eu	1.10	1.22	0.75	0.39	0.37	0.21
Gd	3.48	2.24	2.75	0.51	0.76	0.98
Tb	0.60	0.35	0.57	0.13	0.12	0.22
Dy	2.57	1.68	3.05	0.62	0.72	1.41
Ho	0.46	0.30	0.58	0.12	0.15	0.27
Er	1.47	0.92	1.94	0.43	0.43	0.88
Tm	0.24	0.15	0.31	0.07	0.07	0.15
Yb	1.58	0.87	1.94	0.49	0.47	1.14
Lu	0.23	0.15	0.29	0.07	0.06	0.18
REE tot	117.90	164.65	100.49	14.27	14.82	20.26

Tab. 3.2: Whole-rock geochemical composition of Paleoproterozoic rocks from the OML. Analyses of samples BA0001 and BA0003 provided by F. Melcher (BGR Hannover, Germany). Oxides in wt.-%, n.d. = not detected, N. a. = not analysed.

Locality	Farkfontein	Berg Aukas	Berg Aukas	Berg Aukas	Berg Aukas	Keilberg
Sample	CL53	CL 14A	CL 14B	BA0003	BA0001	CL181
Rock type	Diorite	Anorthositic Gabbro	Anorthositic Gabbro	Diorite	Syenodiorite	Gneiss
SiO2	55.70	46.95	47.23	54.78	59.94	78.29
Al2O3	14.19	16.50	16.58	15.41	17.25	10.75
Fe2O3	10.91	13.35	13.54	9.58	8.98	3.63
MgO	4.35	4.56	4.63	3.05	2.67	0.84
CaO	4.43	9.56	9.66	4.13	2.70	0.23
Na2O	2.57	2.91	2.92	2.26	4.22	0.15
K2O	2.39	0.81	0.81	2.81	2.77	3.49
TiO2	1.05	1.72	1.76	1.76	1.75	0.39
P2O5	0.39	0.44	0.45	0.51	0.51	0.01
Cr2O3	0.006	0.002	0.002	n.a.	n.a.	0.001
LOI	2.80	2.60	1.90	4.96	3.03	2.10
TOT/C	0.21	0.23	0.20	n.a.	n.a.	0.17
TOT/S	0.01	0.24	0.23	n.a.	n.a.	0.01
Total	99.92	99.64	99.73	99.61	99.22	99.94
A.S.I.	1.51	1.24	1.24	1.68	1.78	2.78
Ba	610.80	446.00	459.00	453.00	453.00	737.70
Sc	32.00	38.00	39.00	38.50	38.50	10.00
Mo	0.40	0.50	0.40	<2	<2	0.30
Cu	140.70	177.10	168.60	477.00	2926.00	3.10
Pb	5.40	2.20	2.10	21.00	11.00	3.00
Zn	75.00	77.00	67.00	101.00	78.00	16.00
As	0.80	< 0.5	< 0.5	21.00	18.00	0.60
Sb	< 0.1	< 0.1	< 0.1	<5	<5	< 0.1
Ag	< 0.1	0.10	0.10	0.10	0.10	< 0.1
Au	1.40	6.70	5.80	6.50	6.50	1.70
V	253.00	311.00	319.00	211.00	229.00	68.00
Rb	95.80	11.50	12.20	64.00	63.00	131.80
Sr	153.40	427.80	424.10	306.00	238.00	32.80
U	2.30	< 0.1	0.10	6.00	<3	0.60
Th	7.60	0.20	0.50	<5	6.00	16.60
Y	26.00	45.00	45.80	41.00	39.00	24.90
Zr	139.00	199.60	215.20	281.00	343.00	120.90
Nb	7.20	12.80	12.90	16.00	17.00	10.00
Cs	8.80	0.30	0.30	13.00	11.00	3.60
Ga	18.40	22.10	22.50	22.00	24.00	11.90
Rb/Sr	0.62	0.03	0.03	0.21	0.26	4.02
La	30.20	27.90	27.90	44.00	40.00	23.40
Ce	60.60	69.60	68.30	71.00	80.00	179.60
Pr	7.10	8.60	8.55	n.a.	n.a.	7.11
Nd	26.80	41.60	40.80	n.a.	n.a.	27.70
Sm	5.50	9.00	9.20	n.a.	n.a.	4.60
Eu	1.36	2.01	2.13	n.a.	n.a.	1.06
Gd	4.69	8.46	8.81	n.a.	n.a.	3.02
Tb	0.84	1.47	1.45	n.a.	n.a.	0.77
Dy	4.65	7.54	7.82	n.a.	n.a.	4.20
Ho	0.96	1.40	1.50	n.a.	n.a.	0.81
Er	2.89	4.48	4.86	n.a.	n.a.	2.37
Tm	0.40	0.63	0.67	n.a.	n.a.	0.35
Yb	2.52	3.97	4.28	n.a.	n.a.	2.07
Lu	0.44	0.57	0.62	n.a.	n.a.	0.31
REE tot.	148.95	187.23	186.89	115.00	120.00	257.37

Tab. 3.2 (continued) : Whole-rock geochemical composition of Paleoproterozoic rocks from the OML. Analyses of samples BA0001 and BA0003 provided by F. Melcher (BGR Hannover, Germany). Oxides in wt.-%, n.d. = not detected, N. a. = not analysed.

In addition to the granite and diorite clasts found in diamictites of the Keilberg Anticline (Werner, 2005), detrital biotite and clasts of brecciated granites mixed with foliated gneisses provide an insight into the composition of the late Neoproterozoic eroded basement highs. The feldspars show almost complete sericitisation. Biotite grows in shear bands and occurs together with rutile and opaque phases, reflecting higher greenschist facies conditions during a pre-Pan-African metamorphic event.

Quartzitic micaschists from Keilberg (sample CL181 Fig. 3.2, Table 3.2) and similar rocks observed in the central Gauss Anticline are highly siliceous (quartz 30-60%, white mica 20-25%) and exhibit distinct sc-patterns traced by white mica and crenulation of mica fishes (Fig. 3.4d). Depending on the grade and type of alteration, the light pink colour of these rocks turns into red or green. Allothigene quartz and hornblende clasts are enclosed in the foliated matrix, the latter ones of which being extremely altered and exhibiting biotite strain shadows. Scarce outcrops of phyllitic micaschists with a SE-dipping cleavage are spatially related to the quartzitic micaschists.

3.4.2 Geochemistry

Main and trace element data for igneous rocks from the Grootfontein Inlier are given in Table 3.2 and depicted in Fig. 3.5-9. The igneous bodies of the Grootfontein Inlier have SiO_2 concentrations between 47 and 78 wt.% (Table 3.2, Fig. 3.5). Three groups can be distinguished by their main element composition: 1) granitic to alkali granitic rocks (CL48, CL52, CL102), 2) dioritic rocks (CL53, CL92, CL21, BA0001, BA0003) and 3) gabbroic rocks (CL14A, CL14B) (Fig. 3.5). The abundances of CaO, MgO, TiO_2, Fe_2O_3 and V decrease with increasing SiO_2 content (Fig. 3.5, 6c). Except for gabbroic sample 14A, the same is observed for the SiO_2/P_2O_5 ratio. K_2O and Rb increase in the dioritic and gabbroic rocks with increasing SiO_2. Granitic to alkali granitic rocks show a pronounced variation in K_2O and Rb at a limited SiO_2 variation (Fig. 3.5g, 3.6e). The A.S. index (Aluminium Saturation Index: molar $Al_2O_3/CaO+Na_2O+K_2O$; Shand, 1951) varies between 1.33 and 1.92 (Fig. 3.6f). The Cr_2O_3 and Zn contents decrease with increasing SiO_2 in the diorites and granites (Fig. 3.6a, b). Gabbros from Berg Aukas (CL14A, B) reveal a strong variation of Cr_2O_3 and Zn and an A.S. index of ca. 1.24.

Selected major and trace element profiles of the granites and gabbros reflect contrasting distributions of the incompatible elements (Fig. 3.7a, b). With the exception of Zr, Mo and As, the variation of trace element abundances increases with decreasing incompatibility. Pb, Zr, Y, Sc, V, Zn and Cu abundances are high in the dioritic and gabbroic samples compared to the granitic samples. Samples from the Berg Aukas area have the highest V and Cu contents. The gabbroic rocks show lower Rb, but higher Sr contents than the diorites and granites. The distribution pattern of the Keilberg quartzitic micaschist (CL181) is similar to that of the granitic rocks (Fig. 3.7b). Previous data of Van der Westhuizen (1984, LOT082 and LOT172) are well comparable to the granitic rocks analysed in this study at least in their Pb, V, Zn and Cu abundances (Fig. 3.7).

Bulk-Earth-normalised trace element-diagrams (Fig. 3.8; Hickey et al., 1986) display a uniform distribution pattern for the dioritic rocks with decreasing relative abundances of more compatible trace elements. The Keilberg quartzitic micaschist (CL181) shows a similar pattern, differing only in higher Ce and lower Sr values. Trace element distribution patterns of the granitic rocks display high variations, but generally decrease with increasing element compatibility in alkaligranites (CL102) and pegmatites (CL52). Granite CL48 has the lowest Nb value of all samples. Sr and Zr values are similar to those of the diorites and interrupt along with Nb the generally decreasing distribution patterns of the higher compatible elements. The more compatible trace elements (La to Yb) in the gabbroic rocks reveal a pattern similar to the dioritic rocks, slightly decreasing with compatibility. The more incompatible elements (Cs to Nb) are less abundant in the gabbroic rocks with very low values especially for Th.

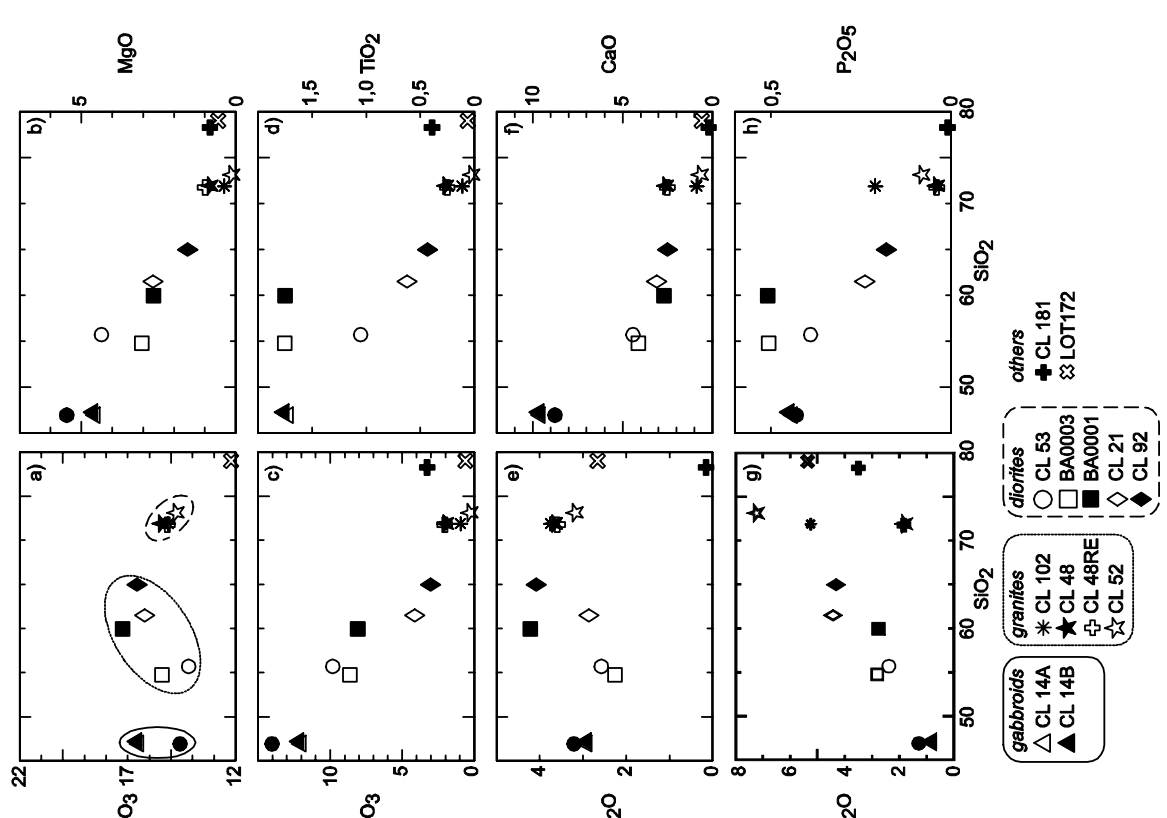

Fig. 3.5: Major element plots of the investigated rocks of the Grootfontein Inlier. Additional data from the Grootfontein Metamorphic Complex by Melcher (Melcher, 2004) and Van der Westhuizen (1984) also shown.

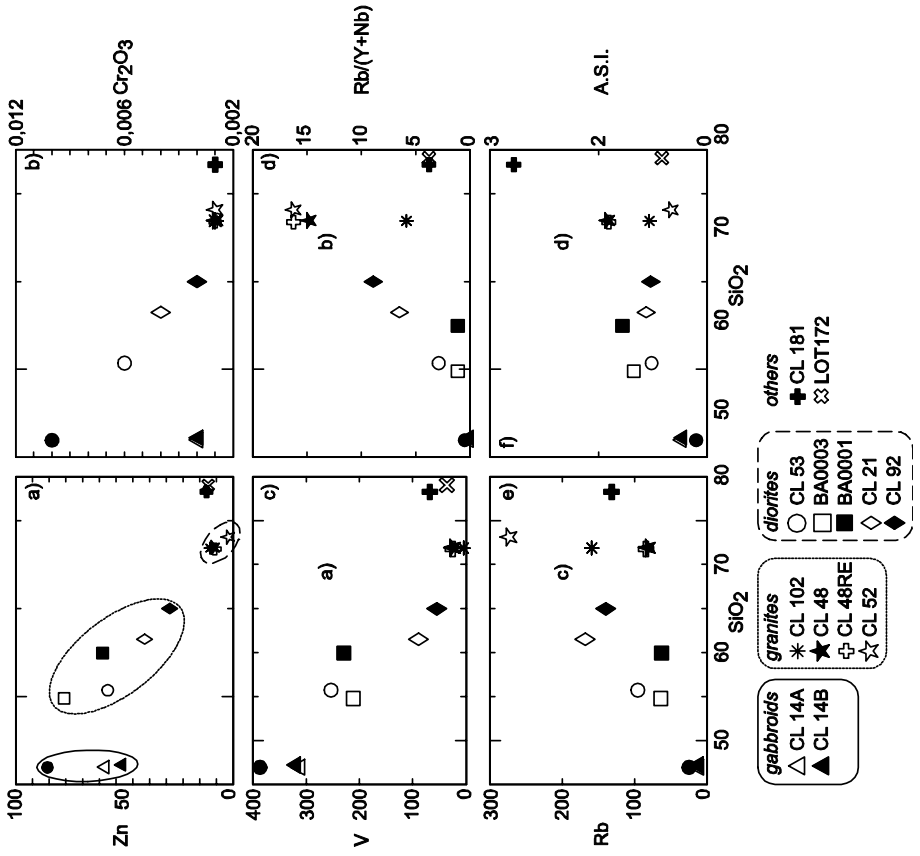

Fig. 3.6: Selected trace element plots for the investigated rocks of the Grootfontein Inlier. Additional data from the Grootfontein Metamorphic Complex by Melcher (unpublished BGR-report, 2004) and Van der Westhuizen (1984) also shown.

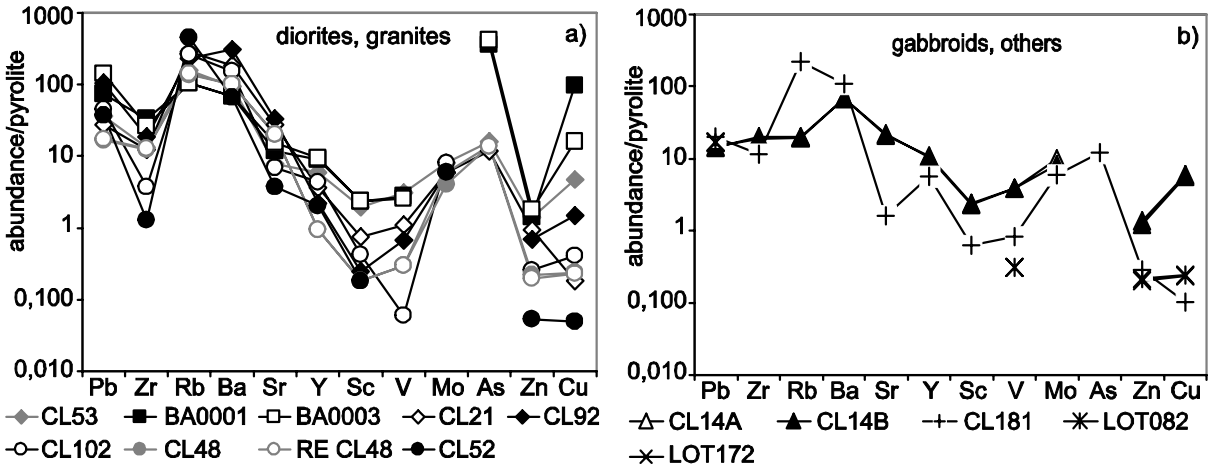

Fig. 3.7: Pyrolite-normalised trace element profiles. a) diorites and granites, b) for gabbroids and others (normalising values from McDonough and Sun, 1995). Elements in order of increasing compatibility towards the right.

REE analyses of the gabbroic and dioritic rocks and alkali granite (Cl102) reveal similar patterns for the light REE and a general decrease in relative abundances towards the heavier REE (Fig. 3.9). The gabbroic rocks are enriched in HREE compared to the diorites. With the exception of sample CL102, the granitic rocks display distinct variation in their REE pattern. The granite and pegmatite samples from the Farkfontein Farm (CL48, 52) have the lowest LREE abundances of all analysed basement rocks. CL52 and CL102 show a distinct negative and CL48 a positive Eu anomaly. Except for the positive Ce anomaly, the REE distribution pattern of quartzitic micaschists from Keilberg (CL181) is similar to that of the dioritic group.

3.4.3 Rb-Sr dating

Rb-Sr isotopic data for the sample of white mica separated from a pegmatitic dyke at Farkfontein Farm (sample CL52) are given in Table 3.3. The mica has very high Rb and low Sr contents (Rb/Sr = 93.6). The $^{87}Rb/^{86}Sr$ ratio is about 880 and the Sr is highly radiogenic with $^{87}Sr/^{86}Sr$ = 23.71. Therefore, the unknown initial $^{87}Sr/^{86}Sr$ ratio of that mica is insignificant for calculating a model age. Assuming an

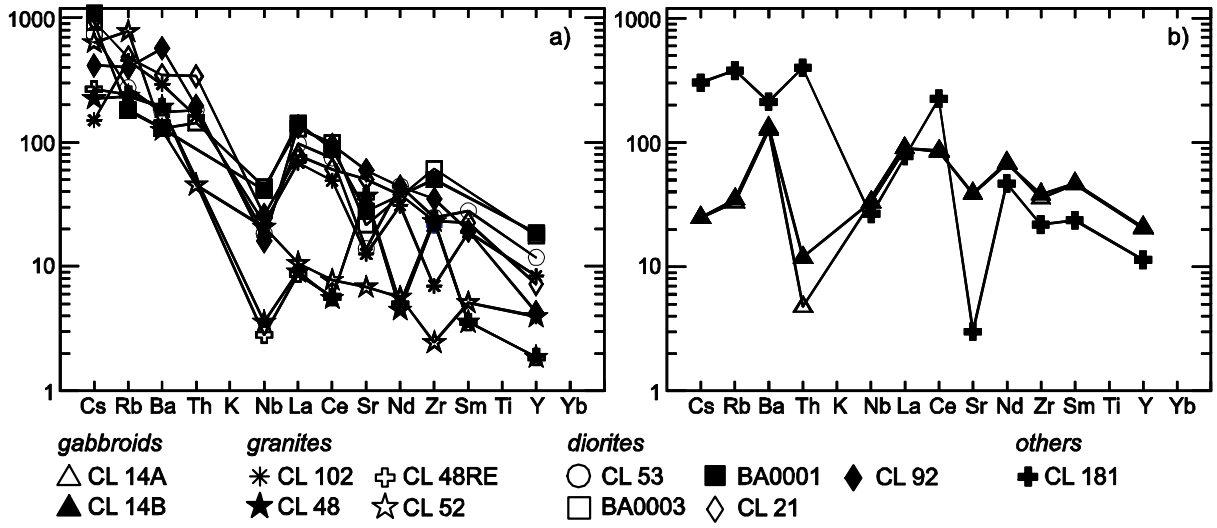

Fig. 3.8: Bulk Earth normalised trace element-diagrams (after Hickey et al., 1986). a) diorites and granites, b) for gabbroids and others. K and Ti not shown because of normalised values well below 1.

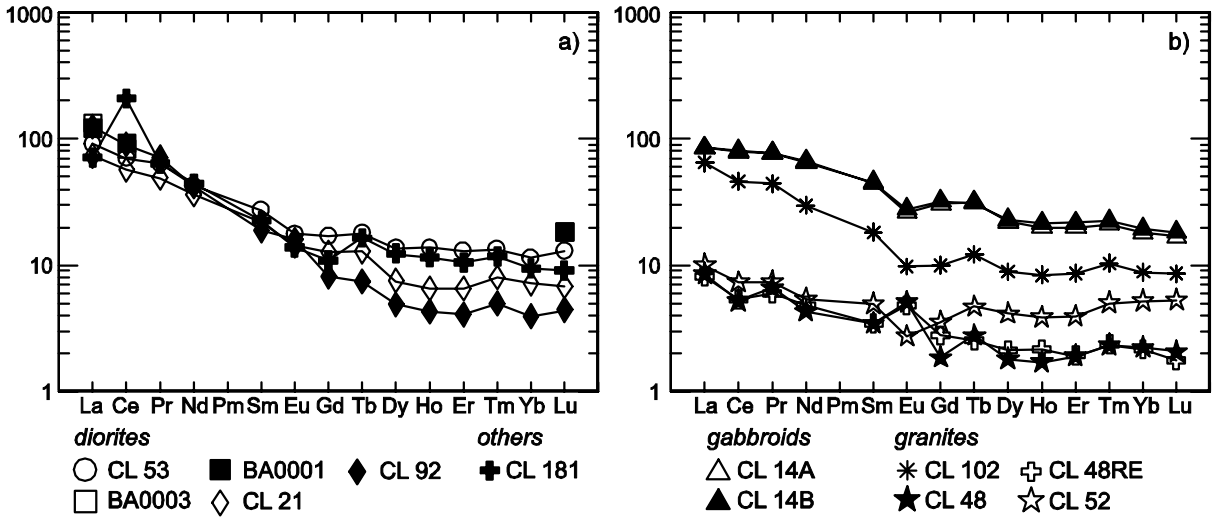

Fig. 3.9: Chondrite normalised REE plots (Nakamura, 1974) for rocks from the Grootfontein Inlier. a) diorites and quartzitic micaschist CL181. b) gabbroids and granites.

average crustal value of $^{87}Sr/^{86}Sr = 0.71$ for the initial Sr, a model age of 1.816 ± 23 Ma is obtained. This late Eburnean age is significantly younger than the Pb-Pb whole rock age of 1.946 +299/-333 Ma reported by Armstrong (1988) for gabbroic rocks from the area SE of Grootfontein, and most likely dates the emplacement of pegmatites during a late magmatic stage in the GMC Overall, the age of 1.816 Ma corresponds well to ages in the 1.880 - 1.680 Ma range reported for the Franzfontein granitic suite in the Kamanjab Inlier farther W (Burger et al., 1976).

3.5. Discussion

Based on petrographical observation and geochemical data, three major types of plutonic rocks have been distinguished in the Grootfontein Inlier, a granitic, a dioritic and a gabbroic group. This is in accordance with Söhnge (1957), who postulated an extreme compositional variation of the granites of the Grootfontein Inlier, depending on the extent of contamination from the older basement. Van der Westhuizen (1984 cf.; Fig. 3.3, 3.5, 3.6) also reported the presence of highly siliceous granites from the Grootfontein Inlier, whose overall geochemical composition is, except for their extremely low Al_2O_3 content, comparable to the granitic rocks analysed in this study. Furthermore, trace element patterns of the diorites from the eastern Toggenburg Syncline and at Berg Aukas are similar to those of the gabbroic samples from Berg Aukas, which are interpreted to belong to the GMB (Fig. 3.7; 3.8). Significant differences are confined to relatively lower abundance of more incompatible elements in the GMB, such as Cs, Rb and Th (Fig. 3.8). Conversely, the diorites match in their distribution of incompatible trace elements with the other samples of the GMC. This points to a regional change of the trace element distribution which could have originated from distinct magma sources or differential contamination from older basement rocks.

The tectonic setting of the pre-Damaran basement rocks in the OML may be inferred from geochemical discrimination diagrams. In a Rb vs. Y+Nb diagram (Pearce et al., 1984; Fig. 3.10), the granites and alkali granites of the OML plot close to the boundary of

Sample	Sample wt. [mg]	Rb [ppm] ± 2σ	Sr [ppm] ± 2σ	$^{87}Rb/^{86}Sr$ ± 2σ	$^{87}Sr/^{86}Sr$ ± 2σ
CL52	5.2	1088.7 ± 12.3	11.63 ± 0.17	880.24 ± 11.68	23.708 ± 0.017

Table 3. Rb-Sr isotopic data for pegmatite-related white mica from Farkfontein Farm.

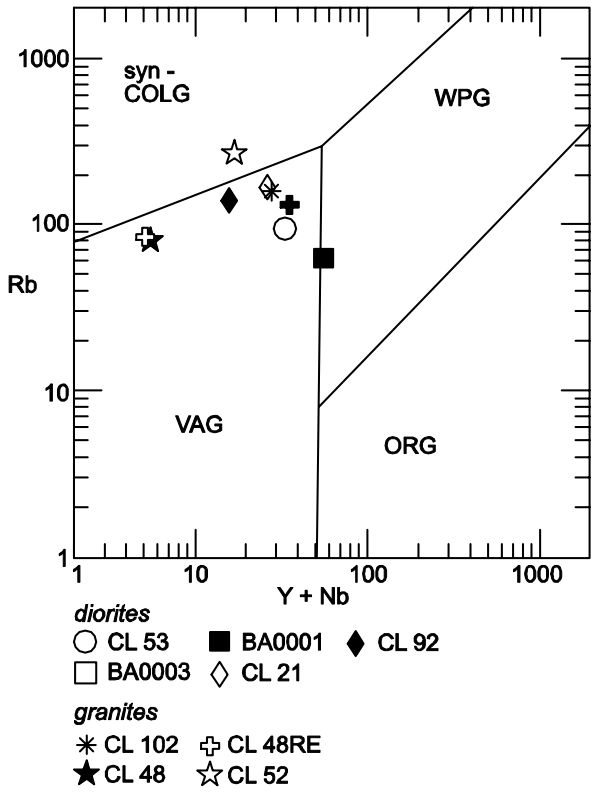

Fig. 3.10: Rb/(Y+Nb) (Pearce et al., 1984) of the diorites and granites from the Grootfontein Inlier and the quartzitic micaschist from Keilberg.

volcanic arc granites (VAG) and syn-collisional granites (syn-COLG). Rb-poor source rocks or a low fluid content could have caused a lower Rb/(Y+Nb) ratio, moving some of the granites into the VAG field. The only granite sample that can be classified as a syncollisional granite is the pegmatite sample CL52, which is clearly younger than the granitic wall rock. The dioritic rocks reflect a VAG setting, with the exception of samples from Berg Aukas (BA0001, BA0003) which plot on the boundary between the VAG and WPG (within plate granites) fields. In Fig. 3.6d, most of the diorites and granites show a positive linear correlation. The aberrant behaviour of granite CL102 cannot be explained by a regional metamorphic overprint alone, because other rocks (e.g. CL53) following the linear trend display even stronger metamorphic alteration. Since the pegmatite sample CL52 displays vein-like chloritic alteration, its Rb depletion and Y preservation may be explained by the chloritisation process.

A greenschist to amphibolite facies overprint is indicated by the alteration of the mineral assemblage of granites and diorites of the GMC. The degree of alteration varies throughout the OML and the different types of the rocks of the GMC without any general trend. The metamorphic overprint is possibly related to deformational processes during the Pan-African orogeny, as indicated by syn-deformationally grown epidote and actinolite in diorites of the Toggenburg Anticline (sample CL53). Both the diorites and pegmatites show grain boundary migration, resulting in a bimodal grain size distribution. This can be produced by a partially dynamic recrystallisation under medium grade metamorphic conditions (Passchier and Trouw, 1998). Perthitic segregation and polysynthetic twinning of the feldspars, already described by Söhnge (1957), are partly obliterated by bulging of quartz. A pre-Damaran age for the first metamorphic overprint of the GMC is suggested by biotites in shear bands that are restricted to basement clasts in the Damaran Ghaub Formation and in the Nabis Formation, and a mineral assemblage that reflects low to medium grade metamorphism. The possible timing of this metamorphic overprint could be late Eburnean or Kibaran, as suggested by isotopic resetting of other basement rocks in the Damara Belt (Porada, 1979). Negative Sr anomalies observed in some of the diorites (CL53, BA0001, BA0003), the granites (CL102) and the gabbroic rocks from Berg Aukas could imply weathering and erosion processes. Clifford et al. (1969) suggested a weathering period in the late Middle Proterozoic for the Franzfontein granitic suite.

The stratigraphic column of the Congo Craton basement at the northern margin of the Damara Belt (Table 3.1) and the Rb-Sr age of 1816 ± 23 Ma obtained for pegmatite CL52 in the OML restrict the list of comparable pre-Damaran basement rocks in central and northern Namibia. Martin (1965) and Söhnge (1964) compared the Grootfontein Inlier with the Abbabis Formation of the Abbabis Complex in the SW Central Zone of the Damara Belt. Orthogneisses and granitic rocks of the Abbabis Complex were grouped together into the Narubis Granitoid Complex by Brandt (1987). These rocks display distinct foliation, whereas none of our samples from the OML basement reflects comparable deformation patterns. However, this might not be a valuable discrimination for both basement complexes because of their different tectonostratigraphic positions: the Abbabis Complex is situated in the central Damara Belt, whereas the Grootfontein Inlier is positioned at the northern tip of the Damara Belt. Moreover, our study reveals indications for a detachment zone at the bottom of the Nosib Group, represented by the Keilberg quartzitic

micaschists and adjacent phyllites, which may accommodate strain that is related to the "northward"-moving Damaran orogenic front.

Hedberg (1979) related the Grootfontein granites to the Franzfontein granites. The majority of the Franzfontein granitic suite is composed of middle to coarse-grained alkali granites with mineral alteration and deformation features equivalent to those of the granites from the Toggenburg Anticline. Plagioclase is sericitised, epidote is an alteration product of K-feldspar and muscovites are bent (Clifford et al., 1969). Main element contents of the OML granites generally correspond to the composition of the Franzfontein granites (Fig. 3.11), but only granites in the Gauss Anticline have an alkaline composition that matches that of the Franzfontein granitic suite (Fig. 3.3). In contrast to this, Mesoproterozoic samples from the same basement complex comprise a broad spectrum of syenodioritc and alkalidioritc rocks (Fig. 3.3). The composition of the dioritic rocks of the OML is similar to that of Archean units in the Huab Massif, which may indicate the existence of pre-Eburnean rocks also in the OML. Especially diorites from the eastern Nosib Anticline (Fig. 3.2) have compositions comparable to those of equivalent rocks in the Archean Huab Massif (Seth et al., 1998; Fig. 3.11; Table 3.2). The Paleoproterozoic granitoids in the central Kaoko Belt underwent amphibolite facies metamorphism during the Eburnean orogeny (Dingeldey, 1997; Seth et al., 1998). A pre-Damaran metamorphic event is also evident in the GMC, as reflected by low- to medium grade basement clasts, embedded in the

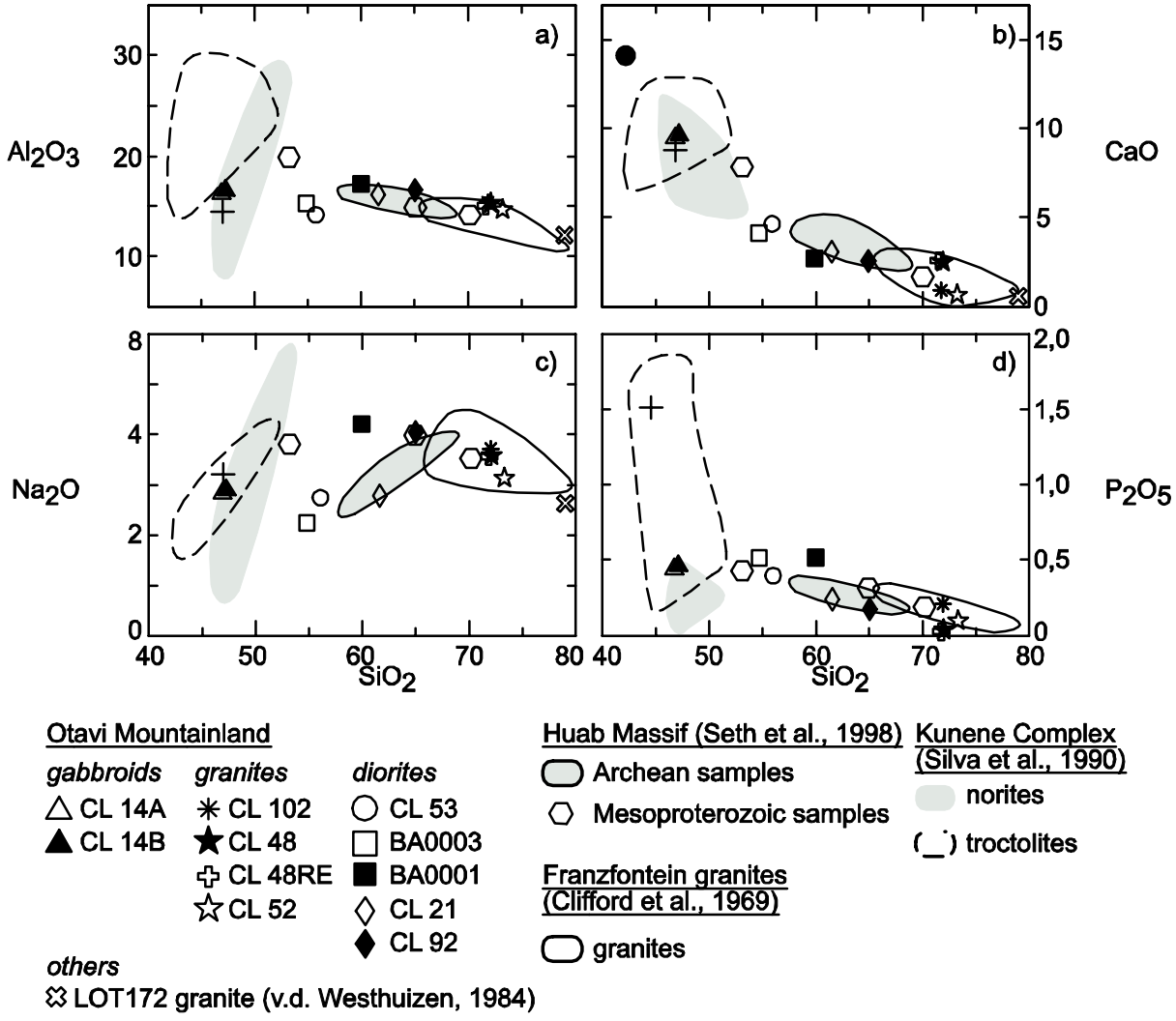

Fig. 3.11: Plots of selected main elements for rock samples from the Grootfontein Inlier. Additional data from the Grootfontein Metamorphic Complex by Melcher (Melcher, 2004) and Van der Westhuizen (1984) as well as published data of comparable basement complexes of the southern part of the Congo Craton are also shown (references see legend, values given in wt%).

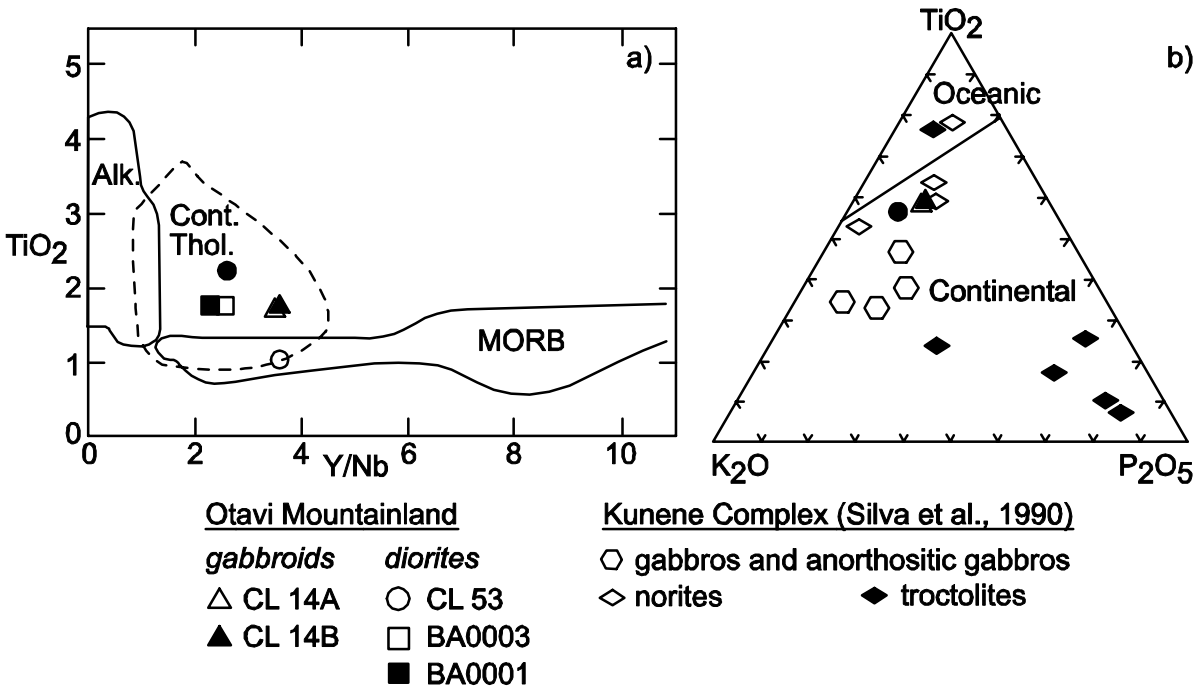

Fig. 3.12: a) TiO_2-Y/Nb discrimination diagram for basalts (Floyd and Winchester, 1975), b) triplot of $K_2O/P_2O_5/TiO_2$ for subalkaline basalts (Pearce et al., 1975), showing rock samples from the Grootfontein Inlier and the Kunene Complex in NW Namibia (data from Silva, 1990).

Damaran sedimentary sequence.

The gabbros (CL14) and some diorites in the Grootfontein Inlier can be classified as continental tholeiites based on a TiO_2-Y/Nb discrimination diagram (Floyd and Winchester, 1975; Fig. 3.12a). The Farkfontein diorite (CL53) also reflects a tholeiitic composition but could have been emplaced either in continental or oceanic crust. A continental environment for the subalkaline basaltic rocks of the GMB (Berg Aukas gabbros, samples CL14A,B) can be inferred from a K_2O-P_2O_5-TiO_2 triplot (Pearce et al.,1975; Fig. 3.12b). A possible equivalent to the Grootfontein Mafic Body (GMB) is the Kunene Complex (KC, Fig. 3.1) in the southern part of the Congo Craton which consists mainly of massive anorthosite with minor gabbroic bodies (Mayer et al., 2004). A southern part with an An content of 53 ± 5% has been distinguished from a northern part with An 70 ± 5% (Morais et al., 1998). The geochemical composition of gabbroics from Berg Aukas in the GMB and the norites and troctolites of the Kunene Complex (Silva, 1990; Mayer et al., 2004) appear to be similar (Fig. 3.3, 3.11). The subalkaline norites reflect either an oceanic or continental tectonic setting, which highlights the uncertainties in the interpretation of the tectonic setting of the gabbroic rocks in the OML.

3.6 Conclusions

The Paleoproterozoic basement lithologies of the Grootfontein Inlier, NE Namibia, have been characterised by field evidence, petrographical, geochemical and geochronological data. Plutonic rocks in the Grootfontein Metamorphic Complex (GMC) record a magmatic evolution from a dioritic to a granitic composition, with a final stage of pegmatitic intrusions during the late Eburnean, as evidenced by a Rb-Sr age of 1.816 ± 23 Ma obtained for pegmatite-related white mica. This age would be in agreement with both a scenario in which the Paleoproterozoic basement of the OML forms part of the southern Congo Craton that had been affected by crust-forming events during the Eburnean orogeny (Tegtmeyer and Kröner, 1985), and with the model of an Eburnean collision between a Paleoproterozoic Kamanjab-Bangweulu arc terrane with the Archean Tanzanian Craton and its subsequent accretion to the southern margin of the Congo Craton during the Kibaran orogeny (Rainaud et al., 2005).

Geochemical data indicate an emplacement of the GMC in a convergent tectonic setting, while the gabbros of the Grootfontein Mafic Body (GMB) were emplaced in a continental regime. The field

occurrence, petrographic character and geochemistry of the Paleoproterozoic magmatites in the OML show great similarity to other basement complexes in northern Namibia, suggesting that all these rock units located along the southern margin of the Congo Craton underwent a more or less common tectonometamorphic evolution. A pre-Pan-African low- to medium grade metamorphic overprint reflected by basement rocks in the central OML may be of Eburnean or Kibaran age, whereas a second, low- to medium grade metamorphism is most likely of Pan-African age. This overprint is also known from other pre-Pan-African basement areas at the southern Congo Craton, such as the Franzfontein granitic suite (550 Ma, Clifford et al., 1969). Indications were found for a Pan-African detachment zone, comprising quartzitic micaschists in the basal part of the Nabis Fm, separating the pre-Damaran basement of the Grootfontein Inlier from the Damaran sedimentary successions.

Acknowledgements

We thank Arno Günzel (Ongopolo Mining and Processing Limited, Tsumeb) for the introduction into the field. We acknowledge the logistic support by Hartwig Frimmel (University of Würzburg), Andries Nethling (Ongopolo Mining and Processing Limited, Tsumeb) and Volker Petzel (Namibia Geological Survey). We greatly thank Frank Melcher (BGR) for providing analytical data of samples from the Grootfontein Inlier. Georg Werner kindly provided unpublished material and helped together with Nathan Kang to prepare the samples for geochemical studies. We are grateful to Urs Schaltegger (University of Geneva) and Albrecht von Quadt (ETH Zurich) for giving unlimited access to all cleanlab and mass spectrometry facilities. We are indebted to Deutsche Forschungsgemeinschaft (DFG) for financing this study in the framework of the “Graduiertenkolleg 273 on Rock-water interaction” at Heidelberg University. Further financial support was provided by the DAAD-financed Internationales Promotionsprogramm (IPP) at the Faculty of Chemistry and Geosciences, Heidelberg University.

Part 4: Geology, geochemistry and metallogenetic significance of Cryogenian volcanic and siliciclastic rocks in the Otavi Mountainland (Namibia)

Abstract

Field observations, petrographical, geochemical, and geochronological data on Neoproterozoic rock units in the Otavi Mountainland (NE Namibia) have been used in combination to put constraints on the geotectonic evolution of these units and to assess their significance as a possible metal source for ore deposits in overlying sedimentary strata. The Neoproterozoic Damara Supergroup consists of the siliciclastic/volcanic Nosib Group, platform carbonates of the Otavi Group, and late Ediacaran siliciclastic rocks of the Mulden Group. The Otavi Group is the host of various styles of hydrothermal base metal mineralisation.

Middle Neoproterozoic (Cryogenian) volcanic and siliciclastic rocks of the low grade metamorphic Nosib group overlying the Paleoproterozoic basement have been identified not only in the southern, but also in the central OML. There, a possible Pan-African detachment zone separates the Paleoproterozoic basement from the Neoproterozoic sedimentary successions. Main and trace element data of Nosib Group metavolcanic rocks of the Askevold Formation reflect a pre-Pan-African rifting phase at the southern margin of the Congo Craton during the early Cryogenian due to opening of the Adamastor Ocean in the W, up to the final stage of the deposition of the Nosib Group. Rifting was accompanied by tholeiitic magmatism and the formation of VMS mineralisation. Magnetites from Askevold volcanic rocks which postdate VMS mineralisation yield an early middle Ediacaran Pb-Pb age of 587 ± 12 Ma that dates a period of metamorphic overprint prior to Pan-African D2 deformation, thereby giving a maximum age for the Pan-African collision of the Congo and Kalahari Cratons in the Northern Zone of the Damara Belt.

Comparative geochemical studies on the Neoproterozoic Nosib Group and galena from base metal mineralisations hosted by Abenab and Tsumeb Supergroup carbonate sequences support that the Neoproterozoic Askevold Formation and related VMS-type deposits represent viable metal sources.

4.1 Introduction

Metamorphic rocks are considered worldwide to be important sources of metal ores concentrated in overlying sedimentary sequences (Misra, 2000, amongst others). The concept of “basement brines”, i.e. ore-forming fluids derived from deep-seated metamorphic rocks, plays a major role in the metallogenetic interpretation of many economically important ore provinces (Pirajno, 1993; Yardley, 1997). Fluids of this type may be expelled e.g. along shear zones and vein systems during compressive orogenic deformation (Thompson, 1997) or seismic pumping in extensional settings (Sibson et al., 1975).

Neoproterozoic carbonate sequences of the Otavi Mountainland (OML), NE Namibia, are the host of numerous hydrothermal base metal mineralisations, some of which represent world-class deposits for Cu-Pb-Zn, Ge, Ag, and V (Melcher, 2006). The major mineralisation style, represented by hypogene Cu-Zn-Pb-sulphide-dominated mineralisation, may have originated from ore fluids mobilised during the compaction and dewatering of the Neoproterozoic sediments (Pirajno and Joubert, 1993) and/or during the amalgamation of the Congo and Kalahari Cratons (Fig. 4.1), i.e., the Pan-African orogeny (ca. 580-473 Ma; Miller, 1983a; Pirajno and Joubert, 1993; Frimmel, 2004; Goscombe et al., 2005; Part 2). The carbonate successions that host mineralisation are underlain by Paleoproterozoic metamorphic basement rocks and Cryogenian siliciclastic and volcanic rocks, which have been considered by many authors (Pirajno and Joubert, 1993; Chetty and Frimmel, 2000; Frimmel et al., 2004) as a possible source reservoir for the base metals. Verwoerd (1957) considered the magmatic rocks occurring in the basement as the main source of vanadium for the karst-related, supergene V-deposits (Part 6). However, little is known about the geology and geochemical nature of these Proterozoic units. This paper aims to characterise some of the Neoproterozoic siliciclastic and intercalated volcanic rocks in the OML by means of their field occurrence

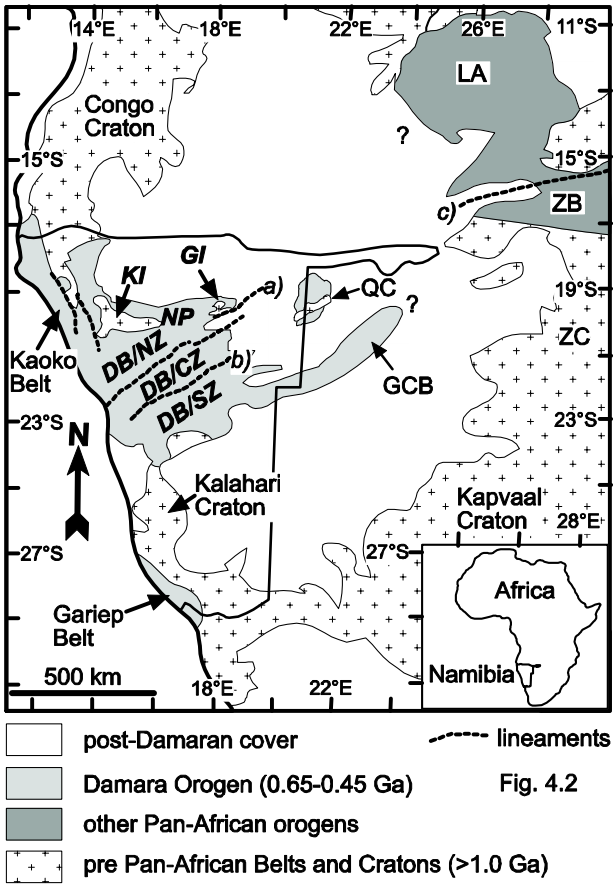

Fig. 4.1: Proterozoic mobile belts and Cratons of south-western Africa with selected lineaments and metamorphic zones of the Damara Belt; Lineaments: a) - Grootfontein Lineament, b) - Okahandija Lineament; c) - Mwembeshi shear zone; DB – Damara Belt, CZ – Central Zone, NZ – Northern Zone, SZ – Southern Zone, GCB – Ghanzi-Chobe Belt, GI – Grootfontein Inlier, KI - Kamanjab Inlier, LA – Lufilian Arc, QC – Quangwadum Complex, ZB – Zambezi Belt, ZC - Zimbabwe Craton (Map modified after GSN, 1999; Rainaud et al., 2005; Singletary et al., 2003).

and main and trace element geochemistry, and to assess their significance as possible sources for base metals concentrated in the overlying strata. Furthermore, some Pb-Pb data are presented that allow us to better constrain the geochronological evolution of these Proterozoic units in north-eastern Namibia.

4.2 Geology

4.2.1 The Neoproterozoic Damara Supergroup in the OML

The Paleoproterozoic basement in northern Namibia is unconformably overlain by Neoproterozoic sequences of the Damara Supergroup (Fig. 4.2). These comprise from bottom to top the siliciclastic Nosib Group with intercalated bimodal volcanics in the upper part, the platform carbonate sequence of the Otavi Group and the molasse-like Mulden Group. Basement highs of the Grootfontein Inlier controlled the depositional environment, tectonic structures and pathways of metal-bearing brines (Söhnge, 1972).

The structural evolution of the OML commenced with rifting initiated by the opening of the Adamastor Ocean and its eastern branch during the Cryogenic, finally leading to the evolution of the Khomas Trough and subsidiary basins (Kukla and Stanistreet, 1991; Unrug, 1997), which strike parallel to the later Damara Belt (ENE-WSW). The rudaceous lower Nosib Group in the central OML reflects the composition of the subjacent basement (Hedberg, 1979), with deep pre- or syn-Nosib valleys having formed in ENE to E direction. Small basins are filled with siliciclastic rocks of the Nabis Formation (Fig. 4.2) accompanied by a mixed assemblage of diamictites, pyroclastics and ironstones, which are part of the Chuos Formation (or Varianto Formation) and bimodal volcanic rocks of the Askevold Formation in the southern OML. The irregular presence of the Nabis Formation is interpreted to be both of a sedimentary and erosional origin. South of the Grootfontein Lineament, in the greenschist-facies, Northern Zone (Fig. 4.1, 4.2), the original contact to the underlying basement and the overlying Otavi Group is obliterated by the Pan-African orogeny. Hedberg (1979) described an onlap of the Nosib Group onto a north-eastern striking basement high, roughly along a line from the Gauss Anticline to Abenab. The Askevold Formation is characterised by the presence of volcanic metabasites and has been correlated with the Naauwpoort Formation in the Northern Zone. The Naauwpoort Formation revealed U-Pb zircon ages of 742 ± 25 Ma (Burger and Coertze, 1973) and 746 ± 2 Ma (Hoffmann et al., 1996). The metavolcanic rocks crop out in two almost EW-striking belts, each about 1.5 km wide (Söhnge, 1957). Widespread epidotisation

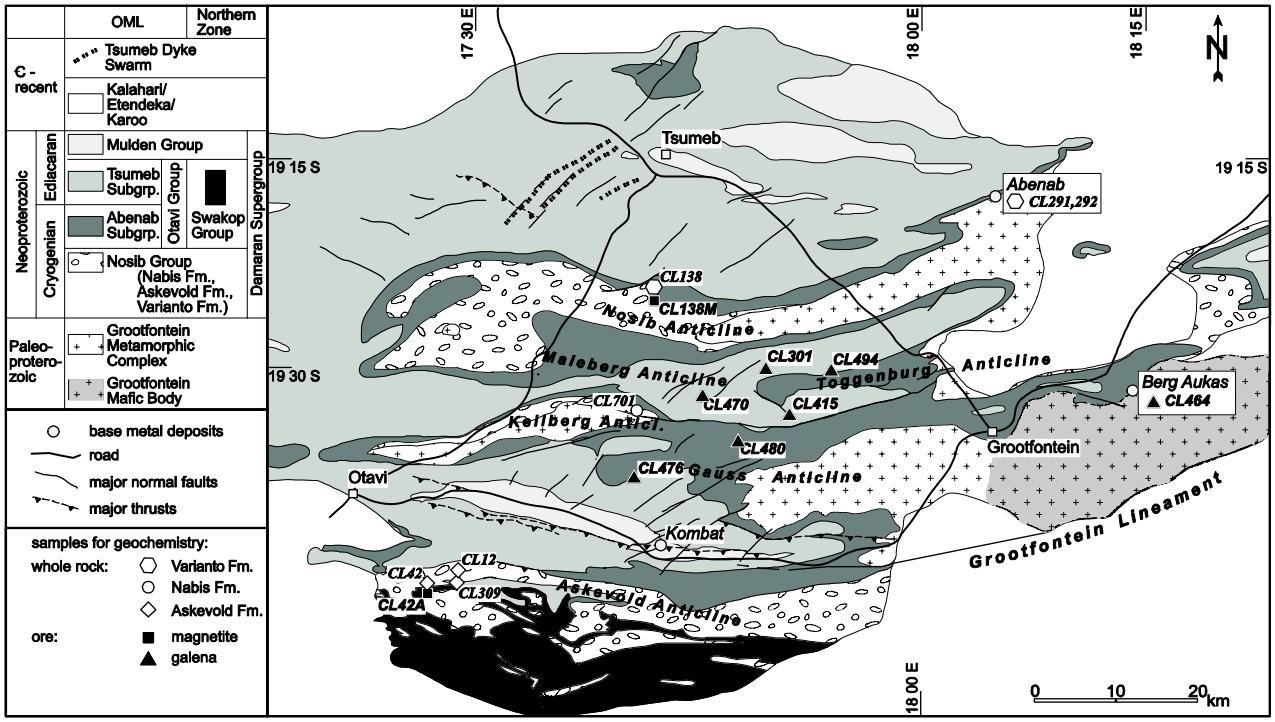

Fig. 4.2: Geological map of the OML with tectonic structures and sample locations.

("epidosites") could have resulted from their extrusion into shallow water (Van der Merwe Smit, 1959). A detailed description of the petrography is given in Söhnge (1957). The schists between metavolcanic rocks and overlying dolomites of the upper Nosib Group contain possibly VMS-type Cu-Fe-deposits, which were exploited in the Deblin mine. The Deblin orebody may have formed by leaching of metals from the Cu- and Fe-rich Askevold Formation. The genetic relationship between the Askevold Formation and the Nabis Formation is veiled by the Pan-African overprint. Söhnge (1957) assumed an intrusive or sheared contact of the epidosites with dolomitic marbles and related the Askevold Formation to the upper Nosib Group, or to a separate volcanic phase restricted to the lower Abenab Subgroup.

The Otavi Group consists mainly of dolomitic rocks, which were deposited in a platform setting (Miller, 1983a) from the Middle Cryogenian to the Middle Ediacaran (Fig. 4.2). This up to 3000 m thick sequence can be subdivided into a lower and an upper part, the Abenab and Tsumeb Subgroups, respectively. Both are separated by diamictites of the Ghaub Formation (635.5 ± 1.2 Ma, U-Pb zircon, Hoffmann et al., 2004). The Abenab Subgroup lies unconformably on the Nosib Group or older basement rocks (e.g. Eastern Gauss Anticline, Toggenburg Anticline; Fig. 4.2). Like the Nosib Group, at least the lower parts of the Abenab Subgroup accumulated partly in the morphological depressions of the basement. South of the Otavi Valley, the Nosib Group and the overlying Otavi Group carbonates display isoclinal folding. Recumbent folding and northward thrusting resulted in thinning and tectonically induced repetition of the Damara Supergroup (Söhnge, 1972; Innes and Chaplin, 1986). Schoch (1958) and Brandt (1955) described sheared contacts of the Nosib Group with the basement and the Abenab Subgroup.

4.2.2 Base metal mineralisation in the OML

The Neoproterozoic carbonate sequence in the OML is the host for various types of important base metal deposits (Wartha and Schreuder, 1992; Pirajno and Joubert, 1993; Frimmel et al., 1996a; Part 6). Furthermore, chlorite schists intercalated in metavolcanic rocks and dolomites of the Askevold Formation in the southern OML, contain volcanogenic sulphides, whose mineralogy is dominated by chalcopyrite, bornite, pyrite, pyrrhotite and chalcocite as supergene phase. Similar deposits were described also from other Nosib Group occurrences in central Namibia (e.g. Oamites Mine: Lee and Glenister, 1976).

The major base metal deposits in the OML are hosted by carbonates of the Otavi Group, which build

up the eastern end of the Northern Platform of the Damara Belt (Pirajno and Joubert, 1993). The two major types of mineralisation were defined as the Berg Aukas- and the Tsumeb-type (Hughes, 1987). Detailed summaries of the geological setting and possible genesis of these mineralisation styles are given in Pirajno and Joubert (1993), Frimmel et al. (1996a) and Melcher (2003). The stratabound Berg Aukas-type mineralisation consists of Zn-Pb dominated sulphides, which carry very limited amounts of Cu and Ag as well. These sulphides should have been precipitated by saline brines (ca. 23 wt.% NaCl eq.) of low to moderate formation temperatures (137 - 255°C), which could have resulted from basin dewatering prior to the Pan-African orogeny (Misiewicz, 1988, Pirajno and Joubert, 1993, Chetty and Frimmel, 2000). Conversely, Hughes (1979) suggested a Pan-African age for Berg Aukas-type sulphides. Even if no absolute ages were recorded so far for the Berg Aukas-type ore, recent age datings of about 562 to 436 Ma (Rb-Sr; Part 5) obtained from Zn-silicates (willemite) derived from sulphides belonging to the latter type, imply an even older age for the primary ores. Tsumeb-type mineralisation comprises Pb, Cu and Zn sulphides and occurs in pipe-like deposits hosted by the middle to upper Tsumeb Subgroup (Fig. 4.2). The paragenetic sequence of the hypogene mineralisation determined by Lombaard et al. (1986) in the Tsumeb Mine starts with early pyrite, followed by the main mineralised assemblage, consisting of Cu-Fe-Ge(-Zn) sulphosalts and sulphides. A subsequent phase of sulphide mineralisation was dominated by Zn-Cu-sulphides, which were finally displaced by galena. Apart from the high As concentration, Melcher et al. (2006) emphasised in the Tsumeb-type ores a high amount of Cu thiogermanates like germanite and renierite. Preliminary Re-Os data for sulphide ores from the Tsumeb deposit point to an age of about 530 Ma for Tsumeb-type mineralisation (Melcher et al., 2003). This age could indicate a strict relationship between mineralisation and the main phase of the Pan-African orogeny (ca. 535 Ma, Goscombe et al., 2004).

4.3 Sampling and analytical methods

A total of 7 samples of Neoproterozoic siliciclastics/rift volcanics of the Nosib Group, as well as 8 galena samples from diverse base metal mineralisations were taken in the OML for petrography and geochemical analysis during field seasons from 2003 to 2005. Sample types and locations are given in Table 4.1 and 4.2. The samples were taken from field outcrops and studied in thin section (Fig. 4.2 for location).

Whole rock powders were prepared using a jaw crusher and a tungsten-carbide mill at the University of Heidelberg. Analysis of the main and trace elements was performed by ACME Analytical Laboratories Ltd. (Canada). For whole rock analysis, 2.5 g of sample pulp was treated with $LiBO_2$ fusion and subsequent digestion using dilute HNO_3. Major oxides and minor elements were measured by ICP-ES and trace elements measured by ICP-MS. Sample CL48 was remeasured by ACME Analytical Laboratories Ltd. and labelled as CL48RE.

From epidosite samples CL42 and CL138 (Askevold Formation, Hohentwiel and Varianto-Toppa Farms), pure magnetite splits were produced from the crushed rocks by magnetic separation and subsequent sieving (samples CL42A and CL138M). Main and trace element analysis was performed by ACME Analytical Laboratories Ltd. with an ICP-MS, by initially leaching sample splits of 0.5g with hot (95°C) aqua regia. From the same samples, three additional separates of euhedral magnetite (grain size fractions > 400 µm and 400-250 µm from CL138 and grain size > 400 µm from CL42) were analysed for their Pb isotopic composition. Prior to analysis, the separates were cleaned twice in a cleanlab with doubly distilled water (DDW) using ultrasonic treatment, and subsequently leached for 15 min. in hot 2 N HF to remove possible silicate contaminants. After repeated rinsing with DDW, the samples were dried, weighed into Teflon screw-top vials and decomposed in aqua regia on a hot plate at 120°C. Lead was chemically separated with 3 N HNO_3 using EICHROM Sr resin on 50 µl Teflon columns. After rinsing with 1 ml 3 N HNO_3 and 1 ml H2O, Pb was stripped from the column with 1 ml 6 N HCl. The Pb cut was further processed through a 50 µl column containing precleaned EICHROM Pre Filter Resin.

For mass spectrometry, Pb was loaded onto single Re filaments using silica gel-H_3PO_4 bedding. Isotopic measurements were performed at ETH Zurich (Switzerland) on a FINNIGAN MAT 262 solid-source mass spectrometer running in static multicollection mode. Pb isotopic ratios were corrected for mass fractionation using a mean discrimination factor of 0.085 ± 0.006 (2σ) %/[amu], based on replicate measurements of the NBS SRM 981 common lead

(n=35) standard. Errors and error correlations were calculated after Ludwig (1980). Individual uncertainties (2σ) are given for Pb isotope ratios elemental concentrations and isotope ratios (Table 4.3). Total procedure blanks amounted to 20 pg Pb, and were found to be negligible. Pb-Pb ages were calculated after Ludwig (2001) using the ISOPLOT/Ex version 2.49 program, errors on the ages are quoted at the 2σ level.

4.4 Results

4.4.1 Field relationships and petrography

The middle Neoproterozoic Nosib Group in the OML comprises the siliciclastic Nabis Formation, the volcanic Askevold Formation and diamictites of the Chuos (or Varianto) Formation (Hedberg, 1979). Major occurrences of the greenschist-facies Askevold Formation are located in the southernmost OML (Fig. 4.2) and comprise metamorphosed basaltic rocks, sometimes represented only by clasts in mature siliciclastic sediments of the Nabis Fm, and chlorite schists (Söhnge, 1957). Additional outcrops of magnetite-rich pyroclastics were found in the northern Nosib Anticline (Varianto-Toppa Farm, CL138). The genetic relationship between the metavolcanics and the surrounding strata is, where accessible, obliterated by tectonic overprint. Alternation of the metavolcanic rocks and dolomitic marbles of the upper Nosib Group at Hohentwiel (locality of sample CL42) is accompanied by isoclinal folds and boudinage in the marbles. Strain partitioning in this interbedding results in deformation features mainly developed in the

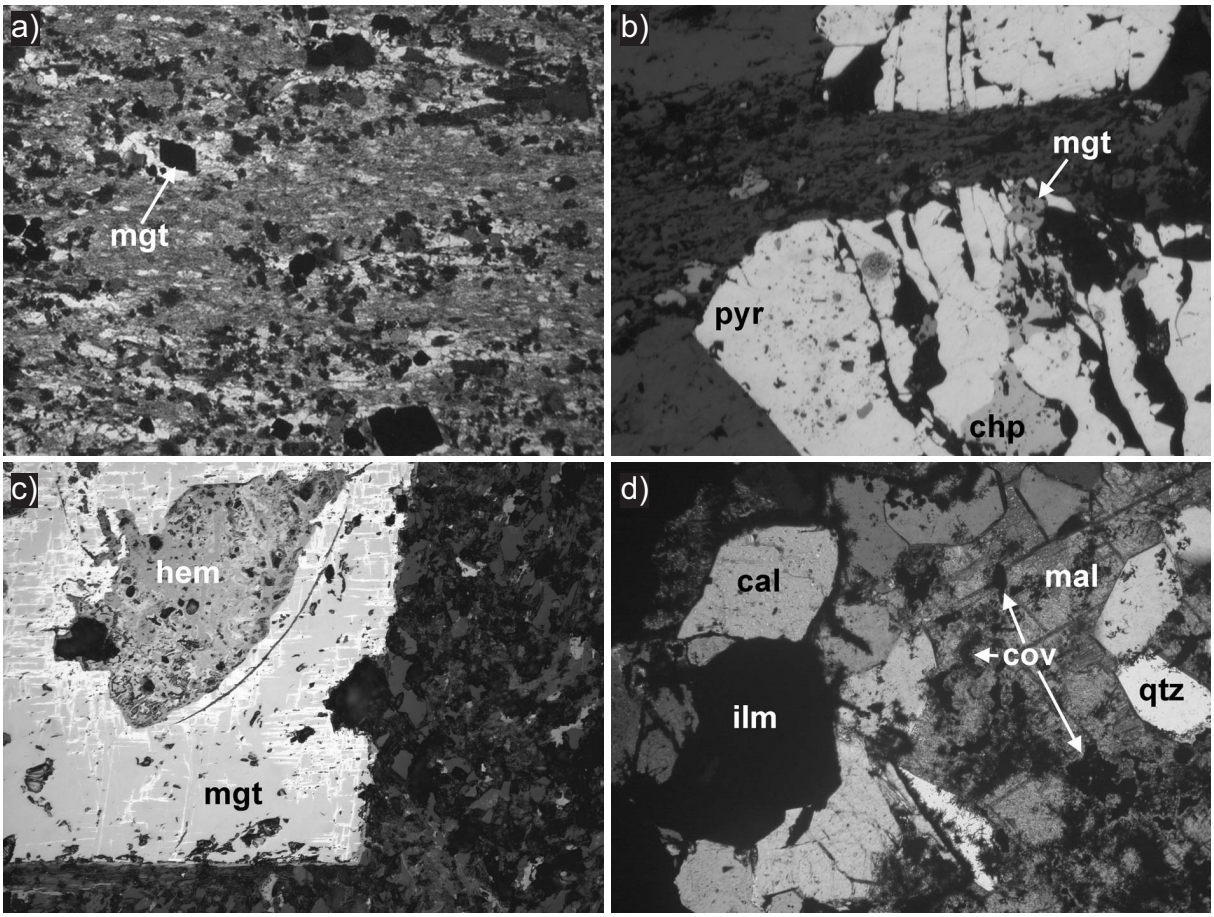

Fig. 4.3: Hand specimens and thin sections of samples from the Askevold Formation. a) sulphide mineralisation in chlorite schist, crossed nicols, bottom width 1.6 mm, b) chalcopyrite replacing pyrite and magnetite healing fractures plus strain shadow, reflected light, bottom width 0.8 mm, c) magnetite showing strain shadow, chlorite schist, parallel nicols, bottom width 5 mm, d) ilmenite exsolution in titanomagnetite, volcanoclastic rock (CL42), reflected light, bottom width 0.9 mm. cal: calcite, chp: chalcopyrite, cov: covellite, hbl: hornblende, hem: hematite, ilm: ilmenite, mgt: magnetite, mk: muscovite, pyr: pyrite, qtz: quartz.

volcanic rocks, resulting in a southeast dipping SC-fabric and a crenulation cleavage. In the Nosib Anticline, metavolcanics are intercalated in the Chuos Formation. The Askevold Formation consists mainly of chlorite schists and altered pyroclastics. The chlorite schists comprise green chlorite, quartz, muscovite, sericite, biotite, amphibole, and calcite as major components. Calcite and quartz can be accumulated in phacoids. Opaque phases are pyrite, chalcopyrite, pyrrhotite, covellite, magnetite and ilmenite in mineralised areas (e.g. Deblin Mine, CL309, Fig. 4.3a), In barren units, magnetite represents the only opaque mineral. Pyrite displays brittle deformation with chalcopyrite replacing the pyrite and magnetite partly healing the fractures (Fig. 4.3b). In the sulphide-free sequences magnetite is subhedral to euhedral and reveals quartz and phyllosillicate strain shadows (Fig. 4.3c). In reflected light, ilmenite exsolutions in the primary titanomagnetite are visible (Fig. 4.3d). Quartz and calcite phacoids, pyrite, amphibole, mica and biotite display strain shadows which mainly consist of chlorite, quartz and biotite and sometimes have several growth increments. Metapyroclastic rocks of the central OML (CL138) show no penetrative foliation and therefore less deformation at microscopic scale than equivalent samples from the southern OML.

4.4.2 Geochemistry

Geochemical data for metavolcanic rocks of the Askevold Formation and siliciclastic rocks of the Chuos (CL291) and Nabis Formations (CL701) are listed in Table 4.1 and depicted in Fig. 4.4 - 4.7 SiO_2 contents of the metavolcanic rocks vary between 40 and 57 wt.% (Table 4.1, Fig. 4.4). The least siliceous rocks are tholeiitic rocks (CL12) and chlorite schists

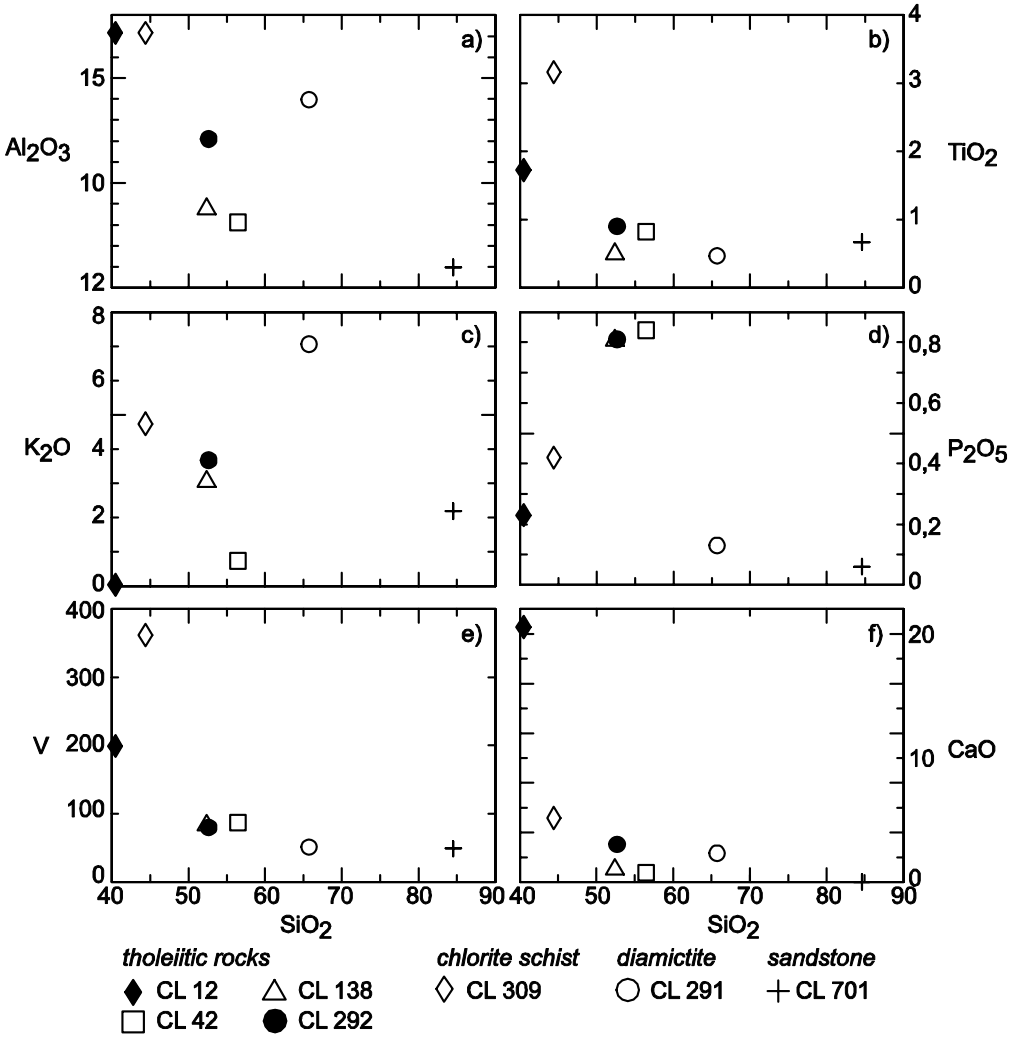

Fig. 4.4: Main and selected trace element plots for rock samples from the Askevold Formation, enclosed magnetites and related rocks of the Nabis and Chuos Formation.

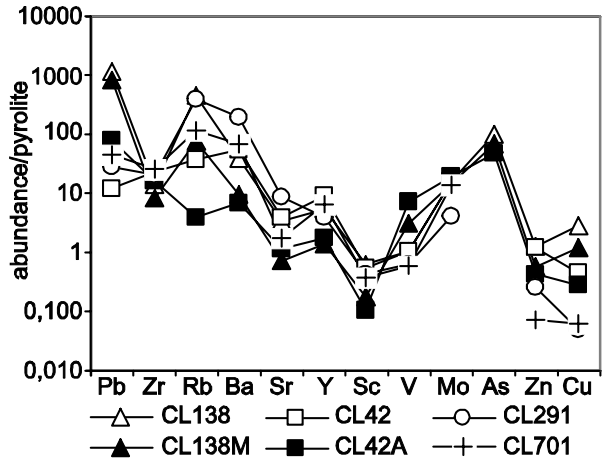

Fig. 4.5: Pyrolite-normalised trace element profiles (McDonough and Sun, 1995) for rock samples from the Askevold Formation, enclosed magnetites and related lithologies. Elements in order of increasing compatibility towards the right.

(CL309) from the Deblin Mine in the southern OML. The abundance of Al_2O_3 decreases with increasing SiO_2. Conversely, P_2O_5 shows a positive correlation with SiO_2. Samples with higher SiO_2 content (CL138, CL292, CL42) have almost constant TiO_2/SiO_2, P_2O_5/SiO_2 and V/SiO_2 ratios.

Patterns of selected trace elements allow the discrimination of high-SiO_2 rocks (Askevold Fm) from low-SiO_2 rocks, as represented by sample CL12 from the Deblin Mine (Fig. 4.5). Especially the Rb, Ba and Sr contents differ greatly. With the exception of the Rb, Ba, Mo and As abundances, the high-SiO_2 rocks exhibit a decreasing trend with increasing element compatibility. Pb, Mo and Cu show large variations. The magnetite samples CL42A and CL138M and their corresponding host rocks (CL42, CL138) display similar patterns, with exception of the Rb and Ba contents. The host rocks generally have slightly higher trace element contents, excepting Pb, V, and Mo, which are enriched in magnetite CL42A relative to its corresponding host. Trace elements in Chuos diamictites (CL291) and Nabis sandstones (CL701) show roughly the same pattern as those of the high-SiO_2 rocks of the Askevold Fm.

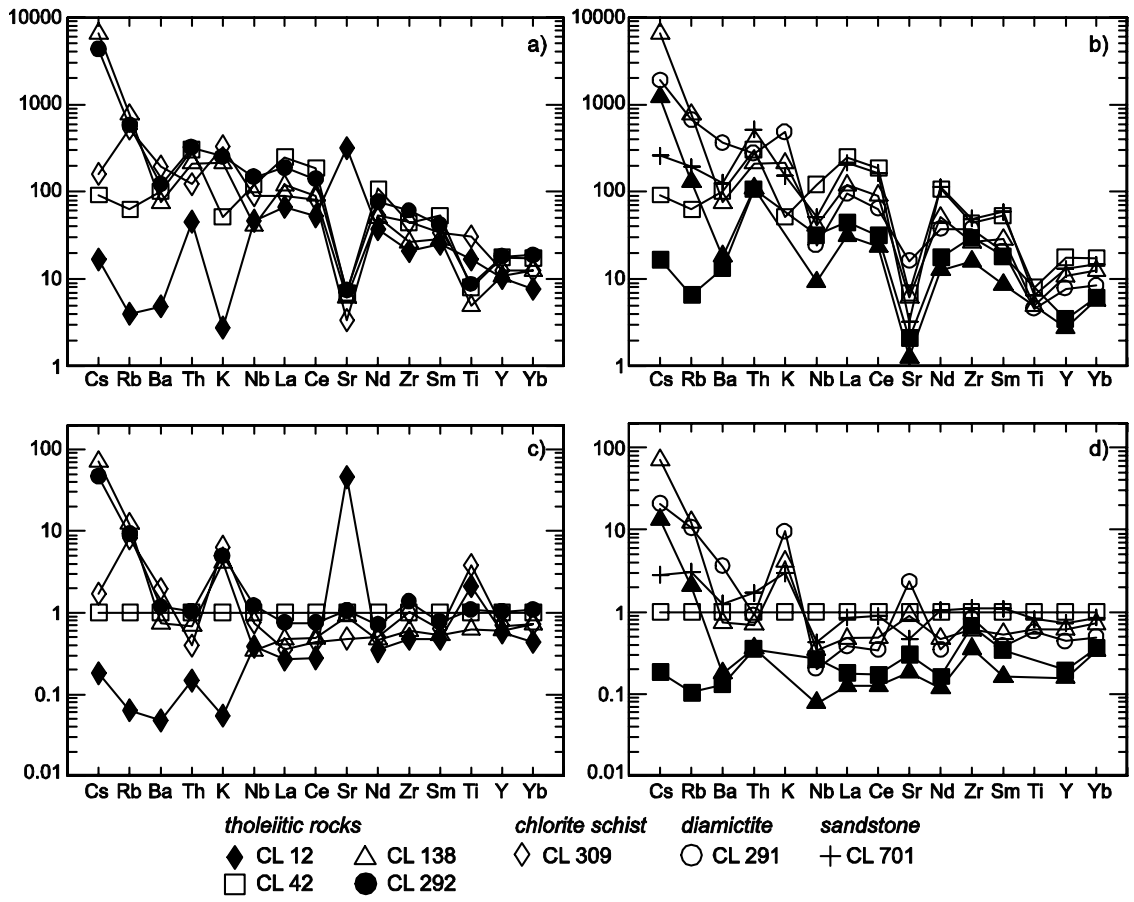

Fig. 4.6: Bulk Earth-normalised trace element-diagram (Hickey et al., 1986) for a) rock samples from the Askevold Formation, b) enclosed magnetites and related rocks; c) and d) sample (CL42)-normalised trace element diagrams.

Locality	Neuwerk	Neuwerk	Hohentwiel	Varianto-Toppa	Abenab	Abenab	Keilberg
Sample	CL309	CL12	CL42	CL138	CL291	CL292	CL701
Rock type	Chlorite schist	Metavolcanic	Metavolcanic	Metavolcanic	Diamictite	Diamictite	Sandstone
SiO2	44.42	40.46	56.45	52.40	65.70	52.65	84.55
Al2O3	17.15	17.15	8.12	8.81	13.97	12.10	5.98
Fe2O3	12.07	13.68	24.91	23.99	4.58	17.58	4.45
MgO	5.43	1.23	1.89	3.13	1.34	3.46	0.61
CaO	5.18	20.56	0.76	1.10	2.32	3.04	0.02
Na2O	0.07	0.33	0.01	0.01	0.83	0.85	0.03
K2O	4.74	0.04	0.74	3.08	7.06	3.67	2.19
TiO2	3.16	1.73	0.82	0.51	0.47	0.90	0.67
P2O5	0.42	0.23	0.84	0.81	0.13	0.81	0.06
Cr2O3	0.021	0.009	0.009	0.006	0.00	0.01	0.00
LOI	6.90	4.00	5.30	6.00	1.37	1.60	2.67
TOT/C	0.94	0.62	0.03	0.10	n.a.	n.a.	n.a.
TOT/S	2.19	0.01	0.01	0.01	0.01	0.33	0.01
Total	102.69	100.05	99.89	99.96	97.78	97.00	101.24
A.S.I.	1.72	0.82	5.38	2.10	-	-	-
Ba	684.60	16.90	352.90	262.30	1269.30	420.30	443.30
Sc	34.00	21.00	9.00	10.00	7.00	10.00	6.00
Mo	5.00	0.20	0.80	0.80	0.20	1.10	0.70
Cu	1646.00	1.50	13.20	83.80	1.50	9.60	1.90
Pb	10.10	3.60	1.80	175.20	4.20	10.60	6.90
Zn	127.00	12.00	67.00	68.00	14.00	41.00	4.00
As	5.80	0.60	< 0.5	4.90	< 0.5	3.00	< 0.5
Sb	< 0.1	< 0.1	< 0.1	0.40	0.10	0.10	< 0.1
Ag	0.30	0.10	0.20	0.20	< 0.1	0.10	< 0.1
Au	2.00	2.20	< 0.5	0.90	1.90	2.70	0.50
V	362.00	199.00	87.00	85.00	51.00	80.00	49.00
Rb	182.80	1.40	22.10	268.90	234.30	203.10	67.80
Sr	36.80	3488.70	76.20	68.00	176.70	81.40	35.70
U	2.10	0.20	1.70	1.20	1.70	3.60	1.60
Th	5.10	1.90	12.80	8.80	11.60	13.30	21.80
Y	27.20	22.50	39.00	23.60	17.10	39.90	28.60
Zr	252.00	117.20	247.40	147.80	209.20	339.50	275.00
Nb	35.30	18.20	46.90	16.00	9.50	57.20	20.10
Cs	1.90	0.20	1.10	78.00	22.60	51.20	3.10
Ga	22.90	40.50	12.90	13.10	15.40	17.20	7.10
Rb/Sr	4.97	0.00	0.29	3.95	1.33	2.50	1.90
La	28.00	20.60	77.50	36.80	29.80	58.20	66.40
Ce	66.40	42.10	150.80	73.30	51.80	112.90	133.90
Pr	8.01	5.39	17.15	8.05	6.35	13.05	18.60
Nd	32.40	22.30	64.80	30.50	22.50	46.40	68.10
Sm	6.60	5.00	10.50	5.60	4.00	8.10	11.50
Eu	1.65	1.99	2.06	1.24	1.00	1.79	2.24
Gd	5.72	4.96	7.14	4.06	3.03	6.29	7.17
Tb	0.90	0.85	1.18	0.75	0.51	1.10	1.11
Dy	4.92	4.42	6.71	3.82	3.11	6.54	5.63
Ho	0.95	0.78	1.28	0.80	0.58	1.32	0.95
Er	2.64	2.17	3.76	2.46	1.91	4.25	2.77
Tm	0.40	0.29	0.58	0.39	0.26	0.68	0.48
Yb	2.60	1.60	3.61	2.61	1.77	3.94	3.08
Lu	0.39	0.21	0.53	0.41	0.28	0.59	0.47
REE tot.	161.58	112.66	347.60	170.79	126.90	265.15	322.40

Tab. 4.1: Whole-rock geochemical composition of Cryogenian rocks from the OML. Oxides in wt.-%; n.d. = not detected, n.a. = not analysed.

Locality	Hohen-twiel	Varianto-Toppa	Berg Aukas	Uitsab	Wolken-hauben	Teco	Driehoek	Border	Border RE	Harasib III
Sample	CL42A	CL138M	CL464	CL415	CL476	CL470	CL480	CL494	CL494	CL301
mineral	Magnetite	Magnetite	Galena	Galena	Galena	Galena	Galena	Galena	Galena	Galena
K	0.05	0.36	< 0.02	< 0.02	< 0.02	< 0.02	< 0.02	< 0.02	< 0.02	< 0.02
Ti	0.22	0.10	< 0.001	< 0.001	< 0.001	< 0.001	< 0.001	< 0.001	< 0.001	< 0.001
Ba	46.00	63.00	3.20	26.00	15.00	2.10	3.20	23.00	2.90	15.00
Sc	1.70	2.90	< 0.1	< 0.1	< 0.1	< 0.1	< 0.1	< 0.1	< 0.1	0.10
S	< 0.04	< 0.04	10.00	7.93	8.66	10.00	8.89	10.00	10.00	7.16
Mo	0.98	0.74	< 0.05	0.64	< 0.05	0.27	0.17	0.41	0.11	0.13
Cu	8.28	36.96	791.35	255.14	435.69	2754.00	130.30	40.40	33.79	2855.09
Pb	11.77	121.61	n.a.	n.a.	n.a.	n.a.	n.a.	n.a.	n.a.	n.a.
Zn	23.70	31.10	>10000	124.80	4516.40	147.70	730.10	2371.10	1577.20	>10000
As	2.40	3.40	37.10	83.90	1.10	708.30	1.90	91.80	92.20	40.20
Sb	0.08	0.81	162.45	35.52	157.46	95.72	73.83	432.07	416.34	118.28
Ag	65.7	62.1	115023.0	83140.0	>200000	156800.0	103852.0	>200000	>200000	157581.0
Au	< 0.1	< 0.1	< 0.1	< 0.1	< 0.1	< 0.1	< 0.1	< 0.1	< 0.1	< 0.1
V	580.00	254.00	< 1	< 1	< 1	< 1	< 1	< 1	< 1	1.40
Rb	2.30	45.80	0.50	0.20	0.30	0.20	0.20	0.60	0.20	0.90
Sr	23.00	14.00	5.00	141.00	30.00	4.00	19.00	4.00	3.00	9.00
U	1.20	1.10	0.30	1.30	0.10	1.10	0.10	0.10	0.10	0.10
Th	4.50	4.60	0.10	0.20	0.10	< 0.1	0.10	0.10	< 0.1	0.30
Y	7.60	6.10	0.10	< 0.1	0.10	< 0.1	0.10	< 0.1	< 0.1	0.40
Zr	165.90	88.20	0.70	< 0.2	< 0.2	0.50	< 0.2	0.20	0.20	0.60
Nb	12.45	3.64	< 0.04	< 0.04	< 0.04	< 0.04	< 0.04	< 0.04	< 0.04	0.05
Cs	0.20	14.50	0.10	0.10	0.10	0.10	0.10	0.10	0.10	0.10
Ga	7.91	6.01	0.45	0.02	0.05	2.02	0.07	0.50	0.46	7.59
Rb/Sr	0.10	3.27	0.10	0.00	0.01	0.05	0.01	0.15	0.07	0.10
La	13.90	9.71	< 1	< 1	< 1	< 1	< 1	< 1	< 1	< 1
Ce	25.70	18.96	0.41	0.19	0.17	0.25	0.29	0.20	0.10	1.06
Pr	2.70	1.90	< 0.1	< 0.1	< 0.1	< 0.1	< 0.1	< 0.1	< 0.1	0.10
Nd	10.60	7.60	0.20	0.10	0.10	0.10	0.10	0.10	< 0.1	0.40
Sm	3.60	1.70	0.10	< 0.1	< 0.1	< 0.1	< 0.1	< 0.1	< 0.1	0.10
Eu	0.50	0.30	< 0.1	< 0.1	< 0.1	< 0.1	< 0.1	< 0.1	< 0.1	< 0.1
Gd	1.40	1.00	< 0.1	< 0.1	< 0.1	< 0.1	< 0.1	< 0.1	< 0.1	0.10
Tb	0.20	0.10	< 0.1	< 0.1	< 0.1	< 0.1	< 0.1	< 0.1	< 0.1	< 0.1
Dy	1.30	1.00	< 0.1	< 0.1	< 0.1	< 0.1	< 0.1	< 0.1	< 0.1	0.10
Ho	0.30	0.20	< 0.1	< 0.1	< 0.1	< 0.1	< 0.1	< 0.1	< 0.1	< 0.1
Er	0.90	0.80	< 0.1	< 0.1	< 0.1	< 0.1	< 0.1	< 0.1	< 0.1	< 0.1
Tm	0.20	0.10	< 0.1	< 0.1	< 0.1	< 0.1	< 0.1	< 0.1	< 0.1	< 0.1
Yb	1.30	1.20	< 0.1	< 0.1	< 0.1	< 0.1	< 0.1	< 0.1	< 0.1	0.10
Lu	0.20	0.20	< 0.1	< 0.1	< 0.1	< 0.1	< 0.1	< 0.1	< 0.1	< 0.1
REE total	62.80	44.77	0.71	0.29	0.27	0.35	0.39	0.30	0.10	1.96

Tab. 4.2: Geochemical composition of magnetite and galena samples from the OML. (Ag in ppb; K, Ti, S in wt.-%; other elements in ppm; n.d. = not detected, n.a. = not analysed.

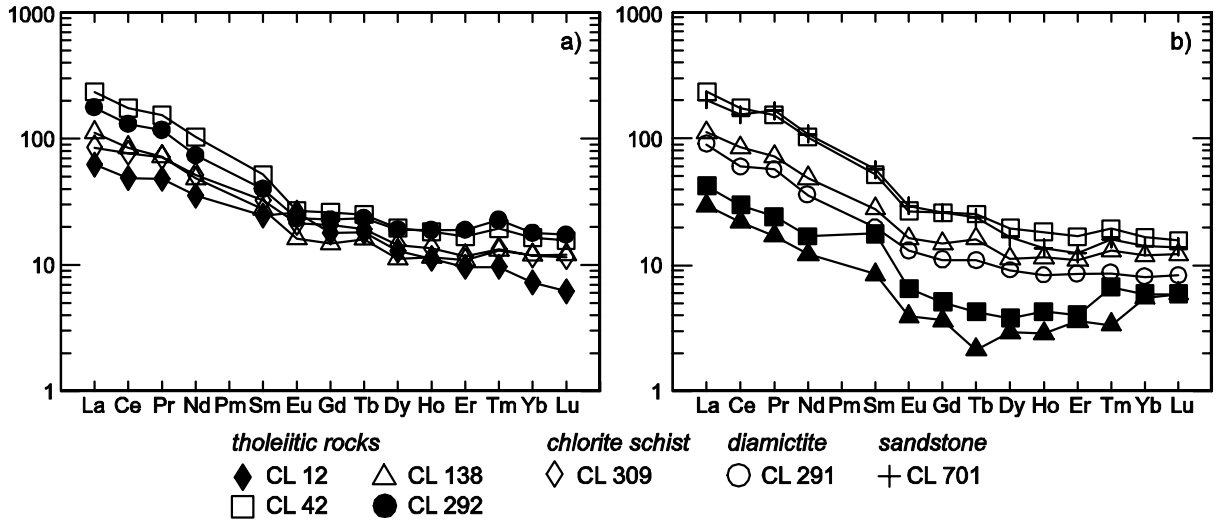

Fig. 4.7: Chondrite-normalised REE plots (Nakamura, 1974) for rock samples from a) the Askevold Formation, b) enclosed magnetites and related rocks.

The distribution of Bulk Earth-normalised trace elements of the Askevold Fm samples and related sediments of the Nabis and Chuos Formations are separated into two patterns (Fig. 4.6). The incompatible elements from Cs to K are highly variable in most of the samples, whereas the more compatible elements from Nb to Ti and Y display a similar distribution pattern. An exception is the Sr content of tholeiites from the Deblin Mine (CL12) which is higher by two orders of magnitude. Apart from CL12 and Sr, decreasing values with higher compatibility are visible. Only samples CL138 and CL292 reveal almost the same values over the entire range of measured elements. Incompatible elements from Cs to K attain higher values in the magnetite samples (CL42A, CL138M) than in the corresponding host rocks (CL42, CL138), whereas trace elements from Nb to Yb are depleted in the magnetites relative to their hosts.

Chondrite-normalised REE patterns for the Askevold Fm show an almost parallel, generally decreasing trend towards the HREE (Fig. 4.7) with a cumulative dispersion from the middle REEs to the lighter and heavier REEs, respectively. The magnetite samples have significantly lower REE contents than their corresponding host rocks. The REE patterns for magnetite reflect positive Sm anomalies in both analysed samples. Magnetite CL138M has negative Tb and Tm anomalies, while sample CL42A shows a positive Tm peak. The REE pattern of diamictite CL291 runs parallel to the decreasing trend of Askevold metavolcanic rock CL138, whereas the REE pattern of Nabis sandstone CL701 is virtually identical to that of metabasalt sample CL42 from Hohentwiel.

4.4.3 Pb-Pb dating

Pb isotope data of three magnetite separates from two whole rock samples of the Askevold Formation taken at Hohentwiel Farm and Varianto-Toppa Farm (CL42 and CL138, Fig. 4.2) are listed in Table 4.3 and plotted in conventional Pb-Pb diagrams in Fig. 4.8. While magnetite sample CL42 has a common lead composition with $^{206}Pb/^{204}Pb$ = 18.249, the magnetite separates from sample CL138 clearly show radiogenic Pb components with $^{206}Pb/^{204}Pb$ = 34.991 and 44.052. In the $^{207}Pb/^{204}Pb$ vs. $^{206}Pb/^{204}Pb$ space, the three data points define a statistically well-supported regression line (MSWD = 0.53) the slope of which corresponds to a Pb-Pb isochron age of 587 ± 12 Ma. In a $^{208}Pb/^{204}Pb$ vs. $^{206}Pb/^{204}Pb$ diagram, the samples are also linearily correlated but display enhanced scatter of the data points around the regression line. This points to the presence of a contaminating (silicate?) mineral phase characterised by distinct thorogenic Pb, possibly forming inclusions in magnetite at the submicron scale. However, the relatively limited data scatter around the line indicates that the interference of Pb from this possible, yet unidentified contaminant with the Pb-Pb systematics of magnetite is not very significant and the excellent linearity in the uranogenic Pb plot suggests consistent U-Pb-Pb systematics of magnetite and possible inclusions. Therefore, we interpret the Pb-Pb

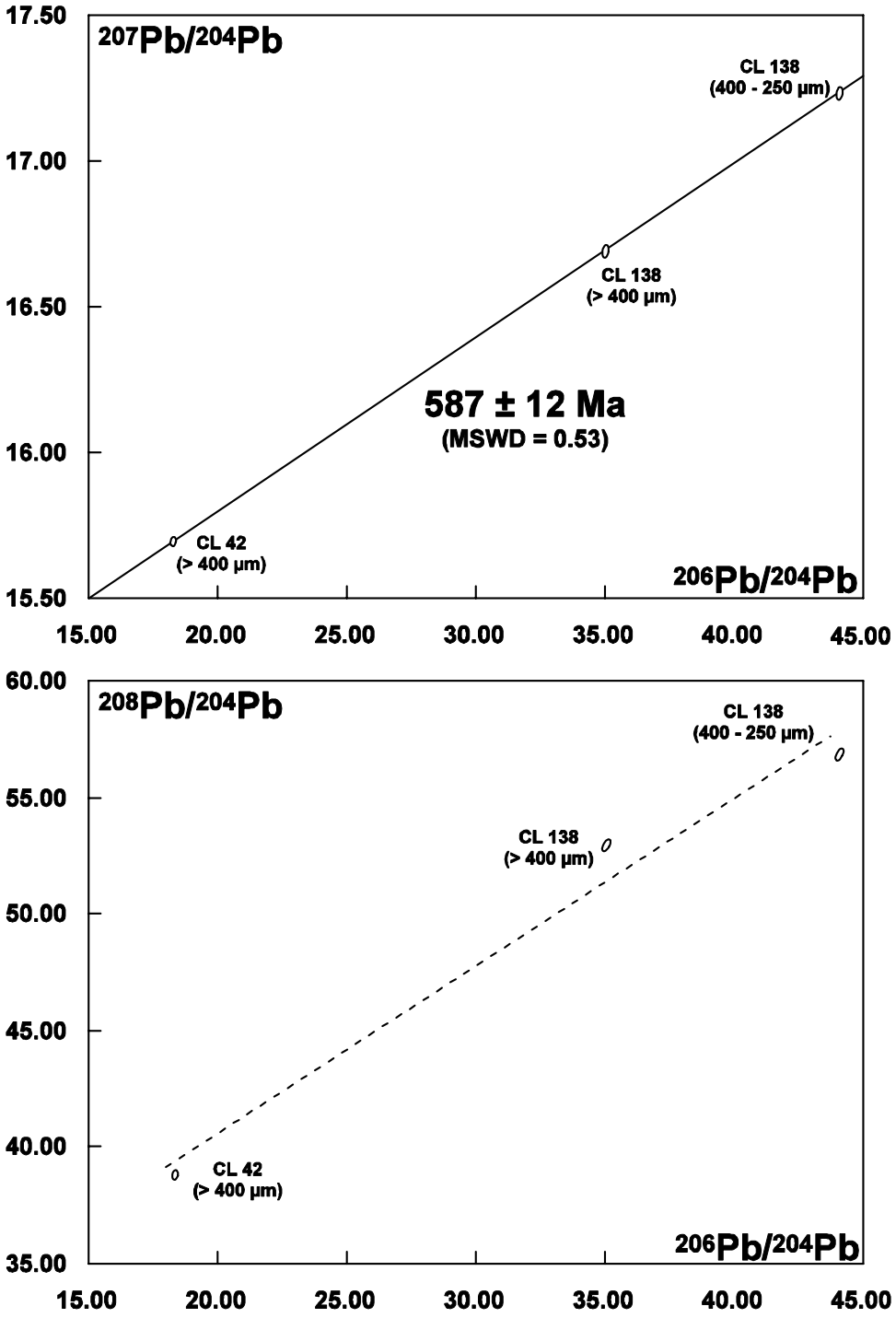

Fig. 4.8: Pb-Pb diagrams for magnetite separates from Askevold Formation volcanic rocks.

age of 587 ± 12 Ma to be geochronologically significant. Since the Askevold metavolcanic rocks can be parallelised with the Naauwpoort Formation in the Northern Zone, which revealed U-Pb zircon ages of 742 ± 25 Ma (Burger and Coertze, 1973) and 746 ± 2 Ma (Hoffman et al., 1996), the early middle Ediacaran age of 587 Ma for the Askevold magnetites most likely records a metamorphic reset age.

4.5. Discussion

As described by Söhnge (1957), the major deposits of the metavolcanic Askevold Formation crop out in the southernmost OML, in the vicinity of the Askevold range. Our petrographical (Fig. 4.3) and geochemical data (Fig. 4.4 - 7), have identified some more possible candidates that could be assigned to the Askevold Fm in the central OML, e.g. samples CL138 and CL292 from the Nosib Anticline (Fig. 4.2). A characterisation of samples from the Askevold Fm using discrimination diagrams is hampered by their metamorphic nature. Their mineral assemblage implies an at least greenschist facies overprint, which is also evident for the metavolcanic rocks of the Nosib Anticline. This indicates that Pan-African greenschist facies metamorphism has affected not only the Northern Zone, but also rock sequences in the central OML. Biotite-quartz strain shadows of opaque phases indicate even higher metamorphic conditions, but the pure brittle deformation of pyrites indicates pT-conditions lower than 400°C and 3kbar (Atkinson, 1975). The Zr/4-Y-Nb*2 triplot (Fig. 4.9a) could point to a within-plate setting for the metavolcanic rocks. However, it has to be considered that this classification is based on basalt analyses with a total CaO+MgO between 12 and 20 % (Meschede, 1986) and most of the Askevold metavolcanic rocks presented here have a total CaO+MgO less than 12 wt.%, which could have been caused by a substantial Ca loss due to retrograde metamorphism during the waning stages of the main Pan-African orogenic phase (M1, peak at. ca. 535 Ma, Goscombe et al., 2004) or late Pan-African regional metamorphism (M2, ca. 481 - 459 Ma, Laukamp et al., 2006 and references therein). Only sample CL12 from the Neuwerk Farm has an extreme high CaO content (20.56 wt. %), which can be explained by tectonically inserted, Calcite-rich phacoids from adjacent lithologies. Low K values (Table 4.1, Fig. 4.4) argue for rift-related volcanism. The higher abundance of incompatible trace elements, such as Ba and Zr, implies crustal contamination or originated from mixing of metavolcanic rocks (e.g. CL42) with siliciclastic rocks of the Nabis Fm. The latter interpretation is supported by similar main and trace element distribution patterns for the metavolcanic and siliciclastic rocks (Fig. 4.4 - 7). A continental setting for the Askevold metavolcanic rocks can be inferred from a La/10-Nb/8-Y/15 triplot (Cabanis and Lecolle, 1989; Fig. 4.9b). In addition to metamorphic events, strong hydrothermal overprinting of the Askevold rocks is suggested by the local occurrence of VMS-type mineralisation (e.g. Farm Neuwerk, sample CL309), which also display post-mineralisation alteration (Fig. 4.3b). The mineralised chlorite schist from the Deblin Mine (CL309) is strongly enriched in Cu, Mo and As, whereas adjacent metavolcanic rocks (CL12) are depleted in these elements (Table 4.1, Fig.

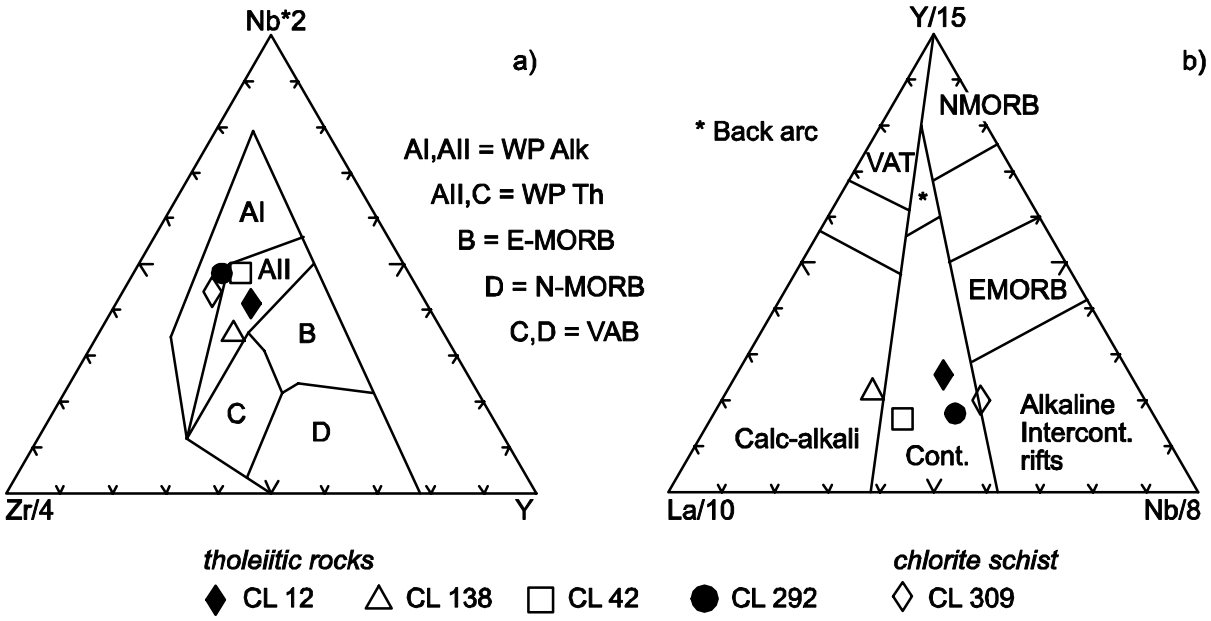

Fig. 4.9: Discrimination diagrams showing rock samples from the Askevold Formation. a) triplot of Zr/4-Y-Nb*2 (Meschede et al., 1986), b) La/10-Y/15-Nb/8 diagram for basalts (Cabanis and Lecolle, 1989).

4.5). This suggests a partitioning of chalcophile elements into the sulphide phase during crystallisation of the mafic magmas (Naldrett, 1989), leading to an enrichment of sulphide ore in distinct layers. Cu sulphides occurring in single layers of the chlorite schists seem to have survived even the Pan-African deformational event.

The origin of the Askevold metavolcanic rocks as well as of the petrographically and geochemically similar formations in the central and eastern Nosib Anticline awaits explanation. The emplacement of Askevold volcanic rocks south of the Otavi Valley has been integrated in the Cryogenian rifting of the Khomas Trough, accompanying the final stages of the deposition of the Nosib Group (Söhnge, 1957; Hoffmann et al., 1996). Our geochemical data support the classification of the Askevold metavolcanics as intracontinental rift-related volcanics. Therefore, the metavolcanics north of the Grootfontein basement high could have intruded into the Nabis Formation in a subsidiary graben in the northern central OML. Considering the strong foliation of almost all the samples of the Askevold Formation and the strong Pan-African deformation observed in the southern OML (Van der Merwe Smit, 1959; Maclaren, 1991), the metavolcanic rocks in the north may also represent thrust slices, generated during the main phase of the Pan-African orogeny (D2). The Pan-African age of this foliation is indicated by strain shadows of magnetite in the metavolcanics that have a Pb-Pb age of 587 ± 12 Ma. These magnetites clearly postdate the VMS-type mineralisation. Furthermore, our field observations revealed a schistose unit between the basement and the Nosib Group in the Eastern Keilberg Anticline (CL181). The SC pattern of the Keilberg quartzitic micaschist is related to the Pan-African orogeny and reflects upper greenschist facies conditions, as indicated by the presence of biotite strain shadows attached to extraformational clasts in a mica-quartz-dominated mineral assemblage. Allothigene quartz clasts suggest a siliciclastic educt of the Keilberg quartzitic micaschist (CL181), and its composition possibly identifies granites in the Grootfontein Inlier as source rocks, as already suggested by Hedberg (1979) (Part 3). Its spatial relationship to schistose units implies a major zone of deformation (detachment?) at the contact of the pre-Damaran basement and the Nosib Group in the central OML. The quartzitic micaschist shows a significant loss in Na_2O that could have been caused by metamorphism.

Hydrothermal base metal mineralisation in the OML has been interpreted by many authors (Söhnge, 1957; Frimmel et al., 1996a) to be the product of metamorphic brines that leached ore-forming elements from siliciclastic rocks of the Nosib Formation, epidosites of the Askevold Fm, phyllites of the Kombat Formation, and shales of the upper Abenab Subgroup. This implies that D2-contemporary fluids derived from compaction and dewatering of sediments, which were deposited in pre-Pan-African grabens, could have leached the siliciclastic and volcaniclastic rocks (Pirajno and Joubert, 1993). Likewise, the Paleoproterozoic basement of the Grootfontein Inlier was considered as possible source for base metal mineralisation in the OML (Pirajno and Joubert, 1993; Chetty and Frimmel, 2000) as well. Frimmel et al. (2004) proposed a mixture of basement-derived Pb (and other base metals) and more radiogenic Pb, which was added through syn-orogenic brines. Pan-African lineaments, reverse faults and large thrusts located at the southern margin of the Congo Craton, could have been the conduits of such ore-forming metamorphic fluids, released by dehydration reactions at very deep crustal levels (Kasch, 1983).

Our petrographical and geochemical data reflect the alteration of VMS-type mineralisation in the southern OML (Deblin mine, Fig. 4.2). Greenschist facies metamorphism may be related to the main phase D2 of the Pan-African orogeny. As with other locations, the Deblin orebody is confined to zones of intensive deformation (Van der Merwe Smit, 1959). However, the formation of Cu-sulphides and the growth of magnetite in these metavolcanic rocks occurred pre-D2. This is confirmed by layers of magnetite, outlining mesoscopic folds in the Kombat Mine (Innes and Chaplin, 1986). Along with the proved Pan-African deformation of Cu-sulphides in the southern OML, this indicates that the genesis of VMS-type mineralisation in the OML is not related to the Pan-African orogeny. The VMS-type mineralisation could have acted as a precursor for base metal deposits in the Otavi Valley (e.g. Kombat, Fig. 4.2). The new exploration of metavolcanic rocks of the Askevold Fm in the Nosib Anticline implies the possibility of further VMS-type deposits in the central OML, buried under the platform carbonates of the Otavi Group.

Trace element diagrams for galena (Fig. 4.10) show distribution patterns characterised by distinct variations of the single relative element abundances arranged around a slightly decreasing trend towards

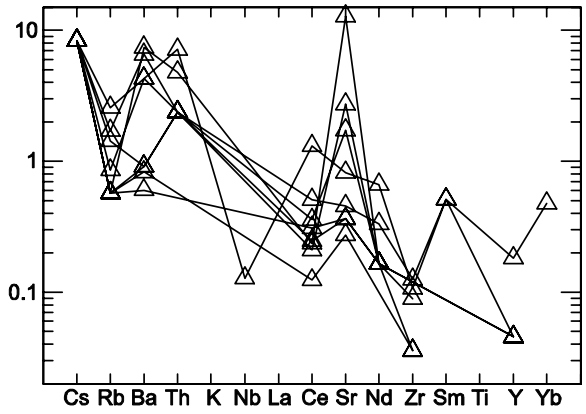

Fig. 4.10: Bulk Earth-normalised trace element diagram (Hickey et al., 1986) for galena samples from the OML. For sample locations see Fig. 2.

the more incompatible elements. This trend, characterised by positive Cs, Th and Nd / negative Sr, Zr and Ti anomalies, is similar to the trace element distribution patterns detected in the Askevold rocks and differs from the high relative abundance of incompatible trace elements observed in the samples of the GMC (Part 3). Therefore, the influence of the Askevold Fm as source rock of base metal mineralisation in the OML might be more significant than that of the GMC.

4.6 Conclusions

Middle Neoproterozoic (Cryogenian) volcanic and siliciclastic rocks of the Nosib group overlying the Paleoproterozoic basement have been known mainly from the southern OML. However, our petrographical and geochemical data suggest the presence of such rocks also in the central OML farther north. Although the origin of metavolcanic rocks of the Askevold Formation (Nosib Group) is almost obliterated by Pan-African deformational features, main and trace element data confirm their relationship with a pre-Pan-African rifting phase at the southern margin of the Congo Craton (Porada, 1985) during the early Cryogenian. The rifting up to the final stage of the deposition of the Nosib Group was accompanied by the intrusion of tholeiitic magmas into the upper Nosib Group and the formation of widespread VMS mineralisation, whose age could not be definitely assessed. The Pb-Pb age of 587 ± 12 Ma obtained from the magnetite occurring in the Askevold volcanic rocks records a metamorphic phase during the early middle Ediacaran, just prior to D2 deformation and the subsequent deposition of the late Ediacaran Mulden Group. It therefore gives a minimum age for the Pan-African collision of the Congo and Kalahari Cratons in the Northern Zone of the Damara Belt.

Comparative geochemical data on volcanic rocks from the Nosib Group and on galena from base metal ores hosted by the Abenab and Tsumeb Supergroups carbonate successions support the Askevold Fm and related VMS-type deposits as precursors for base metal ore deposits in the overlying platform carbonates of the OML.

Acknowledgements

We thank Arno Günzel (Ongopolo Mining and Processing Limited, Tsumeb) for the introduction into the field. We acknowledge the logistic support by Hartwig Frimmel (University of Würzburg), Andries Nethling (Ongopolo Mining and Processing Limited, Tsumeb) and Volker Petzel (Namibia Geological Survey). Georg Werner kindly provided unpublished material and helped together with Nathan Kang to prepare the samples for geochemical studies. We are grateful to Urs Schaltegger (University of Geneva) and Albrecht von Quadt (ETH Zurich) for giving unlimited access to all cleanlab and mass spectrometry facilities. We are indebted to Deutsche Forschungsgemeinschaft (DFG) for financing this study in the framework of the "Graduiertenkolleg 273 on Rock-water interaction" at Heidelberg University. Further financial support was provided by the DAAD-financed Internationales Promotionsprogramm (IPP) at the Faculty of Chemistry and Geosciences, Heidelberg University.

Part 5: Willemite (Zn_2SiO_4) as a possible Rb-Sr geochronometer for dating nonsulphide Zn-Pb mineralisation: examples from the Otavi Mountainland (Namibia)

Abstract

The zinc silicate willemite (Zn2SiO4) is the main carrier of zinc in a number of high-grade, carbonate-hosted nonsulphide deposits located in the southern hemisphere that have been recently reinterpreted to be of hypogene-hydrothermal origin. The timing of willemite mineralisation in these deposits is only poorly constrained. In this pilot study, willemite has been evaluated as a potential Rb-Sr geochronometer that can be used to directly date nonsulphide ore deposits. We have analyzed samples of economic-stage willemite from the Berg Aukas and Abenab West deposits, Otavi Mountainland (Namibia), which are hosted by Neoproterozoic, dolomitised and tectonised carbonate rocks. Rb-Sr elemental concentration levels and ranges of $^{87}Rb/^{86}Sr$ and $^{87}Sr/^{86}Sr$ ratios in these willemite samples are comparable to those observed for the Zn sulphide sphalerite, which has been already successfully used for direct Rb-Sr dating of carbonate-hosted (MVT) deposits. This reflects similar Rb-Sr partitioning mechanisms into Zn ore minerals that precipitate either as sulphides from reduced or as silicates from oxidised hydrothermal fluids, respectively. The Rb-Sr results on willemite presented here reflect mostly low, but variable $^{87}Rb/^{86}Sr$ ratios, sufficient to generate radiogenic ^{87}Sr over time. This clearly shows that willemite is suitable as a Rb-Sr geochronometer and should be further evaluated for direct Rb-Sr dating of nonsulphide Zn deposits.

Isochron regressions combining samples from Berg Aukas and Abenab West willemites yield Rb-Sr ages in the range of ca. 500 to 560 Ma. These values are geochronologically doubtful at first sight due to high excess data scatter (MSWD = 2000 to 3000). Massive, fine-grained willemite samples from Abenab West alone (n = 3) give a - still statistically unacceptable (MSWD = 60) - isochron regression corresponding to a Rb-Sr age of 574 ± 84 Ma. More reliable ages are obtained from two statistically adequate small-scale Rb-Sr isochron regressions for samples of coarse-grained, well-crystallised Berg Aukas willemite, which yield 499 ± 63 Ma (MSWD = 2.6) and 493 ± 2 Ma (MSWD = 1.2), respectively.

Regardless of the quality of isochron regressions in terms of MSWD, the Rb-Sr ages obtained in this study are fully compatible with other available geochronological data that reflect distinct tectonothermal events in the study area. Therefore, on a regional scale, they appear to be at least geologically reasonable, which has yet to be verified by further studies. Comparable mineralisation ages in the range of ca. 490 to 550 Ma are also reflected by the few other known economic, hypogene willemite deposits in the southern hemisphere, for which direct geochronological information is mostly lacking. This may point to a global period of hydrothermal activity in the Cambrian to Lower Ordovician under conditions that favoured the formation of hypogene nonsulphide Zn mineralisation.

5.1 Introduction

Oxidised ores from nonsulphide Zn-Pb deposits were the prime source for zinc metal production for hundreds of years but lost their significance during the early 20th Century due to the development of flotation and smelting techniques for zinc sulphides. During the last years, however, nonsulphide Zn-Pb deposits have gained renewed attention and are now considered to be of major importance for the future production of zinc metal (e.g.,+ Large, 2001; Hitzman et al., 2003 and references therein). They may contain huge reserves of high-grade ores, are easy to exploit, and their ores can now be efficiently processed using improved hydrometallurgical techniques (e.g., Woollett, 2005). Many carbonate-hosted nonsulphide Zn-Pb deposits, especially in the southern hemisphere, contain the zinc nesosilicate willemite (Zn2SiO4) in economic concentrations (Hitzman et al., 2003). Willemite was discovered for the first time in 1829 in a “calamine” orebody in Belgium, scientifically described by A. Lévy (1843) and dedicated to King Willem of Orange. It is one of the very few silicate minerals that have a trigonal-rhombohedral symmetry (e.g., Simonov et al., 1977). The average density of willemite is 4.05 and its colour varies from transparent to red-brown and black.

It occurs as thin, transparent, mm-sized crystals with hexagonal-prismatic terminations as well as granular masses which often replace associated primary sulphides. Therefore, willemite has been traditionally considered as a product of low-temperature supergene alteration of zinc sulphide ores. However, a number of fluid inclusion studies suggest that willemite may also form at higher temperatures (100 to 250°C) under oxidizing hypogene-hydrothermal conditions (Sweeney et al., 1991; Brugger et al., 2003, see also Hitzman et al., 2003), both in deposits where willemite replaces primary Zn sulphides and in entirely nonsulphide mineralisation styles. In fact, most carbonate-hosted economic willemite deposits in the southern hemisphere (Vazante, Brazil, ca. 28.5 Mt @ 18% Zn; Kabwe and Star Zinc, Zambia, ca. 13 Mt @ 20 to 25% Zn; Berg Aukas and Abenab West, Namibia, ca. 3.5 Mt @ 15 to 25% Zn; and Beltana, Australia, ca. 0.86 Mt @ 38% Zn, see Hitzman et al., 2003) are now interpreted to be of hypogene-hydrothermal origin (Large, 2001; Brugger et al., 2003; Groves et al., 2003; Hitzman et al., 2003). According to Brugger et al. (2003) and Hitzman et al. (2003), the precipitation of willemite, instead of sphalerite, from saline hydrothermal fluids is preferred under oxidizing (hematite-stable) conditions at neutral to basic pH, low a HS- and elevated temperatures (>100 to 150°C).

The fact that economic willemite concentrations may have formed by hypogene-hydrothermal processes and are not necessarily associated with pre-existing zinc sulphides has ultimate implications for successful exploration strategies, as these may largely depend on the predictions provided by genetic models developed for these deposits (Brugger et al., 2003). It is therefore crucial to understand the geological factors that control the formation of willemite deposits in the presence or absence of known primary zinc sulphide accumulations, i.e., whether these nonsulphide ores have formed by supergene or hypogene-hydrothermal processes, or a combination of both.

For any viable genetic concept, a good knowledge on the age of mineralisation is of critical importance. With a few exceptions (e.g., Dejonghe and Boni, 2005; Monteiro et al., 2006), little is known about the actual timing of willemite mineralisation relative to the age of associated "primary" deposits as well as in the absence of pre-existing sulphide orebodies. Radiometric dating of ore-stage minerals is the prime tool to study these aspects and thereby could decisively help to better understand the genesis of nonsulphide Zn-Pb mineralisation. As with other types of economic mineral deposits, determining numerical ages for nonsulphide Zn-Pb mineralisation is a difficult task, as there are no major ore phases known in these deposits that are a priori amenable to direct radiometric dating using conventional isotopic systems. In a recent study, Groves et al. (2003) presented K-Ar ages of 437 ± 5 and 430 ± 5 Ma, respectively, obtained for late-mineralisation stage coronadite (MnPbMn6O14) from the Beltana willemite deposit located in the northern Flinders Ranges (Australia), which point to a minimum age of this mineralisation during the early Silurian.

In this study we have evaluated the mineral willemite as a possible Rb-Sr geochronometer that may be useful for direct dating of nonsulphide Zn-Pb mineralisation. We present some Rb-Sr data for willemite from two nonsulphide Zn-Pb deposits located in the Otavi Mountainland (OML), Namibia, that contain both primary base metal sulphides and Zn-Pb silicate/carbonates. These will allow us to draw preliminary conclusions on the possible timing of nonsulphide mineralisation in the Otavi Mountainland relative to regional geotectonic events.

5.2 Geological setting and mineralisation

5.2.1 Regional geology

The Otavi Mountainland (OML, Fig. 5.1) covers an area of about 10,000 km2 in the north-eastern foreland of the Damara Orogen, Namibia. The lithologies in the OML mainly comprise calcareous, dolomitic and siliciclastic rocks of the Neoproterozoic Damara Supergroup (Fig. 5.2) which unconformably overly a poorly outcropping Paleoproterozoic (Eburnean, 2.1 to 1.65 Ga, Miller, 1983a; Frimmel et al., 2004) basement, known as the Grootfontein Inlier or Grootfontein Metamorphic Complex (GMC). The GMC crops out in the nuclei of E-W anticlinal folds (Fig. 5.1) which have been interpreted as paleotopographic highs predating the deposition of the Damara Supergroup. The basement mainly consist of various, intensely deformed and metamorphosed alkaline and calcalkaline granites (Clifford et al.,

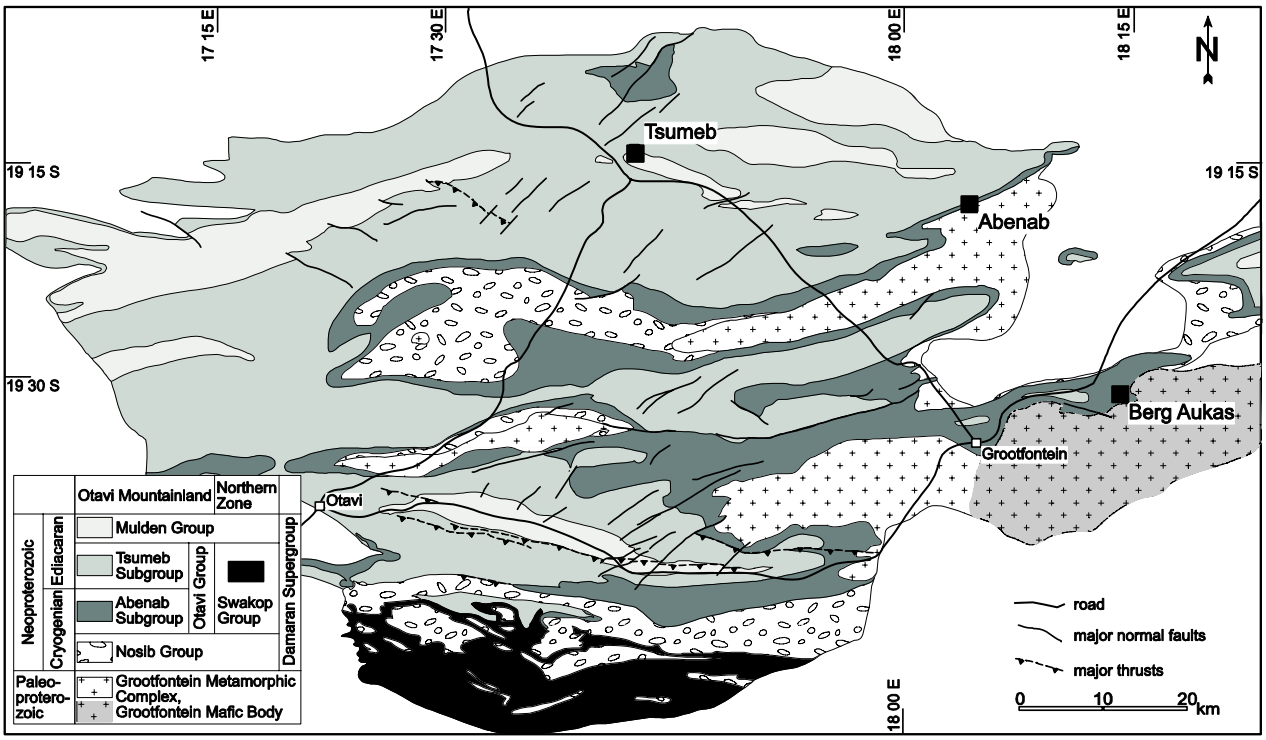

Fig. 5.1 Location map and geology of the Otavi Mountainland (OML), Namibia.

1969), and gabbros. In the south-eastern OML, this metamorphic basement is represented by the Grootfontein Mafic Body (Fig. 5.2).

The structural evolution of the OML during the Neoproterozoic commenced with rifting of a small eastern branch of the Adamastor ocean in the early Cryogenian, eventually leading to the evolution of the Khomas Trough and parallel running, subsidiary basins (Miller, 1983a). The volcaniclastic Nosib Group (747 ± 2 Ma, U-Pb zircon age obtained for the Askevold Fm; Hoffman et al., 1996) was deposited in a horst-graben system that follows ENE-trending lineaments. The Nosib group is overlain by platform carbonates of the Otavi Group (Fig. 5.2) which has been subdivided into the Abenab and Tsumeb Subgroups, respectively (Miller, 1983a). The age of the Otavi Group is poorly constrained. Frimmel et al. (2004) proposed an evolution of the carbonate platform between 746 Ma and 550 Ma. Hoffmann et al. (2004) obtained an U-Pb zircon age of 635.5 ± 1.2 Ma for diamictites of the glaciogenic Ghaub Fm, situated at the base of the Tsumeb Subgroup. Synorogenic molasse sediments of the Mulden Group overly the Tsumeb Subgroup and are also found in an extensive network of pre-Mulden paleokarst dissolution cavities. Cambrian to Mesozoic, Tertiary and Quaternary siliciclastic rocks of the Karoo and Kalahari sequences (Fig. 5.2) cover the Proterozoic rocks towards the north, east and south of the OML and also the deeply eroded, E-W striking anticlines (e.g., DWA et al., 2002). Several karstification periods occurred in the late Neoproterozoic and from the Tertiary onwards, up to recent times (Lombaard et al., 1986; Van der Westhuizen et al., 1988; Geyh, 1995; BGR, 1997; Bäumle, 2003).

The structural evolution of the OML during the Pan-African orogeny is characterised by three main deformational phases (Fig. 5.2). D1 folding and thrusting in the southernmost part of the OML was initiated by continental convergence in the Kaoko region in the west. Following karstification of the uppermost Otavi Group and deposition of the Mulden Group, north-vergent, partly overturned folds, a penetrative foliation and thrusts in the southern OML were generated by Pan-African collision of the Kalahari and Congo microplates (D2 after Frimmel et al., 1996b). According to Kröner and Clauer (1979) the age of the metamorphic peak M1 in the Northern Platform is around 535 to 530 Ma (K-Ar ages of clay fractions < 2 µm separated from pelitic Mulden sediments). After Goscombe et al. (2004), the D2 phase passes into late to post-Pan-African, mainly

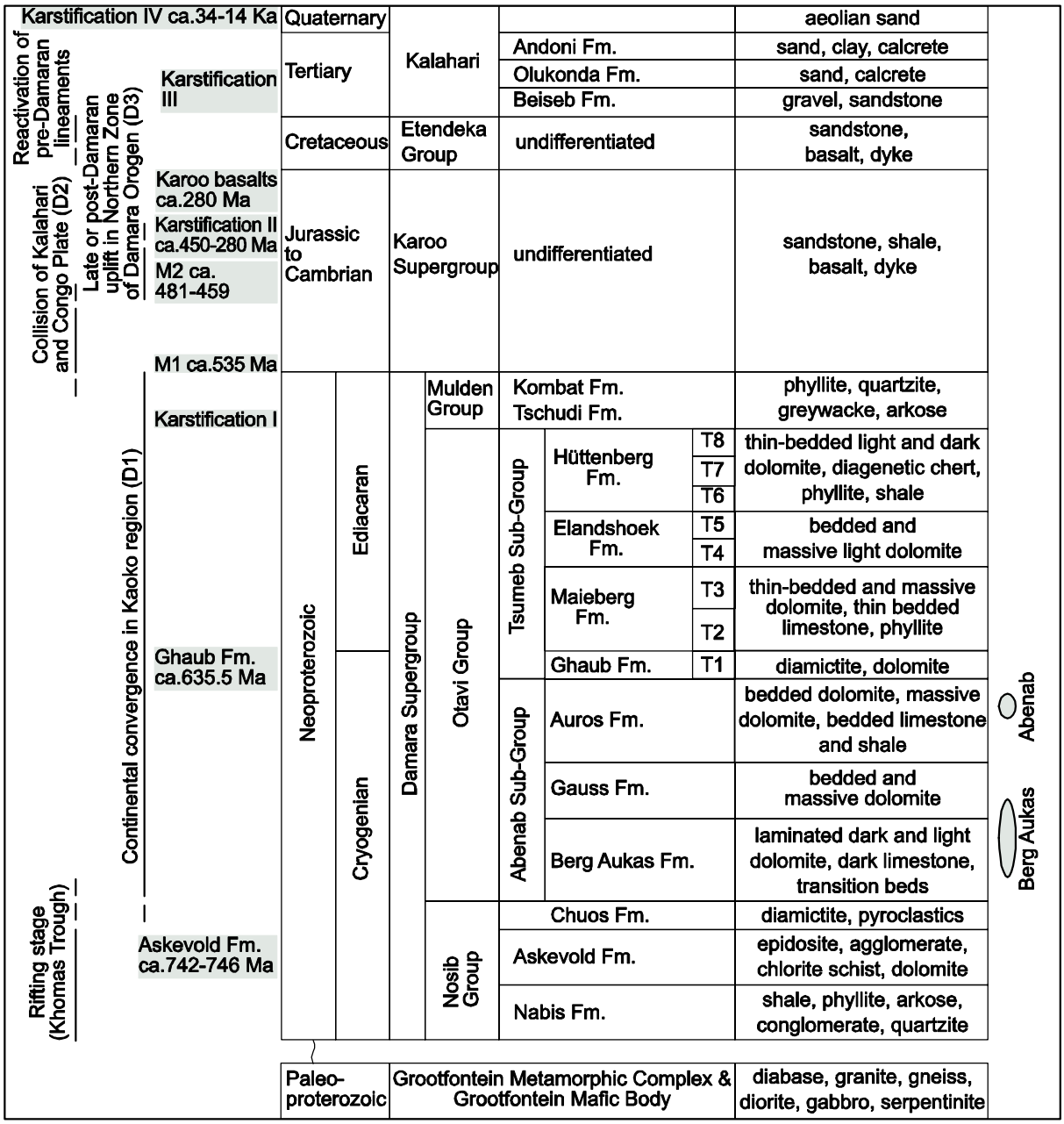

Fig. 5.2 Lithologies and tectonostratigraphic evolution in the Otavi Mountainland and stratigraphic position of the Abenab West and Berg Aukas deposits. Compiled from Burger and Coertze (1973), Kröner and Clauer (1979), Haack et al. (1980), Haack and Martin (1983), Frimmel et al. (1996a), Hoffman et al. (1996), Bäumle (2003, and references therein), Frimmel (2004), Frimmel et al. (2004), Goscombe et al. (2004) and Hoffmann et al. (2004).

extensional deformation D3. Kröner and Clauer (1979) and Kröner (1982) suggested that a late phase of regional metamorphism M2 occurred in the OML at ca. 481 to 459 Ma, even though this may be a consequence of uplifting.

5.2.2 Base metal mineralisation in the OML

Most base metal deposits in the OML contain both sulphide and nonsulphide mineralisation and are hosted by shallow-water carbonate successions of the Otavi Group. Based on a number of geological/geochemical criteria and variable metal contents, two main mineralisation styles have been distinguished: the Berg Aukas (Zn-Pb>Cu)- and the Tsumeb (Pb>Cu>Zn)-type deposits (Pirajno and Joubert, 1993; Melcher, 2003). Most deposits reflect a multistage evolution and display a strong structural control (Lombaard et al., 1986; Pirajno and Joubert, 1993; Frimmel et al., 1996a). Mineralised brittle shear

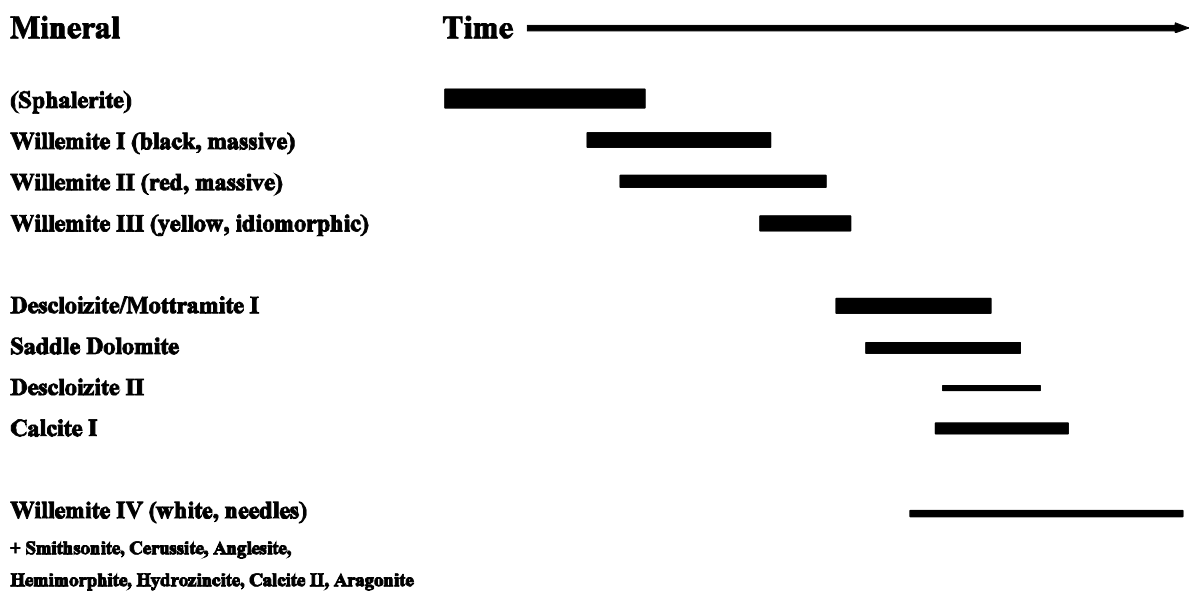

Fig. 5.3 Simplified paragenetic sequence of nonsulfide base metal mineralisation in the Otavi Mountainland, based on own observations. Note that the nonsulfide assemblage also occurs in the absence of sphalerite.

zones indicate the importance of flexural shear folds and small-scale thrusts for mineralisation. This relates to the formation of primary sulphide deposits (e.g., Tsumeb orebody, Lombaard et al., 1986) and, based on own observation, also to part of the nonsulphide deposits.

Nonsulphide Zn-Pb ores in the OML are mostly associated with, or even clearly replace, primary base metal sulphides. They partly display complex paragenetic associations, which point to very distinct processes of formation and mineralisation periods (e.g., Lombaard et al., 1986). The economically most important nonsulphide base metal ore minerals are willemite and Pb-Zn-Cu vanadates (descloizite-mottramite), several generations of which have been observed in the nonsulphide mineral paragenesis of the OML deposits (Fig. 5.3). Early, economic willemite forms massive, black and reddish accumulations (willemite I and II, Fig. 5.4a, c, g) but also occurs as yellow-brownish masses consisting of idiomorphic crystals (willemite III) that display characteristic rhombohedral terminations and hexagonal prisms (Fig. 5.4f). These willemite stages (I to III) commonly replace sphalerite or the carbonate host rocks directly (Fig. 5.4a, c-f) but may also occur in the absence of sulphides (Fig. 5.4b, g). Non-economic willemite IV (Fig. 5.4h) displays white needles and is associated with other Zn-Pb nonsulphides, such as cerussite, anglesite, smithsonite, hemimorphite, hydrozincite etc., which clearly represent later formations. They generally replace both primary sulphides and the earlier willemite generations and are characterised by the typical features of supergene weathering products. No reference to the possible age of early willemite mineralisation I-III or of the supergene mineral assemblages including willemite IV has ever been made, with the exception of the descloizite/mottramite precipitates. These have been roughly dated to be of Miocene age, based on vanadate-encrusted mammalian fossil remnants discovered in a network of karstic cavities in several mines (Pickford, 1993).

In the vast literature on the OML base metal ores, willemite has been generally considered to be of supergene origin, formed through weathering processes (Verwoerd, 1957; Misiewicz, 1988; Cairncross, 1997). Hitzman et al. (2003) was the first to consider the economic portion of willemite mineralisation in Namibia to have formed by hypogene-hydrothermal processes, by comparison with similar ores occurring in Zambia (e.g., Star Zinc, Sweeney et al., 1991). The economically most important willemite deposits in the OML are located at Berg Aukas and Abenab (Fig. 5.1).

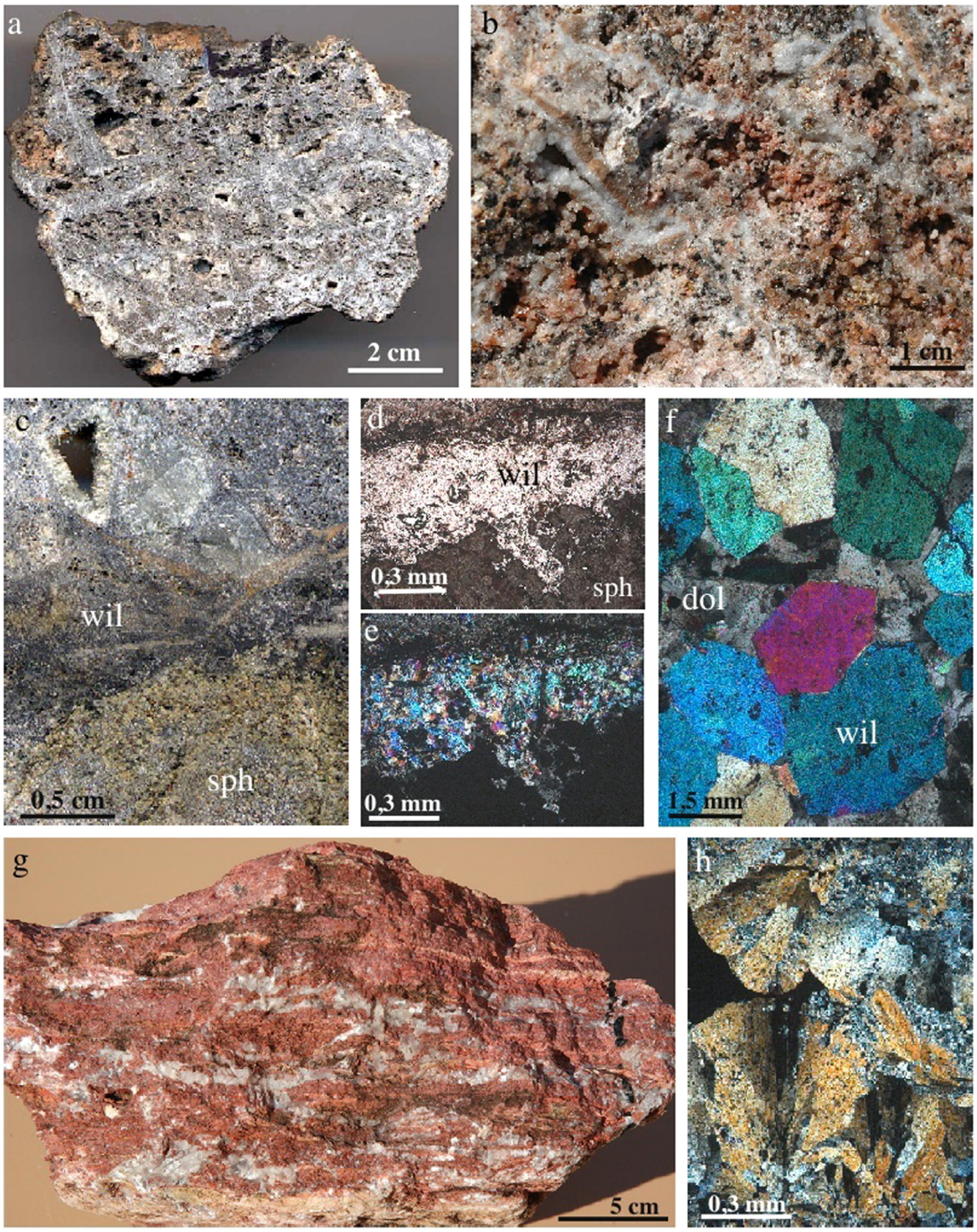

Fig. 5.4 Paragenetic stages, modes of occurrence and textural variations of willemite in the OML. a) Berg Aukas, willemite I in boxwork replacing sphalerite (sample BA 2003-1); b) Berg Aukas, pale-yellow/brownish, idiomorphic willemite III showing semi-massive microcrystalline texture (sample BA 2003-4); c) Berg Aukas, sphalerite (sph) replaced by black and red willemite I and II (will); d) Berg Aukas, willemite III (will) replacing sphalerite (sph), 2.5x, NII; e) Berg Aukas, same sample, 2.5x, N+; f) Berg Aukas, willemite III (will) cemented by clayey-dolomitic matrix (dol), sample NA.R04681; g) Abenab West, "Zinc Reef" mineralisation, red massive willemite II along a sheared contact between dolomite and limestone; in white: macrocrystalline calcite, sample AW 2003-1; h) Abenab West, "Zinc Reef" mineralisation, willemite IV spherules (sample AW 2003-1/I.), 2.5 x, N+.

5.2.3 Berg Aukas deposit

The Berg Aukas Zn-Pb-V deposit is located in the eastern part of the OML, 20 km northeast of Grootfontein, at latitude 19°34'12" S and longitude 18°15'36" E (Cairncross, 1997). The ore grade of the mine averaged 16.8 % Zn, 4% Pb, and 0.93 % V_2O_5. Mineralisation has been traced to a depth of 750 m below the surface, but was mined only to a depth of 600 m. The mine ceased operation in 1978. The Berg Aukas deposit is unique in that it represents one of the largest known accumulations of willemite and vanadium minerals in the world (Misiewicz, 1988). About 40% of the total zinc metal content occurred in form of willemite.

The Berg Aukas deposit is hosted in Neoproterozoic microbial dolostones of the Gauss Formation (Abenab Subgroup, see Fig. 5.2) which overly basal siliciclastic rocks on the northern limb of the E-W trending Berg Aukas syncline. Base metal mineralisation at Berg Aukas is developed along a bedding-parallel fault and has been subdivided into several types of stratigraphically and structurally controlled orebodies (Misiewicz, 1988). Sulphide ores mainly consist of coarse-grained sphalerite and minor galena which are partly intergrown with or even replaced by willemite. Other nonsulphide minerals include smithsonite, hemimorphite, cerussite (all noneconomic), and abundant descloizite and vanadinite (Markham, 1958).

Willemite ore from Berg Aukas forms fine-grained to granular masses which are black to red in colour (willemite I and II, Fig. 5.4a-c). Complete dissolution and replacement of sphalerite by willemite along a network of veins is common and results in a dark willemite boxwork (Fig. 5.4a). Pale-yellow willemite III occurs with a semi-massive microcrystalline texture and comprises closely packed, subhedral, hexagonal grains (Fig. 5.4b, f). Locally, vuggy textures can be observed with late-stage supergene base metal carbonates and willemite IV in the form of coalescing agglomerates of fine, radiating prismatic needles growing in open spaces (Fig. 5.4h, see also Misiewicz, 1988).

5.2.4 Abenab deposit

The Abenab and Abenab West deposits are located approximately 30 km north of Berg Aukas (Fig. 5.1) and were exploited between 1922 and 1958 (Cairncross, 1997). Both deposits are hosted by the Auros Formation (uppermost Abenab Subgroup, Fig. 5.2). The Abenab deposit consists of a pipe-like karst structure filled with descloizite and vanadinite-rich muds that appear to have replaced a precursor Pb-Zn-rich pipe. The combined original Pb-Zn ore reserves of the Abenab and Abenab West deposits amount to ca. 2.35 Mt @ 1 to 2.6 % V_2O_5 (Cairncross, 1997).

The Abenab West deposit is located ca. 100 m southwest of the Abenab pipe and occurs along a steeply dipping, bedding-parallel structural contact. Primary sulphides are extremely rare at Abenab West, however, Verwoerd (1957) described very minor and strongly deformed galena from the lowermost levels of the deposit. Our own observations revealed only very rare, local replacements of sphalerite by willemite. The so-called "Zinc Reef" forms part of the Abenab West deposit and consists of a ca. 450 m long replacement zone of massive, red willemite II and hematitic clay along a sheared and brecciated contact between laminated limestone and dolostone (Verwoerd, 1957, Fig. 5.4a). The development of bedding-parallel cleavage and tectonic brecciation along this contact predates the formation of the zinc silicates. Therefore, willemite mineralisation most probably occurred after the main deformational event of the Pan-African orogeny (D2). Willemite IV in the "Zinc Reef" occurs as radially assembled, needle-like crystals in cavities or along lining fracture surfaces (Fig. 5.4h).

5.3 Methodology

5.3.1 Sampling and sample description

For the present pilot study, willemite samples were collected at the Berg Aukas and Abenab West mining sites during 2003 and 2004 field seasons. As the Berg Aukas underground mine is currently not accessible, samples were taken from the nearby dumps. Abenab West samples were taken from surface outcrops of the "Zinc Reef" mineralisation. Since willemite occurs in several generations and partly complex textural assemblages at both deposits (Fig. 5.4), we have

selected for Rb-Sr analysis only samples that (i) were likely to represent unaltered precipitates which are free of major discernible impurities that could disturb their Rb-Sr system, and (ii) represent main-stage, economic willemite mineralisation styles (willemite I-III, cf. Fig. 5.4). These encompass massive, fine-grained red willemite II as it is found in the "Zinc Reef" mineralisation at Abenab West (Fig. 5.4g) and coarse-grained, well-crystallised, idiomorphic willemite III which is one of the main generations occurring at Berg Aukas (Fig. 5.4b, d-f). Rb-Sr analyses were performed on two samples of red willemite II from Abenab West (AW 2003-1/I, AW 2003-1/II) and on two samples displaying well-crystallised, creamy-yellow prisms of willemite III from Berg Aukas (BA 2003-4, NA.R04681, cf. Fig. 5.4b, f). Some parts of Berg Aukas sample NA.R04681 show a dolomitic matrix containing abundant, yet unidentified clay minerals, cementing the interstitial spaces of coarse-grained willemite crystals. Sparry calcite I (Fig. 5.3) frequently fills remaining fissures in massive, red willemite from Abenab West that follow the same strain direction (Fig. 5.4g).

5.3.2 Sample preparation and Rb-Sr isotope analysis

The willemite specimens from Berg Aukas and Abenab West selected for analysis required different approaches for the sample preparation. Concentrates of coarse-grained, crystallised willemite were extracted from several domains of the two analyzed Berg Aukas samples in order to trace possible small-scale variations in the Rb-Sr system. These subsamples were then sieved to 40 to 60 mesh size fractions, cleaned with deionised water (DW) and carefully handpicked under a binocular microscope. Furthermore, we produced a concentrate of clay minerals from the dolomitic-clayey matrix observed in Berg Aukas sample NA.R04681 for separate Rb-Sr analysis by handpicking, suspecting that these clays may have possibly formed coevally with willemite from the same fluids. Samples of massive, fine-grained willemite from Abenab West were crushed, sieved to <1mm size and cleaned with DW. Fragments of red, massive willemite ore with no visible impurities were then handpicked from these separates. All separates were then leached with 1 N HCl for 10 min. to remove possible carbonate contaminants (calcite, smithsonite), and repeatedly washed with DW prior to Rb-Sr analysis. After drying, sample amounts of 10 to 50 mg were weighed into Teflon screw-top vials and completely dissolved in 22 N HF on a hot plate at ca. 120°C. For comparison, an aliquot of Abenab West sample AW 2003-1/I (massive, fine-grained willemite) was treated with 6 N HCl in order to selectively dissolve the willemite phase and separate it from possible submicroscopic impurities.

All solutions were totally spiked with a highly enriched, mixed 87Rb-84Sr tracer that allows for determination of Sr concentrations by isotopic dilution and $^{87}Sr/^{86}Sr$ ratios from one mass-spectrometric run. Rubidium and strontium were chemically separated and purified with 3 N HNO3 using EICHROM Sr resin on 50 µl Teflon columns, following the methods of Horwitz et al. (1991b). Sr was stripped from the columns with 1 ml of DW. For mass spectrometry, Sr was loaded with TaCl5-HF-H3PO4 solution (Birck, 1986) onto W single filaments. Rb was loaded with DW onto the evaporation ribbon of a Ta double-filament assemblage. All Rb and Sr isotopic measurements were performed on a six-collector FINNIGAN MAT 261 solid-source mass spectrometer running in static multicollection mode. Sr isotopic ratios were normalised to $^{88}Sr/^{86}Sr = 0.1194$. Repeated static measurements of the NBS 987 standard over the duration of this study yielded an average $^{87}Sr/^{86}Sr$ ratio of 0.71025 ± 4 (2σ mean, n = 13). Rb isotope ratios were externally corrected for mass fractionation by normalization to replicate analyses of unspiked, natural Rb (the $^{85}Rb/^{87}Rb$ ratio of which was taken to be 2.59265) separated from whole-rock samples (n = 9). The reproducibilities of $^{87}Sr/^{86}Sr$ and $^{87}Rb/^{86}Sr$ ratios obtained from standard measurements and replicate runs amounted to 0.004 % (2σ) and 1.3 % (2σ), respectively. Total procedure blanks did not exceed 30 pg for Sr and 2 pg for Rb, and were found to be negligible with respect to the sample weights.

Linear regressions according to the isochron model were calculated after Ludwig (2001) using the ISOPLOT/Ex version 2.49 program. All isochron regressions are based on individual analytical errors. The goodness of fit has been tested by means of the MSWD parameter, according to Wendt and Carl (1991). The decay constant used for the age calculations was λ87Rb = 1.42 x 10-11 a-1 (Steiger and Jäger, 1977) and errors on the model ages are quoted at the 2σ level.

Sample	Sample Weight [mg]	Rb [ppm] ± 2σ	Sr [ppm] ± 2σ	87Rb/86Sr ± 2σ	87Sr/86Sr ± 2σ
BERG AUKAS					
BA 2003-4 domain 1	12.2	0.582 ± 0.006	1.977 ± 0.80	0.853 ± 0.011	0.71692 ± 0.00003
BA 2003-4 domain 2	15.4	0.368 ± 0.004	2.433 ± 0.025	0.438 ± 0.004	0.71401 ± 0.00002
BA 2003-4 domain 3	11.4	0.132 ± 0.001	2.382 ± 0.022	0.161 ± 0.001	0.71200 ± 0.00002
NA.R04681 domain 1	13.7	0.111 ± 0.001	0.653 ± 0.007	0.492 ± 0.005	0.71723 ± 0.00004
NA.R04681 domain 2	18.8	0.185 ± 0.001	0.645 ± 0.003	0.828 ± 0.009	0.71954 ± 0.00002
NA.R04681 Clay mineral separate	10.2	16.49 ± 0.12	4.250 ± 0.031	11.317 ± 0.041	0.79321 ± 0.00005
ABENAB WEST					
AW 2003-1/I	44.2	8.883 ± 0.12	0.743 ± 0.008	35.57 ± 0.42	0.99762 ± 0.00008
AW 2003-1/I 6 N HCl leachate	15.6	1.499 ± 0.016	1.058 ± 0.009	4.11 ± 0.05	0.73894 ± 0.00006
AW 2003-1/II	31.2	1.232 ± 0.012	0.786 ± 0.008	4.55 ± 0.07	0.74531 ± 0.00004

Table 5.1: Rb-Sr data for willemite samples and related material from the Berg Aukas and Abenab West deposits, Otavi Mountainland (Namibia).

5.4 Results and interpretation

Rb-Sr analytical data for 8 willemite samples and the one sample of clay minerals separated from the matrix of Berg Aukas sample NA.R04681 are given in Table 5.1. The willemite samples display variable Rb-Sr isotopic ratios, with $^{87}Rb/^{86}Sr$ = 0.16 to 35.6 and $^{87}Sr/^{86}Sr$ = 0.71200 to 0.99762. The Rb and Sr elemental concentrations are generally low (Rb = 0.1 to 8.9 ppm, Sr = 0.64 to 4.25 ppm). The clay mineral concentrate of sample NA.R04681 has a relatively high $^{87}Rb/^{86}Sr$ ratio (11.317) and radiogenic Sr ($^{87}Sr/^{86}Sr$ = 0.79321), as can be expected for this type of material. The HF-dissolved aliquot of AW 2003-1/I has the highest $^{87}Rb/^{86}Sr$ ratio (35.57) and radiogenic Sr ($^{87}Sr/^{86}Sr$ = 0.99762) of the entire sample suite. As this could be due to contamination e.g., by detrital, submicroscopic mica with high Rb/Sr and $^{87}Sr/^{86}Sr$ we have treated a quantity of the same sample with 6 N HCl in order to selectively dissolve the willemite portion (cf. Ramdohr, 1954; Clauer at al., 1993; Clauer and Chaudhuri, 1995). This leaching produced a dark yellow solution but no discernible residue. Both the $^{87}Rb/^{86}Sr$ and $^{87}Sr/^{86}Sr$ ratios of the HCl leachate are significantly lower than those of the corresponding HF-dissolved sample (Table 5.1). Since we observed neither possible contaminating mineral phases in thin section that could be responsible for the high Rb-Sr isotopic ratios nor any undissolved material after the leaching experiment, we are currently unable to explain the discrepancy in the analytical results for sample AW 2003-1/I. However, the second analyzed, HF-dissolved willemite sample from Abenab West, AW 2003-1/II, has $^{87}Rb/^{86}Sr$ and $^{87}Sr/^{86}Sr$ ratios that

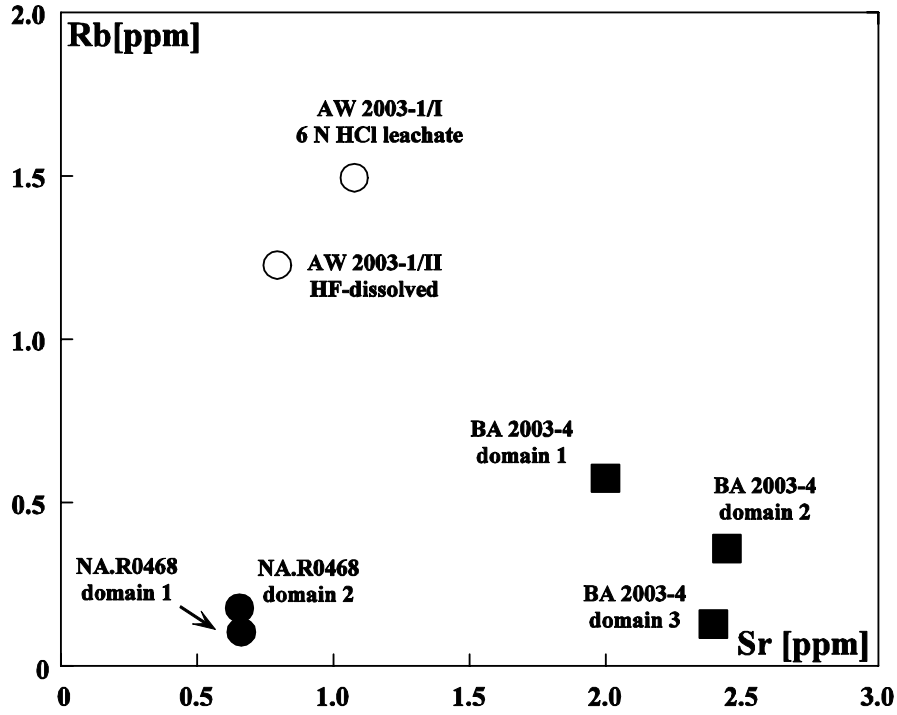

Fig. 5.5 Rb [ppm] vs. Sr [ppm] variation diagram for willemite samples from Berg Aukas and Abenab West.

are nearly identical to those of the AW 2003-1/I HCl leachate. This may indicate that the Rb-Sr results of these analyses are more representative for massive willemite from Abenab West than those of the HF-dissolved aliquot of sample AW 2003-1/I.

Figure 5.5 shows a Rb vs. Sr diagram for the analyzed willemites samples, with those from Abenab West having the highest Rb concentrations. Berg Aukas willemites are similar in their Rb contents but the trace Sr in willemite analyzed from sample NA.R04681 is significantly lower than that of BA 2003-4 willemite samples, remaining at the ppb level. Willemite concentrates extracted from three different domains of sample BA 2003-4 from Berg Aukas have Sr concentrations in a relatively narrow range from 1.97 to 2.43 ppm whereas Rb shows more variation (0.13 to 0.58 ppm). This results in variable $^{87}Rb/^{86}Sr$ ratios between 0.16 and 0.85. Willemites obtained from two domains of Berg Aukas sample NA.R04681 are comparable to the analyses of sample BA 2003-4 in their Rb-Sr characteristics, but display more limited ranges in both their Rb-Sr isotopic ratios and Rb and Sr elemental concentrations. These discrepancies in the Rb and Sr elemental concentrations may indicate the presence of different willemite generations or geochemically distinct fluids that were involved in mineralisation.

In a $^{87}Sr/^{86}Sr$ vs. $^{87}Rb/^{86}Sr$ diagram (Fig. 5.6), all Berg Aukas and Abenab West samples are correlated along a straight line (R = 0.999) with a slope corresponding to a Rb-Sr isochron model age of 561 ± 20 Ma, implying an initial $^{87}Sr/^{86}Sr$ ratio of ca. 0.71. However, a high MSWD value of 1979 for the regression indicates considerable excess scatter of the data points which cannot be explained by the analytical errors alone. In the $^{87}Sr/^{86}Sr$ vs. $1/^{86}Sr$ space (not shown) no systematic data arrangement is observed which indicates that binary mixing can be excluded. Also, time-integrated paleomixing calculations according to Schneider et al. (2003) yielded no interpretable results. Therefore, the line in Fig. 5.6 could represent a disturbed "errorchron" the scatter of which may result e.g., from post-formational alteration processes. Isochron regression excluding sample AW 2003-1/I (HF-dissolved) yields a model age of 503 ± 27 Ma (MSWD = 2298). The Abenab West samples (n = 3) alone give 574 ± 84 Ma (MSWD = 60, not shown). However, all these isochron regressions are statistically meaningless and their geochronological significance therefore remains doubtful.

Figure 5.7 shows a $^{87}Sr/^{86}Sr$ vs. $^{87}Rb/^{86}Sr$ correlation diagram for the Berg Aukas samples. Isochron regression for willemite separates from the three different domains of sample BA 2003-4 yields

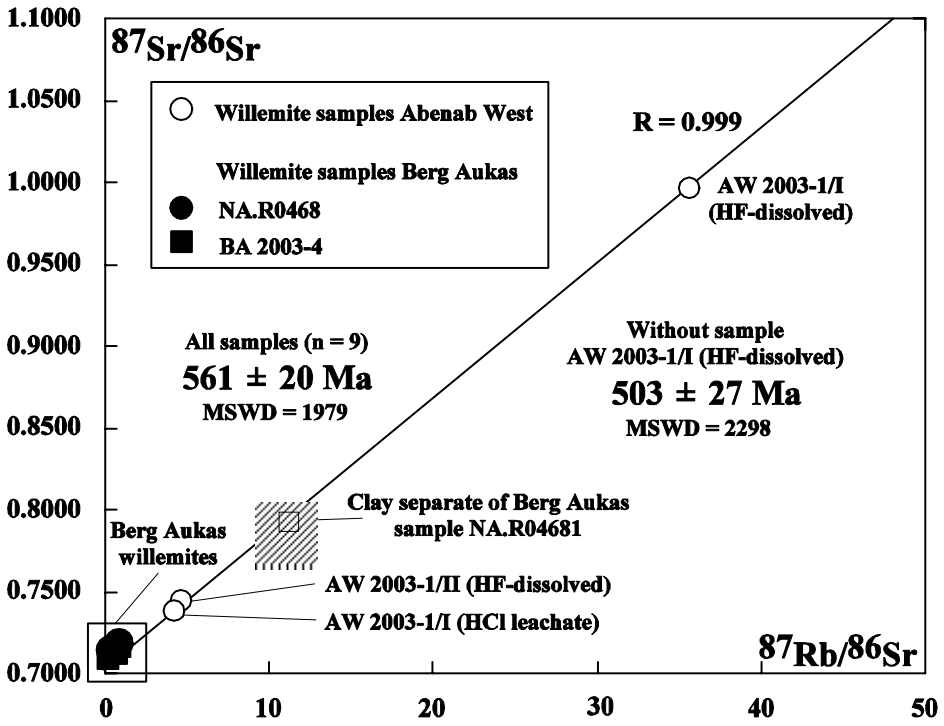

Fig. 5.6 $^{87}Sr/^{86}Sr$ vs. $^{87}Rb/^{86}Sr$ correlation diagram displaying all analyzed samples from Berg Aukas and Abenab West.

499 ± 63 Ma (MSWD = 2.6) whereas two willemite separates and the clay mineral sample extracted from NA.RO468 give 493 ± 2 Ma (MSWD = 1.2). The good correlation and statistically robust regression for NA.RO468 sample separates may indicate that willemite and its associated clays are coprecipitates of the same ore-forming fluid, implying a non-detrital origin of these clays. However, this is currently not supported by independent mineralogical and geochemical evidence. Excluding the clay sample, a two-point age of 483 ± 17 Ma is obtained from the two willemite separates of sample NA.RO468 alone (Fig. 5.7). Nevertheless, the ages calculated for Berg Aukas samples all agree within error and are also compatible with the "errorchron" age of 503 ± 27 Ma (Abenab sample AW 2003-1/I HF-dissolved excluded) displayed in Fig. 5.6. Figure 5.7 may be interpreted to reflect two parallel, internal small-scale isochrons for samples NA.RO468 and BA 2003-4. Consequently, the distinct initial $^{87}Sr/^{86}Sr$ ratios reflected by these isochrons (0.7138 and 0.7109) imply a coeval formation of willemite at Berg Aukas ca. 480-500 Ma ago involving fluids that had interacted with distinct Sr sources. This interpretation is also supported by the difference in the Sr content of sample NA.RO468 willemite separates (ca. 0.65 ppm) and those of sample BA 2003-4 (ca. 1.9-2.4 ppm, Table 5.1, Fig. 5.5).

5.5 Discussion

5.5.1 The Rb-Sr system in willemite

Our Rb-Sr data (Table 5.1) for willemite from nonsulphide deposits in the OML reflect generally low Rb and Sr elemental concentrations that barely exceed ppb- to lower ppm levels. Moreover, the variation of $^{87}Rb/^{86}Sr$ in willemite appears to be significant, but is limited to values <1 for most samples. The higher $^{87}Rb/^{86}Sr$ ratios of about 4 observed for two samples from Abenab West may still be representative for the willemite phase, whereas the very high $^{87}Rb/^{86}Sr$ value of ca. 35 for the HF-dissolved sample AW 2003-1/I seems unrealistic in the light of the other data and has yet to be explained. Overall, the Rb-Sr system in willemite shows characteristics comparable to that in sphalerite. Rb-Sr dating of sphalerite has been successfully used to directly determine the age of sulphide mineralisation and to constrain models of large-scale migration of mineralizing fluids in a number of studies (e.g., Nakai et al., 1990, 1993; Brannon et al., 1992; Christensen et al., 1995a, b; and references therein). These ages were based on Rb-Sr isochrons that, with a few exceptions (Christensen et al., 1995a; Schneider et al., 2002), displayed a limited

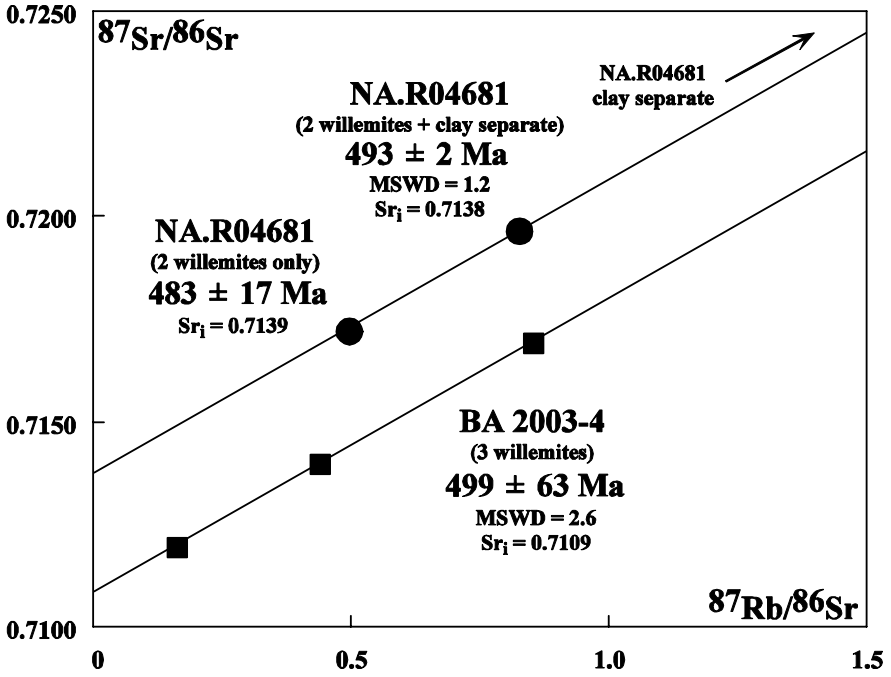

Fig. 5.7 $^{87}Sr/^{86}Sr$ vs. $^{87}Rb/^{86}Sr$ correlation diagram for willemite samples from Berg Aukas.

variation of $^{87}Rb/^{86}Sr$ ratios between 0 and 1 to 2, as we have observed for willemite in this study. Moreover, Rb and Sr concentrations of sphalerite are exactly in the same range (ppb- to lower ppm levels, see references above) as those of most of our analyzed willemite samples. Although sphalerite appears to yield meaningful Rb-Sr ages and the partitioning mechanisms of Rb and Sr between parent fluid and host sphalerite phases were examined in detail by Pettke and Diamond (1996), the siting of trace Rb and Sr and the factors controlling Rb/Sr fractionation in sphalerite remain speculative (Nakai et al., 1990; Halliday et al., 1991). Given the similar range of observed $^{87}Rb/^{86}Sr$ and Rb and Sr elemental concentration levels, the same questions arise in the case of willemite. Nakai et al. (1993) and Christensen et al. (1995a) envisaged kinetic effects during sphalerite growth and suggested that rapidly precipitated sphalerite may preferentially incorporate "exotic" elements such as Rb, which are a priori not compatible with the crystal structure of sphalerite. Conversely, Pettke and Diamond (1996) suggested trapping of Rb and Sr in crystal defects and interstitial octahedral voids of the sphalerite structure and explained the relative, preferential incorporation of Rb over Sr by charge-coupled substitution of two divalent Zn atoms by monovalent Rb plus a trivalent element (e.g., Fe2+-Fe3+), the availability of the latter being possibly controlled by the fluid oxidation potential. All these effects may also account for the currently poorly understood behaviour of Rb and Sr in willemite, which requires further systematic investigation of the Rb-Sr system in this mineral. However, this may be limited by the often complex nature of willemite-bearing nonsulphide mineralisation (see Fig. 5.4) which is commonly characterised by several, possibly non-cogenetic willemite generations as well as mineral assemblages formed by supergene alteration processes that may affect and disturb the Rb-Sr system of earlier hypogene-hydrothermal nonsulphides.

5.5.2 Methodological reliability of the Rb-Sr ages

The Rb-Sr isochron model ages obtained in this study using different combinations of willemite samples are all in the range of ca. 480 to 580 Ma. It is obvious from Fig. 5.5 that isochron regressions of the entire data set, i.e. including both the samples from Berg Aukas and Abenab West, are statistically insignificant (high- to very high MSDW values of up to 2300), even when several possible "outliers" are excluded. Therefore, combining samples from Berg Aukas and Abenab to obtain a common Rb-Sr age seems unrealistic. A three-point isochron regression for the Abenab West samples (n = 3) alone has a greatly reduced MSWD of 60 but (i) this value is still

statistically meaningless, and (ii) the resulting model isochron is dominated by the very high $^{87}Rb/^{86}Sr$ and $^{87}Sr/^{86}Sr$ ratios of sample AW 2003-1/I (HF-dissolved). It remains very questionable whether these high isotopic ratios are held in the willemite phase of this sample or result from submicroscopic impurities (e.g., detrital mica with high Rb/Sr). Considering the results from the leaching experiment performed on the same sample, the latter option appears to be more plausible. However, even the moderate $^{87}Rb/^{86}Sr$ ratios of about 4 obtained from the 6 N HCl leachate of sample AW 2003-1/I and the HF-dissolved, second sample AW 2003-1/II are sufficiently high to generate radiogenic Sr over time. Therefore, massive, red willemite from Abenab West could be further evaluated successfully as a Rb-Sr geochronometer. However, this will be compromised by the overall fine-grained texture of the samples and the possible presence of intergrown contaminants that may disturb the Rb-Sr system in the willemite phase. In this sense, the Rb-Sr age of about 570 Ma obtained in this study for Abenab West may serve only as a first approximation to the maximum age of this willemite mineralisation.

Some more reliable age information may be derived from statistically significant small-scale internal model isochrons defined by coarse-grained yellow willemites from the two Berg Aukas samples BA 2003-4 and NA.RO468 (Fig. 5.6). The well-crystallised Berg Aukas willemites, from which pure separates could be easily produced, have much lower $^{87}Rb/^{86}Sr$ ratios than the massive ones from Abenab West, but isochron regressions for Berg Aukas samples agree within error at an age of about 500 Ma. In terms of precision and statistical significance, the Rb-Sr age of 493 ± 2 Ma derived from the three-point isochron (MSDW = 1.2) defined by willemite from two domains of sample NA.RO468 and associated clay minerals is currently our best estimate for the age of nonsulphide mineralisation at Berg Aukas, provided that the clays are cogenetic with willemite. However, in the absence of independent proof for this assumption, it is currently more plausible to report ages for the willemite phase only. Excluding the NA.RO468 clay sample, which has high Rb/Sr and $^{87}Sr/^{86}Sr$ ratios and therefore dominates the regression, a two-point isochron calculation for the NA.RO468 willemite samples alone yields an age of 483 ± 17 Ma, which is still consistent with the other age calculations for Berg Aukas samples.

5.5.3 Geological significance of the Rb-Sr ages

It has to be emphasised here that all our isochron regressions presented above, even the ones that are statistically adequate in terms of MSWD, are based on two or three data points only. This may cast doubts on their geochronological significance. However, whether our Rb-Sr ages reflect accurate mineralisation ages for willemite or not can also be evaluated by comparison with other dated geological events that have affected the study area. Ages for willemite mineralisation at Abenab West in the range of 500 to 570 Ma could be related to early Mulden karst phenomena and/or hydrothermal fluid flow during D2 deformation and metamorphism (e.g., Clauer and Kröner, 1979; Miller, 1983a), whereas an even older age of about 570 Ma could point to a formation of the Abenab nonsulphide deposit during the first Pan-African metamorphic phase D1 (Clauer and Kröner, 1979; Haack et al., 1980; 1988). This, however, would conflict with the observation that willemite precipitation at Abenab West appears to postdate major, D2-related structural elements (see section 2.4.).

Ages of ca. 480 to 500 Ma for the Berg Aukas deposit would be consistent with the waning stages of the Pan-African orogeny and uplift phase (e.g., Haack 1976). Blaxland et al. (1979) and Haack et al. (1980) have presented Rb-Sr ages in the range of 480 to 520 Ma for late-tectonic granitic rocks from the central, intracratonic branch of the Damara Orogen, south of the OML. Some mineral and combined mineral-whole-rock isochrons for these granites yielded Rb-Sr ages of 495 ± 3 Ma, 505 ± 5 Ma and 484 ± 9 Ma. Ahrendt et al. (1978) presented a K-Ar isochron age of 495 ± 10 Ma for the emplacement of the Naukluft nappes at the southern margin of the Damara Belt. These ages are all in perfect agreement with our Rb-Sr ages for the Berg Aukas willemite mineralisation. In this scenario, the same tectonothermal processes that were responsible for the emplacement of late granitic plutons and nappe complexes in the Damara Orogen may have triggered the circulation of mineralizing hydrothermal fluids in the OML further north. These events would also be coeval with a low-grade metamorphic overprint of Mulden group pelites in the OML ca. 460 to 500 Ma ago, as proposed by Clauer and Kröner (1979) on the basis of Rb-Sr and K-Ar ages for clay fractions <2 µm, which they assigned to a third D3 tectonometamorphic episode in the Damara Orogen.

If the timing of willemite mineralisation at Abenab

and Berg Aukas can be plausibly linked to the tectonothermal evolution of the Damara Belt, then this may indicate an overprint of primary Zn-Pb sulphides by hypogene-hydrothermal nonsulphide ores rather than a typical supergene alteration of pre-existing sulphides due to weathering processes. This would imply that associated primary sulphide ores must be even older. The absolute timing of primary base metal sulphide mineralisation in the OML is, however, not well constrained. Many age estimates are based on galena Pb-Pb model ages (e.g., Allsopp et al., 1981; Hughes, 1987; Kamona et al., 1999; see also Innes and Chaplin, 1986; Lombaard et al., 1986) which are insignificant for geochronological interpretations (e.g., Haack, 1993; Frimmel et al., 2004). A maximum age for "Tsumeb-type" deposits is given by mineralised, feldspathic arenites occurring within the pipe-like Tsumeb and Kombat orebodies, which have been interpreted to represent karst fills derived from the clastic Mulden Group (ca. 570 to 530 Ma; Lombaard et al., 1986; Frimmel et al., 1996a, 2004). Melcher et al. (2003) reported an age of 527 Ma for Tsumeb based on preliminary Re-Os analyses of Ge-rich sulphide ores. In the absence of better isotopic age constraints, most authors agree that "Tsumeb-type" sulphide mineralisation formed syntectonically from orogenic fluids expelled during D2 deformation (e.g., Innes and Chaplin, 1986; Frimmel et al., 1996a, 2004; cf. Fig. 5.2). In contrast, a much earlier, synsedimentary-syndiagenetic formation (maximum 750 Ma) of the stratabound Berg Aukas sulphide ores from basinal brines in an extensional setting has been favoured by Frimmel et al. (1996a, 2004). Overall, the current age interpretation of primary sulphide mineralisation in the OML does not conflict with the mostly younger Rb-Sr ages of 480 to 500 Ma obtained for willemite from OML nonsulphide deposits in this study. Even a hypothetical maximum age of ca. 560 to 570 Ma for the virtually sulphide-free Abenab deposit may still be interpreted to reflect a possible coeval formation of sulphide and some nonsulphide base metal deposits in different areas of the OML. At Berg Aukas, distinct fluid systems of possibly small scale that had interacted with different Sr sources were most likely involved in willemite mineralisation, as indicated by the contrasting initial $^{87}Sr/^{86}Sr$ ratios of the Rb-Sr isochrons obtained for samples NA.RO468 and BA 2003-4 (Fig. 5.7). The latter may be explained by differential contamination of the ore-forming fluids by Sr derived from the carbonate host rocks of mineralisation. Since the initial $^{87}Sr/^{86}Sr$ ratios (0.7109 and 0.7138, respectively) reflected by the Berg Aukas small-scale Rb-Sr isochrons are significantly more radiogenic than contemporaneous Neoproterozoic seawater ($^{87}Sr/^{86}Sr$ = 0.7068 to 0.7088; e.g., Derry et al., 1992; Jacobsen and Kaufman, 1999; Yoshioka et al., 2003), a major input of pristine Sr derived from the Abenab Group host carbonates can be excluded. However, Frimmel et al. (1996a) described distinct textural types of dolomite cements from the Berg Aukas deposit, characterised by a systematic increase in $^{87}Sr/^{86}Sr$ from least-altered, fine-grained dolomite I ($^{87}Sr/^{86}Sr$ = 0.7078 to 0.7104) to late to post-mineralisation stage, sparry dolomite IV ($^{87}Sr/^{86}Sr$ = 0.7137 to 0.7174). Primary sulphides at Berg Aukas are associated with medium to coarse-grained dolomite III, the $^{87}Sr/^{86}Sr$ ratios of which vary between 0.7095 and 0.7138. The $^{87}Sr/^{86}Sr$ ratios of dolomite IV were found to correlate systematically with the Sr contents, reflecting differential binary mixing between the pre-existing dolomite generation III and a fluid enriched in radiogenic Sr. The observed, wide range in $^{87}Sr/^{86}Sr$ of epigenetic dolomite cements from the Berg Aukas deposit is mirrored by the differing initial $^{87}Sr/^{86}Sr$ ratios of the small-scale Rb-Sr isochrons obtained in this study for Berg Aukas willemites. Therefore, these can be plausibly explained by small-scale mobilization of Sr from certain pre-existing, preferably late-stage dolomite cements during willemite mineralisation. Alternatively, willemite and part of the dolomite cements may represent coprecipitates that have formed from the same fluid systems.

5.5.4 Timing of hypogene, economic willemite mineralisation on a global scale

The currently known, major economic willemite deposits that have been recently reinterpreted to originate from structurally controlled, hypogene-hydrothermal fluid flow are confined to the southern hemisphere and arranged along roughly the same latitude (see Fig. 5.2 in Hitzman et al., 2003). These are Vazante (Brazil), Kabwe and Star Zinc (Zambia), Berg Aukas and Abenab West (Namibia), and Beltana-Aroona (Australia). They all occur in tectonised and mostly dolomitised, Neoproterozoic carbonate successions (see Hitzman et al., 2003; and references therein), with the exception of Beltana, which has

Lower Cambrian host carbonates overlying the Neoproterozoic (Groves et al., 2003). The common Late Proterozoic to Early Cambrian age of the carbonate rocks that host this type of hypogene willemite mineralisation worldwide provide a background to place constraints on the timing of these nonsulphide deposits relative to each other. No direct radiometric age constraints are yet available for willemite mineralisation at Vazante (Brazil) and Kabwe/Star Zinc (Zambia). Monteiro et al. (2000, 2006) related the formation of sulphide ores and willemite in the Vazante district to the late stages of the Brasiliano orogeny (ca. 630 to 500 Ma). Moreover, there is some evidence for large-scale flow of mineralizing fluids in the 500 to 550 Ma range from Pb-Pb dating of Neoproterozoic carbonate rocks (520 ± 53 Ma; Babinski et al., 1999) from the Bambuí Group in the Sao Francisco Basin. The Sao Francisco Basin is closely adjacent to the external part of the Brasília orogenic belt in this area, the Vazante Group, which hosts the Vazante Zn deposits. Based on structural relationships, Kamona and Friedrich (1994) interpreted the Zn-Pb mineralisation at Kabwe to have occurred prior to the last deformational phase of the Lufilian orogeny (ca. 650 to 500 Ma), which would be in the same age range. Groves et al. (2003) proposed a younger, early Silurian age of about 435 Ma for the formation of the Beltana-Aroona willemite deposits in the Adelaide basin in the northern Flinders Ranges (Australia) from K-Ar dating of coronadite ($MnPbMn_6O_{14}$). They related this mineralisation age to a period of exhumation following the Delamerian orogeny (523 to 490 Ma). However, coronadite is one of the late phases in the paragenetic sequence (see Groves et al., 2003) and may therefore significantly postdate the economic willemite stage at Beltana. Furthermore, exhumation processes are more likely to produce supergene mineralisations - including minerals like coronadite - from enhanced weathering of pre-existing sulphides and nonsulphides (Boni and Large, 2003). Therefore, it appears to be plausible that the formation of hypogene willemite mineralisation in the Beltana-Aroona area may also be related to a distinct, but yet unknown period of hydrothermal fluid flow during the Delamerian orogeny at 523 to 490 Ma.

In the absence of direct radiometric ages for willemite, the existing evidence for the timing of epigenetic, hypogene willemite deposits at Vazante, Kabwe and Beltana may indicate mineralisation events in the range of ca. 490 to 550 Ma. This would be in good agreement with the first Rb-Sr ages obtained directly for willemite from the Abenab West and Berg Aukas deposits (Namibia) in this study.

5.6 Conclusions

In this pilot study, the zinc silicate willemite has been evaluated by means of its Rb-Sr characteristics and suitability as a Rb-Sr geochronometer for the first time. Even though we are currently unable to present statistically well-supported ages for suites exceeding 2-3 samples, our study clearly demonstrates that willemite appears to be suitable for Rb-Sr geochronometry and direct dating of nonsulphide Zn-Pb mineralisation. Willemite may display significant, albeit limited, variation in Rb/Sr, sufficient to define Rb-Sr isochrons. The Rb-Sr system in willemite shows striking similarities to that in sphalerite, which in several studies has been already successfully used as a Rb-Sr geochronometer for directly dating sulphide deposits. The comparable Rb and Sr concentration levels and $^{87}Rb/^{86}Sr$ ranges observed in willemite and sphalerite suggest that the partitioning of trace Rb and Sr into hydrothermal zinc ore minerals may be largely independent from the pH and oxidation potential of the mineralizing fluids. Therefore, it is unlikely that a differential availability of trivalent cations, controlled by the fluid oxidation potential, for the coupled substitution $M^{3+} + Rb^{+} \leftrightarrow 2\ Zn^{2+}$ (Pettke and Diamond, 1996) can explain the variability of Rb in hydrothermal zinc minerals. Instead, other mechanisms have to be invoked that may be capable of generating $^{87}Rb/^{86}Sr$ variations in both sulphide and nonsulphide zinc ores that precipitate from reduced and oxidised hydrothermal fluids, respectively. This awaits further studies to better understand the Rb-Sr system in willemite and to fully evaluate its potential for Rb-Sr dating, which will be compromised, however, by the various and often complex willemite ore textures observed in nonsulphide deposits. Therefore, a careful sample selection has to be made prior to any geochronological work, favouring well-defined willemite generations that can be easily separated and purified. In other cases, leaching experiments may help to interpret Rb-Sr isotope data.

The surprisingly “old” Rb-Sr ages of 490-560 Ma obtained in our pilot study for the formation of willemite mineralisation in the OML need to be

verified and better constrained but, at first sight, appear to be geologically reasonable on a regional and a global scale. They are fully compatible with numerous published radiometric data that reflect distinct tectonothermal events in the study area. We therefore propose that the genesis of economic nonsulphide mineralisation in the OML may be strongly linked to hydrothermal sulphide-replacement processes initiated by these events rather than simply to supergene weathering of associated pre-existing sulphides. In the absence of isotopic ages obtained from willemite directly, most available data for the few other, currently known economic willemite deposits of hypogene origin in Brazil, Zambia and southern-central Australia that are hosted by Neoproterozoic to Early Cambrian carbonate rocks also suggest mineralisation ages in the range of 490 to 550 Ma. This may point to a global period of hydrothermal activity in the Cambrian to early Ordovician, under conditions that favoured the formation of nonsulphide Zn deposits. From this, the question arises why these mineralisations are restricted to areas that are now located in the southern hemisphere and why major, structurally controlled hypogene-hydrothermal willemite deposits have never been found in younger strata. Further attempts of direct dating of willemite and associated sulphides are required to resolve the timing and genesis of nonsulphide Zn mineralisation on a global scale as well as relative to the age of their host rocks and possible pre-existing sulphide ores.

Acknowledgements

We are grateful to R. Frei and F. Melcher for providing thoughtful reviews that significantly helped us to improve the manuscript and figures. The invaluable support of H.A. Gilg is acknowledged with gratitude. U. Haack is thanked for giving access to the cleanlab and TIMS facilities of the University of Giessen (Germany).

Part 6: Vanadate ores in the Otavi Mountainland (Namibia): geological setting, mineralogy, geochemistry, formation timing and relation with the "African Erosion Cycle"

Abstract

The Zn-Cu-Pb vanadate ores (descloizite, mottramite and vanadinite) in the Proterozoic dolomites of the Otavi Mountainland (OML) were considered the greatest vanadium deposits in the world, with resources estimated at several Mt of V ore. The deposits, now mostly exhausted, occurred in collapse breccias and solution cavities related to a karstic network, deep in the carbonates of the Otavi Group. Despite the past economic importance, the genesis of the vanadate ores in the OML is still controversial. However, because they were associated with oxidised sulphide ores, a supergene origin was generally accepted.

Here we present the geological setting of the main deposits, ore mineralogy and petrography, major and trace element geochemistry of the vanadate ore minerals and gangue carbonates, along with fluid inclusion microthermometry, O, C, Sr, and Pb isotope analyses and direct U-Th/He thermochronometry of descloizite. Our results indicate that most vanadate deposits were formed at temperatures of ~40 to 50°C by meteoric waters interacting with Proterozoic shales, carbonates and Pan-African orogeny-related primary sulphide ores, which were subject to multiple weathering phenomena in a karst environment. Minor contribution of vanadium and metals from Paleoproterozoic basement rocks cannot be excluded. The age of most deposits appears to be confined to the Tertiary, with descloizite formation dated at 26-29 Ma.

The OML V-deposits represent a special low-temperature, arid-weathering related nonsulphide ore type, also fairly widespread in other areas of southern Africa (Zambia, Angola). They are genetically related to the most important erosional episodes of the "African Cycle", controlled by the tectono-morphological evolution after Atlantic rifting spanning the period from the end of Cretaceous to Pleistocene.

6.1 Introduction

The element vanadium (V) occurs in more than 60 different minerals. The majority of these (carnotite, descloizite-mottramite, patronite, roscoelite and vanadinite) are considered to be of secondary origin, formed by oxidation and/or weathering of primary vanadium sources. These sources are usually found in basic and ultrabasic igneous rocks, carbonatite complexes, titaniferous magnetite complexes (V-rich magnetite ores) and chromite, uranium, iron and manganese deposits. Vanadium also occurs in black shales and phosphatic rocks and can be associated with uranium in sandstones and calcretes. It is present in coal and crude oils in organic complexes and commercial production from petroleum ash holds promise as an important source of the element. Vanadium is an important carbide stabiliser in making steels and for this reason 80% of the vanadium now produced is used as ferrovanadium or as an additive in high strength steels. Another use is in the production of aerospace titanium alloys.

Most of the vanadium-bearing ores in the United States occur in Arkansas, Colorado, and Idaho (associated with sandstone uranium), while other abundant sources include Canada, South Africa (Bushveld Complex), Chile and Australia. Among the newly discovered deposits, an estimated 60 M tonn of reserves (currently increasing) @ 0.73 V_2O_5 in form of ferrovanadium ore has recently been reported by Aurox Resources at Balla Balla in Western Australia (Aurox Resources Ltd., 2006). Another economically promising resource is represented by the Langer Heinrich uranium mine in Southern Namibia, going into production in 2006 (Paladin Resources Ltd., 2006) and contained in Tertiary fluviatile sediments and calcretes of the Naukluft-Namib region. At Langer Heinrich, vanadium pentoxide (used in ceramics, as a catalyst, and to produce superconductive magnets) produced from carnotite $K_2(UO_2)_2(VO_4)_2 \cdot 3H_2O$, is a valuable by-product (1-2% V) of the U ore (Wartha and Schreuder, 1992).

Since the early last century, vanadium occurrences have been known to exist in the northern areas of the Otavi Mountainland (OML), Namibia. Mining for vanadium, secondary to the exploitation of base metal ores, started here in 1920, with increasing production

from 1943 to 1960 (Wartha and Schreuder, 1992). The OML deposits represent a special type of low-temperature nonsulphide ore, also fairly widespread in several other areas of Southern Africa such as Zambia (Pelletier, 1930; Taylor, 1954; Kamona and Friedrich, 1994) and Angola (Millman, 1960). Mottramite was the first vanadium mineral recognised in the Tsumeb orebody (OML) by W. Maucher in 1908, but the first complete geological and mineralogical descriptions of the vanadium ores in the OML were given by Schneiderhöhn (1929) and Diefenbach (1930). Since then, a considerable number of deposits, some of great economic significance (Berg Aukas, Abenab, Tsumeb West and Baltika), have been described throughout the OML (Schwellnus, 1946; Misiewicz, 1988; Verwoerd, 1957; Van der Westhuizen, 1984 etc.). Due to the fact that the last producing vanadium mine was abandoned in 1978, very little geological and geochemical investigation of this mineralisation type has been performed utilizing modern methods. In the better known deposits located in the Neoproterozoic carbonates of the OML, vanadium occurs in the form of vanadinite [$Pb_5(VO_4)_3Cl$] or, more often, as Pb-Zn-Cu-vanadates belonging to the descloizite-mottramite series [$PbZn(VO_4)(OH)$ - $PbCu(VO_4)(OH)$], in which vanadium occurs in the +5 oxidation state.

Most vanadium concentrations are peripheral to, or in close contact with, primary sulphide deposits, as well as with complex other Zn-Pb nonsulphide assemblages, containing both the Zn-silicate willemite and a great number of metal carbonates-sulphates related to the oxidation of sulphide ores. This led to the conclusion that the vanadium mineralisation in the OML was also supergene in origin, having formed during the same weathering processes that produced the ample variety of nonsulphide minerals occurring in the oxidation zone of the main ore occurrences (cfr. Tsumeb: Keller, 1984; Berg Aukas: Cairncross, 1997 etc.). At the same time, most authors realised that the V-rich bodies did not form at the same time as the sulphides, but rather accumulated as secondary minerals in vein and karst environments produced after the Pan-African orogeny (Miller, 1983a). Vanadium ores are quite distinct from other nonsulphide concentrations with respect to their specific mineralogy, position in the mineral paragenesis of the OML, and their siting, which appears to be always slightly detached from that of other nonsulphide bodies (Misiewicz, 1988; Part 5). Estimates of the provenance of such a high quantity of vanadium, as well as on the timing of mineralisation vary greatly. More cautious workers like Misiewicz (1988) quote only a post-Damaran genesis, while others have indicated a broad Mesozoic to Tertiary interval for ore emplacement. Verwoerd (1957) recognised that the vanadium mineralisation occurred substantially later than sulphide emplacement and that it was related to karst filling. Van der Westhuizen (1984) favoured a Tertiary age based on geomorphological evidence and the absence of Karoo sediments together with vanadium ores in the karst fills. Later, Van der Westhuizen et al. (1989) suggested that the vanadium mineralisation was related to Quaternary karstification episodes. Pickford (1993), on the basis of paleontological evidence (mammalian bones encrusted by vanadates in karst filling deposits), considered the vanadium ores to have precipitated during several distinct phases spanning in age from the middle Miocene to the Quaternary.

In this study, we present the geological setting and detailed ore mineralogy and petrography of the OML vanadates and their gangue minerals. New geochemical data, including major and minor elements content, O, C, Sr and Pb isotopes, and direct (U-Th)/He thermochronology of descloizite will help us to constrain the origin (hypogene? supergene?), precipitation mechanisms, and timing of ore formation.

6.2 Geological and geomorphological setting

The Otavi Mountainland (OML, Fig. 6.1) covers an area of about 10,000 km^2 in the northern foreland of the Damara Orogen, Namibia (Miller, 1983a). The OML lithologies comprise calcareous, dolomitic and siliciclastic rocks of the Neoproterozoic Damara Supergroup, which unconformably overlie a poorly outcropping Paleoproterozoic (Eburnean, 2.1-1.65 Ga: Miller, 1983a; Frimmel et al., 2004) basement, generally known as the Grootfontein Metamorphic Complex (GMC). The basement mainly consists of various, intensely deformed and metamorphosed alkaline and calcalkaline granites (Clifford et al., 1969), and gabbros. In the south-eastern OML, this metamorphic basement corresponds to the Grootfontein Mafic Body (GMB). The structural evolution of the OML during the Neoproterozoic started with the rifting of a small eastern branch of the Adamastor Ocean in the early Cryogenian, eventually

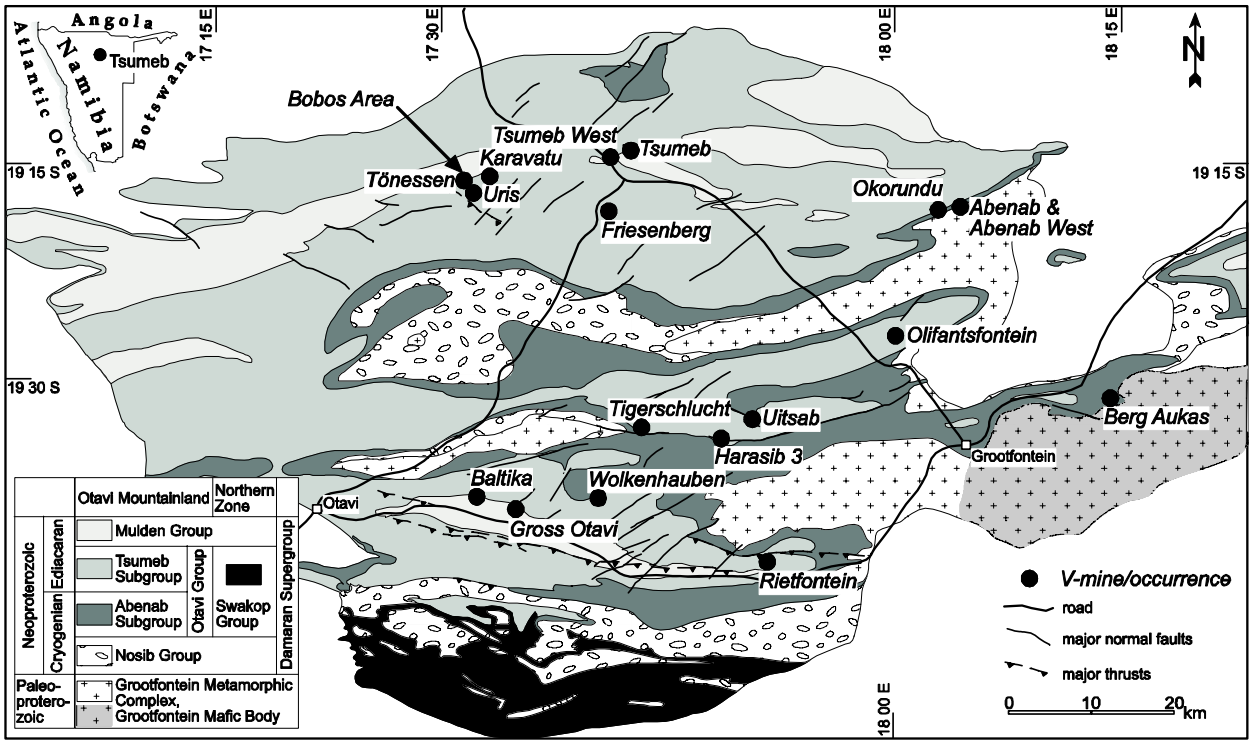

Fig. 6.1 - Geological map of the Otavi Mountainland marking the most important localities where vanadium ores have been exploited.

leading to the evolution of the Khomas Trough and of other parallel, subsidiary basins. The volcaniclastic Nosib Group (747 ± 2 Ma, U-Pb zircon age obtained for the Naauwpoort Fm, Hoffman et al., 1996) was deposited in such a horst-graben-system along ENE-trending lineaments. The Nosib Group (Fig. 6.2) is overlain by platform carbonates of the Otavi Group, which have been subdivided into the Abenab and Tsumeb Subgroups (Miller, 1983a). The age of the Otavi Group (Fig. 6.2) is poorly constrained. Frimmel et al. (2004) proposed an evolution of the carbonate platform between 746 Ma and 550 Ma. Hoffmann et al. (2004) obtained an U-Pb zircon age of 635.5 ± 1.2 Ma for the diamictites of the glaciogenic Ghaub Fm, situated at the base of the Tsumeb Subgroup. The synorogenic molasse sediments of the Mulden Group (Fig. 6.2), overlie the Tsumeb Subgroup and are also found in an extensive network of pre-Mulden paleokarst dissolution cavities.

The structural evolution of the OML during the Pan-African orogeny is characterised by three main deformational phases. D1 folding and thrusting in the southernmost part of the OML was initiated by continental convergence in the Kaoko region to the West. Following karstification of the uppermost Otavi Group and deposition of the siliciclastic (molasse-type?) Mulden Group, north-trending, partly overturned folds, a penetrative foliation and thrusts in the southern OML were generated by Pan-African collision of the Kalahari and Congo microplates (D2 after Frimmel et al., 1996a). The D2 phase was then followed by the late to post-Pan-African, mainly extensional D3 deformation (Goscombe et al., 2004). According to Kröner and Clauer (1979) the age of the metamorphic peak M1 in the Northern Platform is 535-530 Ma, whereas a late phase of regional metamorphism (M2) occurred at ca. 481-459 Ma.

Paleozoic to Mesozoic, Tertiary and Quaternary mainly siliciclastic rocks of the Karoo and Kalahari sequences (Fig. 6.3) covered the Proterozoic rocks towards the north, east and south of the OML and also the deeply eroded, E-W striking Pan-African anticlines (e.g. DWA, 2002). The thick sedimentary and volcanic rocks of the Permian to Jurassic Karoo succession, occurring primarily in the south-eastern and north-western parts of Namibia, have been extensively intruded by dolerite sills and dyke swarms. These are associated with a number of alkaline subvolcanic intrusions, but are predominantly related to effusive basaltic volcanism (e.g., the Etendeka Group) which probably extended more than 250 km inland from the recent coastline and up into the OML. The

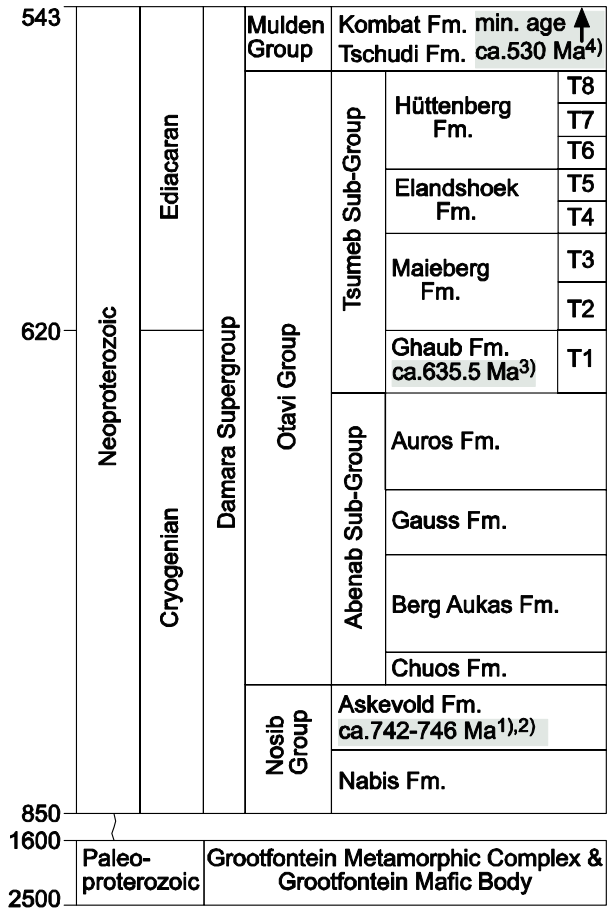

Fig. 6.2 - Tectonostratigraphic evolution and ages of the Damara Supergroup (Neoproterozoic) in the Otavi Mountainland. [1)]Burger and Coertze, [2)]Hoffman et al., 1996, [3)]Hoffmann et al., 2004, [4)]Melcher et al., 2003.

abovementioned volcanic successions marked the break-up of Gondwana and the formation of the South Atlantic Ocean beginning in the Early Cretaceous (Fig. 6.3).

In the OML there is no evidence of Karoo sediments, but small outcrops of the Etendeka volcanites (Fig. 6.3) have been locally encountered at its southern boundary (Marsh et al., 2003). In addition, some strongly weathered sills (so called "kersantites", Söhnge, 1957) of possible Cretaceous age occur in the Tsumeb mine pipe, while the younger "Tsumeb dyke swarm" has also been observed in the northernmost areas of the OML (Söhnge, 1957). Thick detrital sediments of the Kalahari Formations and calcrete soils are quite widespread in the eastern regions of the OML (King, 1951), and cover the bottom of the ample valleys, like the Otavi valley. The most frequently encountered Tertiary and Quaternary deposits in the OML are, however, the sediments, which were accumulated in karst settings (Pickford, 1993; 2000).

The present landscape of southern Africa is a product of the tectonic processes largely associated with the break-up of Gondwana (King, 1951). The other major influences since the establishment of Africa as a distinct continental block have been continuing episodes of uplift, rifting, volcanism, warping, and subsequent denudation and erosion due to the creation of new base levels. These processes are responsible for specific characteristics of present-day Namibia such as the series of broad upwarps, which in several areas run parallel to the coastline up to 200 km inland. These are flanked on their seaward side by a sharp topographic discontinuity in the form of a major escarpment (the "Great Escarpment"), separating the interior plateau from the coastal regions (Summerfield, 1996), whose maximum peneplanation, coupled by intense lateritic weathering (mainly occurring in South Africa) was reached between Late Cretaceous and Eocene (Fig. 6.3). During the Late Cretaceous, a denudation event eroded a 3 km thick section of Southern Africa and Namibia and reached several hundred km inland, well beyond the boundary of the rifted lithosphere (Gallagher and Brown, 1999). This strong denudation has been mirrored in the high terrigeneous sediment accumulation rate on the SW Africa margin during Cretaceous-Eocene time, when the climate was hot and humid ("greenhouse" period) (Rust and Summerfield, 1990). Raab et al. (2002) proposed an Early and Late Cretaceous reactivation of the pre-Pan-African lineaments (the latter due to a change in the spreading geometry of the southern Atlantic), which could have preferentially controlled the erosion belts (Fig. 6.3).

Although the major processes responsible for the macrogeomorphology of Namibia are fairly well known, the genesis and age of various local landscapes remains highly controversial (King, 1951; Partridge and Maud, 1987; Dardis and Moon, 1988; Burke, 1996). The different interpretations arise from the problems of correlating the erosion surfaces across the Great Escarpment, the difficulties inherent in determining the ages of the surfaces, and the structural control that has affected the progress of the major planations (Dardis and Moon, 1988). Another important issue of the evolution following the Gondwana break-up concerns the climate. As mentioned, a "greenhouse" climate extended over Southern Africa and Namibia during the Cretaceous and Eocene, but these hot and humid conditions did not last. One of the central paradigms of Cenozoic

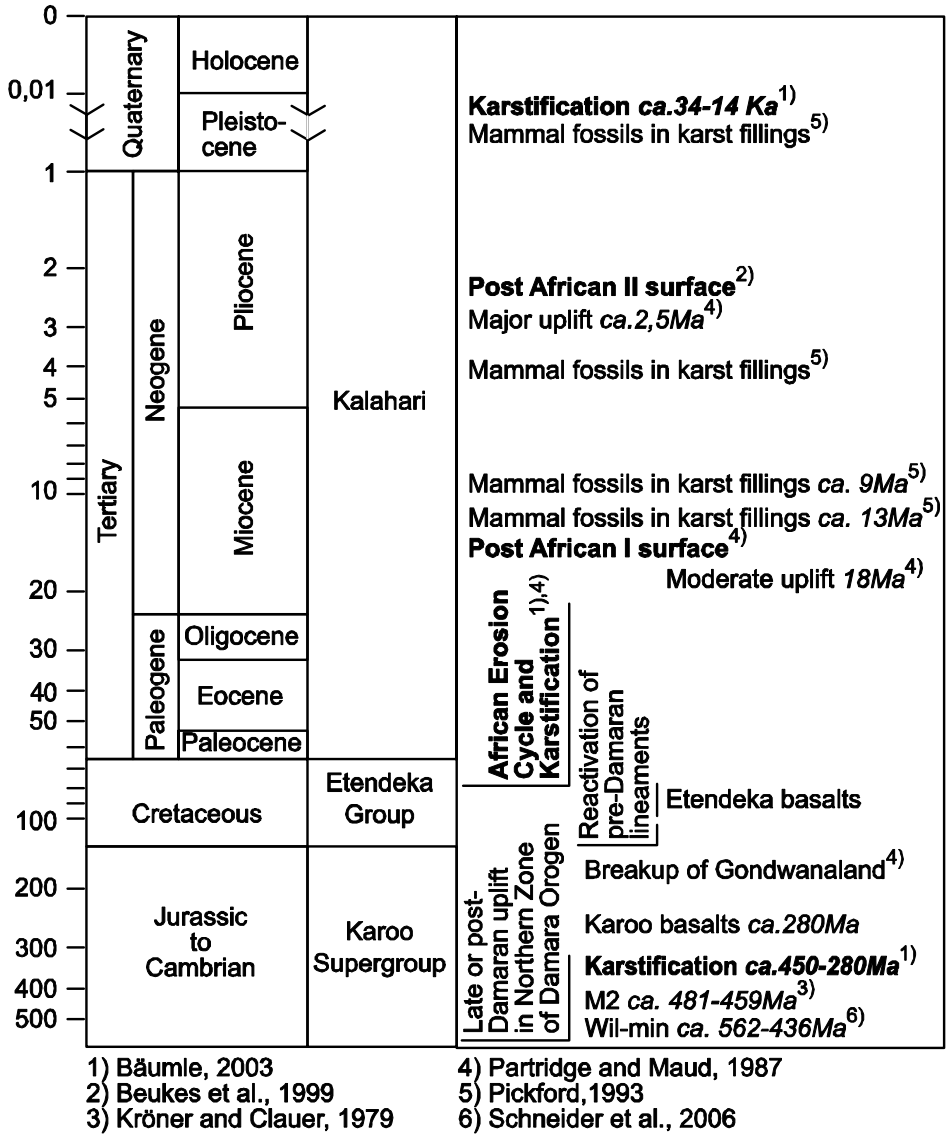

Fig. 6.3 - Tectonostratigraphic evolution of the Otavi Mountainland from Cambrian to Holocene. On the right, the most important morphological stages and the age data key for vanadate mineralisation.

climate evolution in the Southern Hemisphere is that Antarctic cooling and ice sheet development were related to the opening of tectonic gateways, which permitted the unrestricted flow of the ACC (Antarctic Circumpolar Current, Kennett and Barker, 1990). Together with the closure of equatorial gateways and declining atmospheric pCO_2, the development and strengthening of the ACC played an important role in the transition of Earth's climate system from "greenhouse to "icehouse" mode. This transition is expressed in the long-term increase in benthic $\delta^{18}O$ values from the early Eocene to early Oligocene. In Namibia, an evolution towards more arid climates had already started during the Oligocene, ("icehouse") period, which also corresponded to a rapidly declining sedimentation rate along the coastal margin, and lasted up to the Recent. This evolution toward greater aridity, was further accentuated by the Middle Miocene establishment of the cold Benguela current (Wateren and Dunai, 2001). The latter event caused the formation of the Namib and Kalahari deserts, where chemical weathering was extremely limited and the denudation rates of the previously uplifted zones stayed very small.

Some of the best summaries of present-day knowledge about the geomorphic development of southern Africa and Namibia have been presented by Partridge and Maud (1987) and Partridge (1998) (Fig. 6.3), who showed that the macro-scale development of the landscape in all of southern Africa has occurred in

discrete stages. The end of the Cretaceous saw Southern Africa and Namibia transected by an ample planation surface, known in the literature as the "African surface" (related to the African Erosion Cycle) (Fig. 6.3), cut at two levels above and below the Great Escarpment and interrupted locally by elevated mountain massifs, like the highest areas of the OML. The "African surface" was then rejuvenated and intersected by younger erosion planes: the post-African I and II surfaces (Partridge and Maud, 1987). These surfaces, related to discrete uplifts, which took place in Early Miocene and Pliocene and are possibly associated with the "African Superswell" (Nyblade and Robinson, 1994), have not been clearly recognised in the Otavi district.

Several karstification periods occurred in the OML, one in the Late Neoproterozoic, before deposition of the Mulden Group (Lombaard et al., 1986) and another from Mesozoic onwards, up to recent times (Van der Westhuizen et al., 1988; Geyh, 1995; Plöthner et al., 1997; Pickford, 2000; Bäumle, 2003) (Fig. 6.3). Apparently, strong karstic dissolution started only after the erosion of the basaltic cover of the Etendeka volcanites, because their remnants have never been found in the karstic network. An extensive, only partly filled cave system is currently known in the OML, and the internal sediments have been locally dated as Miocene with micromammals-based biostratigraphy (Senut et al., 1992; Pickford, 2000). None of the 32 dated karst sediments in the OML and nearby Kaokoland region, have been found to be older than Middle Miocene; some of them, containing macromammals (Verwoerd, 1957; Robinson, 1959) and hominid bones (Grine et al., 1995) are Pleistocene or younger (Fig. 6.3). These karst deposits reveal no clear link to regional or global geologic or climatic events and were probably forming and eroding away more or less continuously during the Neogene, with rates of karstic erosion of about 15 m per million years (Pickford, 2000). As anticipated, the karstic network, which includes solution-enlarged fractures, is the preferential (if not the only) site for the accumulation of the vanadium ores.

6.3 Base metal sulphide and nonsulphide mineralisation in the OML

Most base metal deposits in the OML, consisting of both sulphide and nonsulphide mineralisation are hosted by carbonate successions of the Otavi Group. Based on a number of geological/geochemical criteria and variable metal contents, two main mineralisation styles have been distinguished: the Berg Aukas (Zn-Pb>Cu)- and the Tsumeb (Pb>Cu>Zn)-type deposits (Pirajno and Joubert, 1993; Melcher, 2003). Most deposits reflect a multistage evolution and display a strong structural control (Lombaard et al., 1986; Pirajno and Joubert, 1993; Frimmel et al., 1996a). Mineralised brittle shear zones indicate the importance of flexural shear folds and small-scale thrusts as controls on mineralisation. This relates particularly to the formation of primary sulphide deposits (e.g. Tsumeb orebody: Lombaard et al., 1986) and also, in part, the formation of nonsulphide deposits. Nonsulphide Zn-Pb ores in the OML are mostly associated with, or even clearly replace, primary base metal sulphides. They sometimes display complex paragenetic associations, which probably indicate very distinct processes of formation and mineralisation (Lombaard et al., 1986). The most economic nonsulphide base metal ore minerals are willemite and Pb-Zn-Cu vanadates (descloizite-mottramite), several generations of which have been observed in the nonsulphide mineral paragenesis of the OML deposits.

The absolute timing of primary base metal sulphide mineralisation in the OML is not well constrained. Many age estimates are based on galena Pb-Pb model ages (e.g., Allsopp et al., 1981; Holmes and Cahen, 1957; Innes and Chaplin, 1986; Lombaard et al., 1986; Hughes, 1987; Kamona et al., 1999), which are not significant for geochronological interpretations (Haack, 1993; Frimmel et al., 2004). A maximum age for "Tsumeb-type" deposits is given by mineralised feldspathic arenites occurring within the pipe-like Tsumeb and Kombat orebodies, which have been interpreted to represent karst fills derived from the clastic Mulden Group (ca. 570-530 Ma; Lombaard et al., 1986; Frimmel et al., 1996a, 2004). Melcher et al. (2003) reported an age of 530 Ma for the Tsumeb main ore phase, based on preliminary Re-Os analyses of Ge-rich sulphide ores. In the absence of better isotopic age constraints, most authors agree that the "Tsumeb-type"

sulphide mineralisation formed syntectonically from orogenic fluids released during D2 deformation (Innes and Chaplin, 1986; Frimmel et al., 1996a, 2004). In contrast, Chetty and Frimmel (2000) and Frimmel et al. (1996a; 2004) favour a much earlier, synsedimentary-syndiagenetic formation of the stratabound Berg Aukas sulphide ores, from basinal brines in an extensional setting.

A recent study by Schneider et al. (in press) used the nonsulphide mineral willemite, which replaces sphalerite in several localities of the OML, as a Rb-Sr geochronometer. The isochron regressions, combining samples of willemites from the two mines of Berg Aukas and Abenab West, yielded Rb-Sr ages in the range of ca. 493-560 Ma, similar to the hypothesised ages of "Tsumeb"-type sulphide ores.

6.4 Vanadate mines and prospects in the OML

The regional distribution of the more important vanadium mines and prospects in the OML is shown in Fig. 6.1. Their position within the stratigraphic succession, as well as their past production, is recorded in Table 6.1. Most vanadium occurrences are hosted by the Tsumeb Subgroup, proximal to primary sulphide concentrations. The Abenab Subgroup contains the two largest former producers, Berg Aukas and Abenab, where (at least in the case of Berg Aukas), large Zn-Pb sulphide and nonsulphide orebodies have also been exploited (Wartha and Schreuder, 1992). Vanadate orebodies do not show the same deformation patterns as the Proterozoic host dolomites or the primary sulphide deposits (Verwoerd, 1957). They follow the horizontal, locally incised, "African erosion surface" and peter out at various depths, sometimes extending to several hundred meters (e.g. at Berg Aukas; Wartha and Schreuder, 1992). The most important structural control on the vanadate ore occurrences are the fractures in the dolomite where the vanadate-bearing solutions could circulate and eventually precipitate. Therefore, the majority of the deposits are related to brittle host rocks, and/or associated with faults of regional or local importance, which controlled the karst network. Larger deposits are located where the intersection of several structural lineaments favoured a more intense brecciation and collapse, which, paired with karstic dissolution, provided regions where ground water could circulate freely in large aquifers. Several different types of ore concentrations have been observed, the most common of which are (a) breccia-filled deep pipes and veins located along important structural lineaments and at stratigraphic discontinuities (e.g., at Abenab, Okorundu, Uris, Toenessen and Berg Aukas), and (b) the so-called "sand sacks" (Fig. 6.4), consisting of carbonate- and vanadate-cemented detrital sediments, filling a maze of relatively shallow karstic cavities (Schwellnus, 1946;

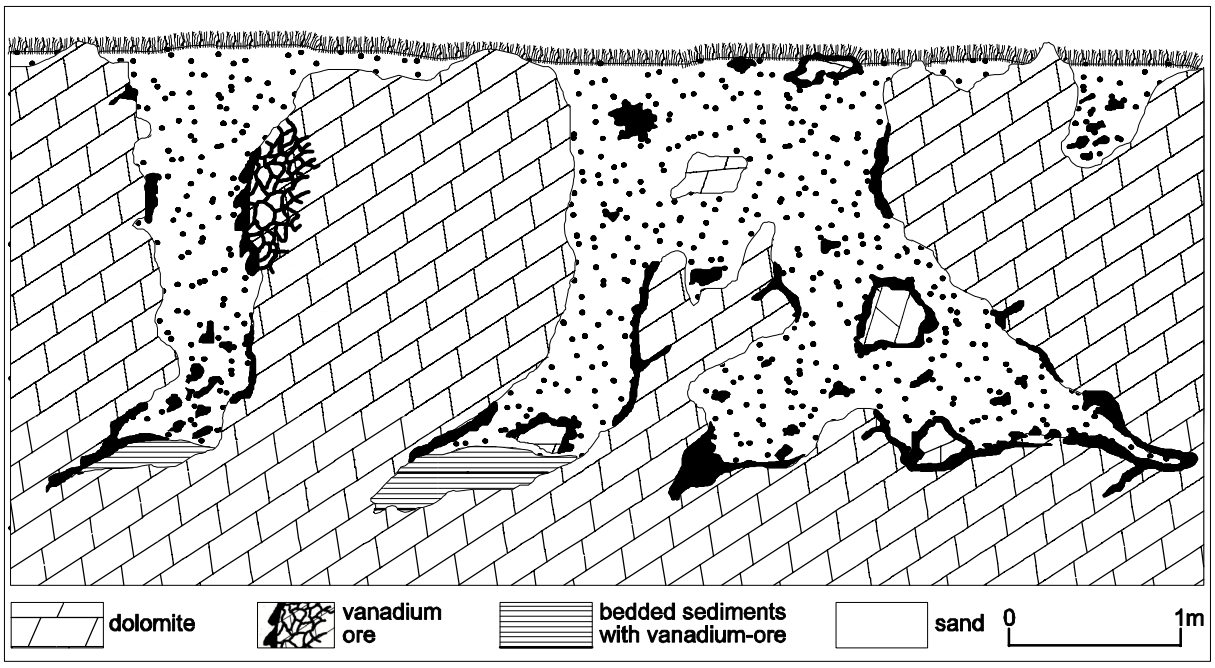

Fig. 6.4 - Schematic section of vanadate ore in "sand sacks" (from Schwellnus, 1946, modified).

Verwoerd, 1957). The "sand sacks" often also contain gossanous material, derived from previous sulphide mineralisations, bone beds, and they are usually capped by Kalahari sands. Owing to the dating of part of the fossils in the bone beds (Senut et al., 1992; Pickford, 1993), the timing of the vanadate mineralisation in the "sand sacks" has been suspected to range from the Late Tertiary to Pleistocene. A further detrital concentration with fragments of descloizite-mottramite also occurred from the Pleistocene up to the present in the upper parts of the cave systems. Supergene Zn-Pb carbonates in variable proportions, calcite, newly formed dolomite and jasperoidal silica are all associated with vanadium ore minerals. Fe and Mn oxides and hydroxides can also occur together with the vanadates, but they are generally derived from weathering processes, which occurred under higher fO2 conditions. A widespread silicification and/or calcitisation were locally described as a typical alteration phenomenon, related to vanadium enrichment of either the (a) or the (b) type (Wartha and Schreuder, 1992).

6.4.1 Berg Aukas

The Berg Aukas Zn-Pb-V deposit (Fig. 6.1, 6.5) is located in the eastern region of the OML, 20 km northeast of Grootfontein (Misiewicz, 1988). This occurrence is geologically unique because it is probably the world's largest known deposit of willemite and descloizite (with vanadium averaging 1% V_2O_5). Small-scale alluvial operations started in 1920 and yielded some 700 t of vanadium concentrate, while exploitation on an industrial scale was initiated in 1950 with the production of gravity concentrates, and ceased in 1978. Vanadium production at Berg Aukas between 1950 and 1978 exceeded 162,000 t of Pb-V_2O_5 concentrate. There is not much literature on Berg Aukas, with the exception of doctoral (Chadwick, 1993), master (Misiewicz, 1988) and honour (Gavine, 1979) theses, as well as several unpublished company reports (Markham, 1958; Weilers, 1959). Both primary sulphide mineralisation and secondary metal silicates/carbonates and vanadates at Berg Aukas are hosted in Neoproterozoic dolostones of the Gauss

Ore Deposit	Host Rock	Ore Type	Productions	Exploitation's Years
Karavatu	Hüttenberg Fm	Zn-Mottramite	5,234 t (together with Uris) @ 11.87% V_2O_5 [2]	1919-1924; 1931-1938 [2]
Tsumeb West	Hüttenberg Fm	Mottramite	3,900 t @ 8% V_2O_5 [2]	1920-1929 [2]
Tönessen	Hüttenberg Fm	Cu-Descloizite	112 t of V_2O_5 high grade concentrate [4]	1920s [2]
Baltika	Hüttenberg Fm	Cu-Descloizite	5,820 t of high grade concentrate @ 9% V_2O_5 [5]	1931-1942 [5]
Gross Otavi	Hüttenberg Fm	Mottramite	70 t of high grade concentrate @ 17% V_2O_5 [5]	1939-1941 [5]
Uris	Elandshoek Fm	Zn-Mottramite	5,234 t @ 18.75% V_2O_5, 45.57% Pb, 9.99% Cu, 4.12% Zn [2]	1919-1924; 1931-1938 [2]
Uitsab Pit	Elandshoek Fm	Cu-Descloizite	60,000 t @ 1.3% V_2O_5 [4]	1920-1940 [4]
Friesemberg	Elandshoek Fm	Zn-Mottramite	10,116 t @ 2.6% V_2O_5 , 5.9% Pb, 1.1% Cu [2]	1924-1928 [5]
Tigerschlucht	Elandshoek Fm	Cu-Descloizite	Prospect	1940 [2]
Wolkenhauben	Elandshoek Fm	Descloizite	Prospect	1943 [2]
Olifantsfontein	Elandshoek Fm	Cu-Descloizite	No data about production	1940s [2]
Abenab Pipe	Maieberg Fm	Descloizite	56,600 high grade concentrate @ 18.5% V_2O_5 [3]	1921-1948 [3]
Okorundu Pipe	Maieberg Fm	Descloizite	No data about production	1950s [2]
Abenab West	Auros Fm	Descloizite	0.49 Mt of which 0,07Mt @ 13% V_2O_5, 72% Pb [3]	1947-1958 [3]
Harasib 3	Auros Fm	Cu-Descloizite	800 t of V_2O_5 concentrate together with Harasib 1 & 2[2]	1940s [2]
Berg Aukas	Gauss Fm	Descloizite	4.25 Mt of which 1.6 Mt @ 1.22% V_2O_5, 5.23% Pb 21.79% Zn [2]	1920-1978 [1]

[1] Misiewicz, 1988; [2] Wartha and Schreuder., 1992; [3] Verwoerd, 1957; [4] Van der Westhuizen; 1984; [5] Söhnge, 1967.

Table 6.1 - Stratigraphic position, mineralogy and production of the main vanadate mines in the OML.

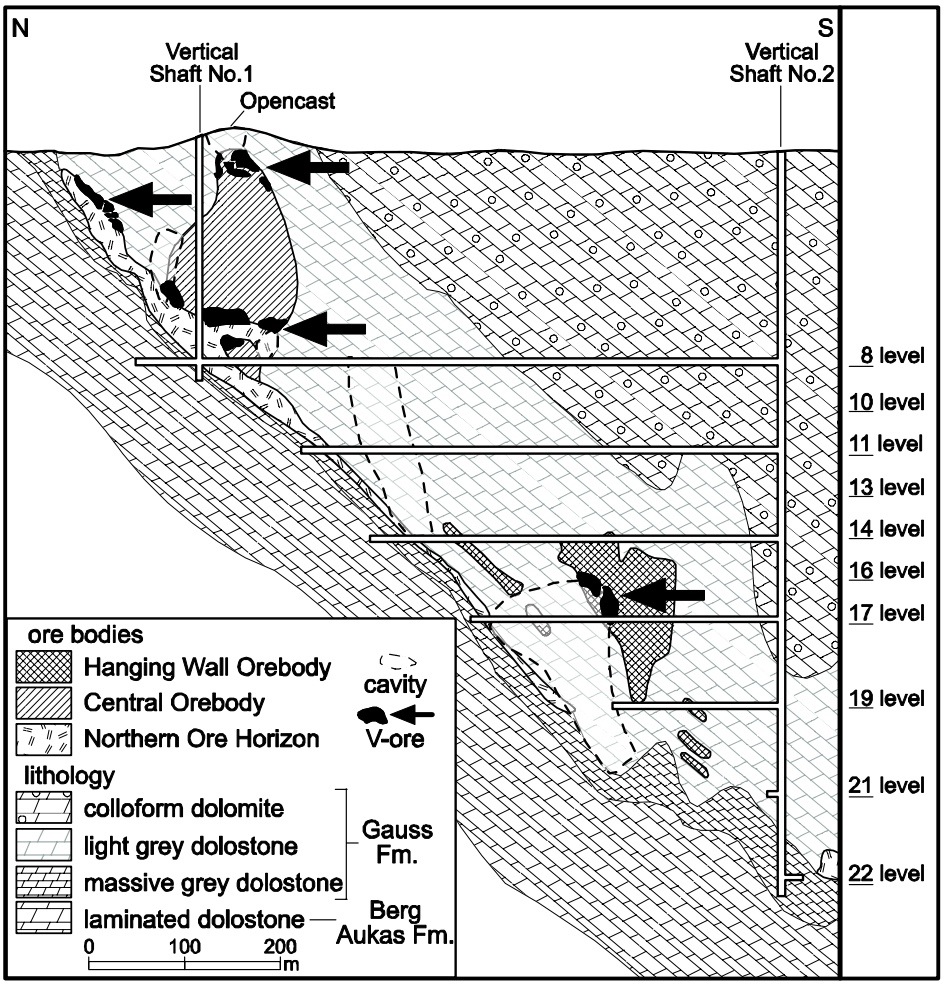

Fig. 6.5: Schematic profile of the Berg Aukas mine with the location of the V-ores (modified from Misiewicz, 1988).

Formation (Abenab Subgroup), developed above basal siliciclastic rocks on the northern limb of the E-W trending, tight Berg Aukas syncline (Misiewicz, 1988). Karst dissolution, collapse breccias and open space filling are ubiquitous, with the exception of the primary massive sulphides lenses (Misiewicz, 1988). Descloizite ore appears to be associated with late supergene (?) mineralisation stages, when metavanadate solutions were introduced into the primary deposit through vertical fractures and karstic conduits (Van der Westhuizen, 1984). Vanadate-enriched muds and caliche are also common. There are three main orebodies, whose distribution is structurally controlled, comprising both sulphide and nonsulphide ore minerals and reaching in depth at least 750 m below the current surface (Fig. 6.5): (1) the Northern Ore Horizon, extending from the surface to the keel of the Berg Aukas syncline, consisted of three fault-related lenses of massive sphalerite and minor galena that underwent repeated brecciation and oxidation. The orebody is zoned away from the fault and grades upward from a sulphide-rich base into a willemite-rich top (Misiewicz, 1988). The Northern Ore Horizon is then capped by brecciated dolomite, cemented by several generations of descloizite and by metal-enriched "saddle"-type dolomite (Fig. 6.5), (2) the Central Orebody, which formed a brecciated, irregular pipe-like lens of semimassive, mainly weathered sulphides and willemite, which extended to a depth of approximately 200 m (Markham, 1958). The orebody was exposed on top of the Berg Aukas hill with an apex, consisting of a series of vanadiferous mud filled fractures ("sand sacks" at the top of karst cavities) and descloizite-lined cavities (Fig. 6.6A). This outcrop led to the actual discovery of the mineralisation in 1913 (Wartha and Schreuder, 1992), and (3) the Hanging Wall Orebody, which was characterised by N-S trending, steeply dipping lenses of ore-filled fractures. Very variable ore grades and differing structural fabrics made this orebody more difficult to mine (Misiewicz, 1988).

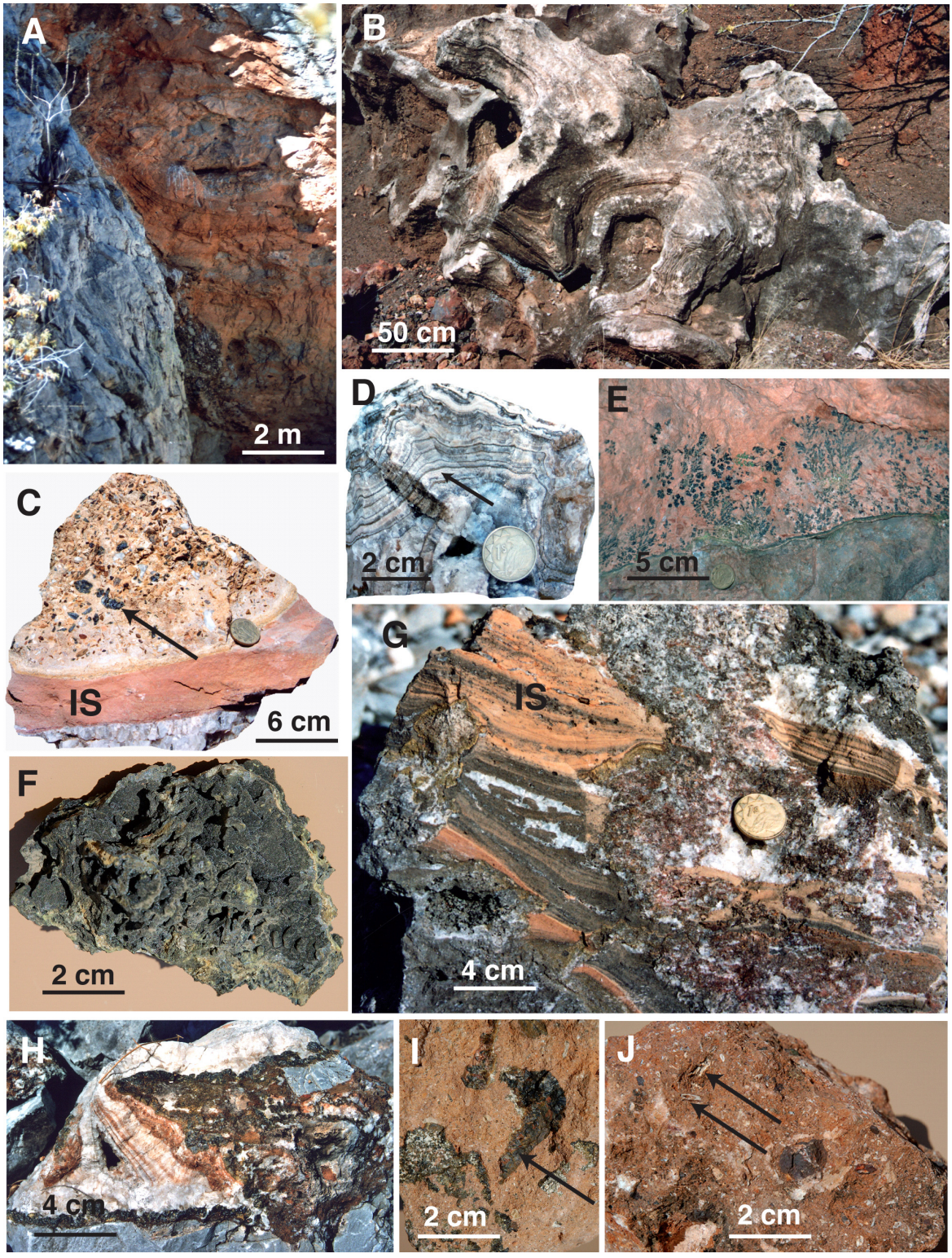

Fig. 6.6 - (A) Karst cavity in the Central Ore Body filled with sandy internal sediments and descloizite concretions (Berg Aukas); (B) Convoluted, late calcite cements (calc 3) at the top of the Uris pit; (C) Sample of internal sediment (IS) with intervals containing detrital descloizite (arrow), (Karavatu); (D) Convoluted, late calcite cements (calc 3) with thin intervals of yellow descloizite (arrow) at Baltika; (E) Mottramite dendrites in karst sediments, (Karavatu); (F) Microcrystalline mottramite concretion (Tsumeb West); (G) Yellow internal karst sediments (IS) and brown descloizite cements (Berg Aukas); (H) Calcite and descloizite cements in a breccia with clasts of dolomite host rock (Baltika); (I) Autigenic descloizite concretions growing in internal sediments (Berg Aukas); (J) Red internal sediment with clasts of gossan and detrital descloizite. The arrows show minute fragments of mammalian bones (Harasib 3).

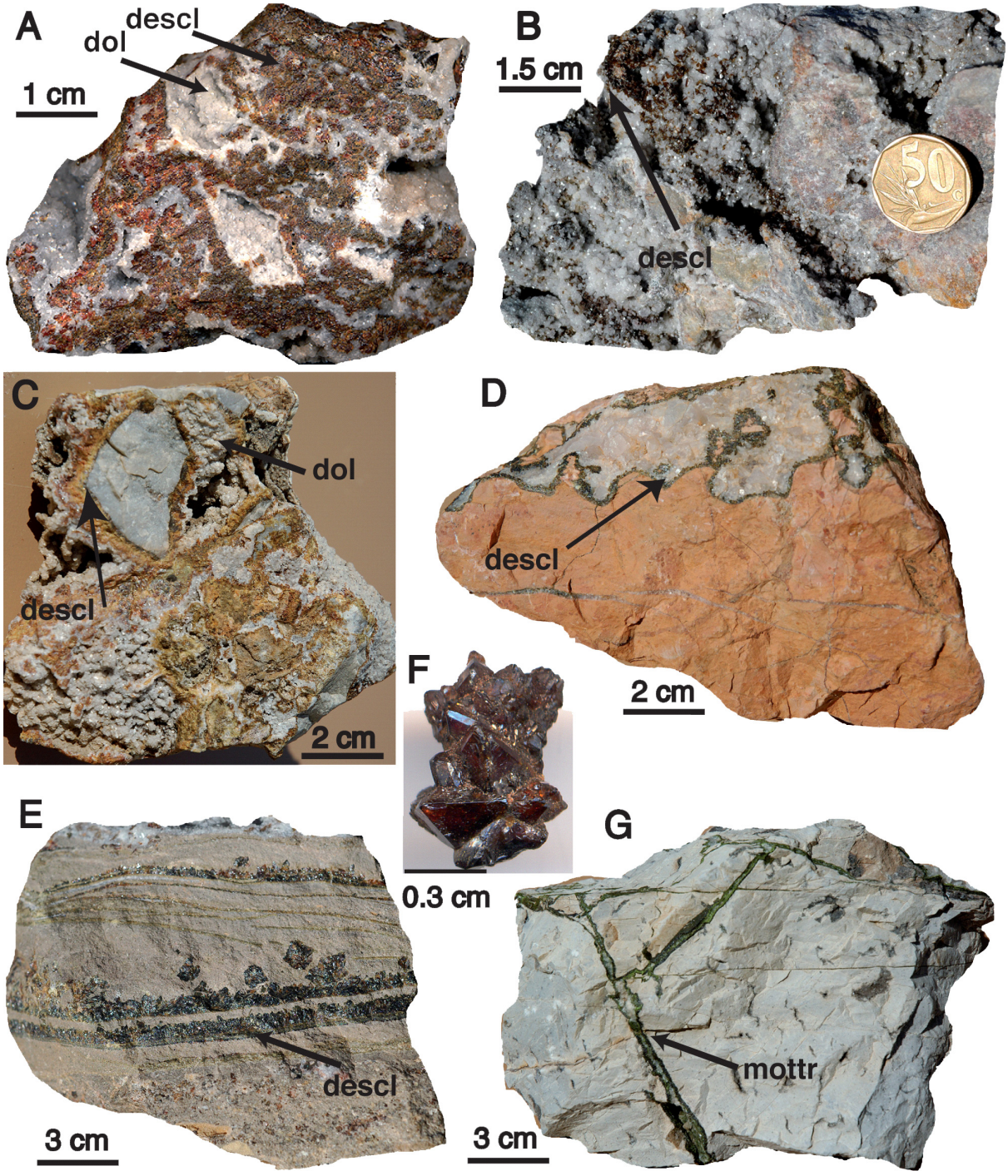

Fig. 6.7 - Typical ore samples from the Otavi Mountainland mining district. (A) Descloizite I (reddish) and "saddle" dolomite gangue (Berg Aukas); (B) "Saddle" dolomite gangue and microcrystals of descloizite II (Berg Aukas); (C) Collapse breccia with Proterozoic dolomite clasts cemented by descloizite I and "saddle" dolomite (Berg Aukas); (D) Cavity filled with descloizite crystals and sparry calcite in the laminated limestone (T3) of the Maieberg Fm. (Okorundu pit); (E) Internal gray sediment from the deeper collapse breccias, with descloizite crystals growing in layers (Berg Aukas); (F) Group of tabular descloizite crystals (Wolkenhauben); (G) Thin veins of mottramite (green) and calcite cutting the dolomite of the Hüttenberg Fm. (Gross Otavi).

Berg Aukas vanadates consist mainly of descloizite, displaying a variety of habits, including pyramidal, prismatic, pseudocubic and tabular (Cairncross, 1997). The crystals (whose diameter often exceeds 1 cm) have colours variable from metallic black, to green black and orange brown. Some of them show spear-shaped terminations. The association with "saddle" dolomite is very common (Fig. 6.7A, B, C), except for the descloizite in the "sand sacks". Calcite, late willemite and Zn-Pb carbonates are less common. In the deepest parts of the mine, internal sediments cemented by carbonates and with descloizite crystals growing in layers parallel to the internal sediments, are fairly common (Fig. 6.7E). "Sand sack"-type descloizite ore occurs in the upper part of the Central Orebody (Misiewicz, 1988). The "sand sacks" consist of the infill of relatively shallow karstic cavities (Fig. 6.6A), containing breccia clasts of various Proterozoic lithotypes in a sandy, reddish matrix. The internal sediments are cemented by carbonates and silica, and locally by a network of descloizite crystals and concretions (Fig. 6.6I). Minor fragments of primary and secondary ores have been found in the karstic network (Fig. 6.6C), as well as accumulations of micromammals bones (Fig. 6.6J), which in the deepest levels are encrusted by descloizite. The micromammals, and hence the encrusting descloizite, have been dated as Middle Miocene, while other fossil findings (among which is also the famous hominoid Otavipithecus namibiensis), located in shallower parts of the cave system, record an Upper Miocene age (Pickford, 1993). Even more surficial caves, where mostly detrital descloizite has been found, contain fossil remnants of Pleistocene age (including a femur attributed to an archaic H. sapiens: Grine et al., 1995.

6.4.2 Abenab, Abenab West, and Okorundu

Vanadium was mined from 1920 to 1947 in the Abenab (A) and Abenab West (AW) mines, located 35 km north of Grootfontein (Schwellnus, 1946; Verwoerd, 1957) (Fig. 6.1, 6.8). These two mines, hosted in the Auros Formation (uppermost Abenab Subgroup), have been considered to be the largest known concentration of vanadate ore in the world (Wartha and Schreuder, 1992). The deposit A (Fig. 6.9) consists of a pipe-like karst structure filled with a breccia of collapsed country rocks associated with compacted red muds, cemented by coarse calcite and descloizite/vanadinite concretions (Verwoerd, 1957; Cairncross, 1997). On the side of the main pipe, a large solution cavity has been exposed, which carries alternate bands of calcite and thin veneers of descloizite (Schwellnus, 1946). The AW deposit, mainly consisting of secondary base metals ores and vanadates, is located ca. 100 m southwest of the Abenab pipe and occurs along a steeply dipping, bedding-parallel structural contact (Fig. 6.8). Primary sulphides are extremely rare at Abenab, however, Verwoerd (1957) described very minor and strongly deformed galena-sphalerite mineralisation from the lowermost levels of the AW deposit.

The Abenab pipe (A) is cylindrical and reaches down to a depth of at least 425 m, but mining operations did not exceed 215 m because of increasing water flow and decreasing economic grade. From 1922 to 1947, 1,360,000 t of ore were mined from the main pipe, yielding 56,000 t of concentrate with a grade of 18.5 % V_2O_5. The Abenab West deposit (B) occurs in dissolution cavities along a narrow deformation zone and is associated with bedding-parallel faults. The known orebody was irregular along strike and ceased rapidly at a depth of less than 100 m. The ore consisted of abundant Zn-Pb nonsulphides and vanadates (descloizite and vanadinite), within a mass of unconsolidated, ferruginous clay containing quartz and detrital galena. The primary sulphides, reached with drilling, consisted of an association of sphalerite-pyrite-galena, with several types of fahlore and secondary copper minerals (Verwoerd, 1957), similar to the Tsumeb-type mineralisation. Abenab West is also famous for its willemite concentrations (Verwoerd, 1957; Part 5). Most of the vanadium ore at Abenab West is contained within a "sand sack" type deposit, where thick descloizite crusts occur as coatings on dolomite boulders in the consolidated sandy infill. Of minor importance are vanadates from a network of small veins in the Auros limestone, where the ore occurs as cryptocrystalline or pseudo-stalactitic masses (Schwellnus, 1946).

At Okorundu, located in the W of the Abenab mining area (Fig. 6.1), several breccia pipes crosscut grey to pink, laminated limestones of the Maieberg Formation (Wartha and Schreuder, 1992). The ore consists of descloizite and minor vanadinite associated with calcite, in the cement of collapse breccias that contain closely packed, angular fragments.

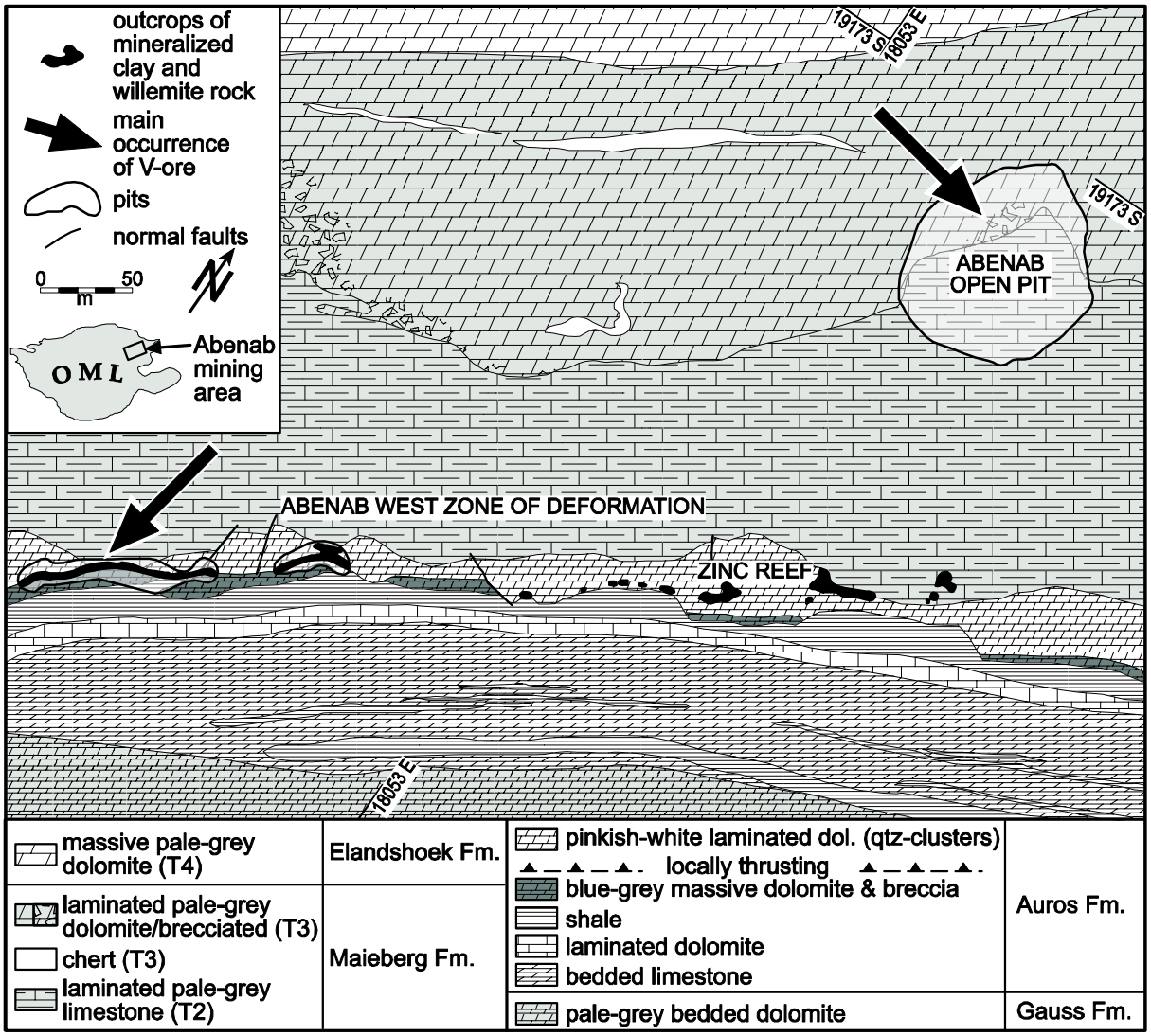

Fig. 6.8 - Geological map of Abenab and Abenab West mining area (from Verwoerd, 1957 modified).

6.4.3 Baltika

This deposit is situated in the area of farm Baltika 515 (Fig. 6.1), was discovered in 1931 and worked until 1942 (Söhnge, 1967), with a total production of vanadium concentrate reaching about 6,000 t at 9 % V_2O_5. At Baltika, the vanadate ore is hosted in carbonate rocks of the northern limb of the Otavi valley syncline, which also contains stratabound Zn-Pb sulphide and willemite bodies. The deposit consists of discrete descloizite concentrations associated with calcite occurring in N-S trending veins, but also as cement in the collapse breccias (Fig. 6.6H) and "sand sack" type ore (Wartha and Schreuder, 1992). The latter type is concentrated in sinkholes of a few meters in diameter, and filled with reddish sands and clays. In the veins and breccia ores, there is strong evidence of multiple generations of karst dissolution and infilling with sediments (Fig. 6.6G, H). Several rhythmically precipitated cement generations have also been observed. At Baltika, calcite is the main gangue carbonate. The latest cement generation consists of speleotheme-like calcite bands (calc 3), alternating with thin descloizite layers and internal sediments (Fig. 6.6D). The zoned calcite/descloizite cements are very similar to the lithotypes occurring in the calcite-filled cavities described by Schwellnus (1946) from the side of the Abenab main pipe.

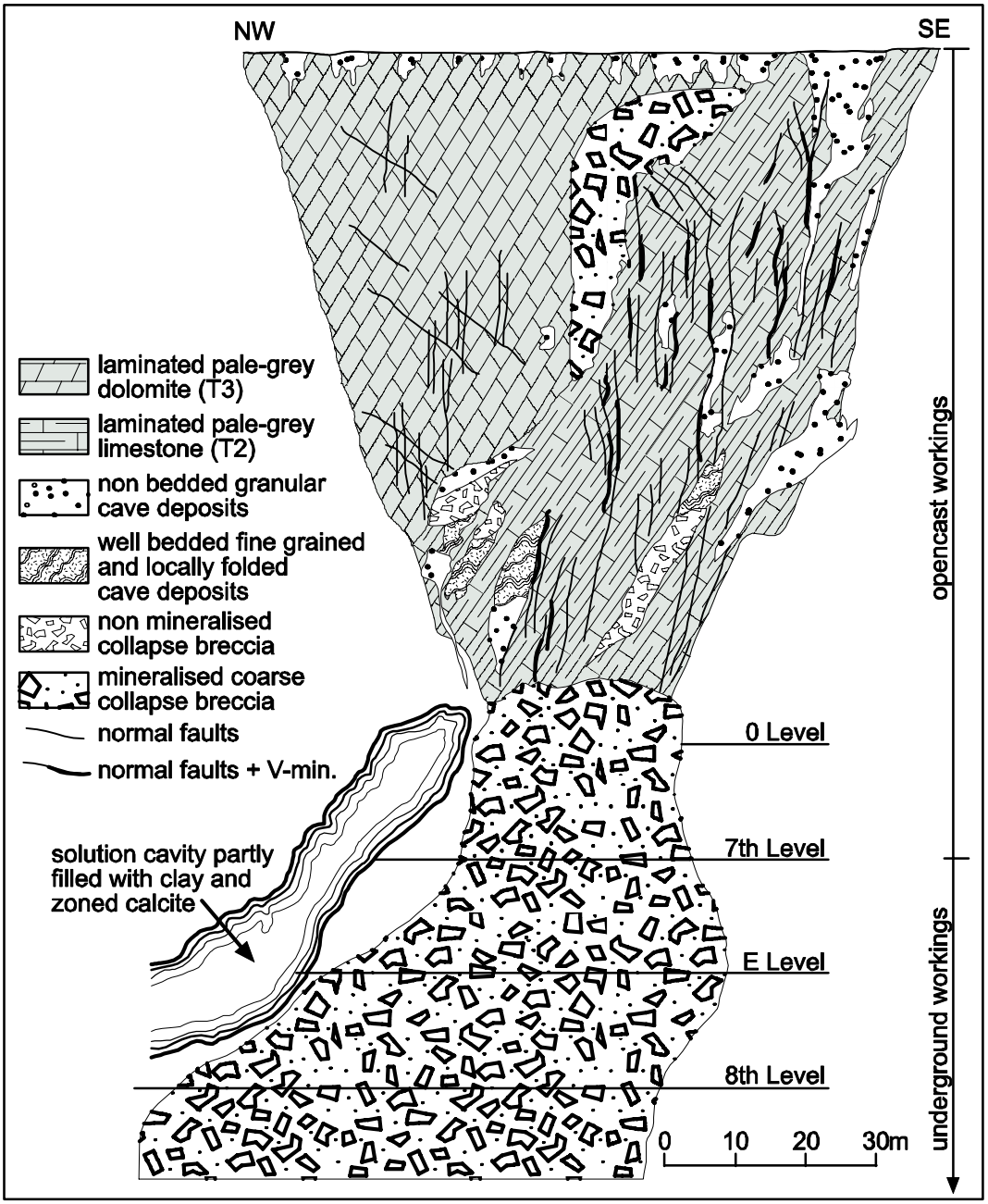

Fig. 6.9 - Schematic section through the Abenab pipe main orebody (from Schwellnus, 1946, modified).

6.4.4 Gross Otavi

The small Gross Otavi vanadium deposit, mined from 1909 to 1941 (Söhnge, 1967) at the farm Andvord, is located east of Baltika (Fig. 6.1) within veined, brecciated and calcitised dolomites of the Hüttenberg Formation (Fig. 6.7G). A network of fractures filled with "sand sack" ore and gangue was also exploited in this locality. The ore minerals consist mainly of Cu-descloizite and mottramite. The main ore sought at Gross Otavi, possibly related to the alteration of primary sulphides like those exploited at the nearby Kombat mine, consisted of supergene Cu sulphides (chalcocite) and Cu carbonates/silicates, often reported as detrital blocks in the "sand sacks". This explains the cupriferous nature of the vanadates at Gross Otavi (Van der Westhuizen, 1984).

6.4.5 Wolkenhauben

The small Wolkenhauben prospect, located in dolomites of the Elandshoek Formation at the Farm Auros (Fig. 6.1), was exploited by the OMEG (Otavi

Minen- und Eisenbahn Gesellschaft) in 1943 and then abandoned (Wartha and Schreuder, 1992). Wolkenhauben is quite famous among mineral collectors for the beautiful descloizite samples recovered, mostly contained in superficial "sand sacks" occurrences at the top of a network of veins.

6.4.6 Harasib 3

Harasib 3 (Harasib 2 in Wartha and Schreuder, 1992) (Fig. 6.1) is a large prospect pit deep in the Elandshoek Fm oolitic carbonates. At this site, large descloizite crystals occurred in bright red breccias, together with reddish, well cemented residuals containing abundant vertebrate bone fossils. The fossil finds, consisting mainly of micromammals, are upper Miocene (9 ± 1 Ma) in age (Senut et al., 1992), similar to the fauna described in the more surficial ore zones of the Berg Aukas mine. Most descloizite concentrations are also reworked from pre-existing, not outcropping, ore occurrences. The main body is capped by a gossan covering an area of about 160 m^2 (Wartha and Scheuder, 1992). It seems clear that the Harasib 3 deposit was formed inside a cave that was open to the old land surface, where temperature and humidity conditions were not very different (perhaps slightly more humid) from those of today.

6.4.7 Uitsab

This small deposit (800 t of V-concentrate were recovered) occurs in the Elandshoek Formation dolomites on the farm Uitsab 654 (Grootfontein) (Fig. 6.1), associated with a north- to northwest trending shear zone. The main minerals are descloizite, vanadinite and pyromorphite. Remnants of Cu- and Pb-sulphides have also been found along the shear zone.

6.4.8 Rietfontein

This prospect occurs at the farm Rietfontein 344 (Fig. 6.1), on the easternmost outcrop of the Elandshoek dolomites along the Otavi Valley. The mineralisation was quite localised in extent and exploited intermittently in dolines filled with detrital descloizite and red internal sediments, as well as along a limited network of fractures in the massive dolomites. In the karst filling, thick descloizite crusts and zincian mottramite crystals growing on mammalian bones of Pleistocene age were locally observed (Schwellnus, 1946; Robinson, 1959; Pickford, 2000).

6.4.9 Tsumeb West - Friesenberg

The countless small vanadate deposits exploited by OMEG during the first decades of the twentieth century around the Tsumeb mining area, and now encountered again by underground sulphide operations recently performed by Ongopolo Company, go under the name of "Tsumeb West vanadium mineralisation" (Fig. 6.1). Most of the vanadium ore at Tsumeb West is Cu-rich and occurs as nodules in sandy sediments filling relatively shallow karst cavities: a typical "sand sack" deposit. Thin stringers of pure mottramite also occur in grapelike concretions (Fig. 6.6F) within solution fissures and along bedding planes of the Hüttenberg Formation carbonates (Wartha and Schreuder, 1992).

The Friesenberg mineralisation occurs a few km to the south of Tsumeb West, and is related to a structural discontinuity in the Elandshoek dolomites. The mine was opened in 1923 and active for less than a decade, producing about 10,000 t of sorted vanadium ore (Söhnge, 1967).

6.4.10 Bobos area

This area represents the westernmost vanadium mineralisation of the OML, occurring in dolomites of the Elandshoek and Hüttenberg Formations. The ore (ranging from Cu-descloizite to mottramite) was exploited in a series of small mines with distinct characteristics. Examples include (Fig. 6.1) Alt Bobos, Karavatu, Uris and Toenessen, which together produced 5,234 t of concentrate averaging 11.87 % V_2O_5. Different types of deposits occur in the Bobos area, from pipe-like and breccia-cement concentrations to "sand sack" sediment infills associated with diagenetic and detrital vanadates. At Uris, a large pipe (20 m in diameter) which pinched out at a depth of 70 m, contained Zn-mottramite and sparry calcite. In the uppermost levels of this mine abundant alluvial deposits and a strongly silicified and rubefied gossan can still be observed. Much younger, draped calcite speleothemes (Fig. 6.6B), similar to the late carbonate generations (calc 3) described in the Baltika mine, occur locally. At Toenessen, the ore is associated with white sparry calcite along veins. Around the whole

area, however, it is common to find vanadate enrichments in "sand sack" dolines (up to 25 m deep, Wartha and Schreuder, 1992), filled with eolian (?) dolomitised sands and clays containing clasts of Proterozoic dolomites and detrital descloizites with fragments of gossan. The small Cu-descloizite and mottramite mine of Karavatu, extensively exploited in the past, shows very interesting features including mineralised fissures and Mn-and V-rich clays wedging out downward, and a morphology consisting of a series of small "sand sacks". In the latter, internal sediments and detrital descloizites (Fig. 6.6C) occur. Generally, the vanadates at Karavatu are either coarse crystalline or show dendritic (Fig. 6.6E) and arborescent growths (Schwellnus, 1946).

6.5 Sampling and methods

An intensive sampling regime has been conducted throughout the OML. Most vanadate deposits, of varying economic importance, have been investigated. However, in the bigger vanadium occurrences, such as Berg Aukas and Abenab, it was almost impossible to sample the descloizites/mottramites in situ due to the inaccessibility of the old workings. Most samples from the latter mine sites have been taken from the ore dumps, and their geological context was deducted from historical literature and mine reports.

Minerals were characterised by stereoscopic, petrographic and reflected light microscopy. Before analysis, pure mineral phases were obtained by a combination of handpicking and gravimetric separation techniques, then cleaned in a sonic bath for 10 minutes to eliminate impurities deposited on crystal surfaces. X-ray powder diffraction analysis (XRPD) was carried out at the Dipartimento di Scienze della Terra, Università di Napoli, Italy, with a SEIFERT MZVI automated diffractometer and CuKα radiation. Synthetic $CaCO_3$ (Mallinckrodt analytical reagent) was used as an internal standard (position of the 1014 reflection for $CaCO_3$ taken to be 3.035 Å, JCPDS-ICDD 5-586).

Ore and gangue samples in polished thin section (~30 µm thick) were examined by conventional and cold cathodoluminescence (CL) petrography utilizing a CITL 8200 Mk3 Cold Cathodoluminescence instrument at the Geologisch-Paläontologisches Institut, University of Heidelberg (Germany), operating at 23-25 kV voltage and 500-550 µA beam current.

SEM observation and semi-quantitative major element analyses were undertaken using a LEO 440 with a Link ISIS EDS at the Mineralogical Institute, University of Heidelberg. Most carbonate analyses were performed at the Natural History Museum (London) on a JEOL5900V scanning electron microscope, with a link EDS detector, operating at 20 kV. These analyses were corrected with INCA software. Chemical analyses of vanadates and carbonates were performed by WDS on a Cameca SX50 electron microprobe (IGAG at the CNR, Rome) operating at 15 kV, 15 nA and 10 µm spot size. Data were corrected using the PAP program (Pouchou and Pichoir, 1991). Minerals and pure elements were used as standards.

Major and trace elements were measured at ACME laboratories in Vancouver, Canada. From each pulverised sample, 2 g were digested with Aqua Regia (HCl - HNO3) at 95°C. The measurements were performed on a Perkin Elmer Elan 6000 ICP-MS in the 1-DX Group (36 elements).

Microthermometric analytical measurements on fluid inclusions of calcite were carried out at the Dipartimento di Scienze della Terra, Università di Napoli, Italy, using a Linkam THMSG 600 heating/freezing stage. The stage was calibrated with synthetic fluid inclusions (Bodnar and Sterner, 1987). The precision of the measurement is better than ± 1°C in the range of interest for this work.

6.5.1 Oxygen and carbon isotopes

Twenty carbonate powders (> 0.2 mg) were analyzed for O and C isotope ratios at the University of Erlangen (Germany). The samples were reacted with concentrated phosphoric acid at 75 °C (Wachter and Hayes, 1985) in an online carbonate preparation line, connected to a Finnigan MAT 252 mass spectrometer. $^{18}O/^{16}O$ and $^{13}C/^{12}C$ ratios were measured simultaneously from the CO_2 gas produced. Calibration was accomplished by assigning a $\delta^{18}O$ value of -2.20 ‰ and a $\delta^{13}C$ value of +1.95 ‰ to the NBS-19 standard. The precision of analyses based on repeated measurement of laboratory and international standards, is about 0.1 ‰ (1σ). The isotopic compositions are reported as δ-values in per mil relative to V-PDB for carbon and SMOW for oxygen. Reproducibility was better than ± 0.02. As suggested by Land (1980), the $\delta^{18}O$ values of dolomites were not corrected for phosphoric acid fractionation.

6.5.2 Lead and strontium isotopes

In total, 15 samples of descloizite, galena and dolomite from different locations in the OML were analyzed for their Pb isotopic composition. Moreover, we have determined the $^{87}Sr/^{86}Sr$ ratios for 17 gangue carbonate (calcite and dolomite) samples. Galena samples were weighed and dissolved in one drop of 8 N HBr and dried. The dry residues were then rewetted with one drop of 14 N HNO3, dried again and redissolved in deionised water (DDW). From these solutions, aliquots containing ca. 200 ng Pb were loaded for mass spectrometry. Descloizite and carbonate samples were completely dissolved in 14 N HNO3. The solutions were then dried at 110°C and subsequently rewetted with 3 N HNO3. Strontium and lead were chemically separated with 3 N HNO3 using EICHROM Sr resin on 50 µl Teflon columns, following the methods of Horwitz et al. (1991a; 1991b). Sr was stripped from the columns with 1 ml of H2O. Subsequently, Pb was eluted from the same column with 1 ml of HCl 6 N. The Pb cut was further processed through a 50 µl column containing precleaned EICHROM Pre Filter Resin.

For mass spectrometry, Sr was loaded with TaCl5-HF-H3PO4 solution (Birck, 1986) onto W single filaments and Pb loaded onto single Re filaments using silica gel-H3PO4 bedding. All isotopic measurements were performed on FINNIGAN MAT 262 solid-source mass spectrometers running in static multicollection mode. Sr isotopic ratios were normalised to $^{88}Sr/^{86}Sr = 0.1194$. Repeated static measurements of the NBS 987 standard over the duration of this study yielded an average $^{87}Sr/^{86}Sr$ ratio of 0.71025 ± 4 (2σ mean, n = 8). Pb isotopic ratios were corrected for mass fractionation using mean discrimination factors of 0.085 ± 0.006 (2σ) %/[amu] and 0.123 ± 0.046 (2σ) %/[amu], respectively, based on replicate measurements of the NBS SRM 981 common lead standard. Errors and error correlations were calculated after Ludwig (1980). Individual uncertainties (2σ) are given for Pb and Sr isotope ratios (Table 6.6). Sr blanks (n=6) amounted to 50 pg maximum, and were found to be negligible (< 0.5 wt-% of the analyzed sample Sr amounts).

6.5.3 (U-Th)/He thermochronometry

(U-Th)/He thermochronometry is based on the production of ^4He from U and Th decay as given by

$$^4He = 8^{238}U(e^{\lambda 238t} - 1) + 7^{235}U(e^{\lambda 235t} - 1) + 6^{232}Th(e^{\lambda 232t} - 1)$$

where ^4He, ^{238}U, ^{235}U, and ^{232}Th are the present-day atoms, λ's are their decay constants, and t is the (U-Th)/He age. Although the U and Th half-lives are fairly long (~10 9-1010 yr), six to eight α particles are produced from each parent because of the multi-step decay chains that yield stable ^{206}Pb, ^{207}Pb, and ^{208}Pb (forming the bases of the well-known U/Pb and Th/Pb dating techniques, Reiners, 2002). When U and Th contained within a given mineral eject alpha particles during radioactive decay, those particles can travel a known distance (usually ~20µm) within the mineral lattice ("stopping distance"; Ziegler, 1977). Daughter products can be lost if decay occurs close the edge of the mineral and erroneously old ages are determined if this loss is not taken into account.

The (U-Th)/He method measures the time at which a given mineral structure cooled to a point where the helium produced by the parent decay was quantitatively retained and in this sense, it is usually a "cooling age" that is determined, rather than a "formation age". The (U-Th)/He age is considered to reflect the age of formation only when the mineral being studied cooled rapidly to below its "helium closure temperature" and remained at low temperatures (<30°C) to the present day. The OML descloizites contain sufficient U and Th to measure and quantitatively retains helium in its lattice. For U-rich samples like this descloizite, the age is determined using equation

$$t = 1/\lambda(\ln[^4He/8^{238}U + 1])$$

For this study, >200 µm diameter shards of descloizite were analyzed at the CSIRO (U-Th)/He Laboratory located in the John de Laeter Centre for Mass Spectrometry at Curtin University of Technology, Western Australia. The fragments were sub-sampled from the interior (>100 microns from the surface) of large (500 µm - 1.0 cm diameter) descloizite megacrysts, so no correction for alpha ejection (Ziegler, 1977) was made. The fragments were homogenised so that all growth zones were mixed and an "average" composition was represented in each aliquot. The samples were loaded into platinum capsules for helium extraction and heated under vacuum using a Nd:YAG laser. Helium content was measured using a quadrupole mass spectrometer. The capsules were removed from the laser, transferred to

Teflon beakers and spiked with 15ppb ^{235}U and 5ppb 230Th prepared in 50% HCl. Spiked standard solutions and reagent blanks (with empty Pt capsules added) were treated similarly to the samples. 200-400 µl of 8 M ultrapure HCl with 0.01 M HF was added to each sample, standard and blank. Solutions were gently heated and treated in an ultrasonic bath for about 1 hour or until the crystals had dissolved and acids had evaporated to incipient dryness. Solutions were then diluted in approximately 5 % HCl and analysed by isotope dilution for U and Th on an Agilent 7500CS mass spectrometer at the University of Western Australia. Further details on (U-Th)/He analytical procedures and data reduction can be found in Evans et al. (2005).

Preliminary step-heating diffusion experiments (Farley et al., 1999) were performed on multi-grain aliquots of descloizite of the same grain size used for (U-Th)/He thermochronometry. A projector bulb furnace was used for all but the final heating step where laser gas extraction was utilised. Experiments began at 250 °C ended at 450 °C. Preliminary Arrhenius plots were produced from which the closure temperature was calculated (see Reiners et al., 2004 for methods as applied to zircon helium diffusion). Diffusion work on the descloizite is continuing in order to produce a more robust estimate of the closure temperature.

6.6 Results

6.6.1 Mineralogy and ore textures of vanadate Ores

Descloizite and mottramite are the most common vanadates occurring in the OML. The vanadium minerals occur either in a network of veins and fractures, or overgrow the walls of dissolution cavities. The most common occurrences are in the form of breccia cements around disaggregated clasts of Neoproterozoic dolomites. Well-crystallised vanadate specimens have been found especially in the Berg Aukas and Abenab mines (Cairncross, 1997). Berg Aukas descloizite displays a variety of habits, including pyramidal, prismatic, pseudocubic and tabular forms. A few specimens have spear-shaped terminations and are highly lustrous. Individual crystals ranging from 1 to 3 cm are relatively common and paragenetically associated with either calcite or dolomite. At Abenab and Abenab West, descloizite occurs as pyramidal and/or tabular crystals either in veins or coating the walls of open cavities. Besides crystalline aggregates, vanadate ores also occur in dendritic (Karavatu, Fig. 6.6E), arborescent and pseudo-stalactitic (Tsumeb West, Fig. 6.6F) forms (Schwellnus, 1946). Vanadates have also been found as fragments in relatively young karst fills (Fig. 6.6C), indicating multiple brecciation events and detrital concentration after the main mineralisation phases.

The vanadium ore minerals are generally coarse-grained, well formed and zoned (Fig. 6.10A, B). The colours range from light to dark green (mottramite and other Cu-varieties, Fig. 6.10A, C) and brown (descloizite and other Zn varieties, Fig. 6.10B, D, E, F). Locally, reddish specks of the Cl-bearing mineral vanadinite [$Pb_5(VO_4)_3Cl$], which is always the first V mineral to be deposited, also occurs with the other vanadates. At Abenab, vanadinite is exceptionally coarse grained (crystals up to a few cm) and red in colour, showing brilliant pleochroism, though lower than descloizite (Verwoerd, 1957). The mineral descloizite is also easily recognised under the microscope: it is strongly pleochroic in shades of yellow (b = c) and brown-yellow (a), and is characteristically zoned. Mottramite is more common (Fig. 6.10C) in the yellow-green variety. The zonation during the growth of vanadate crystals (Fig. 6.10B) points to a prolonged period of deposition subjected to repeated variations in the composition of the depositing solutions (Verwoerd, 1957). In both descloizite and mottramite types, however, compositional zonation is minimal despite the existence of distinct growth zones. Slight enrichment of As compared to V in some zones (Table 6.2) reflects the breakdown of As minerals derived from primary sulphides association (e.g. tennantite).

The vanadates of the OML have always been considered as a paragenetically late phase in the depositional history of the ores (Schwellnus, 1946; Verwoerd, 1957; Van der Westhuizen, 1984, 1986; Misiewicz, 1988). Descloizite was deposited after the main phases of willemite (and vanadinite) deposition both at Abenab West and Berg Aukas, followed only by the formation of some of the supergene Zn-Pb carbonates and silicates, which can be related to the latest weathering phases (Verwoerd, 1957). Calcite shares the same paragenetic position as the vanadates and occurs with the vein- and breccia-related ores and as cement in the deeper parts of the „sand sacks“. After

Verwoerd (1957), transparent, coarsely crystalline calcite (Fig. 6.10A, C, F) should be regarded as a paragenetic associate of vanadate ores in the whole OML. The same author also reported that even plumbean calcite (tarnowitzite) has been found in some mines (Abenab West, Tsumeb etc.).

In a few localities, such as Wolkenhauben, Tsumeb and particularly Berg Aukas, descloizite ores are associated with "saddle" dolomites (Fig. 6.11A, B) of possible hydrothermal origin (Radke and Mathis, 1980). The dolomite crystals generally grow on massive crusts of zoned descloizite (descloizite 1, Fig. 6.7C, 11D, E), which cement the collapse breccias in the deeper cavities of the Berg Aukas mine (top of the Northern Orebody and the Hanging Wall Orebody), and are followed by later, smaller, idiomorphic descloizite crystals (descloizite 2, Fig. 6.11F). At Wolkenhauben, these dolomites replace the Neoproterozoic early diagenetic dolomite host rock (Fig. 6.11J). The two generations can be clearly distinguished not only by their different form, but also by their distinctly different content of base metals, with the host rock dolomites being almost barren. The latest carbonate generations associated with the vanadates consist of calcite, occurring in banded concretions and veins with alternating thin vanadate layers, in the most surficial areas of the old pipes (Uris Mine, Fig. 6.6B). These calcites are morphologically similar to speleotheme cements and are often associated with internal karst sediments of chemical as well as detrital origin. All gangue carbonates, especially the zoned "saddle" dolomites, are either non-luminescent or show cathodoluminescence colours in different shades of blue (Fig. 6.10H), quite different from the brilliant colours observed in the Neoproterozoic dolomites and in the sulphide gangue carbonates (Gross and Vollbrecht, 2003).

	Mottramite			**Descloizite**								**Vanadinite**
	NA.RO.453a			NA.RO.432e			BA.2003.11			BA.2003.9		
V_2O_5	20,06	20,60	21,02	20,37	17,22	20,15	20,09	19,38	19,38	20,08	21,20	14,96
PbO	54,06	53,80	54,29	53,81	55,90	54,47	56,36	54,92	56,26	55,02	54,82	78,22
ZnO	0,39	0,46	0,66	19,76	18,13	18,49	19,00	19,82	19,20	19,38	19,90	1,28
CuO	19,63	19,58	18,90	0,90	1,90	2,08	0,23	0,48	0,26	0,51	0,37	0,00
As_2O_3	2,31	2,06	1,50	1,49	4,09	1,02	0,43	1,04	0,66	1,02	0,17	1,42
CdO	n.d.	0,00	0,06	0,01	0,06	0,02	0,04	0,07	n.d.	n.d.	0,01	0,04
P_2O_5	0,19	0,16	0,07	0,10	0,26	0,06	0,28	0,55	0,32	0,06	n.d.	1,17
TiO_2	0,01	n.d.	0,03	0,00	0,00	0,01	n.d.	n.d.	n.d.	0,02	0,01	n.d.
CaO	1,10	1,00	1,07	0,32	0,28	0,23	0,07	0,07	0,05	0,04	0,09	0,01
MnO	0,06	0,02	0,03	n.d.	0,02	n.d.	0,02	0,03	n.d.	n.d.	n.d.	n.d.
FeO	0,03	0,03	0,02	0,15	n.d.	0,06	n.d.	0,26	n.d.	0,01	0,08	n.d.
NiO	n.d.	n.d.	n.d.	0,05	0,02	0,03	0,01	n.d.	n.d.	n.d.	0,02	0,05
*H_2O	2,50	2,50	2,50	2,48	2,50	2,48	2,47	2,47	2,46	2,46	2,47	
*Cl	--	--	--	--	--	--	--	--	--	--	--	2,49
*-O=Cl_2	--	--	--	--	--	--	--	--	--	--	--	0,56
Total	100,34	100,20	100,14	99,44	100,38	99,32	99,08	99,16	98,63	98,58	99,12	100,87

*calculated from stoichiometry

Table 6.2: (WDS) Microprobe analyses of selected vanadates.

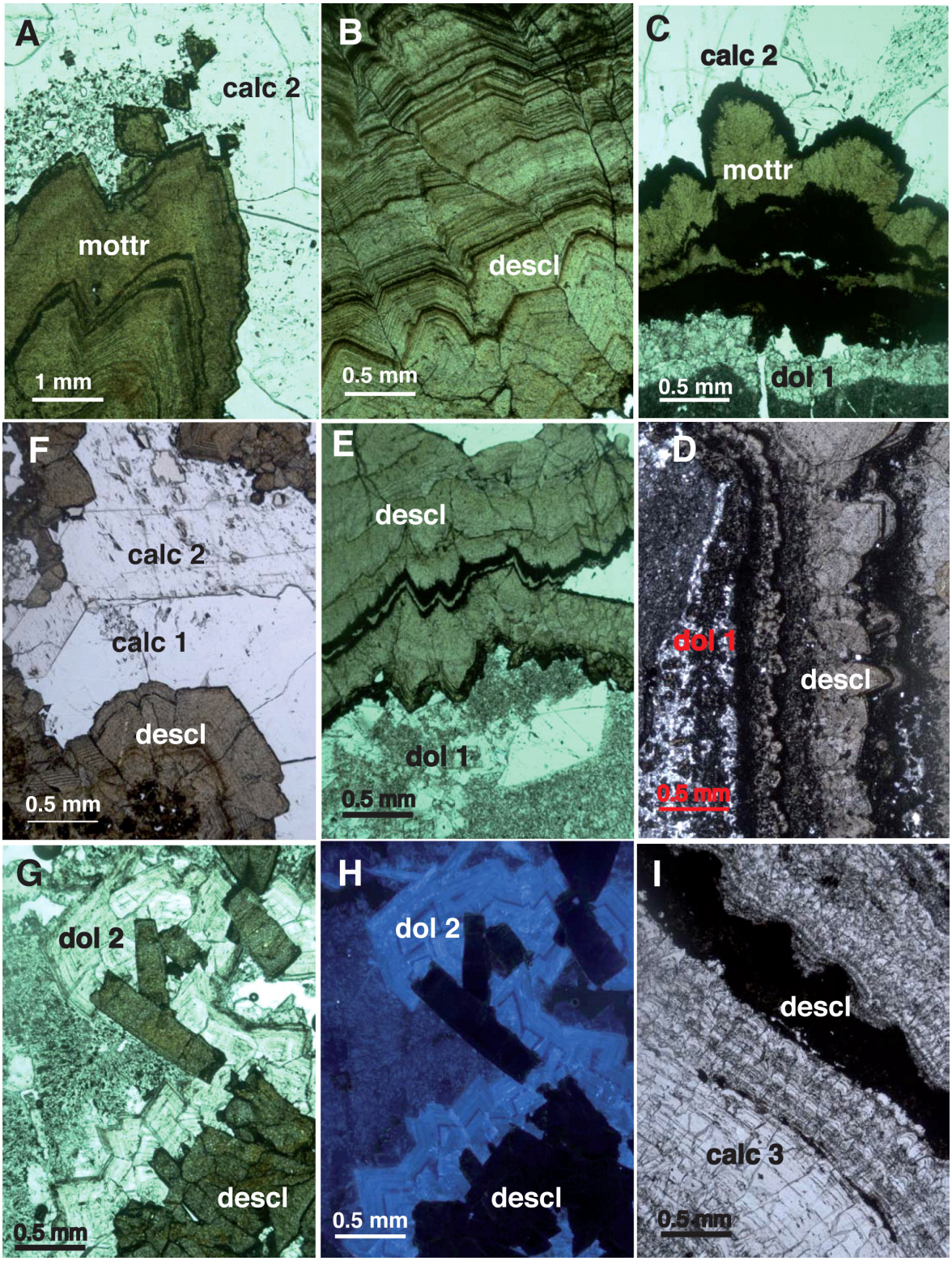

Fig. 6.10 - (A) Zoned mottramite crystals, surrounded by calcite (calc 2). The dark layers have a higher As content than the clear layers (NA.RO.453a, Gross Otavi); (B) Finely zoned Cu-descloizite crystal (NA.RO.432e, Baltika); (C) Poorly zoned, green mottramite growing in a vein (original in Fig. 6.7G) and followed by calcite (calc 2) (NA.RO.452, Gross Otavi); (D) Brownish, zoned descloizite concretions, followed by two generations of calcite (calc 1 and 2) (NA.RO.407, Abenab main pit); (E) Poorly zoned descloizite crusts (NA.RO.432b, Baltika); (F) Brownish descloizite crusts growing on host rock dolomite (left) (NA.RO.434, Baltika); (G) Brownish descloizite crystals, followed by zoned „saddle" dolomite (dol 2) crystals (BA.2003.9, Berg Aukas); (H) same as (G) under catholuminescent light: descloizite is not luminescent, while dol 2 shows a zoned luminescence in shades of blue (BA.2003.9, Berg Aukas); (I) Late generation calcites (calc 3) with thin intercalations of greenish Cu-descloizite (NA.RO.430, Baltika).

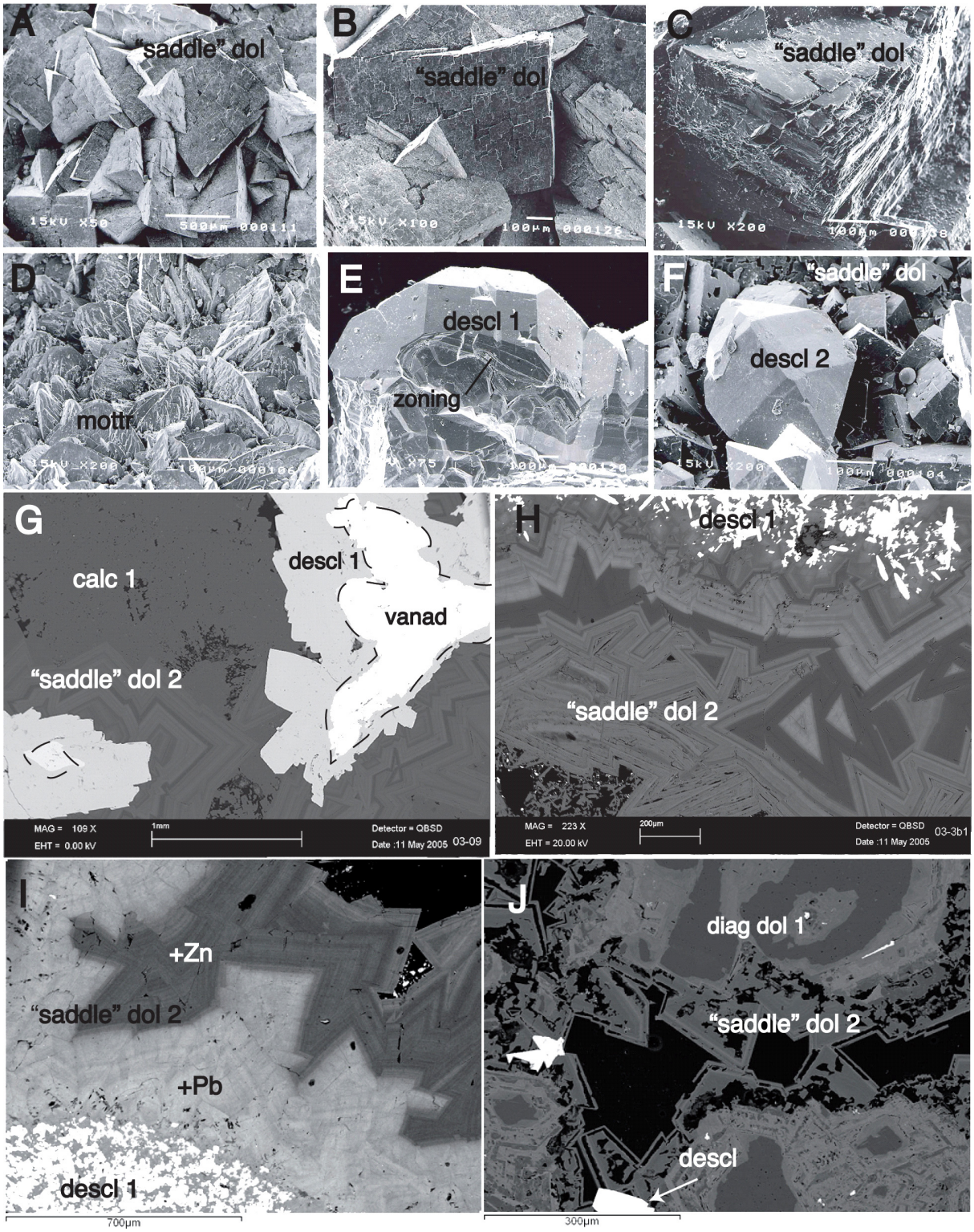

Fig. 6.11 - (A and B) "Saddle"-type dolomite crystals (SEM) (BA.2003.3, Berg Aukas); (C) Zoning in dolomite crystals (SEM) (NA.RO.461, Berg Aukas); (D) Spear-shaped mottramite crystals (SEM) (NA.RO.455, Tsumeb West); (E) Zoned descloizite 1 crystal (SEM) (NA.RO.479, Wolkenhauben); (F) Descloizite 2 crystal growing on corroded „saddle" dolomite 2 (SEM) (NA.RO.450i, Tigerschlucht); (G) Descloizite 1 growing on a nucleus of vanadinite, followed by "saddle" dolomite 2 and then by calcite 1 (EDS) (BA.2003.3, Berg Aukas); (H) Finely zoned "saddle" dolomite 2 (EDS) (BA.2003.3, Berg Aukas); (I) Finely zoned "saddle" dolomite 2 growing on descloizite 1: the dolomite shows two types of bands: Zn-rich (darker) and Pb-rich (clearer) (EDS) (BA.2003.11, Berg Aukas); (H) "Saddle" metal-rich dolomite 2 replacing host rock dolomite 1. Descloizite occurs in resulting porosity (EDS) (NA.RO.478, Wolkenhauben).

6.6.2 Major and trace element geochemistry of vanadate ores and carbonate gangue minerals

Due to their prevailing abundance, we have dedicated most of the analytical work to the descloizite-mottramite series while giving only passing mention to vandadinite. Very high Pb and V contents characterise the vanadate minerals, whereas Cu and Zn contents vary considerably from descloizite (Zn variety) to Cu-descloizite and from Zn-mottramite to mottramite (Cu variety, Table 6.3). All these minerals form a solid solution ranging from the descloizite to mottramite types, with all the varieties in between, as has also been observed in XRD analyses (Table 6.4). The chemical formula $Pb(Zn,Cu)(V,As,P)O_4(OH)$ of this solid solution class of vanadates was identified for the first time by Bannister and Hey (1933). Palache et al. (1951) described its mineralogical class (dipyramidal) and system of crystallization (orthorhombic, 2/m 2/m 2/m). In the mineral lattice of these vanadates there is a complete substitution between the Zn^{2+} (Ionic Radius 0.74 Å) and Cu^{2+} (I.R 0.72 Å) cations, due to the small difference (2.77%) in their ionic radius. However, the total isomorphism between the Zn and Cu end members implies the formal differentiation of the most important members of the series, based on their content in weight % ZnO. According to Millman (1960) this differentiation may be summarised as follows:

- ZnO > 18 wt. %: descloizite
- 18 wt. % < ZnO < 10 wt. %: cuprian descloizite
- 10 wt. % < ZnO < 2 wt. %: zincian mottramite
- ZnO < 2 wt. %: mottramite

The average major element composition of the 15 vanadate ore samples reveals a V content that varies from 10.74 to 11.04 wt. %, while Pb varies from 51.08 to 53.50 wt. % (Table 6.3). The crucial elements Zn and Cu vary in inverse proportion, with Zn values that can reach a maximum of 15-16 wt %. in pure descloizite, and decrease to 12 wt. % in Cu-descloizites. Cu shows maximum enrichment in mottramite (15-16 wt. %) and decreases in Zn mottramite to values of around 10 wt. %. However, Zn is always present in mottramite, often in concentrations below 1 wt. %, and values around 1 wt. % in Cu have been detected in all descloizites. Following Van der Westhuizen (1984, 1986), we correlated the unit cell parameters (derived from XRD analyses) with the chemical composition of the vanadates, with the aim of defining the lattice variation (cell parameters and volume) in the members of the series. Measurements were made on 19 OML descloizite-mottramite samples, which were characterised for chemical homogeneity using a WDS electron microprobe. The chemical analyses of the vanadates and the XRPD results are summarised in Tables 6.3 and 6.4, respectively, and the data plotted in Fig. 6.12. The resulting patterns are very similar to those illustrated by Van der Westhuizen (1984, 1986). In Fig. 6.12A, B and C the relationships between wt. % Cu and the cell dimensions a and c is shown, as well as the relationship between Cu and the volume of the vanadate cell. The clear, though not perfectly linear relationships between the cell parameters and the Cu

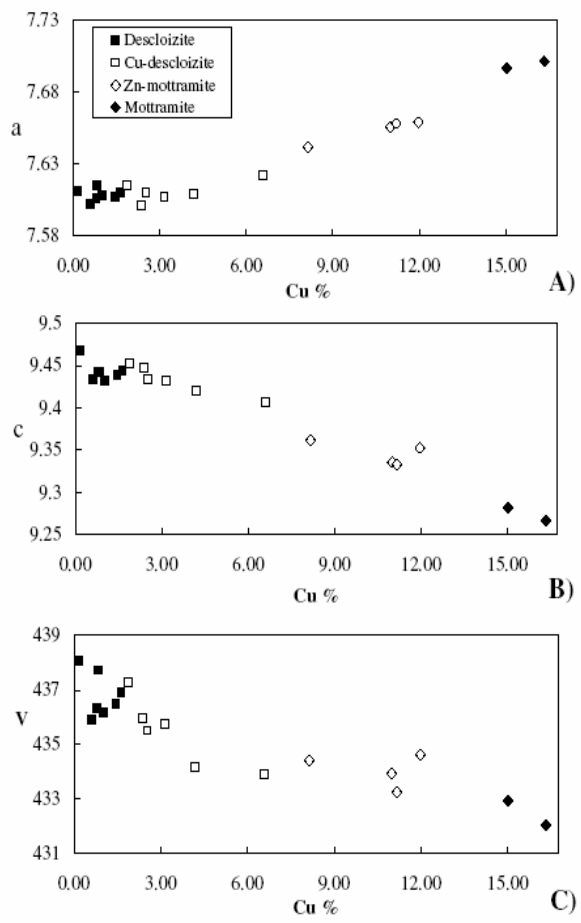

Fig. 6.12 - Correlation between the Cu content (wt. %) of selected vanadates and cell dimensions a (A), c (B) and the cell volume (C), reported in angstrom.

	Zn %	Cu %	Pb %	As %	V %	Ca %	P %	Fe %	Mo ppm	Ni ppm	Co ppm	Cr ppm	Cd ppm	Mn ppm	W ppm	Zr ppm	Y ppm	U ppm
Descloizite																		
NA.RO.407	16,3	0,84	51.89	0.76	10,83	0.11	0,03	0.06	163	109	1	61	11	12	2	23	52	0.5
NA.RO.411b	15,11	1,63	52.39	0.77	10,81	0.06	0,03	0.08	76	128	8	116	18	32	1	31	24	0,24
NA.RO.444a	15,56	1,45	51.08	1.04	10,89	0.31	0,08	n.d.	242	106	6	70	n.d.	n.d.	2	28	4	1
NA.RO.460a	15,79	0,17	53.5	0.09	10,74	0.14	0,01	n.d.	8	8	1	297	337	4	1	1	115	5
NA.RO.462	15,61	0,60	52.57	0.66	10,77	0.12	0,03	n.d.	250	36	4	553	53	11	6	11	13	4
NA.RO.479a(2)	15,93	1,03	51.72	1.81	11,1	0.13	0,04	0.05	158	100	7	215	38	17	3	32	60	1
NA.RO.479c	15,18	1,07	52.33	0.54	11,03	0.05	0,03	0.34	79	196	17	300	44	13	1	54	24	0.5
NA.RO.479d	16,13	0,80	51.62	0.86	11,04	0.09	0,02	0.04	110	173	19	164	47	460	1	11	29	0.5
Cu-Descloizite																		
NA.0803.16	14,37	1,88	48.46	0.54	10,20	0.06	0,02	0.25	10	140	n.d.	150	20	n.d.	n.d	n.d.	n.d.	n.d.
NA.0803.181a	9,18	6,59	52.26	0.92	10,78	0.3	0,04	0.26	150	90	10	270	230	n.d.	n.d	n.d.	n.d.	n.d.
NA.RO.411a	12,25	4,19	52.66	1.72	10,89	0.35	0,08	0.01	170	45	2	481	10	23	2	27	31	1
NA.RO.418	12,98	3,34	51	0.2	10,56	0.34	n.d.	0.24	n.d.	140	n.d.	30	10	n.d.	n.d	n.d.	n.d.	n.d.
NA.RO.419	13.75	1,05	42.45	0.38	9,01	0.18	0,06	0.27	n.d.	120	10	80	10	n.d.	n.d	n.d.	n.d.	n.d.
NA.RO.424	14.34	1,98	51.34	0.57	10,67	0.11	0,02	0.26	n.d.	130	10	90	10	100	n.d	n.d.	n.d.	n.d.
NA.RO.431g	14.02	2,38	51.81	1.36	10,97	0.19	0,05	0.16	52	52	3	113	96	100	1	5	13	0.5
NA.RO.432c	14.05	2,53	51.29	2.96	11,02	0.34	0,07	n.d	162	48	n.d.	148	84	7	9	11	7	1
NA.RO.449b	13.4	3,16	52.43	0.38	11,04	0.12	0,03	0.06	24	114	1	106	41	45	0.0	160	198	0.0
Zn-Mottramite																		
NA.0803.55	6.8	9,36	47.64	1.52	10,21	0.68	n.d.	0.38	40	60	10	450	50	n.d.	n.d	n.d.	n.d.	n.d.
NA.0803.61a	7.65	8,15	48.07	0.95	10,14	0.59	n.d.	0.33	130	60	10	830	40	n.d.	n.d	n.d.	n.d.	n.d.
NA.RO.423b	8.75	6,12	47.9	1.05	9,98	0.42	0,02	1.97	n.d.	90	n.d.	370	20	n.d.	n.d	n.d.	n.d.	n.d.
NA.RO.426	4.05	11,97	48.01	0.61	10,11	1.32	0,01	0.35	n.d.	90	n.d.	860	20	200	n.d	n.d.	n.d.	n.d.
NA.RO.437b	5.95	11,00	52.84	1.3	10,88	0.43	0,02	0.11	141	48	n.d.	991	23	399	2	3	149	2
NA.RO.440	4.69	11,18	49.24	1.37	10,40	1.43	0,05	0.4	170	40	10	1450	210	100	n.d	n.d.	n.d.	n.d.
Mottramite																		
NA.RO.453b	0.65	16,33	52.33	1.63	10,98	0.8	0,06	0.01	123	12	1	375	5	677	0.0	8	209	3
NA.RO.455	0.13	15,02	52.32	0.17	10,75	0.28	0,11	0.07	32	13	4	818	7	572	2	438	303	2

Table 6.3 - ICP-MS analyses of major and trace elements in selected descloizites and mottramites.

(and Zn) concentrations can be attributed to the difference in ionic radii of the two elements resulting in compression or expansion along the crystallographic axes (Van der Westhuizen, 1986). In this regard, the larger ionic radius of copper relative to zinc, might be responsible for the smaller volume of the mottramite cell, compared to that of descloizite (Fig. 6.12C).

Among other major elements, As is present in all samples with values ranging from 0.12 to 1.04 wt % As_2O_3. P is relatively low (from 0.02 up to 0.11 wt. %) and Ca varies from 0.05 to 0.11 wt. %. The average trace element composition of the same samples reveals very high Mo (7-249 ppm, with average of 120 ppm), Cr (61-991 ppm) and Ni (8-195 ppm), whereas Co (max value 19 ppm) and Sb (max value 16.7 ppm) contents are low. Cd (max value 96 ppm) seems to follow the Zn variations while Mn (7-570 ppm) and Fe (100-3400 ppm) are possibly related to the presence of secondary hydroxide/oxide minerals. Zr, La and Y values are quite high: their values range from a few tens to hundreds of ppm. U is relatively depleted in the vanadate ores, ranging up to a few ppm in all samples, with the local exception of descloizite sample BA.2003.10 from the "sand sack" of Berg Aukas (270 ppm U). The high U value in this sample is comparable to the equally high U contents occurring in the Namibian calcretes (Wartha and Schreuder, 1992).

Table 6.2 reports the WDS microprobe analyses of representative crystals of descloizite and mottramite. Samples BA.2003.11 and BA.2003.9 from Berg Aukas show a composition quite close to ideal descloizite, with ZnO around 19.00-19.90 wt. % and CuO well below 1 wt. %. PbO ranges from 55.9 to 57.12 wt. %. Arsenic is ubiquitous, with contents higher than in the bulk chemical analyses, while P and Mo are found in variable amounts (P_2O_5: 0.02-0.5 wt.% and MoO_3: 0.03-0.11 wt. %). The latter data were obtained from sample NA.RO.432e (Baltika), where ZnO is around 19.76-19.95 wt. %, and Cu is slightly enriched (CuO 0.89-1.32 wt. %). As_2O_3 is also relatively high (1.48-

	d1(I_0)(hkl)	d2(I/I_0)(hkl)	d3(I/I_0)(hkl)	a (Å)	± σ	b (Å)	± σ	c (Å)	± σ	cell vol ($Å^3$)	± σ
Descloizite											
Pure member	3,23	2,9	5,12	7,607		6,074		9,446		436,45	
NA.RO.407	3,2265	2,9017	5,1199	7,615	0,011	6,088	0,008	9,442	0,010	437,733	0,739
NA.RO.411b	3,2273	2,9056	5,1196	7,610	0,006	6,080	0,004	9,443	0,005	436,922	0,363
NA.RO.444a	3,2245	2,9044	5,1192	7,607	0,006	6,079	0,004	9,438	0,005	436,486	0,376
NA.RO.460a	3,2289	2,9115	5,1226	7,611	0,006	6,080	0,004	9,468	0,005	438,087	0,363
NA.RO.462	3,2194	2,9055	5,1132	7,602	0,008	6,079	0,005	9,433	0,007	435,913	0,492
NA.RO.479a(2)	3,2263	2,9028	5,1166	7,608	0,005	6,078	0,004	9,433	0,005	436,202	0,336
NA.RO.479d	3,2205	2,9048	5,1114	7,606	0,004	6,075	0,003	9,443	0,004	436,323	0,284
Cu-Descloizite											
NA.0803.16	3,2297	2,9079	5,119	7,615	0,007	6,075	0,005	9,453	0,006	437,268	0,455
NA.0803.181a	3,2261	2,8999	5,0935	7,622	0,004	6,053	0,003	9,406	0,004	433,926	0,272
NA.RO.411a	3,2209	2,9007	5,0972	7,609	0,003	6,057	0,002	9,420	0,003	434,181	0,200
NA.RO.431g	3,2239	2,9048	5,1162	7,601	0,008	6,072	0,005	9,447	0,007	435,961	0,511
NA.RO.432c	3,223	2,9024	5,1031	7,610	0,005	6,066	0,003	9,435	0,004	435,520	0,291
NA.RO.449b	3,2217	2,903	5,1111	7,607	0,004	6,073	0,003	9,432	0,004	435,773	0,280
Zn-Mottramite											
NA.0803.61a	3,2479	2,8838	5,091	7,641	0,005	6,060	0,003	9,362	0,004	434,408	0,297
NA.RO.426	3,2425	2,881	5,0948	7,659	0,008	6,068	0,006	9,353	0,007	434,629	0,534
NA.RO.437b	3,2399	2,8814	5,0947	7,656	0,008	6,071	0,005	9,336	0,007	433,942	0,479
NA.RO.440	3,239	2,8794	5,0902	7,658	0,007	6,062	0,005	9,333	0,006	433,264	0,437
Mottramite											
NA.RO.455	3,2584	2,8671	5,0759	7,697	0,013	6,061	0,009	9,282	0,012	432,939	0,834
NA.RO.453b	3,251	2,8611	5,0687	7,701	0,013	6,054	0,009	9,267	0,012	432,049	0,835
Pure member	3,24	2,87	5,07	7,685		6,020		9,301		430,300	

Table 6.4. Main d value (by intensity), unit cell dimensions and volume of selected vanadates.

3.63 wt. %), as well as CaO (0.21-0.31 Sample NA.RO.453a (Gross Otavi) has all the characteristics of the mottramite end member, with CuO ranging from 17.67 to 20.00 and ZnO from 0.11 to 1.20 wt. %. Arsenic is relatively enriched, ranging from 0.5 to 3.69 wt. %.

In some spots measured on BA.2003.9, vanadinite has also been detected. This mineral has very low Zn (ZnO 1.28 wt. %) and high Pb (PbO 78.22 wt. %). Cu is virtually absent. V is lower than 15 wt.% and As_2O_3 is higher than in the average descloizite samples (1.42 wt. %). After Verwoerd (1957), the vanadinite at Abenab West displays isomorphous replacement of V_2O_5 by almost 3 wt. % of As_2O_5. EDS analyses of descloizite sample BA.2003.9 (Berg Aukas), have shown the presence of a vanadinite nucleus inside the descloizite (Fig. 6.11G), as it was already reported by Verwoerd (1957) for the Abenab mine. In BA.2003.11, also other small solid inclusions of about 10 μm size have been observed inside the descloizite. These inclusions consist of a mineral containing Pb (58-60 wt. %), P (6.35-7.20 wt. %), Ca (4.40-5.50 wt. %) and Cl (2.75 wt. %). Zn can reach 2.10 wt. %. This phase could correspond to a phosphate of the pyromorphite family, where Pb is partially replaced by Ca and by minor Zn.

It is interesting to note that the optical zonation, so common in the OML Zn- and Cu-vanadates, does not correspond to a gross chemical zonation of Zn and Cu, as previously supposed. In fact, Zn and Cu content varies by less than 100 ppm from zone to zone, as also observed by Misiewicz (1988). The strong variability in Zn- and Cu content in the vanadates has been recorded only between samples belonging to genetically distinct generations or even to different mineralised districts. Moreover, from WDS profiles measured on BA.2003.11, NA.RO.432e and NA.RO.453a, the typical zonation of these vanadates seems to be related to the variable (though not abundant as in vanadinite) arsenic content in each zone, which is inversely proportional to the amount of vanadium.

The carbonates associated with vanadate ores consist of both calcite (more common) and dolomite. The main components of Ca carbonates do not vary very much according to ICP-MS analyses. Ca ranges

Sample No.	Carbonate	Ca %	Mg %	Pb %	Zn %	Fe %	P %	Cu ppm	V ppm	Cd ppm	As ppm	Sr ppm	Mo ppm	Ni ppm	Co ppm	Ba ppm	Cr ppm
NA.MA.503	Calcite	36,72	0.44	0,00	0,22	0.02	0.011	2068	n.d	0,4	25	5	0.0	3	0.0	2	n.d
NA.MA.521	Calcite	38,94	0.4	0,27	0,56	0.02	0.054	4	12	12	2	26	0.1	2	0.0	4	1
NA.MA.522(1)	Calcite	36,97	0.37	1,73	0,91	n.d	0.034	92	3506	36	112	23	11	3	1	3	12
NA.MA.522(2)	Calcite	38,31	0.52	0,32	0,83	0.01	0.066	7	8	17	4	29	0.1	2	0.0	5	1
NA.MA.526	Calcite	35,66	0.24	0,65	0,64	0.02	0.05	4	3	39	2	16	0.0	3	0.0	4	1
NA.RO.401	Calcite	38,14	0.12	0,28	0,14	0.02	0.003	2	3	11	1	27	0.0	2	0.0	1	1
NA.RO.430	Calcite	39,02	0.28	0,66	0,95	0.02	0.012	159	1426	87	159	11	0.1	3	0.0	2	5
NA.RO.432c	Calcite	39,01	0.23	0,73	0,21	0.02	0.005	232	1153	591	191	21	2	4	0.0	1	2
NA.RO.437b	Calcite	37,89	0.12	0,02	0,02	0.03	0.002	16	14	34	0,6	14	0.0	4	0.0	0,5	1
NA.RO.439a	Calcite	38,68	0.23	0,02	0,05	0.06	0.005	85	33	266	6	41	0.1	5	0.4	7	1
NA.RO.444d	Calcite	39,44	0.16	n.d.	0,21	0.03	0.012	20	203	23	20	40	0.4	5	0.0	1	1
NA.RO.449b	Calcite	36,44	1.01	0,01	0,46	0.04	0.013	27	16	21	0,5	26	0.0	2	0.0	13	1
NA.RO.477	Calcite	38,22	0.48	0,10	0,08	0.05	0.004	113	198	7	7	10	0.1	4	0.0	4	1
NA.MA.519	Saddle Dolomite	19,21	9.26	5.83	4.83	n.d	0.011	135	4075	820	222	27	26	10	5	3	33
NA.RO.461	Saddle Dolomite	17,76	9.07	6.57	5.08	n.d	0.006	96	1502	n.d	63	31	6	10	2	4	6

Table 6.5 - ICP-MS analyses of major and trace elements in selected V-ore gangue calcites and dolomites.

from 35.66 to 39.44 wt. % and Mg from 0.16 to 1 wt. %. Na is very low (from 0.001 to 0.01 wt. %), as also Fe (from 0.01 to 0.06 wt. %) and Mn (from <1 to 97 ppm). Phosphorus ranges from 0.002 to 0.06 wt. %. The average trace element composition of the same samples reveals relatively high Cu (1.6-232 ppm) and As (2-191 ppm), while all the other metallic elements are in the range of few ppm or ppb. The high Cu value detected in the late calcite from the little Guchab prospect in the Otavi valley, is probably related to microscopic inclusions of secondary Cu minerals. The same could be suspected to explain the highly variable V content (descloizite micro inclusions?) measured in the carbonates (from <2 to 3506 ppm).

Zinc and lead values in the carbonate minerals merit separate evaluation. In the bulk chemical analyses (Table 6.5), Pb is generally very high and varies from 70 ppm (only one sample) to 1.73 wt. % in the zoned, post-descloizite calcites of the Berg Aukas mine. The same variability has been found again at Berg Aukas, also for Zn, ranging from a few hundreds of ppm to 0.91 wt. %. Cd is quite low and does not follow the Zn behaviour. In the ”saddle” dolomites associated with the early descloizite breccias at Berg Aukas, calcium ranges from 17.76 to 10.21 wt. % and Mg from 9.07 to 9.26 wt.%. Also Pb and Zn are in the wt. % range: (Pb varies from 5.83 to 6.57 and Zn from 4.83 to 5.08). Lead seems to substitute partly for Ca and Zn for Mg in these carbonates. Cd is very high and roughly follows Zn (from 820 to >2000 ppm). The same should be said for Mo (5.70 to 25 ppm), Ni, Co, As, Au and Cr, which is an evidence for precipitation of all these metallic elements in reducing conditions in the carbonate lattice. Manganese is very scarce (from 34 to 47 ppm), as is Fe (< 0.1 wt. %). Preliminary EDS analyses of the dolomites associated with vanadate ore at Berg Aukas and Wolkenhauben, have fully confirmed the mentioned values (Fig. 6.11H, I). The analyses reveal also oscillating chemical compositions in the main metallic elements that follow the zonation of the dolomite crystals. Observed in reflected light, the darker bands show higher Zn contents, while the paler ones contain more Pb (Fig. 6.11I). Sample NA.RO.478b from the Wolkenhauben mine has a mixed geochemical signature derived from the coexistence of several dolomite generations. In Fig. 6.11J the replacement of the host rock dolomite (dol 1) by the younger (dol 2) phases is very clear. While the older generations contain only the cations Ca (19.5 wt. %) and Mg (11.40 wt. %), the younger ones, associated with the vanadium minerals, are extremely rich in Zn (from 7 to 11.50 wt. %) and Pb (1.50-3.05 wt. %). In the latter dolomite, Mg and Ca values are proportionally lower: from 6.25 to 8.49 wt. % and from 16.74 to 19.41 wt. % respectively. Zinc replaces Mg while Pb replaces Ca in the dolomite lattice; Cd

irregularly follows the Zn enrichment and can reach values between 0.4 and 0.72 wt. %. In BA.2003.3 (Berg Aukas), the amount of Mg ranges between 7.40 and 9.78 wt. %, while Ca varies between 18.2 and 22.17 wt. %. Lead values oscillate between 2.40 and 6.97 wt. %, Zn between 3.68 and 7.63 wt. % and Cd occurs at 0.40-0.60 wt. %. In BA.2003.11, Mg ranges between 8.59 and 9.70 wt. %, Ca between 17.06 and 20.40 and Zn from 3.04 and 5.30 wt. %. The Pb values in the light coloured bands can be even higher (up to 8.30 wt. %). In some small zones of the dolomite crystals near the boundary with previously deposited willemite, the Cd values can be as high as 1.50 to 3.60 wt. %.

6.6.3 Fluid Inclusions

We could not observe many fluid inclusions in the descloizite-mottramite crystals (due to fine zoning) or in the associated carbonates. The few monophase calcite- and dolomite-hosted fluid inclusions range in diameter from less than 6 µm to up to 18 µm. They occur mostly as isolated inclusions, often along growth zones and less commonly as clusters. For the most part, the inclusions are primary, and only a few of them can be considered as pseudo-secondary and/or secondary. Monophase, possibly liquid inclusions, were also detected in some vanadinite crystals at Abenab West (Verwoerd, 1957): this is a further evidence of vanadinite precipitation under supergene conditions.

The only area in the OML where abundant two-phase fluid inclusions have been found is the old Toenessen prospect and the inclusions were measured in the sparry calcite crystals of a vein that predated the descloizite. The two phases consist of a colourless aqueous liquid and a small vapour bubble with a consistent degree of fill. Homogenization temperatures range from 127 to 230°C, with a mode at 160°C, while ice-melting temperatures are all above 0°C (metastability?). Due to their high HT, it might be possible that the calcite crystals of Toenessen are not associated with the precipitation of the vanadates, but rather with a gangue phase of the primary sulphides, in the interstices of which, descloizite had precipitated.

6.6.4 Oxygen and carbon isotopes

The results of oxygen and carbon isotope measurements on calcite and dolomite samples

Sample No	Description/Paragenesis	$\delta^{13}C_{V\text{-}PDB}$(‰)	± σ	$\delta^{18}O_{SMOW}$(‰)	± σ	$^{87}Sr/^{86}Sr$	± 2σ
NA.RO.401	Sparry Cc with Will in shear	-9,08		20,23		0,71322	0,00002
NA.MA.526	Zoned Cc 3 concretion	-7,35		20,76		0,71143	0,00001
NA.RO.432c	Cc 2 crystals with Des	-8,31		19,84		0,71125	0,00002
NA.RO.444d	Cc 2 crystals with Des	-9,07		21,54		0,70948	0,00001
NA.RO.449b	Cc 1 crystals with Des	-5,13		20,61		0,71237	0,00002
NA.MA.521	Cc 2 crystals post Des	-7,93		20,58		0,71162	0,00001
NA.MA.522(2)	Cc 2 crystals post Des	-8,32		20,66		0,71281	0,00002
NA.RO.409	Cc 1 crystals post Des	-8,13		19,20		0,71071	0,00001
NA.RO.418	Cc 3 crystals post Des	-5,27		21,04		0,71221	0,00001
NA.RO.437b	Cc 2 crystals post Mott	-8,52		20,41		0,71170	0,00002
NA.MA.503	Zoned Cc 3 concretion	-7,31		19,86		0,71298	0,00001
NA.RO.430	Zoned Cc 3 concretion	-7,53		21,13		0,71486	0,00001
NA.RO.439a	Zoned Cc 3 concretion	-8,38		19,85		0,71111	0,00001
NA.RO.477	Cc 1 crystals pre Des	-6,61	0,05	20,43	0,10	0,71064	0,00001
NA.MA.519	Dol 2 with Des	-8,38		22,68		0,71198	0,00001
NA.MA.522(1)	Dol 2 with Des	-7,77		23,49		0,71177	0,00001
NA.MA.520	Dol 2 with Des	-8,40		22,55		n.d.	n.d.
NA.MA.525	Dol 2 with Des	-8,31		22,67		n.d.	n.d.
NA.RO.461	Dol 2 with Des	-8,37		22,65		0,71187	0,00001
NA.RO.478c	Dol 2 (+1) with Des	-7,03	0,03	23,96	0,07	0,71190	0,00001

Cc=Calcite, Dol 2=Saddle Dolomite, Will=Willemite, Des=Descloizite, Mott=Mottramite.

Table 6.6 - Carbon, oxygen and strontium isotope data for gangue calcites and dolomites.

associated to descloizite-mottramite ore are presented in Table 6.6. The $\delta^{13}C$ values of all carbonate minerals are negative and show a moderate range from -9.07 to -5.13 ‰ PDB, with an average value of -7.76 ± 0.05 ‰ (1σ, n = 20). The $\delta^{18}O$ values of the "saddle" dolomite vary between 22.55 and 23.96 with an average value of 23 ± 0.07 ‰ (1σ, n = 6), while calcite yields values between 19.2 and 21.54 ‰ SMOW (average 20.44 ± 0.1 ‰, 1σ n = 14). There is no detectable isotopic difference between calcite generations 1 to 3. The oxygen values of "saddle" dolomites occurring at Berg Aukas and Wolkenhauben are very different from the seawater data for Neoproterozoic dolomites quoted by Jacobsen and Kaufman (1999) and from those of the early diagenetic dolomites (dolomite I) measured by Frimmel et al. (1996a). They overlap only partially with dolomites III and IV described by the latter authors. Gangue calcites yield quite a limited range of oxygen data, not comparable with any of the host rock carbonates mentioned in the OML literature. The 3-4 ‰ enrichment in ^{18}O between calcites and dolomites, is evidence for normal fractionation between both minerals, precipitated from a fluid with similar isotopic characteristics.

6.6.5 Lead and strontium isotopes

Pb isotope data of descloizite/Cu-descloizite (mottramite) samples from selected locations in the OML are given in Table 6.7 and depicted in conventional Pb-Pb biplots in Fig. 6.13. This figure also shows Pb isotopic ratios of associated, primary

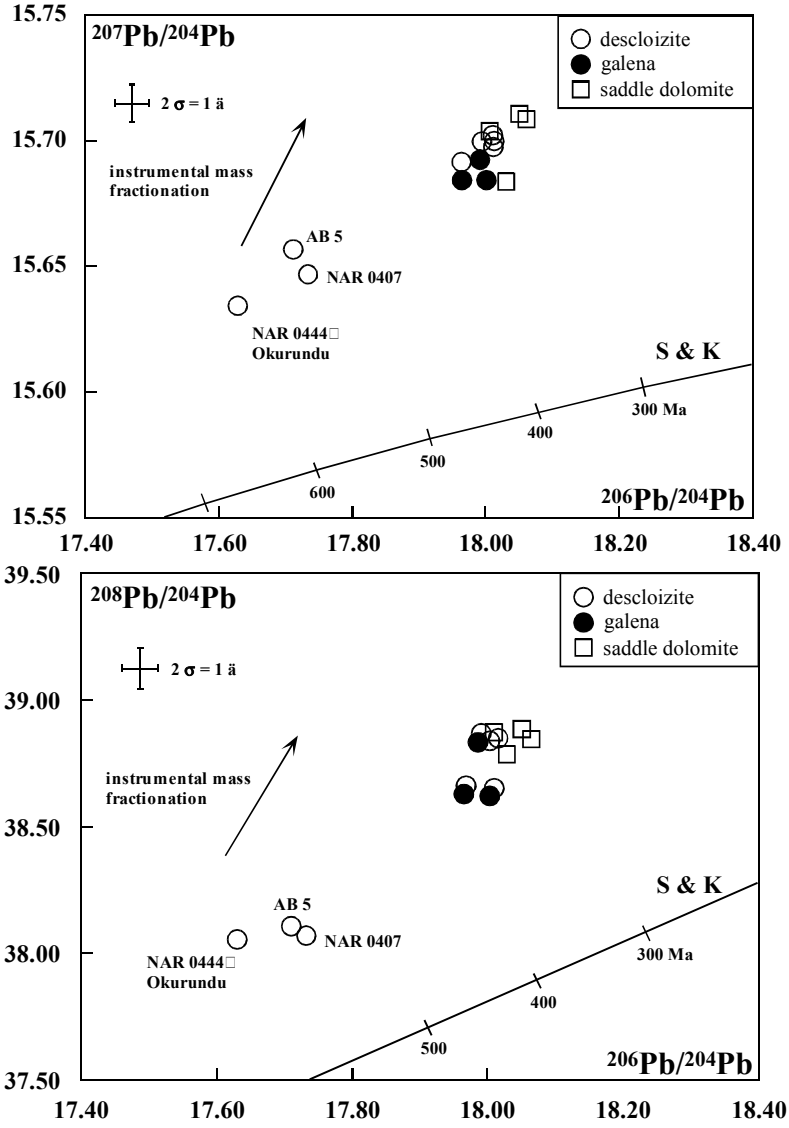

Fig. 6.13 - Pb isotopic composition of descloizite, galena and saddle dolomite samples from vanadate mineralisations.

Sample No	Description/ Paragenesis	Locality	$^{206}Pb/^{204}Pb \pm 2\sigma$	$^{207}Pb/^{204}Pb \pm 2\sigma$	$^{208}Pb/^{204}Pb \pm 2\sigma$
BA 1	descloizite	Berg Aukas	17.995 ± 0.011	15.700 ± 0.014	38.853 ± 0.045
BA 4	descloizite	Berg Aukas	18.007 ± 0.011	15.700 ± 0.014	38.848 ± 0.044
NA.RO.460 a	Cu-descloizite	Berg Aukas	18.009 ± 0.011	15.703 ± 0.014	38.841 ± 0.045
AB 5	descloizite	Abenab pit	17.711 ± 0.010	15.657 ± 0.013	38.106 ± 0.044
NA.RO.407	descloizite	Abenab pit	17.734 ± 0.011	15.647 ± 0.014	38.067 ± 0.044
NA.RO.444	descloizite	Okorundu Pipe	17.630 ± 0.010	15.635 ± 0.014	38.050 ± 0.044
NA.RO.803-16	descloizite	Olifantsfontein	17.966 ± 0.011	15.692 ± 0.014	38.657 ± 0.044
NA.RO.419	descloizite	Uitsab	18.010 ± 0.010	15.699 ± 0.013	38.654 ± 0.044
NA.RO.464 a	galena	Berg Aukas	17.991 ± 0.011	15.693 ± 0.014	38.839 ± 0.044
NA.RO.415	galena	Uitsab	18.003 ± 0.011	15.685 ± 0.014	38.611 ± 0.044
NA.RO.80307	galena	Olifantsfontein	17.966 ± 0.011	15.685 ± 0.014	38.634 ± 0.044
NA.MA.512	Dol 2 (saddle) with descloizite	Berg Aukas	18.009 ± 0.004	15.702 ± 0.004	38.861 ± 0.013
NA.MA.519	Dol 2 (saddle) with descloizite	Berg Aukas	18.053 ± 0.008	15.710 ± 0.007	38.874 ± 0.019
NA.MA.522	Dol 2 (saddle) with descloizite	Berg Aukas	18.062 ± 0.004	15.709 ± 0.004	38.849 ± 0.010
NA.RO.461	Dol 2 (saddle) with descloizite	Berg Aukas	18.030 ± 0.004	15.684 ± 0.004	38.788 ± 0.010

Table 6.7 - Pb isotope analyses of descloizite, galena and saddle dolomite samples from vanadate mineralisations.

galena for three of the deposits. All data points plot well above the average crustal Pb evolution curve of Stacey and Kramers (1975), indicating crustal source rocks containing lead components which evolved in ancient, cratonic reservoirs (Pb growth dominated by ^{235}U decay) and possibly lower crustal domains with elevated Th/U ratios. Descloizite samples from the Abenab and nearby Okorundu deposits display the lowest radiogenic lead ($^{206}Pb/^{204}Pb$ = 17.63 - 17.73), clearly different from the values obtained for descloizites from the Berg Aukas, Olifantsfontein, and Uitsab deposits. These form a tight cluster with $^{206}Pb/^{204}Pb$ = 17.96 - 18.01 in both Pb-Pb diagrams. This may either reflect a time sequence (i.e., derivation of lead from the same source lithologies during different mineralisation periods), or different lead sources for each area at the time of mineralisation, or a combination of both. Where vanadates and primary sulphides from the same deposit were analyzed, their Pb isotope signatures are identical within errors, indicating that the Pb in vanadates derives from their sulphide precursors. Pb isotope ratios of "saddle" dolomite associated with the vanadates at Berg Aukas also display values very similar to the galena and descloizite ores. Small, remaining differences may be attributed solely to instrumental mass fractionation effects.

Strontium isotope data (Table 6.6) of the calcite and dolomite gangue accompanying the vanadate ores, show a large spread of $^{87}Sr/^{86}Sr$ values from 0.709 to a maximum of 0.714. The "saddle" dolomites from Berg Aukas and Wolkenhauben have comparable $^{87}Sr/^{86}Sr$ values between 0.7117 and 0.7120. With few exceptions, the Sr concentration in most samples is lower than 50 ppm, very different from the high concentrations given by Chadwick (1993) for the host carbonate rocks at Berg Aukas (between 70 and 170 ppm in both diagenetic and hydrothermal dolomites). The $^{87}Sr/^{86}Sr$ values also differ from most carbonate categories reported by Allsopp and Ferguson (1970), Chadwick (1993) and Frimmel et al. (1996a). In these studies, the $^{87}Sr/^{86}Sr$ values of the early and late diagenetic dolomites generally range from 0.708 to 0.712, while recrystallised and hydrothermal dolomites associated with sulphide ores have much higher isotopic ratios ($^{87}Sr/^{86}Sr$ up to 0.715 - 0.718).

Sample	He (ncc/g)	U (ppm)	Th (ppm)	Age (Ma)	±2σ
NA.RO.411b Harasib 3	755	0.15	0.23	26.70	1.60
NA.RO.450h Tigerschlucht	2370	0.66	0.21	29.60	1.20
BA.2003.10 Berg Aukas ("Sand Sack" type)	11180	180	0.23	0.37-1.42	0.08-0.16

Note that the precision of the isotopic ratios is typically between 0.5 and 1.5%. Spiked standard solutions yielded mean $^{235}U/^{238}U$ of 0.6970 and $^{230}Th/^{232}Th$ of 0.2554. Age and helium contents given are mean weighted average of n=3.

Table 6.8 - Preliminary (U-Th)/He Thermochronometry results for OML descloizite.

6.6.6 (U-Th)/He thermochronometry

In order to constrain the possible timing of vanadate mineralisation, we have performed preliminary (U-Th)/He analysis (Zeitler et al., 1987; Wolf et al., 1996; Farley et al. 2002; Reiners and Ehlers, 2005) on descloizite sampled from several old mines and prospects (Table 6.8). The (U-Th)/He ages from the OML descloizites fall into two main categories. The first interval, reflected in samples from Tigerschlucht and Harasib 3 are in the 26-30 Ma range, while a sample of Berg Aukas (BA.2003.10, "Sand Sack" type) yielded a series of young ages ranging from 0.35-1.42 Ma. Extreme U enrichment (up to 270 ppm U) was observed in the latter sample. Preliminary results from the Wolkenhauben prospect and from the Abenab main pit may indicate an older period of descloizite formation (40-60 Ma), but this needs to be confirmed.

Preliminary diffusion experiments carried out on the Tigerschlucht descloizite, indicate a closure temperature of 70°C ± 10 °C (assuming a cooling rate of 10°C/My) (Fig. 6.14). This result is by no means robust, but may suggest that the (U-Th)/He ages obtained on the OML vanadates approximate formation ages. If the supergene fluids had quite low temperatures and the area has not been subjected to later heating events (hydrothermal?), then these descloizite crystals have been retaining helium since their formation. More work is being carried out to validate the diffusion experiment results.

6.7 Discussion

6.7.1 Comment on earlier genetic concepts

From the first discovery of the vanadium ores, widely differing opinions on their origin were published (Schwellnus, 1946), and continuously modified to keep pace with the new data derived during deposits exploitation. The most common genetic concepts were: 1) vanadium ores are of hydrothermal origin, and 2) vanadium ores were formed as a consequence of supergene processes (given that this element should have originated either from the primary sulphides, or from the surrounding sedimentary rocks).

The hydrothermal theory was not very popular (an exception being Schneiderhöhn, 1929), considering the absence of alteration around the deposits, the obvious

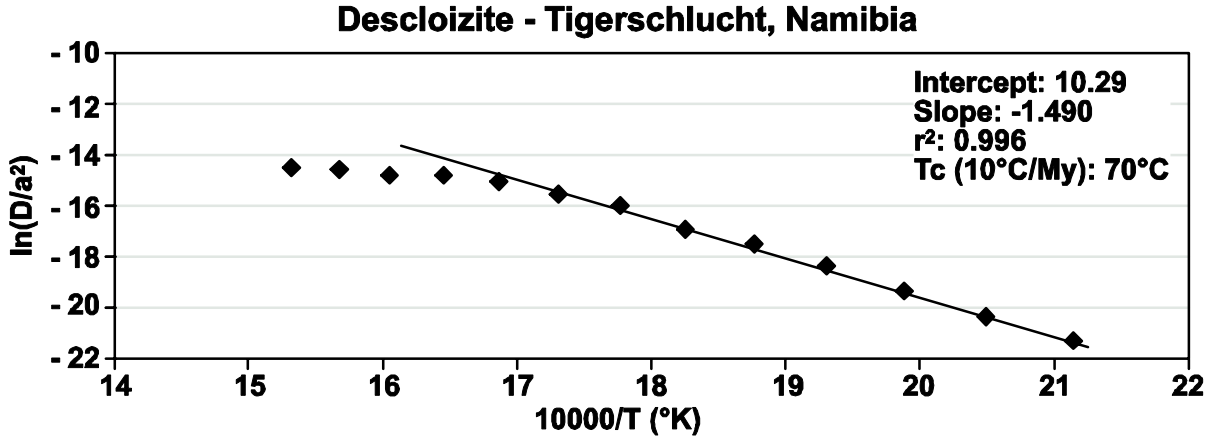

Fig. 6.14 - Arrhenius plot for descloizite step-heating experiments. The sample (descloizite from Tigerschlucht) consisted of abraded 250-350 µ grains, similar to those used for the dating experiments. Steps were at 15°C intervals from 200°C through 380°C. Heating times varied from 8 hours to 1 hour. The fraction of helium released at each stage varied from 1-50 % of the total helium in the sample.

relationships between the vanadate ores and the karstic topography, their proximity to other nonsulphide deposits and the progressive disappearance of the economic concentrations with depth (Schwellnus, 1946; Verwoerd, 1957; Van der Westhuizen, 1984). However, some characteristics of the ores, such as the perfect crystal habits, their frequent occurrence with calcite in veins and geodes, as well as their local association with "saddle"-type dolomite, may have given credence to the hydrothermal hypothesis. An interesting theory presented by Korn and Martin (1937) stated that the vanadate mineralisation was associated with fluids related to Cretaceous sodic magmatism, circulating along north-northwest structural disturbances. However, considering the supergene theory to be most viable for the genesis of the vanadates, we should assume that vanadium in both sulphides and sediments was taken into solution by the ground waters and carried away from the source to be precipitated in favourable sites (cherts and/or shale barriers etc.) with base metals and As, which had been liberated by weathering processes (Schwellnus, 1946). As proposed by Verwoerd (1957) and Van der Westhuizen (1984), vanadium was probably transported as calcium metavanadate $Ca(VO_3)_2$, which then reacted with the metal ions. This must have been a slow process, as shown by the layering in the vanadate crystals. Calcium set free by this reaction may also explain the preferential association of calcite with the descloizite-mottramite series. The local association with dolomite was only cursorily mentioned, and never satisfactorily explained. The primary factors governing the oxidation state and the resulting type of V ions, are pH and Eh. Van der Westhuizen (1984) assumed that the pH of the environment did not change with time and was controlled by the carbonates. However, in the areas where sulphide weathering occurs, pH can vary dramatically, as well as during periods when drastic climate changes take place.

Based on the observation of the secondary mineral assemblages, which are similar to those of the arid regions of South-western United States and South America, Verwoerd (1957) stated that the OML had experienced a period of relative aridity in a not too distant past. Whereas this climate was not particularly favourable to the weathering of primary sulphide ores and their host rocks, it was certainly an important factor for the precipitation of the vanadates, especially for the early deposited vanadinite, a chlorine-bearing mineral. However, the precise timing of vanadate mineralisation in the OML is poorly understood. The only reliable ages so far are those reported by Pickford (1993; 2000) for the vanadates occurring in some karst fillings, which are paleontologically constrained to the Middle to Upper Miocene and Plio-Pleistocene. However, there are still many deposits, like Abenab or Wolkenhauben, which could not be dated, due to lack of fossil content.

6.7.2 A mineralisation model

It has been known for long that the vanadate deposits of the OML are not limited to a distinct geological formation of the Neoproterozoic carbonates (Table 6.1, Fig. 6.1), but occur throughout the Otavi Group (Schwellnus, 1946). There is a close relationship between vanadate ores and the locally deep paleokarst network associated to the post-Gondwana land surface, which shows various degrees of filling. Moreover, the V concentrations seem to be closely spaced along barriers like chert or shale horizons, and are often controlled (directly or indirectly) by late-Pan-African, locally reactivated, structural features (Raab et al., 2002), which seem to have determined the position and the form of the karstic network. There is also a distinct marginal relationship between the most important V concentrations and the Pb-Zn-Cu sulphide/nonsulphide orebodies throughout the OML (Schwellnus, 1946).

Most vanadates are characterised by variable composition, primarily in their Cu (mottramites) and Zn (descloizites) contents. This variability occurs on the regional and on the deposit scale and roughly mirrors the original composition of the primary sulphide deposits in the same area (Van der Westhuizen et al., 1984; 1988). On the contrary, the differences in colour and pleochroism at the crystal scale (zoning), reflect only slight compositional changes (local replacement of V by As in some zones). The zones reflect a prolonged period of formation, and the cyclical changes of the depositional parameters.

The vanadates of the OML occur relatively late in the paragenetic and diagenetic history of the region. Vanadinites, descloizites and mottramites follow not only the deposition of the sulphide ores (some of which are showing clear signs of deformation due to the late Pan-African movements), but also the main phase of willemite formation in the Berg Aukas, Abenab West and Baltika areas (Verwoerd, 1957). The

willemite has a minimum age of 499-493 Ma (Part 5). Therefore, it seems evident that a considerable time gap exists between the deposition of the bulk of the Zn silicates and that of the vanadates. This is also the case for the willemite-vanadate purely "geometrical" association in the Kabwe (Zambia) mineral district (Kamona and Friedrich, 1994, and field observations by M. Boni). Among the OML vanadates, vanadinite always predates descloizite (Verwoerd, 1957; Cairncross, 1997, Fig. 6.11G), while several generations of calcite (calcite 1 and 2) can be associated with each of the later vanadate mineral phase. The "saddle" dolomite (dolomite 2), growing with (or shortly after) descloizite, in the deeper karst breccias of Berg Aukas and at Wolkenhauben, is a rather unusual cement, whose presence has never been seriously discussed in the OML before. The current literature (Radke and Mathis, 1980; Machel, 2005) suggests that "saddle" dolomite requires minimum temperatures of 60-80 °C and reducing conditions in order to precipitate. This type of dolomite is generally associated with burial and/or hydrothermal processes (Machel, 2005). However, "saddle" dolomites seem to have precipitated in the OML at low temperature, as evidenced by the absence of two-phase fluid inclusions, which could not be generated even on freezing. The late calcite generation (calcite 3), consisting of aragonite-like crusts, bands and cave cements, is quite widespread throughout the OML, where it follows the last phases of nonsulphide mineralisation. This calcite generation, with few exceptions (Baltika), has a very limited association with the precipitation of vanadate ores.

The paragenetic position of other nonsulphide minerals relative to the vanadates, such as smithsonite, cerussite etc., is unclear, especially in areas crucial to the understanding of the different oxidation stages, like Tsumeb. There is no doubt that the main depositional phase for these and other secondary, fairly exotic minerals, together with late willemite needles, is syn- or even post-descloizite (Berg Aukas, Abenab West, Guchab etc.). However, there is a compelling evidence that a strong oxidation phase, which also produced Fe(-hydr)oxides and possibly the bulk of the vanadinite, took place before the precipitation of the main vanadate mineralisation (Verwoerd, 1957). Once the vanadates had crystallised, they remained as such and were not redissolved by post-depositional solutions. Later phases seem to form by precipitation from younger solutions, or by physical comminution of primary vanadate ores (Schwellnus, 1946).

To determine the precipitation mechanism and the genesis of the vanadate ores in the OML, it is critical to characterise the nature of the fluids associated with them, and to understand the origin of vanadium and metals involved in the mineralisation process. The origin of the main elements in the vanadates has been investigated through evaluation of the geochemical background of the OML, and by comparing the Pb isotope signatures of the vanadium ores with their associated possible sulphide precursors. It was not possible, either through fluid inclusion or isotopic analysis, to directly determine the nature of the fluids responsible for vanadate precipitation. Therefore, our studies have been carried out on the gangue carbonates that are closely associated with the vanadium minerals throughout the whole district.

It is well known that combining microthermometry and O isotope data on calcite and dolomite enables researchers to characterise the O isotope composition of the corresponding primary fluids. Conversely, by knowing the O isotope composition of the latter as well as the isotopic ratio of the carbonates, a rough estimate of their precipitation temperature can be obtained (Taylor, 1974). While the current $\delta^{18}O$ of the meteoric waters in the OML has a value around -11 ‰ SMOW (Gilg et al., 2004) the $\delta^{18}O$ of the weathering fluid during the main oxidation phases in the same area, deduced from the analysis of Tsumeb supergene kaolinites, was not lower than -7 ‰ SMOW (A. Gilg, pers. comm., 2005).

If we assume that these values are a proxy for the parent (meteoric?) fluid, we can calculate, using the fractionation equation of Friedman and O'Neil (1977), for most calcites associated with the vanadates a formation temperature of between 30 and 50°C. This is quite reasonable considering the general lack of two-phase inclusions in all samples but one. Precipitation temperatures lower than 50 °C are suggested by primary, all liquid fluid inclusions in most calcites. It is quite peculiar, however, that in some mines, such as Berg Aukas and Wolkenhauben, a metal-rich, "saddle"-type dolomite, again bearing only monophase liquid-filled inclusions, occurs as the chief gangue mineral of the vanadates, instead of calcite. Owing to the imprecision of the isotopic parameters for low-temperature dolomite, we cannot be as confident of the formation temperatures for the latter, as we are for calcites. However, using the compilation of Land (1983) as a guide, we could calculate a hypothetical

precipitation temperature also for the dolomite of approximately 30-40 °C. This would contradict current empiric models (Radke and Mathis, 1980; Machel, 2005), suggesting that "saddle" dolomite requires minimum temperatures of 60-80 °C to precipitate.

In summary, most calcite (and probably also the dolomite) precipitated from moderately low temperature fluids with a meteoric water signature (Lohmann, 1987), suggesting that the study area was subjected to deep circulation of slightly heated meteoric fluids at the time of carbonate and vanadate precipitation. Gilg et al. (2004) recorded similar values in several secondary Cu and Pb minerals from the Tsumeb oxidation zone. Moreover, in all carbonates the constant negative $\delta^{13}C$ values point to a strong input of biogenic carbon (from soils, dominated by the decay of C3 plants, and/or paleokarst infills rich in organic matter, Lohmann, 1987) during precipitation of calcite and dolomite. Such negative carbon values have never been reached in the Proterozoic host carbonate rocks, even in the strongly negative diamictite horizons of the Chuos and Ghaub Formations ($\delta^{13}C$ = -5/6 ‰ PDB, Kaufman et al., 1991; Frimmel et al., 1996a; Hoffman et al., 1998; Halverson et al., 2002). However, strongly negative $\delta^{13}C$ values have been reported by Frimmel et al. (1996a) in the vicinity of the Kombat mine in the Otavi valley. Again, these negative carbon values occur both in post-tectonic calcite veins (from -1.8 to -6.4 ‰ $\delta^{13}C$), which are associated with secondary mineralisation and in other coarse brown calcites occurring in the karst fillings ($\delta^{13}C$ = -1.2 to -9.0 ‰). Hughes (1987) also mentioned strongly negative $\delta^{13}C$ values ($\delta^{13}C$ = -8 to -11.9 ‰) in the supergene calcites from Tsumeb, including the calcite growing in the karstic aquifer of the North Break Zone (Lombaard et al., 1986). Again negative $\delta^{13}C$ values (-8.81 to -5.53 ‰) have been quoted by Deane (1993) for the possibly supergene vein calcites sampled at Baltika and in the nearby Guchab and Schlangental prospects. The vanadate ores of OML are therefore related to deep continental weathering involving meteoric waters, which locally display elevated chloride activities (necessary for vanadinite precipitation).

It can be deduced from our Pb isotope data (Fig. 6.13) that the metals contained in the primary sulphide deposits most likely originated from old, cratonic crustal sources, possibly located in the Paleoproterozoic basement. The Abenab and Berg Aukas deposits display clearly distinct Pb isotope signatures, with Abenab having significantly lower Pb isotope ratios than Berg Aukas. This may be explained by different ages of the primary sulphide mineralisations at these locations, or, alternatively, the by the lack of lithologies that could have supplied radiogenic lead at Abenab. The oxidised ores in the OML, and among them the vanadates, do not reflect any input of lead derived from external sources. Their Pb isotopic composition is identical to that of their sulphide precursors, which indicates that lead was remobilised from primary sulphides during formation of the Zn/Cu-vanadates. Also, the "saddle" dolomites accompanying the vanadate ores, which are strongly anomalous in base metals, have Pb-isotopic signatures congruent with the metal ores. However, though the lead content in the descloizite-mottramite series of vanadates does not change, the ratio of Cu/Zn in the latter minerals corresponds to the known ratios of the same elements in the primary sulphides (if present in the area) and/or in the country rock around the vanadate ores (Van der Westhuizen et al., 1984; 1988). Therefore, mottramite and Cu-descloizite are particularly abundant around Cu sulphide deposits (as in Tsumeb West or Gross Otavi), while descloizite occurs in the areas surrounding primary sphalerite (-willemite) orebodies, such as Berg Aukas and Baltika.

Unlike Zn, Pb and Cu, V is contained only in small quantities in the primary sulphides (Melcher, 2003) and its source has instead been sought in the Grootfontein Mafic Body (Verwoerd, 1957), in the clastic Nabis Formation and in the shales intercalated in the Neoproterozoic carbonates, which show a rather anomalous V content (from 140 to 250 ppm, Van der Westhuizen, 1984 and own measurements). Geochemical studies (Part 3) reveal very high vanadium values in the magmatic rocks of the Grootfontein Mafic Body (GMB) (up to 320 ppm V in the gabbros and diorites around Berg Aukas and Abenab), as well as in the Askevold metavolcanites (up to 200 ppm), which also contain V-rich magnetite. However, the latter mineral is not very susceptible to weathering and therefore, the most appreciable source of vanadium is likely to have been either the mafic minerals (biotite, hornblende) from the basement or the newly formed clays in the shales originating from weathered basement. Arsenic shows a rather odd behaviour: its origin is the same as the other metals from the primary sulphides, the element occurring quite abundantly in tennantite associated to the Tsumeb-type orebodies. However, in the secondary

mineralisation phase, most As does not form its own oxidation minerals (with the rare occurrence of late mimetite), but enters a solid solution with V in Zn/Cu-vanadates.

The Sr isotope data for carbonate gangue minerals indicate that in most cases the calcite and dolomite cements associated with the vanadates have inherited their Sr from the host dolomites where the supergene solutions have circulated, with some local contribution of radiogenic Sr from the hydrothermal dolomites associated with primary mineralisation. In some cases, the Sr signature may have been inherited directly from Proterozoic shales or also from the Paleoproterozoic basement.

6.7.3 Timing of vanadate mineralisation

The genesis of the vanadates is strictly related to the geomorphological setting of the OML and to the prevailing climate at the time of mineralisation. Therefore, for a better understanding of this ore forming process, it is crucial to determine its absolute age. As already mentioned, the only dating of the vanadate ores so far has been performed using paleontological methods (Senut et al., 1992; Pickford, 1993, 2000) at several mineralised sites. The vanadate cements (mainly descloizites) are associated with breccias containing fossil remnants ranging from Middle to Upper Miocene at Berg Aukas, Upper Miocene at Harasib 3 and Pleistocene in the uppermost levels of Berg Aukas and at Rietfontein.

Our preliminary U-Th/He data have roughly confirmed the Tertiary age for the bulk of ore deposition, but indicate an interval of mineralisation at 26-29 Ma and perhaps another in Pleistocene times. Reproducibility on the young sample was poor but if substantiated by further analysis, the young ages may suggest either a Pleistocene formation age or partial resetting of helium ages by a more recent heating event. However, given the preliminary closure temperature of 70°C for the Tigerschlucht descloizite and the lack of evidence for recent high temperature fluid circulation throughout the site, it is perhaps more likely that the 26-29 Ma and the Pleistocene ages reflect distinct periods of descloizite formation.

The ages determined here, point to times where arid conditions prevailed in northern Namibia. In addition, similar ages have been determined for a descloizite sample from the Kabwe (Broken Hill) mine in Zambia (26 Ma ± 0.84, unpublished data), perhaps indicating a regional climate effect. Using these preliminary ages, the formation of the OML vanadate deposits can be chronologically framed within the geomorphic evolution of Northern Namibia, from the end of the Mesozoic throughout the Tertiary. Between the Cretaceous and Eocene, the climate was relatively hot and humid, thus favouring intense weathering and erosion and the development of a deep karst network in the carbonate terrains of the OML. A reasonable amount of vanadium could have been supplied from the shales of the Otavi Group, the siliciclastics of the Nosib Group, and eventually from the mafic rocks of the Paleoproterozoic basement. Base metals and As were mobilised from the primary sulphides during prolonged oxidation stages. Deep weathering processes during this period also caused the supergene Zn enrichment exploited at Skorpion, in the Gariep Belt of southern Namibia (McConachy et al., in press). The end of the Cretaceous and Eocene saw Namibia transected by an ample planation surface. It is known in literature as the “African surface” (related to the African Erosion Cycle, Partridge and Maud, 1987), whose traces are recorded in several areas of the OML. The deepest levels of the karst nework started to be filled with detrital and chemical sediments; the first collapse breccias started to accumulate and to be cemented by several generations of silica and carbonates. An evolution towards more arid climates started in Namibia during the Oligocene, and lasted - with short intervals - up to the present. This evolution towards greater aridity was made irreversible during the Middle Miocene because of the inset of the cold Benguela current (Wateren and Dunai, 2001), which caused the formation of the Namib and then the Kalahari deserts. During these periods, chemical weathering was extremely limited, the denudation values of the previously uplifted zones stayed very small and conditions favoured precipitation of several generations of nonsulphide minerals (including vanadates) in the previously established porosity network.

A similar evolution, where already deposited ores (Mn-Fe) in Proterozoic dolomites have been modified through the African Erosion Cycle, can be traced also in other areas of southern (Beukes et al., 1999; Van Niekerk et al, 1999; Pack et al. 2000) and western Africa (Colin et al., 2005). In South Africa, several supergene ferromanganese wad deposits developed as a deep weathering profile in the Neoarchean Malmani Dolomite (Beukes et al., 1999). The wad formed

probably during the late Cretaceous-Early Tertiary African Erosion Cycle, when conditions were humid and warm. Later the climate became more arid and pediment deposits formed during Late Tertiary. 40Ar/39Ar dating of cryptomelane concretions below the Africa I erosion surface (Partridge and Maud, 1987) gave ages ranging from 15 to 12 Ma (Van Niekerk et al. 1999). Pack et al. (2000), described the manganese wad at Ryedale (South Africa) as consisting of ore weathered during the African Erosion Cycle from manganiferous Karoo sediments, which fill a karst network in the Malmani dolomite. Using the $\delta^{18}O$ values of goethite in duricrusts (-1.3 / -1.1 ‰ SMOW), which should have precipitated in equilibrium with meteoric waters during Tertiary at temperatures between 15 and 25°C, the authors calculated for these waters a $\delta^{18}O$ value ranging from -7.1 to -8.6. These values are very similar to those calculated by Gilg et al. (2004) from the kaolinite of Tsumeb, which we have applied to the temperature evaluation of the OML gangue carbonates.

Colin et al. (2005) also detected several age intervals affecting the precipitation of the Mn-lateritic pisolites in Western Africa (Burkina Faso), in relation to the evolution of the African Landsurface. $^{40}Ar/^{39}Ar$ dating of cryptomelane concretions in lateritic crusts has resulted in three main age intervals: 56-59 Ma, 44-47 Ma and 24-27 Ma. The first two ages coincide with the Lower Tertiary "greenhouse"-related weathering period (producing in the country the main bauxite deposits), while the third age may represent a moderate and transitory humid event in a cycle of major aridity, which started in Western Africa at the beginning of the Oligocene.

6.8 Conclusions

The Zn-Pb-Cu vanadate ores, hosted in the OML carbonates of the Otavi Supergroup in Namibia, are genetically related to the most important erosional episodes of the "African Cycle", which took place after the Atlantic rifting. The "African Cycle" spanning the period from the end of Cretaceous to Pleistocene, was controlled by the complex tectono-morphological and climatic evolution of the southern part of the African continent.

The vanadate ores represent a special type of low-temperature, weathering-related mineralisation, deposited during periods of extreme aridity and are clearly distinct in age from the primary sulphides as well as from secondary nonsulphide Zn-Pb concentrations. However, the temperature range of ore deposition and the stable isotope ratios measured in the accompanying carbonates, are very similar to the values found in the minerals of the oxidation zone at Tsumeb. Our study indicates that vanadate deposits of the Otavi Mountainland formed in several stages, during circulation of partly heated meteoric waters (40-50°C) within a karstic network hosted in Proterozoic dolomites. The source of vanadium is thought to be primarily the siliciclastic country rocks of the OML, as well as the mafic rocks of the Paleoproterozoic basement. Base metals and As were derived from primary sulphide deposits undergoing oxidation. The age of vanadium mineralisation spans from Eocene to Pleistocene ((U/Th)-He thermochronology), or it may be limited to few Miocene stages (paleontology). It will be interesting, therefore, to confirm if these differences are real, or if they are due to the discrepancies between two very different methodologies.

Uncertainties are also raised by the slightly elevated temperature (40-50°C) deduced from isotopic analysis of the gangue carbonates, and also confirmed by direct fluid inclusion measurements of the oxidation minerals at Tsumeb (Gilg et al., 2004). This thermal anomaly could be due to the deep precipitation environment (well below 700 m) of the carbonate gangue of the vanadates (Berg Aukas) and of the nonsulphide minerals (Tsumeb) in a "normal" phreatic karst regime. However, it may also reflect the extension of a late Tertiary (20-10 Ma) thermal event into north-eastern Namibia, involving advection of moderately hot fluids or a regional thermal gradient higher than present (30°C/km), similar to that recorded along the West African coast in Angola (Jackson and Hudec, 2005).

Acknowledgements

We want to thank V. Petzel (Geological Survey of Namibia) and A. Günzel (Ongopolo) for their help during the sampling in OML. We thank A. Thomas and C. Scadding for assistance on the Agilent 7500CS mass spec. We are also grateful to B. McDonald for largely developing the descloizite thermochronometry protocols and to F. Melcher (BGR) for helpful discussions.

References

Ahrendt, H., Hunziker, J.C., Weber, K., 1978. Age and degree of metamorphism and time of nappe emplacement along the southern margin of the Damara orogen, Namibia (SW-Africa). Gelogische Rundschau, 67: 719.

Ahrendt, H., Hunziker, J.C., Weber, K., 1978. Age and degree of metamorphism and time of nappe emplacement along the southern margin of the Damara orogen, Namibia (SW-Africa). Gelogische Rundschau, 67: 719.

Ahrendt, H., Behr, H.J., Clauer, N., Hunziker, J.C., Porada, H., Weber, K.., 1983. The Northern Branch; depositional development and timing of the structural and metamorphic evolution within the framework of the Damara Orogen. In: H. Martin, Eder, F.W. (Editor), Intracontinental Fold Belts - Case studies in the Variscan Belt and Damara Belt, pp. 723-743.

Alkmim, F.F., Marshak, S., Fonseca, M.A., 2001. Assembling West Gondwana in the Neoproterozoic; clues from the Sao Francisco Craton region, Brazil. Geology, 29(4): 319-322.

Allsopp, H.L., Ferguson, J., 1970. Measurements realting to the genesis of the Tsumeb Pipe, South West Africa. Earth Planet. Sci. Lett., 9: 448-453.

Allsopp, H.L., Welke, H.J., Hughes, M.J., 1981. Shortening the odds in exploration. Nuclear Active, 24: 8-12.

Armstrong, R.A., 1988. A report on a geochronological study on the Grootfontein Mafic Body.

Atkinson, B.K., 1975. Experimental deformation of polycrystalline pyrite: effects of temperature, confining pressure, strain rate, and porosity. Econ. Geol., 70: 473-487.

Babinski, M., Van Schmus, W.R., Chemale, Jr.F., 1999. Pb-Pb dating and Pb isotope geochemistry of Neoproterozoic carbonate rocks from the Sao Francisco basin, Brazil: implications for the mobility of Pb isotopes during tectonism and metamorphism. Chem. Geol., 160: 175-199.

Bakker, R.J., 2003. Package FLUIDS 1. Computer programs for analysis of fluid inclusion data and for modelling bulk fluid properties. Chem. Geol., 194: 3-23.

Bannister, F.A., Hey, M., 1933. The identity of mottramite and psittacinite with cupriferous descloizite. Mineralogical Magazine, 23: 376-386.

Barra, F., Broughton, D.W., Ruiz, J., Hitzman, M.W., 2004. Multi-stage mineralization in the Zambian Copperbelt based on Re-Os isotope constraints. Abstracts with Programs - Geol. Soc. of America, 36 (5): 516.

Bäumle, R., 2003. Geohydraulic characterisation of fractured rock flow regimes: regional studies in granite (Lindau, Black Forest, Germany) and dolomite (Tsumeb Aquifers, Northern Namibia). Unpublished PhD thesis Thesis, TH Karlsruhe, Karlsruhe.

Beukes, N.J., van Niekerk, H.S., Gutzmer, J., 1999. Post Gondwana African land surfaces and pedogenetic ferromanganese deposits on the Witswatersrand and the West Wits Gold Mine, South Africa. S. Afr. J. Geol., 102 (1): 65-82.

BGR, B.f.G.u.R.-., 1997. Hydrogeology and isotope hydrology of the Otavi Mountainland and its surroundings (KARST_01 AND KARST_02). Vol. D-III, BGR, Windhoek.

Birck, J.L., 1986. Precision K-Rb-Sr isotopic analysis: Application to Rb-Sr chronology. Chem. Geol., 56(73-83).

Blaxland, A.G., E., Haack, U., Hoffer, E., 1979. Rb/Sr ages of late-tectonic granites in the Damara Orogn, Southwest Africa/Namibia. N. Jb. Miner. Mh., 11: 498-508.

Bodnar, R.J., Sterner, M.S., 1987. Synthetic fluid inclusions. In: G.C. Ulmer, Barnes, H.L. (Editor), Hydrothermal Experimental Techniques. John Wiley & Sons, New York, (USA), pp. 423-457.

Bodnar, R.J., 1993. Revised equation and table for determining the freezing point depression of H2=-NaCl solutions. Geochim. Cosmochim. Acta, 57: 683-684.

Boni, M., Large, D., 2003. Nonsulfide Zinc Mineralization in Europe: An Overview. Econ. Geol., 98: 715-729.

Botha, B.J.V., 1958. A report on the geology of the Uris mining area.

Brandt, J.W., 1955. Interim report on the Nosib Mine, South West African Company Limited.

Brandt, R., 1987. A revised stratigraphy for the Abbabis Complex in the Abbabis Inlier, Namibia. S.-Afr.Tydskr.Geol., 90(3): 314-323.

Brannon, J.C., Podosek, F.A., McLimans, R.K., 1992. Alleghenian age of the Upper Mississippi Valley zinc-lead deposit determined by Rb-Sr dating of sphalerite. Nature, 356: 509-511.

Brugger, J., McPhail, D.C., Wallace, M., Waters, J., 2003. Formation of Willemite in Hydrothermal Environments. Econ. Geol., 98: 819-835.

Burger, A.J., Clifford, T.N., Miller, R.McG., 1976. Zircon U-Pb ages of the Franzfontein granitic suite, Northern South West Africa. Prec. Res., 3: 415-431.

Burger, A.J. and Coertze, F.J., 1973. Radiometric age measurements on rocks from southern Africa to the end 1971. Bull. Geol. Surv. S. Afr., 58: 48.

Burke, K., 1996. The African plate. S. Afr. J. Geol., 99: 339-409.

Butler, R.W.H., 1989. The influence of pre-existing basin structure on thrust system evolution in the Western Alps. Geol. Soc. Spec. Publ., 44: 105-122.

Cabanis, B., Lecolle, M., 1989. Le diagramme La/10-Y/15-Nb/8: un outil pour la discrimination des eries valcaniques et la mise en evidence des processus de melange et/ou de contamination crustale. C.R. Acad. Sci. Ser. II, 309: 2023-2029.

Cairncross, B., 1997. The Otavi Mountain Land Cu-Pb-Zn-V Deposits. Mineralogical Record, 28: 109-130.

Chadwick, P.J., 1993. A study of the Berg Aukas-type Pb-Zn-V deposits in the Otavi Mountain Land, Namibia. MSC Thesis, University of Cape Town, Cape Town, 138 pp.

Chetty, D. and Frimmel, H.E., 2000. The role of evaporites in the genesis of base metal sulphide mineralisation in the northern platform of the Pan-African Damara Belt, Namibia; geochemical and fluid inclusion evidence from carbonate wall rock alteration. Mineralium Deposita, 35(4): 364-376.

Christensen, J.N., Halliday, A.N., Vearncombe, J.R., Kesler, S.E., 1995a. Testing models of large-scale crustal fluid flow using direct dating of sulphides: Rb-Sr evidence for early dewatering and formation of Mississippi Valley-type deposits, Canning Basin, Australia. Econ. Geol., 90: 877-884.

Christensen, J.N., Halliday, A.N., Leigh, K.E., Randell, R.N., Kesler, S.E., 1995b. Direct dating of sulphides by Rb-Sr: A critical test using the Polaris Mississippi Valley-type Zn-Pb deposit. Geochim. Cosmochim. Acta, 59: 5191-5197.

Clauer, N., Chaudhuri, S., Kralik, M., Bonnot-Courtois, C., 1993. Effects of experimental leaching on Rb-Sr and K-Ar isotopic systems and REE contents of diagenetic illite. Chem. Geol., 103: 1-16.

Clauer, N., Chaudhuri, S., 1995. Clays in crustal environments - Isotope dating and tracing. Springer, Berlin, 359 pp.

Clauer, N. and Kroener, A., 1979. Strontium and argon isotopic homogenization of pelitic sediments during low-grade regional metamorphism; the Pan-African Upper Damara Sequence of northern Namibia (South West Africa). Earth Planet. Sci. Lett., 43(1): 117-131.

Clifford, T.N., Nicolaysen, L.O., Burger, A.J., 1962. Petrology and age of pre-Otavi basement granite at Franzfontein, northern South-West Africa. J. Petrol., 3: 244-279.

Clifford, T.N., Rooke, J.M., Allsopp, H.L., 1969. Petrochemistry and age of the Franzfontein granitic rocks of northern South-West Africa. Geochim. Cosmochim. Acta, 33: 973-986.

Colin, F., Beauvais, A., Ruffet, G., Hénocque, O., 2005. First 40Ar/39Ar geochronology of lateritic manganiferous pisolites: implications for the Palaeogene history of a West African landscape. Earth Planet. Sci. Lett., 238: 172-188.

Condie, K.C., 2002. Breakup of a Paleoproterozoic supercontinent. Gondwana Research, 5(1): 41-43.

Coward, M.P., 1981. The junction between Pan African mobile belts in Namibia: its structural history. Tectonophysics, 76: 59-73.

Coward, M.P., 1983. The tectonic history of the Damaran Belt. Spec. Publ. geol. Soc. S. Afr., 11: 409-421.

Coward, M.P., Daly, M.C., 1984. Crustal lineaments and shear zones in Africa: Their relationship to plate movements. Prec. Res., 24: 27-45.

Cox, K.G., Bell, J.D., Pankhurst, R.J., 1979. The interpretation of igneous rocks, London, 450 pp.

Daly, M.C., 1986. Crustal shear zones and thrust belts: their geometry and continuity in Central Africa, Philos. Trans. R. Soc. London, London.

Dardis, G.F., Moon, B.P., 1988. Geomorphological Studies in Southern Africa. Balkema, Rotterdam, 509 pp.

De Bever, N.J., 1997. The Guinas Prospect - Report on the Diamond Drilling, Gold Fields Namibia Ltd.

De Carvalho, H., Cantagrel, J.M., Jamond, C., 1983. Geologie de l'Angola oriental: datation K-Ar de quelques roches basiques, leur place dance l'evolution de cette region, Gracia de Orta. Serie de Geologia, 6 (1-2): 151-159.

De Swardt, A.M.J., Drysdall, A.R., 1964. Precambrian geology and structure in central Northern Rhodesia. Geol. Surv. N. Rhod. Mem., 2: 87.

Deane, J.G., 1989. Guchab Project Area. Progress report with further exploration motivations, Gold Fields Namibia Ltd.

Deane, J.G., 1993. The controls on "Contact-type" Cu-Pb (Ag) Mineralization within the Tsumeb Subgroup of the Otavi Valley syncline. MSc thesis Thesis, Univ. of Cape Town, Cape Town, 240 pp.

Deane, J.G., 1995. The structural evolution of the Kombat deposits, Otavi Mountainland, Namibia. Communications of the Geological Survey of Namibia, 10: 99-107.

Dejonghe, L., Boni, M., 2005. The "Calamine-type" Zinc-Lead deposits in Belgium and West Germany: A product of Mesozoic paleoweathering processes. Geologica Belgica, 8/3: 3-4.

Derry, L.A., Kaufman, A.J., Jacobsen, S.B., 1992. Sedimentary cycling and environmental change in

the Late Proterozoic: evidence from stable and radiogenic isotopes. Geochim. Cosmochim. Acta, 56: 1317-1329.

Diefenbach, A., 1930. Mineralogische und chemische Untersuchungen von Descloizit und Mottramit aus dem Otavibergland. Zeitschrift für Kristallographie, 74: 155.

Dingeldey, D.P., 1997. Tectono-metamorphic evolution of the Pan-African Kaoko belt, NW-Namibia, University of Würzburg, Germany, 247 pp.

Dürr, S.B., Dingeldey, D.P., 1996. The Kaoko belt (Namibia): Part of a late Neoproterozoic continental-scale strike-slip system. Geology, 24(6): 503-506.

Dürr, S.B., Dingeldey, D.P. and Prave, A.R., 1997. Tale of three cratons; tectonostratigraphic anatomy of the Damara Orogen in northwestern Namibia and the assembly of Gondwana; discussion and reply. Geology, 25(12): 1149-1151.

DWA-Republic of Namibia-Ministry of Agriculture, W.a.R.D.D.o.W.A., Kreditanstalt für Wiederaufbau and GKW/Bicon, 2002. Tsumeb Groundwater Study Final Report Vol.2. file no. 12/1/2/16/2, Geological/geophysical surveys and borehole siting, Windhoek.

Evans, N.J., Byrne, J.P., Keegan, J.T., Dotter, L.E., 2005. Determination of uranium and thorium in zircon, apatite and fluorite: application to laser (U-Th)/He thermochronology. Journal of Analytical Chemistry, 60: 1158-1164.

Farley, K.A., Reiners, P.W., Nenow, V., 1999. An apparatus for measurement of noble gas diffusivities from minerals in vacuum. Analytical Chemistry, 71: 4223-4229.

Farley, K.A., 2002. (U-Th)/He dating: Techniques, calibrations and applications. In: D. Procelli, Ballentine, C.J., Wieler, R. (Editor), Noble Gases in Geochemistry and Cosmochemistry: Reviews in Mineralogy and Geochemistry, pp. 819-844.

Floyd, P.A., Winchester, J.A., 1975. Magma-type and tectonic setting discrimination usinmg immobile elements. Earth Planet. Sci. Lett., 27: 211-218.

Foster, D.A., Gray, D.R., 2000. The structure and evolution of the Lachlan Fold Belt (Orogen) of Eastern Australia. Ann. Rev. Earth Planet. Sci., 28: 47-80.

Frets, D.C., 1969. Geology and structure of the Huab-Welwitschia area, South West Africa. Prec. Res., 5.

Friedman, I., O'Neil, J.R., 1977. Compilation of stable isotope fractionation factors of geochemical interest. United States Geological Survey Professional Papers, 440, 12 pp.

Frimmel, H.E., Deane, J.G., Chadwick, P.J., 1996a. Pan-African tectonism and the genesis of base metal sulphide deposits in the northern foreland of the Damara Orogen, Namibia. Special Publication, Society of Economic Geologists, 4: 204-217.

Frimmel, H.E., Klötzli, U.S., Siegfried, P.R., 1996b. New Pb-Pb single zircon age constraints on the timing of Neoproterozoic glaciation and continental break-up in Namibia. J. of Geol., 104: 459-469.

Frimmel, H.E., 2004. Formation of a late Mesoproterozoic supercontinent: the South Africa - East Antarctica connection. In: P.G. Eriksson, Altermann, W., Nelson, D.R., Mueller, W.U., Catuneanu, O. (Editor), The Precambrian Earth: Tempos and Events. Developments in Precambrian Geology 12, pp. 240-255.

Frimmel, H.E., Jonasson, I.R., Mubita, P., 2004. An Eburnean base metal source for sediment-hosted zinc-lead deposits in Neoproterozoic units of Namibia: Lead isotopic and geochemical evidence. Mineralium Deposita, 39: 328-343.

Frimmel, H.E., Fölling, P.G., 2004. Late Vendian closure of the Adamastor Ocean; timing of tectonic inversion and syn-orogenic sedimentation in the Gariep Basin. Gondwana Research, 7(3): 685-699.

Gadd-Claxton, D.L., 1972. Report on geological map of the Farm Bobos and environs, South-West Africa. Portion of Grant M46/3/132A.

Gallagher, K., Brown, R.B., 1999. Denudation and uplift as passive margins: the record of the Atlantic margins of Southern Africa, Philos. Trans. R. Soc. London, pp. 835-859.

Galloway, C., 1988. The geology of the Kombat Mine and environs., TCL, Tsumeb.

Gavine, G.H., 1979. Aspects of the geology of the Berg Aukas Zn-Pb-V deposit. unpublished Geology Honours Project Thesis, University of Cape Town, 37 pp.

Geyh, M.A., 1995. Geochronologische Aspekte paläohydrologischer und paläoklimatischer Befunde in Namibia. Geomethodica, 20: 75-99.

Gilg, H.A., Hochleitner, R., Keller, P., Struck, U., 2004. A Fluid inclusion and stable isotope study of secondary oxidation minerals from the Tsumeb Cu-Pb-Zn deposit, Namibia. Extended Abstract ECROFI Siena 2005, 2 pp.

Goscombe, B., Gray, D., Hand, M., 2004. Variation in Metamorphic Style along the Northern Margin of the Damara Orogen, Namibia. J. Petrol., 45(6): 1261-1295.

Goscombe, B., Gray, D., Armstrong, R., Foster, D.A., Vogl, J., 2005. Event geochronology of the Pan-African Kaoko Belt, Namibia. Prec. Res., 140: 103-131.

Goscombe, B.D., Hand, M., Gray, D., 2003. Structure of the Kaoko Belt, Namibia: progressive evolution

of a classic transpressional orogen. Journal of Structural Geology, 25: 1049-1081.

Gray, D.R., Foster, D.A., Goscombe, B., Passchier, C.W., Trouw, R.A.J., 2006. 40Ar/39Ar thermochronology of the Pan-African Damara Orogen, Namibia, with implications for tectonothermal and geodynamic evolution. Prec. Res., 150: 49-72.

Grine, F.E., Jungers, W.L., Tobias, P.V., Pearso, O.M., 1995. Fossil Homo femur from Berg Aukas, Northern Namibia. American Journal of Physical Anthropology, 97: 151-185.

Gross, C., Vollbrecht, A., 2003. Cathodoluminescence studies on carbonates from the Otavi Mountain Land, Namibia, Interim Report "BGR-Hochschulvergabeprojekt 81", GWZ Universität Göttingen, Göttingen.

Groves, I.M., Carman, C.E., Dunlap, W.J., 2003. Geology of the Beltana Willemite Deposit, Flinders Ranges, South Australia. Econ. Geol., 98: 797-818.

GSN (Geological Survey of Namibia)., 1999. Preliminary geological map of the Otavi Mountainland. Geological Survey of Namibia, Windhoek.

Guj, P., 1970. The Damara Mobile Belt in the South-Western Kaokoveld South West Africa. PhD Thesis, University of Cape Town, Cape Town.

Haack, U., 1976. Rekonstruktion der Abkühlungsgeschichte des Damara-Orogens in Südwest-Afrika mit Hilfe von Spaltspuren-Altern. Geologische Rundschau, 65(3): 967-1002.

Haack, U., Gohn, E., Klein, J.A., 1980. Rb/Sr Ages of Granitic Rocks Along the Middle Reaches of the Omaruru River and the Timing of Orogenetic Events in the Damara Belt (Namibia). Contrib. Mineral. Petrol., 74: 349-360.

Haack, U., Martin, H., 1983. Geochronology of the Damara Orogen - A Review. In: H. Martin, Eder, F.W. (Editor), Intracontinental Fold Belts - Case studies in the Variscan Belt and Damara Belt.

Haack, U., Gohn, E., Brandt, R., Feldmann, H., 1988. Rb-Sr Data on the Otjimbingwe Alkali Complex in the Damara Orogen, South West Africa, Namibia. Chem. Erde, 48: 131-140.

Haack, U., 1993. Critical note on lead-lead model ages. In: P. Möller, Lüders, V. (Editor), Formation of hydrothermal vein deposits - A case study on the Pb-Zn, barite and fluorite deposits of the Harz Mountains. Monograph Series on Mineral Deposits, pp. 115-116.

Halliday, A.N., Ohr, M., Mezger, K., Chesley, J.T., Nakai, S., DeWolf, C.P., 1991. Recent developments in dating ancient crustal fluid flow. Reviews in Geophysics, 29: 577-584.

Halverson, G.P., Hoffmann, P.F., Schrag, D.P., Kaufmann, J.A., 2002. A major perturbation of the carbon cycle before the Ghaub glaciation (Neoproterozoic) in Namibia: Prelude to snowball Earth? Geophysics, Geochemistry, Geosystems, 3.

Hanson, R.E., Wardlaw, M.S., Wilson, T.J., Mwale, G., 1993. U-Pb zircon ages from the Hook granite massif and Mwembeshi dislocation: constraints on Pan-African deformation, plutonism, and transcurrent shearing in central Zambia. Prec. Res., 63: 189-209.

Hartnady, C., Joubert, P., Stowe, C., 1985. Proterozoic Crustal Evolution in Southwestern Africa. Episodes, 8(4): 236-244.

Hedberg, R.M., 1979. Stratigraphy of the Ovamboland Basin, South West Africa. Bulletin - University of Cape Town, Department of Geology, Chamber of Mines Precambrian Research Unit, 24: 324.

Hickey, R.L., Frey, F.A., Gerlach, D.C., 1986. Multiple sources for basaltic arc rocks from the Southern volcanic zone of the Andes: Trace element and isotopic evidence for contributions from subducted oceanic crust, mantle and continental crust. J. Geophys. Res., 91: 5963-5983.

Hitzman, M.W., Reynolds, N.A., Sangster, D.F., Allen, C.R., Carman, C.E., 2003. Classification, Genesis, and Exploration Guides for Nonsulfide Zinc Deposits. Econ. Geol., 98: 685-714.

Hoffman, P.F., Hawkins, D.P., Isachsen, C.E., Bowring, S.A., 1996. Precise U-Pb zircon ages for early Damaran magmatism in the Summas Mountains and Welwitschia Inlier, northern Damara belt, Namibia. Geological Survey of Namibia Communications, 11: 47-52.

Hoffman, P.F., Kaufman, A.J., Halverson, G.P., Schrag, D.P., 1998. A Neoproterozoic snowball Earth. Science, 281: 1342-1346.

Hoffman, P.F., 2004. 28th Debeers Alex. DuToit Memorial Lecture, 2004. On Cryogenian (Neoproterozoic) ice-shett dynamics and the limitations of the glacial sedimentary record. South African Journal of Geology, 108: 557-577.

Hoffmann, K.H., Condon, D.J., Bowring, S.A., Crowley, J.L., 2004. U-Pb zircon date from the Neoproterozoic Ghaub Formation, Namibia: Constraints on Marinoan glaciation. Geology, 32(9): 817-820.

Holmes, A., Cahen, L., 1957. Geochronologie africaine156; resultats acquis aut (super er) juillet 1956, 5, 169 pp.

Horwitz, E.P., Dietz, M.L., Fischer, D.E., 1991a. SREX: a new process for the extraction and recovery of strontium from acidic nuclear waste streams. Solv. Extr. Ion Exch., 9: 1-25.

Horwitz, E.P., Dietz, M.L., Fischer, D.E., 1991b. Separation and preconcentration of Sr from biological, environmental and nuclear waste samples by extraction chromatography using a crown ether. Analytical Chemistry, 63: 522-525.

Hughes, M.J., 1979. Some aspects of the genesis of the Tsumeb ore body, South West Africa, and of its subsequent deformation, Geokongres 79, 18th congress of the geological society of S.A., pp. 200-206.

Hughes, M.J., 1987. The Tsumeb Ore Body, Namibia, and related dolostone-hosted base metal ore deposits of Central Africa. PhD Thesis, University of the Witwatersrand, Johannesburg.

Hughes, M.J., Welke, H.J. and Allsopp, H.L., 1984. Lead isotopic studies of some late Proterozoic stratabound ores of central Africa. Prec. Res., 25(1-3): 137-139.

Innes, J., Chaplin, R.C., 1986. Ore bodies of the Kombat Mine, South West Africa/Namibia. Mineral Deposits of Southern Africa, I & II: 1789 - 1805.

Jackson, M.P.A., Hudec, M.R., 2005. The great West African Tertiary coastal uplift: fact or fiction? A perspective from the Angolan divergent margin. Tectonics, 24: 1-23.

Jacob, R.E., Kröner, A., Burger, A.J., 1978. Areal extent and first U-Pb age of the Pre-Damara Abbabis complex in the Central Damara belt of South West Africa (Namibia). Geol. Rdsch., 67 (2): 706-718.

Jacobsen, S.B., Kaufman, A.J., 1999. The Sr, C and O isotopic evolution of Neoproterozoic seawater. Chem. Geol., 16: 37-57.

Johns, C.C., Liyungu, K., Mabuku, S., Mwale, G., Sakungo, F., Tembo, D., Vallance, G., 1989. The stratigraphic and structural framework of Eastern Zambia: results of a geotraverse. J. Afr. Earth Sci., 9(1): 123-136.

Johnson, S.P., Rivers, T., DeWaele, B., 2005. A review of the Mesoproterozoic to early Palaeozoic magmatic and tectonothermal history of south-central Africa: implications for Rodinia and Gondwana. J. Geol. Soc., 162: 433-450.

Kamona, A.F., Friedrich, G., 1994. Die Blei-Zink-Lagerstätten Kabwe in Zentral Sambia. Erzmetall, 47: 34-44.

Kamona, A.F., Léveque, J., Friedrich, G., Haack, U., 1999. Lead isotopes of the carbonate-hosted Kabwe, Tsumeb, and Kipushi Pb-Zn-Cu sulphide deposits in relation to Pan African orogenesis in the Damaran-Lufilian Fold Belt of Central Africa. Mineralium Deposita, 34: 273-283.

Kasch, K.W., 1983. Continental Collision, suture progradation and thermal relaxation: A plate tectonic model for the Damara Orogen in central Namibia. Spec. Publ. geol. Soc. S. Afr., 11: 423-429.

Kaufman, A.J., Hayes, J.M., Knoll, A.H. and Germs, G.J.B., 1991. Isotopic compositions of carbonates and organic carbon from upper Proterozoic successions in Namibia; stratigraphic variation and the effects of diagenesis and metamorphism. Prec. Res., 49(3-4): 301-327.

Keller, P., 1984. Tsumeb. Lapis, 7/8: 13-63.

Kennett, J.P., Barker, P.F., 1990. Latest Cretaceous to Cenozoic climate and oceanographic developments in the Weddell Sea, Antarctica, An ocean drilling Perspective: Proceedings of the Scientific Results, ODP, Weddell Sea, Antarctica, pp. 937-960.

Key, R.M., Ayres, N., 2000. The 1998 edition of the National Geological Map of Botswana. J. Afr. Earth Sci., 30 (3): 427-451.

King, C.H.M., 1990. The geology of the Tsumeb Carbonate Sequence and associated Lead-Zinc occurrences on the farm Olifantsfontein, Otavi Mountainland, Namibia. MSc Thesis, Rand Afrikaans University.

King, L.C., 1951. South African scenery, Edinburgh, 379 pp.

Korn, H., Martin, H., 1937. Geological report on the vanadium deposits of Abenab, Baltika, Uitsab and Berg Aukas. Open File Report EG, 030. Ministry of Mines and Energy, Geological Survey, Windhoek, Namibia, 8 pp.

Kretz, R., 1983. Symbols for rock-forming minerals. American Mineralogist, 68: 277-279.

Kröner, A., Clauer, N., 1979. Isotopic dating of low-grade metamorphic shales in northern Namibia (South West Africa) and implications for the orogenic evolution of the Pan-African Damara Belt. Prec. Res., 10: 59-72.

Kröner, A., 1982. Rb-Sr Geochronology and tectonic evolution of the Pan-African Damara Belt of Namibia, Southwestern Africa. Am. J. of. Sci., 282: 1471-1507.

Kukla, P.A., Stainstreet, I.G., 1991. Record of the Damaran Khomas Hochland accretionary prism in central Namibia: Refutation of an "ensialic" origin of a Late Proterozoic orogenic belt. Geology, 19: 473-476.

Land, L.S., 1980. The isotopic and trace element geochemistry of dolomite: the state of the art. In: D.H. Zenger, Dunham, J.B., Ethington, R.L. (Editor), Concepts and models of dolomitization. Society for Sedimentary Research (SEPM) Special Publication, pp. 87-110.

Land, L.S., 1983. The application of stable isotopes to studies of the origin of dolomite and to problems of diagenesis of clastic sediments. In: M.A. Arthur,

Anderson, T.F. (Editor), Stable Isotopes in Sedimentary Geology. Soc. Paleont. Miner. Short course, pp. 4.1-4.22.

Large, D., 2001. The Geology of Non-Sulphide Zinc Deposits - An Overview. Erzmetall, 54: 264-276.

Laukamp, C., Bechstädt, T., Boni, M., 2004. Influence of Pan-African shear zones on Tsumeb-type mineralization in the Otavi Mountainland (OML), Namibia. In: B. Holdsworth, McCaffrey, K., Clegg, P. (Editor), TSG Annual General Meeting, Durham, pp. 95.

Laukamp, C., Petzel, V., Bechstädt, T., 2006. Structural control of fluid flow on a carbonate platform margin: an example from the Otavi Mountainland. In: S. Phillipp, Leiss, B., Vollbrecht, A., Tanner, D., Gudmundsson, A. (Editor), TSK11, Göttingen, pp. 123-125.

Lee, J.E., Glenister, D.A., 1976. Stratiform sulphide mineralisation at Oamites Copper Mine, South West Africa. Econ. Geol., 71: 369-383.

Lévy, A., 1843. Description de plusieurs espéces minérales appartenant à la famille du zinc. Annales des Mines (Paris), 4ème sèrie/4: 507-520.

Littmann, S., Cook, N., Teigler, B., Okrusch, M, 1997. Das ökonomische Potential des Kunene-Anorthosit-Komplexes und seiner Satellit-Intrusionen, NW-Namibia: Erste Beobachtungen. Mainzer naturwiss. Archiv, 19: 47-48.

Lohmann, K.C., 1987. Geochemical patterns of meteoric diagenetic systems and their application to studies of paleokarst. In: N.P. James, Choquette, P.W. (Editor), Paleokarst. Springer Verlag, New York, pp. 58-80.

Lombaard, A.F., Günzel, A., Innes, J., Krüger, T.I., 1986. The Tsumeb Lead-Copper-Zinc-Silver Deposit, South West Africa/Namibia. Mineral Deposits of Southern Africa, I & II: 176 - 1787.

Ludwig, K.R., 1980. Calculation of uncertainties of U-Pb isotope data. Earth Planet. Sci. Lett., 46: 212-220.

Ludwig, K.R., 2001. Users manual for ISOPLOT/Es rev. 2.49. A geochronological toolkit for Microsoft Excel, 1a. Berkeley Geochron. Cent. Spec. Publ., 56 pp.

Machel, H.G., 2005. Concepts and models of dolomitization: a critical reappraisal. In: C.J.R. Braithwaite, Rizzi, G., Darke, G. (Editor), The geometry and Petrogenesis of Dolomite Hydrocarbon Reservoirs. Geological Society of London Special Publications, pp. 7-63.

Maclaren, A.H., 1991. An interpretation of the structure of the Otavi Mountain Land, Namibia; The identification of mineralisation controls, and the generation of exploration targets, Gold Fields Namibia Ltd.

Maloof, A.C., 2000. Superposed folding at the junction of the inland and coastal belts, Damara Orogen, NW Namibia. Communications of the Geological Survey of Namibia. Department of Economic Affairs, 12: 89-98.

Markham, N.L., 1958. Mineralogy of the Berg Aukas vanadium and secondary lead-zinc ores, South West Africa Company Limited.

Marsh, J.S., Swart, R.S., Philips, D., 2003. Implications of a new 40Ar/39Ar age for a basalt flow interbedded with the Etjo Formation, Northeast Namibia. S. Afr. J. Geol., 106: 281-286.

Martin, H., 1965. The Precambrian Geology of South West Africa and Namaqualand. The Precambrian Research Unit: 159.

Mayer, A., Hofmann, A.W., Sinigoi, S., Morais, E., 2004. Mesoproterozoic Sm-Nd and U-Pb ages for the Kunene Anorthosite Complex of SW Angola. Prec. Res., 133: 187-206.

McConachy, T., Evans, N.J., Boni, M., Yang, K., McDonald, B., in press. Potential new techniques in non sulphide base metal exploration: spectral reflectance and U-Th/He thermochronology. Journal of Geochemical Exploration.

McDonough, W.F., Sun, S.-s., 1995. The composition of the earth. Chem. Geol., 120: 223-253.

Meert, J.G., 2003. A synopsis of events related to the assembly of eastern Gondwana. Tectonophysics, 362: 1-40.

Meert, J.G., Torsvik, T.H., 2003. The making and unmaking of a supercontinent: Rodina revisited. Tectonophysics, 375: 261-288.

Melcher, F., 2003. The Otavi Mountain Land in Namibia: Tsumeb, Germanium and Snowball Earth. Mitt. Österr.Miner.Ges., 148: 413-435.

Melcher, F., Oberthür, T., Vetter, U., Gross, C., Vollbrecht, A., Brauns, M., Haack, U., 2003. Germanium in carbonate-hosted Cu-Pb-Zn mineralization in the Otavi Mountain Land, Namibia.

Melcher, F., Lodziak, J., Vetter, U.K., 2004. Sulfide mineralization in the Otavi Mountain Land, Namibia, BGR, Hannover.

Melcher, F., Oberthür, T., Rammlmair, D., 2006. Geochemical and mineralogical distribution of germanium in the Khusib Springs Cu-Zn-Pb-Ag sulfide deposit, Otavi Mountain Land, Namibia. Ore Geology Reviews.

Meschede, M., 1986. A method of discriminating between different types of mid-ocean ridge basalts and continental tholeiites with the Nb-Zr-Y diagram. Chem. Geol., 56: 207-218.

Miller, R.M., 1980. Geology of a portion of central Damaraland, South West Africa/Namibia. Memoirs of the Geol. Surv. of Namibia, 6: 78.

Miller, R.M., 1983a. The Pan-African Damara Orogen of South West Africa/Namibia. Spec. Publ. Geol. Soc. S. Afr., 11: 431-515.

Miller, R.M., 1983b. Economic implications of plate tectonic models of the Damara Orogen. Spec. Publ. geol. Soc. S. Afr., 11: 385-395.

Miller, R.M., 1997. The Owambo Basin of Northern Namibia. In: R.C. Selley (Editor), Sedimentary Basins of the World, pp. 237-268.

Millman, A.P., 1960. The descloizite-mottramite series of vanadates from Minas Do Lueca, Angola. American Mineralogist, 45: 763-773.

Misiewicz, J.E., 1988. The Geology and Metallogeny of the Otavi Mountain Land, Damara Orogen, SWA/Namibia, with particular reference to the Berg Aukas Zn-Pb-V deposit - A model or ore genesis. MSC Thesis, Rhodes University, Grahamstown.

Misra, K.C., 2000. Understanding Mineral Deposits. Kluwer Academic Publishers.

Monteiro, L.V.S., Bettencourt, J.S., Spiro, B., Graca, R., DeOliveira, T.F., 2000. The Vazante zinc mine, Minas Gerais, Brazil: Constraints on willemitic mineralization and fluid evolution. Exploration and Mining Geology, 8: 21-42.

Monteiro, L.V.S., Bettencourt, J.S., Juliani, C., DeOliveira, T.F., 2006. Geology, petrography, and mineral chemistry of the Vazante non-sulphide and Ambrósia and Fagundes sulphide-rich carbonate-hosted Zn-(Pb) deposits, Minas Gerais, Brazil. Ore Geology Reviews, 28: 201-234.

Morais, E., Singoi, S., Mayer, A., Mucana, A., Miquel, L-G., Rufino, N.J., 1998. The Kunene gabbro-anorthosite complex; preliminary results based on new field and chemical data. African Geoscience Review, 5 (4): 485-498.

Nakai, S., Halliday, A.N., Kesler, S.E., Jones, H.D., 1990. Rb-Sr dating of sphalerites from Tenessee and the genesis of Mississippi Valley-type ore deposits. Nature, 346: 354-357.

Nakai, S., Halliday, A.N., Kesler, S.E., Jones, H.D., Kyle, J.R., Lane, T.E., 1993. Rb-Sr dating of sphalerites from Mississippi Valley-type (MVT) ore deposits. Geochim. Cosmochim. Acta, 57: 417-427.

Nakamura, N., 1974. Determination of REE, Ba, Fe, Mg, Na and K in carbonaceous and ordinary chondrites. Geochim. Cosmochim. Acta, 38: 757-775.

Naldrett, A.J., Grünewaldt, G., 1989. Association of platinum-group elements with chromitite in layered intrusions and ophiolite complexes. Econ. Geol., 84: 180-187.

Nyblade, A.A., Robinson, S.W., 1994. The African Superswell. Geophysical Research Letter, 21: 765-768.

Oliver, J., 1986. Fluids expelled tectonically from orogenic belts: Their role in hydrocarbon migration and other geologic phenomena. Geology, 14: 99-102.

Osterman, C., 1990. Geology and soil geochemical survey of the anomaly 3 grid, Tsumeb Grant, M46/3/132A, Otavi Mountain Land. M46/3/132A, Gold Fields Namibia Ltd.

Pack, A., Gutzmer, J., Beukes, N.J., van Niekerk, H.S., Hoernes, S., 2000. Supergene ferromanganese wad deposits derived from Permian Karoo strata along the Late-Cretaceous-Mid Tertiary Land Surface, Ryedale, South Africa. Econ. Geol., 95: 203-220.

Palache, C., Berman, H., Frondell, C., 1951. The system of mineralogy. John Wiley, New York, pp. 816.

Partridge, T.C., Maud, R.R., 1987. Geomorphic evolution of southern Africa since the Mesozoic. S. Afr. J. Geol., 90 (2): 179-208.

Partridge, T.C., 1998. Of diamonds, dinosaurs and diastrophism: 150 million years of landscape evolution in southern Africa. S. Afr. J. Geol., 101: 167-184.

Passchier, C.W., Trouw, R.A.J., 1996. Microtectonics. Springer, 289 pp.

Passchier, C.W., Trouw, R.A.J., Goscombe, B., Gray, D., Kröner, A., in press. Intrusion mechanisms in a turbidite sequence: the Voetspoor and Doros plutons in NW Namibia. Journal of Structural Geology.

Pearce, A.P., Harris, N.B.W., Tindle, A.G., 1984. Trace element discrimination diagrams for the tectonic interpretation of granitic rocks. J. Petrol., 25(4): 956-983.

Pearce, T.H., Gorman, B.E., Birkett, T.C., 1975. The TiO2-K2O-P2O5 diagram: a method of discriminating between oceanic and non-oceanic basalts. Earth Planet. Sci. Lett., 24: 419-426.

Pelletier, R.A., 1930. The zinc, lead and vanadium deposit of Broken Hill, N.Rhodesia. South African Mining and Engineering, 40: 91.

Pettke, T., Diamond, L.W., 1996. Rb-Sr dating of sphalerite based on fluid inclusion-host mineral isochrons: A clarification of why it works. Econ. Geol., 91: 951-956.

Petzel, V.F.W., 1992. The Kombat Mine, its economic potential and future, Otavi Valley Grant M46/3/132D, Gold Fields Namibia Ltd.

Petzel, V.F.W., 1993. Progress report on exploration conducted in the Tsumeb Grant Area M46/3/132A.

Pickford, M., 1993. Age of supergene ore bodies at Berg Aukas and Harasib 3a, Namibia.

Communications of the Geological Survey of Namibia. Department of Economic Affairs, 8: 147-150.

Pickford, M., 2000. Neogene and Quaternary vertebrate biochronology of the Sperrgebiet and Otavi Mountainland, Namibia. Communications of the Geological Survey of Namibia, 12: 359-365.

Pirajno, F., 1993. Hydrothermal ore deposits - Principles and fundamental concepts for the Exploration Geologist. Springer Verlag, 708 pp.

Pirajno, F. and Joubert, B.D., 1993. An overview of carbonate-hosted mineral deposits in the Otavi mountain land, Namibia; implications for ore genesis. J. Afr. Earth Sci., 16(3): 265-272.

Plöthner, D., Schmidt, G., Kehrberg, S., Geyh, M.A., 1997. Hydrogeology and isotope hydrology of the Otavi Mountain Land and its surroundings, KARST_01 and KARST_02, BGR, Windhoek, Hannover.

Porada, H., 1979. The Damara-Ribeira orogen of the Pan-African-Brasiliano cycle in Namibia (Southwest Africa) and Brazil as interpreted in terms of continental collision. Tectonophysics, 57 (2-4): 237-265.

Porada, H., 1985. Stratigraphy and facies in the upper Proterozoic Damara Orogen, Namibia, based on a geodynamic model. Prec. Res., 29: 235-264.

Porada, H., 1989. Pan-African rifting and orogenesis in southern to equatorial Africa and eastern Brazil. Prec. Res., 44(2): 103-136.

Porada, H., Berhorst, V., 2000. Towards a new understanding of the Neoproterozoic-Early Paleozoic Lufilian and northern Zambezi Belts in Zambia and the Democratic Republic of Congo. J. Afr. Earth Sci., 30(3): 727-771.

Pouchou, J.-L., Pichoir, F., 1991. Quantitative analysis of homogeneous or stratified micro-volumes applying the model "PAP". In: K.F.J. Heinrich, Newbury, D.E. (Editor), Electron Probe Quantification. Plenum Press, New York, pp. 31-75.

Prave, A.R., 1996. Tale of three cratons; Tectonostratigraphic anatomy of the Damara Orogen in northwestern Namibia and the assembly of Gondwana. Geology, 24(12): 1115-1118.

Prave, A.R., 1997. Tale of three cratons: Tectonostratigraphic anatomy of the Damara Orogen in northwestern Namibia and the assembly of Gondwana: Reply. Geology, 25 (12): 1150-1151.

Pretorius, D., 1984. The Kalahari Foreland, its marginal troughs and overthrust belts, and the regional structure of Botswana. 169, Economic Geology Research Unit, University of the Witwatersrand.

Raab, M.J., Brown, R.W., Gallagher, K., Carter, A., Weber, K., 2002. Late Cretaceous reactivation of major crustal shear zones in northern Namibia: constraints from apatite fission track analysis. Tectonophysics, 349: 75-92.

Radke, B.M., Mathis, R.L., 1980. On the formation and occurrence of saddle dolomite. Journal of Sedimentary Petrology, 50: 1149-1168.

Rainaud, C., Master, S., Armstrong, R.A., Robb, L.J., 2005. Geochronology and nature of the Palaeoproterozoic basement in the Central African Copperbelt (Zambia and the Democratic Republic of Congo), with regional implications. J. Afr. Earth Sci., 42: 1-31.

Ramdohr, P., 1954. Klockmann's Lehrbuch der Mineralogie. Enke, Stuttgart, 669 pp.

Reiners, P.W., 2002. (U/Th)/He chronometry experiences a renaissance. Eos, 83: 21-27.

Reiners, P.W., Spell, T.L., Nicolescu, S., Zanetti, K.A., 2004. Zircon (U/Th)/He thermochronometry: He diffusion and comparisons with 40Ar/39Ar dating. Geochim. Cosmochim. Acta, 68: 1857-1887.

Reiners, P.W., Ehlers, T., 2005. Thermochronometry, Reviews in Mineralogy and Geochemistry, pp. 1-622.

Robinson, J.T., 1959. The occurrence of fossils on the Otavi Plateau. Der Kreis: Afrikanische Monatshefte für Pflege des Heimatgedankens und deutsche Kultur, 2: 224-226.

Rust, D.G., Summerfield, M.A., 1990. Isopach and borehole data as indications indicators of rifted margin evolution in southwestern Africa. Marine and Petroleum Geology, 7: 277-287.

Schneider, J., Heijlen, W., Muchez, Ph., Haack, U., 2002. Rb-Sr dating of sphalerites from Pomorzany, Upper Silesia (Poland). Geochim. Cosmochim. Acta, 66 (S1): A 683.

Schneider, J., Haack, U., Stedingk, K., 2003. Rb-Sr dating of epithermal vein mineralization stages in the eastern Harz Mts. (Germany) by paleomixing lines. Geochim. Cosmochim. Acta, 67: 1803-1819.

Schneiderhöhn, H., 1929. Das Otavi-Bergland und seine Erzlagerstätten - Ein Führer für die Exkursionen anläßlich des XV. Internationalen Geologen Kongresses 1929. Zeitschrift für praktische Geologie, 37. Jahrgang: 85-116.

Schoch, A.E., 1958. Report on the Nosib Mine and Environs, South West Africa Company Limited.

Schwellnus, C.M., 1946. Vanadium deposits in the Otavi mountains, South-West Africa. Verhandelinge van die Geologiese Vereniging van Suid Afrika = Transactions of the Geological Society of South Africa, 48: 49-73.

Senut, B., Pickford, M., Mein, P., Conroy, G., Van Couvering, J.A., 1992. Discovery of 12 new late

Cainozoic fossiliferous sites in paleokarsts of the Otavi Mountainland, Namibia. Comptes Rendus Acadèmie des Sciences de Paris, 314: 727-733.

Seth, B., Kröner, A., Mezger, K., Nemchin, A.A., Pidgeon, R.T., Okrusch, M., 1998. Archean to Neoproterozoic magmatic events in the Kaoko belt of NW Namibia and their geodynamic significance. Prec. Res., 92: 341-363.

Seth, B., Jung, S., Hoernes, S., 2002. Isotope constraints on the origin of Pan-African granitoid rocks in the Kaoko belt, NW Namibia. S. Afr. J. Geol., 105: 179-192.

Shand, S.J., 1951. Eruptive rocks. Their genesis, composition, classification and their relation to ore deposits, London, 488 pp.

Sibson, R.H., More, J.M., Rankin, A.J., 1975. Seismic pumping - a hydrothermal fluid transport mechanism. Geol. Soc. London J., 131: 653-659.

Silva, Z.C.G., 1990. Geochemistry of the gabbro-Anorthosite Complex of Southwest Angola. J. Afr. Earth Sci., 10 (4): 683-692.

Simonov, M.A., Sandomirskii, P.A., Egorov-Tismenko, Y.K., Belov, N.V., 1977. The crystal structure of willemite Zn2[SiO4]. Soviet Physics Doklady, 22: 622-623.

Simpson, E.S.W., Otto, J.D.T., 1960. On the pre-Cambrian anorthosite mass of southern Angola, 21st Int. Geol. Cong., Copenhagen, pp. 216-227.

Singletary, S.J., Hanson, R.E., Martin, M.W., Crowley, J.L., Bowring, S.A., Key, R.M., Ramokate, L.V., Direng, B.B., Krol, M.A., 2003. Geochronology of basement rocks in the Kalahari Desert, Botswana, and implications for regional Proterozoic tectonics. Prec. Res., 121: 47-71.

Söhnge, P.G., 1957. Geology of the Otavi Mountain Land, Tsumeb Corporation Ltd.

Söhnge, P.G., 1964. The geology of the Tsumeb mine. Geol. Soc. South Africa Proc., 65: 367-382.

Söhnge, P.G., 1967. Tsumeb. A historical sketch. Scientific Research in South West Africa, 5th series. Committee of the S.W.A. Scientific Society, Windhoek, 94 pp.

Söhnge, P.G., 1972. Application of basement structure, sedimentation and paleophysiography to exploration in the Tsumeb district, Tsumeb Corp. Ltd., Tsumeb.

Söhnge, P.G., 1976. Exploration in the environs of Tsumeb, South West Africa, Tsumeb Corp. Ltd., Tsumeb.

Stacey, J.S., Kramers, J.D., 1975. Approximation of terrestrial lead isotope evolution by a two-stage model. Earth Planet. Sci. Lett., 26: 207-221.

Steiger, R.H., Jäger, E., 1977. Subcommission on geochronology: Convention on the use of decay constants in geo- and cosmochronology. Earth Planet. Sci. Lett., 36: 359-362.

Summerfield, M.A., 1991. Global Geomorphology. Longman Scientific & Technical, Harlow UK, 537 pp.

Sweeney, M.A., Patrick, R.A.D., Vaughan, D.J., 1991. The nature and genesis of Willemite deposits of Zambia. In: M. Pagel, Leroy, J. (Editor), Source, Transport, and Ore Deposition of Metals. Balkema, Rotterdam, pp. 139-142.

Tankard, A.J., Jackson, M. P. A., Eriksson, K. A., Hobday, D. K., Hunter, D. R., Minter, W. E. L., 1982. Crustal evolution of southern Africa: 3.8 billion years of Earth history. Springer, New York, 523 pp.

Taylor, J.H., 1954. The lead-zinc-vanadium deposits at Broken Hill, Northern Rhodesia. Colonial Geological Survey Bulletin, 4: 335-365.

Taylor, K.P.J., 1974. The application of oxygen and hydrogen isotope studies to problems of hydrothermal alterration and ore deposition. Econ. Geol., 69: 843-883.

Tegtmeyer, A., Kröner, A., 1985. U-Pb zircon ages for granitoid gneisses in northern Namibia and their significance for Proterozoic crustal evolution of southwestern Africa. Prec. Res., 28: 311-326.

Thomas, R.J., von Veh, M.W., McCourt, S., 1993. The tectonic evolution of southern Africa: an overview. J. Afr. Earth Sci., 16 (1/2): 5-24.

Thompson, A.B., 1997. The evolution of fluids through the metamorphic cycle. In: B. Jamtveit, Yardley, B. (Editor), Fluid flow and transport in rocks. Chapman and Hall, London, pp. 297-307.

Trompette, R., 1997. Neoproterozoic (~600 Ma) aggregation of Western Gondwana: a tentative scenario. Prec. Res., 82: 101-112.

Unrug, R., 1983. The Lufilian Arc; a microplate in the Pan-African collision zone of the Congo and the Kalahari cratons. Prec. Res., 21(3/4): 181-196.

Unrug, R., 1996. The assembly of Gondwanaland. Scientific results of IGCP Project 288: Gondwanaland sutures and mobile belts. Episodes, 19: 11-20.

Unrug, R., 1997. Rodinia to Gondwana: The geodynamic map of Gondwana supercontinent assembly. GSA Today, 7(1): 1-39.

Van der Merwe Smit, J.M., 1959. The geology of the southern part of the Otavi Mountain Land, S.W.A. MSC Thesis, University of Pretoria, Pretoria.

Van der Westhuizen, W.A., 1984. The nature, genesis and geochemistry of the supergene vanadium ores of the Otavi Mountain Land, University Orange Free State, Bloemfontein, 196 pp.

Van der Westhuizen, W.A., de Bruyin, H., Tordiff, E.A.W., Botha, B.J.V., 1986. The descloizite-

mottramite series of vanadates from the Otavi Mountain Land, South West Africa: an X-ray study. Mineralogical Magazine, 50: 137-140.

Van der Westhuizen, W.A., Tordiffe, E.A., de Bruiyn, H., Beukes, G.J., 1988. The composition of the descloizite-mottramite in relation to the trace element distribution of Pb, Zn, Cu and V in the Otavi Mountain Land, South West Africa/Namibia. Journal of Geochemical Exploration, 34: 21-29.

Van der Westhuizen, W.A., Tordiffe, E.A., Loock, J.C., de Bruiyn, H., 1989. Quaternary karstification and vanadium mineralization in the Otavi Mountain Land, South West Africa/Namibia. Palaeocology of Africa and the Surrounding Islands, 19: 391-403.

Van Niekerk, H.S., Gutzmer, J., Beukes, N.J., Phillips, D., Kiviets, G.B., 1999. An 40Ar/39Ar age of supergene K-Mn oxyhydroxides in a post-Gondwana soil profile on the Highveld of South Africa. South African Journal of Science, 95: 450-454.

Veldsman, J.H., 1977. Die Geologie van ´n gedeelte van die Tsumeb-Sinklinorium met spesiale verwysing na litostratigrafie, struktur en diagenese. MSc Thesis, Universiteit van Stellenbisch.

Venter, D.M., 1977. Preliminary report on the geology, geochemistry and mineralization of the Bobosberg-Grobler area (Grant M46/3/132A - Tsumeb Block), TCL.

Verwoerd, W.J., 1957. The mineralogy and genesis of the lead-zinc- vanadium deposit of Abenab West in the Otavi mountains, South West Africa. Annale Universiteit van Stellenbosch, Serie A, 33: 235-319.

Wachter, E., Hayes, J.M., 1985. Exchange of oxygen isotopes in carbon-dioxide-phosphoric acid systems. Chem. Geol., 52: 365-374.

Wartha, R.R., Schreuder, C.P., 1992. Minerals Resource Series - Vanadium. Ministry of Mines and Energy, Geological Survey of Namibia, Windhoek, 16 pp.

Wateren, F.M.V., Dunai, T.G., 2001. Late Neogene passive margin denudation history - cosmogenic isotope measurements from the central Namib desert. Global and Planetary Change, 30: 271-307.

Weber, K., Ahrendt, H., Hunziker, J.C., 1983. Geodynamic aspects of structural and radiometric investigations on the northern and southern margins of the Damara orogen, South West Africa/Namibia. Spec. Publ. geol. Soc. S. Afr., 11: 307-319.

Weilers, B.F., 1959. A contribution to the geology of the lead-zinc-vanadate mine at Berg Aukas, South Western Africa Company Limited.

Wendt, I., Carl, C., 1991. The statistical distribution of the mean squared weighted deviation. Chem. Geol., 86: 275-285.

Werner, G., 2005. Geolgische Kartierung und laterale Faziesanalyse von Mixtit Ablagerungen im Otavi Bergland, Namibia, Ruprecht-Karls-Universität, Heidelberg.

Wilson, M., 1989. Igneous petrogenesis. Unwin Hyman, London, 466 pp.

Wolf, R.A., 1996. Helium diffusion and low-temperature thermochronometry of apatite. Geochim. Cosmochim. Acta, 60(21): 4231-4240.

Woollett, A., 2005. The Processing of Non-Sulphide Zinc Deposits. In: M. Boni, Gilg, A. (Editor), ESF Exploratory Workshop "Nonsulphide Zn-Pb Deposits", Iglesias (Sardinia, Italy), pp. 39.

Yardley, W.D., 1997. The evolution of fluids through the metamorphic cycle. In: B. Jamtveit, Yardley, B. (Editor), Fluid flow and transport in rocks. Chapman and Hall, London, pp. 99-121.

Yoshioka, H., Asahara, Y., Tojo, B., Kawakami, S., 2003. Systematic variations in C, O, and Sr isotopes and elemental concentrations in Neoproterozoic carbonates in Namibia: implications for a glacial to interglacial transition. Prec. Res., 124: 69-85.

Ypma, P.J.M., 1978. Fluid inclusions and ore genesis in the Otavi Mountains, South West Africa. Part 1: Geothermometry and barometry, Department of Economic Geology, University of Adelaide, Australia.

Zeitler, P.K., Herczeg, A.L., McDougall, I., Honda, M., 1987. U-Th-He dating of apatite; a potential thermochronometer. Geochim. Cosmochim. Acta, 51(10): 2865-2868.

Ziegler, J.F., 1977. Helium: Stopping Powers and Ranges in all Elemental Matter. Pergamon Press, 367 pp.

Acknowledgements

I would like to thank the Deutsche Forschungsgemeinschaft (DFG) for financing this study in the framework of the “Graduiertenkolleg 273 on rock-water interaction” at Heidelberg University. Further financial support was provided by the DAAD-financed Internationales Promotions-programm (IPP) at the Faculty of Chemistry and Geosciences, University of Heidelberg.

Maria Boni, Universita di Napoli, introduced me to the secrets of economic geology. She was a great “Doktormutter” and always pushed me forward.

Thilo Bechstädt, University of Heidelberg, initiated this project and gave me as my supervisor all liberties in the realisation of my studies.

Hartwig Frimmel, University of Würzburg, is not only thanked for the logistic support and the review of my thesis, but also for his friendly advices during my studies.

Guy Spence, University of Heidelberg, is thanked for his helpful comments in the field and during the completion of my thesis. The time with him in the field was very challenging and I have to thank him for the realisation, that my “Denglisch” is better than speaking no English at all.

Jens Schneider, K.U. Leuven, greatly helped me to improve the papers and explained the tricks of isotope geochemistry in an understandable way. Rosario Terracciano, Universita di Napoli, was an excellent "compagno di vaggio di scientifico" during all the field trips we did together. Noreen Evans, CSIRO Perth, is thanked for the (U-Th)/He-studies. Frank Melcher, BGR Hannover, provided analytical data from the Grootfontein Inlier and is thanked for discussions about the development of sulphides and nonsulphides in the OML. Ronald Bakker, University of Leoben, is thanked for introducing me to the secrets of fluid inclusion analysis. Damien Foster and Tom Blenkinsop, JCU Townsville, are thanked for discussions about my papers and the conclusion of my thesis.

Volker Petzel, Geological Survey of Namibia, convinced Maria Boni and Thilo Bechstädt, to start this project in the Otavi Mountainland. He gave a great introduction to the field and deliberately shared all his experience from field work in the OML. Gabi Schneider and staff from the GSN are thanked for the logistic support.

Arno Günzel, "Mr. Otavi Mountainland" and geologist at OMPL, gave a great introduction into the field and shared his wide-spread knowledge about the geology of the OML. He always supported me, to develop my own ideas. Andries Nethling, Hafeni Hiveluah, Tinus Prinsloo and all the other staff from OMPL are thanked for their great support. Eusebius Shiweda and his family are thanked for their great hospitality at the Tsumeb Geophysical Research Station. The farmers of the Otavi Mountainland are thanked for their great hospitality.

Dr. Kevin Carrière, Dr Emmanuel Lavarret, Dr. Gael Le Roux, Dr Zbynek Veselovsky and all the other promising scientists, which were members of the GRK and/or the IPP, showed the pleasant life in and outside of the University of Heidelberg to me. Rike Bauer, Sonja Pabst, Jorham Contreras and all the other current PhD-students at INF 234 and INF 236 are thanked for their moral support. Roswitha Marioth, Tanja van der Beek and Francisco Cueto, were involved in managing the GRK 273 and the IPP and enabled funding for conferences and field work. Furthermore, they always gave me a great moral support. Georg Werner helped in the field and provided some detailed information about the Keilberg area. Together with Alke Rehling and Nathan Kang, he was part of the Hiwis, which made the preparation of the samples possible. Bernd Kober, University of Heidelberg, is thanked for discussions about my thesis and beautiful musical evenings at the Tsumeb Geophysical Research Station. Michael Hanel, University of Heidelberg, is thanked for opening me the gates to the Ramdohr-Sammlung. Thomas Ludwig, University of Heidelberg, greatly improved my knowledge about the instruments at INF 236. Ulrich A. Glasmacher, Reinhold Greiling, Jens C. Grimmer, Agnes Kontny, Carsten Vahle and Rainer Zühlke, all at University of Heidelberg, are thanked for various geological discussions.

Ringrazoio molto il mio compagno di stanza R108 Fabio Lapponi, che sará per sempre uno dei miei migliori amici.

I greatly thank my room mate and friend Thomas Angerer, Raum 108, who went a long way with me. Without his help, I would have never had the choice to get this fascinating project.

Schließlich möchte ich meiner Familie und meinen Freunden danken, die mich auf all meinen Wegen unterstützt haben.

Danke Iris

Appendix

Mineral abbreviations ([1] acc to Kretz, 1983) and chemical formulas.

abbreviation	mineral	chemical formula
act[1]	actinolite	$KAl_3(SO_4)_2(OH)_6$
ang	anglesite	$PbSO_4$
azu	azurite	$Cu_3(CO_3)_2(OH)_2$
bt[1]	biotite	$K_2(Mg,Fe)_{6-4}(Fe,Al,Ti)_{0-2}(Si_6\text{-}5Al_{2-3}O_{20})(OH,F)_4$
bn[1]	bornite	Cu_5FeS_4
calc/cal[1]	calcite	CaCO3
cer	cerussite	$PbCO_3$
cc[1]	chalcocite	Cu_2S
ccp[1]	chalcopyrite	$CuFeS_2$
chl[1]	chlorite	$(Mg,Al,Fe)_{12}((Si,Al)_8O_{20})(OH)_{16}$
Ge-col	Ge-collusite	$Cu_{26}V_2(As,Ge)_6S_{32}$
cv[1]	covellite	CuS
descl	descloizite	$PbZn(VO_4)(OH)$
dol[1]	dolomite	$CaMg(CO_3)_2$
ena	enargite	Cu_3AsS_4
ep[1]	epidote	$Ca_2(Al,Fe^{3+})_3(SiO_4)_3(OH)$
-	fahlore	ten-tet-series
gn[1]	galena	PbS
ger	germanite	$Cu_{26}Fe_4Ge_4S_{32}$
hs[1]	hastingsite	$NaCa_2(Fe_4,Mg_4)(Al,Fe)Al_2Si_6O_{22}(OH,F)_2$
hem[1]	hematite	Fe_2O_3
hmm	hemimorphite	$Zn_4Si_2O_7(OH)_2*H_20$
hbl[1]	hornblende	$(Na,K)_{0-1}Ca_2(Mg,Fe,Al)_5(Si_{6-7}Al_{2-1}O_{22})(OH,F)_2$
hz	hydrozincite	$Zn_5((OH)_3/CO_3)_2$
ilm[1]	ilmenite	$FeTiO_3$
kln[1]	kaolinite	$Al_4(SiO_{10})(OH)_8$
kfs[1]	k-feldspar	$(K,Na)(AlSi_3O_8)$
mgt	magnetite	Fe_3O_4
mal	malachite	$Cu_2(CO_3)(OH)_2$
mim	mimetite	$Pb_5(AsO_4)_3Cl$
mottr	mottramite	$PbCu(VO_4)OH$
mk	muscovite	$K_2Al_4(Si_6Al_2O_{20})(OH,F)_4$
dg[1]	neodigenite/digenite	Cu_9S_5
pea-pol	pearcite-polybasite	$(Ag,Cu)_{16}As_2S_{11}$
pl[1]	plagioclase	$(Na,Ca)(Si,Al)_4O_8$
pym	pyromorphite	$Pb_5(PO_4)_3Cl$
po[1]	pyrrhotite	$Fe_{1-x}S$
pyr	pyrite	FeS_2
qtz[1]	quartz	SiO_2
ren	renierite	Zn_3AsS_4
smi	smithsonite	$ZnCO_3$
sp[1]	sphalerite	ZnS
ten	tennantite	$(Cu,Zn,Fe)_{12}As_4S_{13}$
tet	tetrahedrite	$(Cu,Zn,Fe)_{12}Sb_4S_{13}$
tmg	titanomagnetite	$Fe(Fe,Ti)_2O_4$
van	vanadinite	$Pb_5(VO_4)_3Cl$
wil	willemite	Zn_2SiO_4
vanad	vanadate	-

Other abbreviations

D	deformational event
Fm	formation
Gp	group
M	metamorphic event

- Hiermit erkläre ich, Carsten Laukamp (geb. 15.02.1974 in Hanau, Hessen), an Eides statt, dass ich die vorgelegte Dissertation selbst verfasst und mich dabei keiner anderen als der von mir ausdrücklich bezeichneten Quellen und Hilfen bedient habe.

- Ich, Carsten Laukamp (geb. 15.02.1974 in Hanau, Hessen), erkläre zudem an Eides statt, dass ich an keiner anderen Stelle ein Prüfungsverfahren beantragt habe, dass ich die Dissertation nicht in dieser oder anderer Form bereits anderweitig als Prüfungsarbeit verwendet habe und dass ich sie an keiner anderen Fakultät als Dissertation vorgelegt habe.

Heidelberg, den 01.12.2006

Hiermit erkläre ich, Carsten Laukamp (geb. 15.02.1974 in Hanau, Hessen), dass ich folgende Leistungen zu den zur Veröffentlichung eingereichten Artikel dieser kumulativen Dissertation erbracht habe:

Titel: Geodynamic Evolution of the Otavi Mountainland (Namibia): Implications for Pan-African Damara Orogeny and Metallogeny

Autoren: Carsten Laukamp, Thilo Bechstädt, Maria Boni

Status: Submitted to Journal of African Earth Sciences

Carsten Laukamp unternahm die Probennahme und sämtliche strukturgeologischen Analysen und entwickelte eine Neuinterpretation der geodynamischen Entwicklung des Otavi Berglandes. Thilo Bechstädt und Maria Boni halfen bei der Interpretation sedimentologischer und lagerstättenkundlicher Befunde.

_____ _____

Thilo Bechstädt (Betreuer) Maria Boni (Koautor)

Titel: Geochemistry and geochronology of Paleoproterozoic basement rocks of the Grootfontein Inlier (Namibia)

Autoren: Carsten Laukamp, Jens Schneider, Maria Boni, Thilo Bechstädt

Status: Submitted to Precambrian Research

Carsten Laukamp unternahm die Probennahme und die Interpretation geochemischer Analysen der Paläoproterozischen Grundgebirgsgesteine und stellte, unter der Zuhilfenahme der von Jens Schneider durchgeführten Rb-Sr Analysen, einen Vergleich mit weiteren Grundgebirgskomplexen des südlichen Sao Francisco-Congo Kratons an. Maria Boni und Thilo Bechstädt initiierten die Studie des Paläoproterozoischen Grundgebirges des Grootfontein Inliers.

_____ _____

Thilo Bechstädt (Betreuer) Maria Boni (Koautor)

Titel: Geology, geochemistry and metallogenetic significance of Cryogenian rift volcanics in the Otavi Mountainland (Namibia)

Autoren: Carsten Laukamp, Jens Schneider, Maria Boni, Thilo Bechstädt

Status: Submitted to South African Journal of Geology

Carsten Laukamp unternahm die Probennahme und die Interpretation geochemischer Analysen der sedimentären und vulkanische Gesteine und der darin enthaltenen Erze. Maria Boni und Thilo Bechstädt initiierten die Studie an diesen Neoproterozoischen Gesteinen des Otavi Berglandes und halfen bei der Interpretation lagerstättenkundlicher Befunde.

_____ _____

Thilo Bechstädt (Betreuer) Maria Boni (Koautor)

Titel: Willemite (Zn_2SiO_4) as a possible Rb-Sr geochronometer for dating nonsulphide Zn-Pb mineralisation: examples from the Otavi Mountainland (Namibia)

Autoren: Jens Schneider, Maria Boni, Carsten Laukamp, Thilo Bechstädt, Volker Petzel

Status: Accepted by Ore Geology Reviews

Carsten Laukamp half bei der Probennahme, beschrieb den geologischen Rahmen und lieferte Lösungsvorschläge zur Entwicklung der sulfidfreien Zn-Lagerstätten. Jens Schneider unternahm Versuche zur Verwendung der Zinksilikate als Rb-Sr geochronometer. Maria Boni initiierte das Projekt und unternahm den Großteil an den verschiedenen Analysen der Zinksilikate. Thilo Bechstädt und Volker Petzel halfen bei der Probennahme und trugen zur Interpretation der Daten bei.

_____	_____
Thilo Bechstädt (Betreuer)	Jens Schneider (Koautor)

Titel: Vanadate ores in the Otavi Mountainland (Namibia): geological setting, mineralogy, geochemistry, formation timing and relation with the "African Erosion Cycle"

Autoren: Maria Boni, Rosario Terracciano, Noreen Evans, Carsten Laukamp, Jens Schneider, Thilo Bechstädt

Status: Submitted to Economic Geology

Carsten Laukamp half bei der Probennahme, unternahm petrographische Beschreibungen, beschrieb den geologischen Rahmen und lieferte Lösungsvorschläge zur Entwicklung der sulfidfreien V-Lagerstätten. Maria Boni initiierte das Project, unternahm einen Großteil der petrographischen Analysen an den Vanadaten und entwickelte ein Modell zur Bildung der sulfidfreien V-Lagerstätten. Rosario Terracciano half bei der Probennahme und unternahm Beschreibungen und Analysen zur Petrographie der Vanadate. Noreen Evans führte (U-Th)/He Analysen an den Vanadaten durch. Jens Schneider unternahm Analysen zur Isotopengeochemie der Vanadate, Sulphide und begleitender Karbonate. Thilo Bechstädt half bei der Probennahme und trug zur Interpretation der Daten bei.

_____	_____
Thilo Bechstädt (Betreuer)	Rosario Terracciano (Koautor)

_____

Carsten Laukamp

Heidelberg, den 01.12.2006